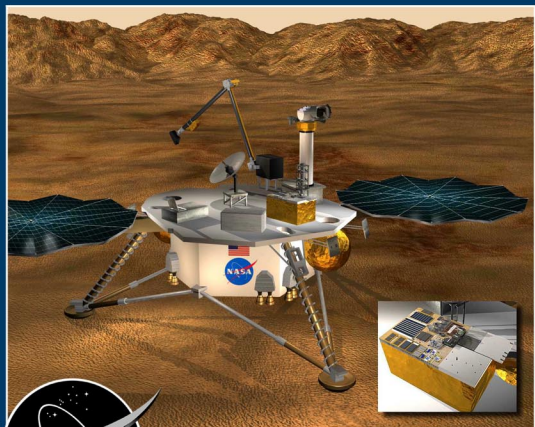
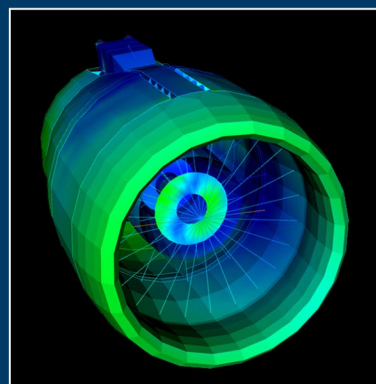
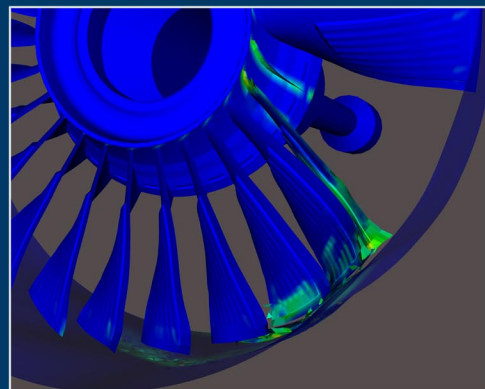


R&T



Glenn Research Center
at Lewis Field
Cleveland • Ohio
NASA/TM-2001-210605



2000 Research and Technology

ERRATA

NASA Technical Memorandum 2001-210605

RESEARCH & TECHNOLOGY 2000

March 2001

Page x: The heading "Communications Technology" should have been displayed above the article on page 67, "Accurate Time-Dependent Traveling-Wave Tube Model Developed for Computational Bit-Error-Rate Testing."

Pages 18, 19, 30, 34, 50, 51, 58, 69, 79, 106, 107, 108, 124, 126, 127, and 155: The Roman letters shown in the courier font (a lighter, typewriter-style font) should have been displayed as their corresponding Greek letters. That is,

a should be α

f should be ϕ

s should be σ

b should be β

G should be γ

w should be ω

D should be Δ

g should be γ

e should be ϵ

q should be θ

Page 50, paragraph 3, line 3: The dimension "12 mm" should be "12 μm ."

Page 67: The main heading "Communications Technology" should have been displayed above the article title "Accurate Time-Dependent Traveling-Wave Tube Model Developed for Computational Bit-Error-Rate Testing."

Page 69, paragraph 3, line 4: The dimension "300-mm-thick" should be "300- μm -thick."

Page 199: "Veres, Jenise" should be "Veris, Jenise" and "Veres, Dr. Kim A." should be "Veris, Dr. Kim A."

About the cover:

Top column: Left: Commodity-based cluster “Aeroshark” (pp. 10–11). Middle: Full-scale business jet empennage model inside NASA Ames’s 40- by 80-ft wind tunnel (pp. 89–90). Right: Researchers can use an interactive wand to zoom in for closeups of their models. This fan interaction simulation shows the dramatic results of a blade loss (pp. 176–177).

Middle column: Left: Kurt Blankenship, Dr. Judy Van Zante, and Arlette Haeberle (from left to right) in the Icing Research Tunnel providing details on an icing experiment during the live video tour (pp. 11–12). Middle: Researchers Eric Dao (University of Houston) and Brian Motil (Glenn) work on a packed bed reactor experiment on NASA’s KC–135 aircraft (pp. 152–154). Right: Glenn engineers, in collaboration with industry partners, model jet engines to predict loads due to blade loss. When displayed in a time sequence on the ImmersaDesk, subtle effects become apparent (pp. 176–177).

Bottom column: Left: Artist’s conception of Mars-2001 Surveyor Lander, with an inset showing the DART experiment package (pp. 37–38). Middle: Dr. Mrityunjay Singh holds an ARCJoint ceramic component (pp. 192–193). Top right: The sapphire refractive secondary concentrator enables high-temperature solar power and propulsion applications (pp. 56–57). Bottom right: Self-field MPD thruster (pp. 41–42).

Research & Technology 2000



National Aeronautics and
Space Administration

Glenn Research Center
Cleveland, Ohio 44135-3191

NASA/TM—2001-210605

Trade names or manufacturers' names are used in this report for identification only. This usage does not constitute an official endorsement, either expressed or implied, by the National Aeronautics and Space Administration.

Available from

NASA Center for Aerospace Information
7121 Standard Drive
Hanover, MD 21076
Price Code: A10

National Technical Information Service
5285 Port Royal Road
Springfield, VA 22100
Price Code: A10

Available electronically at <http://www.grc.nasa.gov/WWW/RT>



Introduction

The NASA Glenn Research Center at Lewis Field, in partnership with U.S. industries, universities, and other Government institutions, is responsible for developing and transferring critical technologies that address national priorities in aeropropulsion and space applications. Our work is focused on research for new aeropropulsion technologies, aerospace power, microgravity science fluids and combustion, electric propulsion, and communications technologies for aeronautics, space, and aerospace applications.

As NASA's premier Center for aeropropulsion, aerospace power, and turbomachinery, our role is to conduct world-class research and to develop and transfer key technologies to U.S. industries. We contribute to economic growth and national security through safe, superior, and environmentally compatible U.S. civil and military aircraft propulsion systems. Our Aerospace Power Program supports all

NASA Enterprises and major programs, including the International Space Station, Advanced Space Transportation, and new initiatives in human and robotic exploration.

The Glenn Research Center leads NASA's research in the microgravity science disciplines of fluid physics, combustion science, and acceleration measurement. Almost every shuttle and Mir science mission has had an experiment managed by the Center, and developments are under way to conduct a wide array of similar experiments on the International Space Station.

We are committed to enabling U.S.-based aerospace and nonaerospace industries to benefit directly from the technologies developed through our programs. Technology spinoffs from our efforts are found in all aspects of our daily lives, from solar cells to pagers. Our goal is to maximize the benefit of our activities to the Nation and to optimize the return on each taxpayer's investment.

Over 3300 civil service employees and support service contractor personnel staff Glenn. Scientists and engineers comprise more than half of our workforce, with technical specialists, skilled workers, and an administrative staff supporting them. We aggressively strive for technical excellence through continuing education, increased diversity in our workforce, and continuous improvement in our management and business practices so that we can expand the boundaries of aeronautics, space, and aerospace technology.

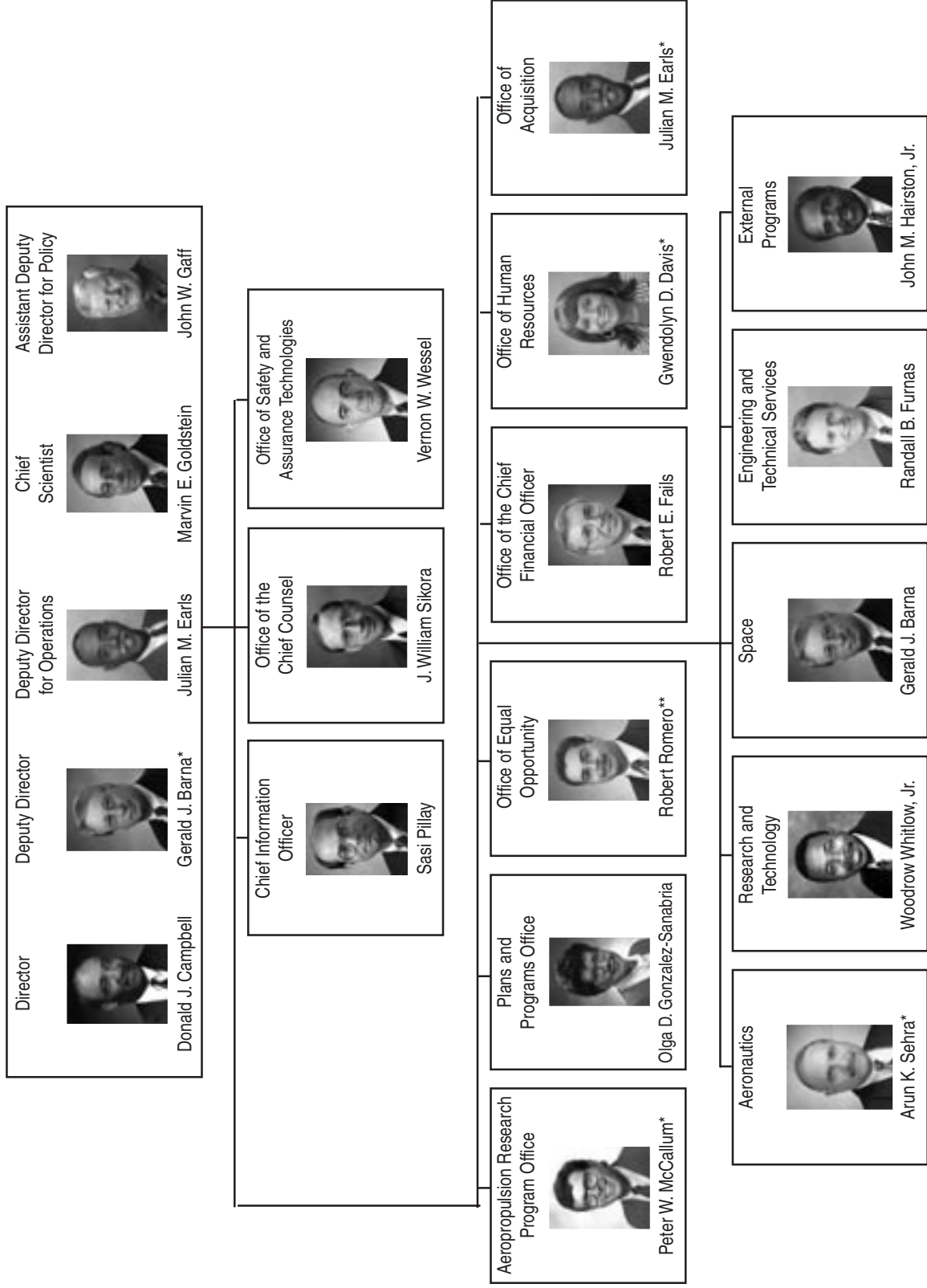
The Glenn Research Center is a unique facility located in the southwest corner of Cleveland, Ohio. Situated on 350 acres of land adjacent to the Cleveland Hopkins International Airport, Glenn comprises more than 140 buildings, including 24 major facilities and over 500 specialized research and test facilities. Additional facilities are located at Plum Brook Station, which is about 50 miles west of Cleveland.

Knowledge is the end product of our activities. The R&T report helps make this knowledge fully available to potential users—the aircraft engine industry, the space industry, the energy industry, the automotive industry, the aerospace industry, and others. It is organized so that a broad cross section of the community can readily use it. Each article begins with a short introductory paragraph that should prove valuable for the layperson. These articles summarize the progress made during the year in various technical areas and portray the technical and administrative support associated with Glenn's technology programs.

We hope that this information is useful to all. If additional information is desired, readers are encouraged to contact the researchers identified at the end of each article and to visit NASA Glenn on the World Wide Web at <http://www.grc.nasa.gov>. This document is available online (<http://www.grc.nasa.gov/WWW/RT/>).


Donald J. Campbell
Director

NASA Glenn Research Center Senior Management



*Acting

**** Interim Chief**

CD-48534

March 2001

V



Contents

Aeronautics

Ultra-Efficient Engine Technology

Ultra-Efficient Engine Technology (UEET) Program	2
--	---

Propulsion Systems Analysis

Probabilistic Risk-Based Approach to Aeropropulsion System Assessment Developed	4
---	---

Computing and Interdisciplinary Systems

EngineSim: Turbojet Engine Simulator Adapted for High School Classroom Use	6
Numerical Propulsion System Simulation—A Common Tool for Aerospace Propulsion Being Developed	7
Onyx-Advanced Aeropropulsion Simulation Framework Created	9
Cost/Performance Ratio Achieved by Using a Commodity-Based Cluster	10
NASA Research Being Shared Through Live, Interactive Video Tours	11
Coupled-Flow Simulation of HP–LP Turbines Has Resulted in Significant Fuel Savings	13

Research and Technology

Materials

Software Package Completed for Alloy Design at the Atomic Level	16
Thermodynamics of Titanium-Aluminum-Oxygen Alloys Studied	18
Laser High-Cycle Thermal Fatigue of Pulse Detonation Engine Combustor Materials Tested	19
Improved Method Being Developed for Surface Enhancement of Metallic Materials	22
GRCop-84 Developed for Rocket Engines	24
High-Flow PMR-Polyimide Composites Developed With Mechanical Properties Comparable to Other High-Temperature Systems	26
Long-Term Durability of a Matrix for High-Temperature Composites Predicted	27
PMR Extended Shelf Life Technology Given 2000 R&D 100 Award	29
Thermodynamics of Volatile Silicon Hydroxides Studied	30
Remote, Noncontact Strain Sensing by Laser Diffraction Developed	31
Creep/Rupture Behavior of Melt-Infiltrated SiC/SiC Composites Being Investigated	32
Environment-Conscious Ceramics (Ecoceramics)	33
Feasibility of Actively Cooled Silicon Nitride Airfoil for Turbine Applications Demonstrated	34
Upper Temperature Limit of Environmental Barrier Coatings for Enabling Propulsion Materials Established	35
Cooled Ceramic Matrix Composite Panel Successfully Tested in Rocket Exhaust	36

Power and On-Board Propulsion Technology

DART: Instrument Package Developed for Investigating Atmospheric Dust on Mars	37
Mars Array Technology Experiment Developed to Test Solar Arrays on Mars	39
Lightweight Sun Position Sensor Developed	40
High-Power Magnetoplasmadynamic Thruster Being Developed	41

1000 Hours of Testing Completed on 10-kW Hall Thruster	42
Lightweight Radiators Being Developed for Advanced Stirling Radioisotope Power Systems	43
MEMS Device Being Developed for Active Cooling and Temperature Control	44
Flywheel Energy Storage Technology Being Developed	46
Atomic Oxygen Interactions With Silicone Contamination on Spacecraft in Low Earth Orbit Studied	47
Specimens Prepared for Materials International Space Station Experiment	48
Effect of Air and Vacuum Storage on the Degradation of X-Ray-Exposed Aluminized-Teflon Investigated ..	49
Effects of Vacuum Ultraviolet Radiation on Thin Polyimide Films Evaluated	50
Chemical State of Surface Oxygen on Carbon and Its Effects on the Capacity of the Carbon Anode in a Lithium-Ion Battery Investigated	51
Surface Texturing Investigated for a High Solar Absorptance Low Infrared Emittance Solar Collector	52
International Test Program for Synergistic Atomic Oxygen and Vacuum Ultraviolet Radiation Exposure of Spacecraft Materials	53
Electronics for Low-Temperature Space Operation Being Evaluated	54
Assessment of Stirling Technology Has Provided Critical Data Leading Toward Flight Readiness of the Stirling Converter	55
High-Efficiency Solar Thermal Vacuum Demonstration Completed for Refractive Secondary Concentrator ..	56

Instrumentation and Controls

Packaging Technology Developed for High-Temperature Silicon Carbide Microsystems	58
Thermally Stable Ohmic Contacts on Silicon Carbide Developed for High-Temperature Sensors and Electronics	59
Atomically Flat Surfaces Developed for Improved Semiconductor Devices	60
Borescope Imaging System Developed for Luminescent Paint Measurements	62
Training Data Optimized and Conditioned to Learn Characteristic Patterns of Vibrating Blisks and Fan Blades	63
Active Control of Rotating Stall Demonstrated for a Multistage Compressor With Inlet Distortion	64
Pulse Detonation Engine Modeled	66
Accurate Time-Dependent Traveling-Wave Tube Model Developed for Computational Bit-Error-Rate Testing	67
Power and Efficiency Optimized in Traveling-Wave Tubes Over a Broad Frequency Bandwidth	68
Ferroelectric/Semiconductor Tunable Microstrip Patch Antenna Developed	69
High-Efficiency Wide-Band Suspended Patch Antenna Array Demonstrated	71
Microelectromechanical Systems (MEMS) Actuator for Reconfigurable Patch Antenna Demonstrated	72

Turbomachinery and Propulsion Systems

Complex Flow Separation Pattern on Transonic Fan Airfoils Revealed by Flow Visualization	73
Flow Range of Centrifugal Compressor Being Extended	74
Compressor Stall Recovery Through Tip Injection Assessed	75
One-Dimensional Spontaneous Raman Measurements Made in a Gas Turbine Combustor	76
Optical Diagnosis of Gas Turbine Combustors Being Conducted	78
Laser Absorption Measurements of Equivalence Ratios Studied Along With Their Coupling to Pressure Fluctuations in Lean Premixed Prevaporized (LPP) Combustion	79
Solid Hydrogen Particles Analyzed for Atomic Fuels	82
Safer Aircraft Possible With Nitrogen Generation	84
Safer Aviation Materials Tested	85
Hydrogen/Air Fuel Nozzle Emissions Experiments	86

Wind Tunnel Tests Conducted to Develop an Icing Flight Simulator	87
Icing Effects on a Full-Scale Business Jet Empennage	89
Thermocouple Rakes for Measuring Boundary Layer Flows Extremely Close to Surface	90
Dynamic Pressure Probes Developed for Supersonic Flow-Field Measurements	91
Development of a Hybrid RANS/LES Method for Turbulent Mixing Layers	92
Restraint of Liquid Jets by Surface Tension in Microgravity Modeled	94
Zero-Boiloff Cryogenic Storage Cryocooler Integration Test	95

Structures and Acoustics

Damage Assessment of Creep Tested and Thermally Aged Metallic Alloys Using Acousto-Ultrasonics	96
Rapid Prototyping Integrated With Nondestructive Evaluation and Finite Element Analysis	97
Silicon Nitride Plates for Turbine Blade Application: FEA and NDE Assessment	99
Local Debonding and Fiber Breakage in Composite Materials Modeled Accurately	101
Micromechanics-Based Inelastic Finite Element Analysis Accomplished Via Seamless Integration of MAC/GMC With ABAQUS	103
Higher-Order Theory for Functionally Graded Materials	105
General Multimechanism Reversible-Irreversible Time-Dependent Constitutive Deformation Model Being Developed	106
Nondestructive Evaluation Approaches Developed for Material Characterization in Aeronautics and Space Applications	107
Nondestructive Evaluation Methodologies Developed for Certifying Composite Flywheels	109
Ceramic Inclusions in Powder Metallurgy Disk Alloys: Characterization and Modeling	111
Test Standard Developed for Determining the Life Prediction Parameters of Advanced Structural Monolithic Ceramics at Elevated Temperatures	112
High Strain Rate Behavior of Polymer Matrix Composites Analyzed	113
Biaxial Testing of High-Strength Fabric Improves Design of Inflatable Radar Domes	114
NASA Software of the Year, GENOA-PFA, Given 2000 R&D 100 Award	115
Uncertainties in the Thermal and Mechanical Properties of Particulate Composites Quantified	118
Transient Reliability Analysis Capability Developed for CARES/Life	119
High-Frequency Focused Water-Coupled Ultrasound Used for Three-Dimensional Surface Depression Profiling	122
Ultrasonic Data Display and Analysis System Developed (Including Fuzzy Logic Analysis) for the Windows-Based PC	123
Fan Flutter Analysis Capability Enhanced	124
Cross-Axis Proportional Gains Used to Control Gyroscopic Effects in a Magnetic-Bearing- Supported Flywheel	124
DC Control Effort Minimized for Magnetic-Bearing-Supported Shaft	125
Synchronous Control Effort Minimized for Magnetic-Bearing-Supported Shaft	126
Fail-Safe Magnetic Bearing Controller Demonstrated Successfully	127
Engine With Regression and Neural Network Approximators Designed	128
Turbofan Noise Studied in Unique Model Research Program in NASA Glenn's 9- by 15-Foot Low-Speed Wind Tunnel	129
New High-Temperature Turbine Seal Rig Installed	131
Rudder/Fin Seals Investigated for the X-38 Re-Entry Vehicle	132
Vapor/Mist Used to Lubricate Gears After Loss of Primary Lubrication System	134
New Gear Transmission Error Measurement System Designed	135
Oil-Free Turbomachinery Being Developed	136

Space

Space Communications

Phased-Array Satcom Antennas Developed for Aeronautical Applications	138
Status of the Direct Data Distribution (D ³) Experiment	139
Aeronautical-Satellite-Assisted Process Being Developed for Information Exchange Through Network Technologies (Aero-SAPIENT)	140

Microgravity Science

Technology Being Developed at Lawrence Berkeley National Laboratory: Ultra-Low-Emission Combustion Technologies for Heat and Power Generation	141
Microscale Particulate Classifiers (MiPAC) Being Developed	143
Ceiling Fires Studied to Simulate Low-Gravity Fires	144
TIGER Burned Brightly in JAMIC	145
Spread Across Liquids Continues to Fly	146
Flame Synthesis Used to Create Metal-Catalyzed Carbon Nanotubes	148
Applications in Bioastronautics and Bioinformatics: Early Radiation Cataracts Detected by Noninvasive, Quantitative, and Remote Means	149
Novel Shapes of Miscible Interfaces Observed	151
Gas-Liquid Two-Phase Flows Through Packed Bed Reactors in Microgravity	152
How Does a Liquid Wet a Solid? Hydrodynamics of Dynamic Contact Angles	154
Diffusivity Measurements Made Instant and Easy	156
Growth and Morphology of Supercritical Fluids, a Fluid Physics Experiment Conducted on Mir, Complete	158
Light Microscopy Module: An On-Orbit Microscope Planned for the Fluids and Combustion Facility on the International Space Station	159
Coarsening Experiment Being Prepared for Flight	161
Physics of Colloids in Space (PCS) Flight Hardware Developed	162
Extensional Rheology Experiment Developed to Investigate the Rheology of Dilute Polymer Solutions in Microgravity	164
Compact Microscope Imaging System Developed	166
Multiuser Droplet Combustion Apparatus Developed to Conduct Combustion Experiments	168
Combustion Module-2 Preparations Completed for SPACEHAB Mission Including the Addition of a New Major Experiment	170
Experiments Developed to Study Microgravity Smoldering Combustion	172

Engineering and Technical Services

Computer Services

Virtual Reality Used to Serve the Glenn Engineering Community	176
---	-----

Facilities and Test Engineering

Multimillion Dollar Construction Project Completed in Glenn's Icing Research Tunnel	178
Abe Silverstein 10- by 10-Foot Supersonic Wind Tunnel Validated for Low-Speed (Subsonic) Operation	179

Engineering Design and Analysis

Sub-Nyquist Distortions in Sampled One- and Two-Dimensional Signals Studied	180
High-Voltage Droplet Dispenser Developed	182
Acoustical Testing Laboratory Developed to Support the Low-Noise Design of Microgravity Space Flight Hardware	183
Microgravity Emissions Laboratory Developed	184
Vibration Test Demonstrated Dynamic Capability of an Operating Stirling Convertor	185
CM-2 Environmental/Modal Testing of Spacehab Racks	187

Commercial Technology

Microarthroscopy System With Image Processing Technology Developed for Minimally Invasive Surgery	190
Dynamic Light Scattering Developed to Look Through the Eye's Window Into the Body	191
Computer Model Used to Help Customize Medicine	192
Affordable, Robust Ceramic Joining Technology (ARCJoint) Developed	192
LIFT Tenant Is Off and Running	193

Appendixes

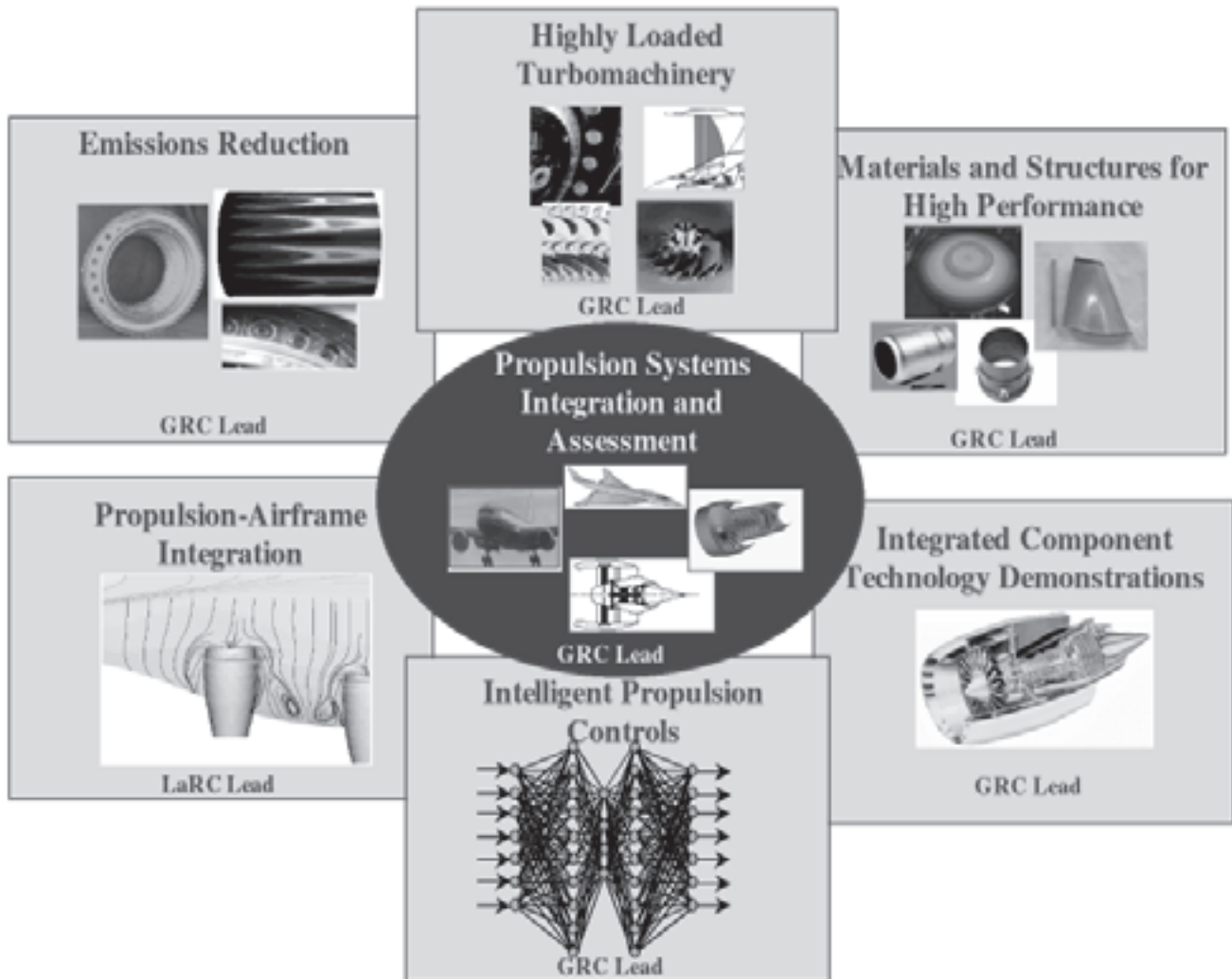
Definitions of NASA Headquarters Program Offices	195
Definitions of Programs and Projects	196
Index of Authors and Contacts	198



2,000 Aeronautics

Ultra-Efficient Engine Technology

Ultra-Efficient Engine Technology (UEET) Program



The Ultra-Efficient Engine Technology (UEET) Program includes seven key projects that work with industry to develop and hand off revolutionary propulsion technologies that will enable future-generation vehicles over a wide range of flight speeds.

A new program office, the Ultra-Efficient Engine Technology (UEET) Program Office, was formed at the NASA Glenn Research Center to manage an important National propulsion program for NASA. The Glenn-managed UEET Program, which began on October 1, 1999, includes participation from three other NASA centers (Ames, Goddard, and Langley), as well as five engine companies (GE Aircraft Engines, Pratt & Whitney, Honeywell, Allison/Rolls Royce, and Williams International) and two airplane manufacturers (the Boeing Company and Lockheed Martin Corporation). This 6-year, nearly \$300 million program will address local air-quality concerns by developing technologies to significantly reduce nitrogen oxide (NO_x) emissions. In addition, it will provide critical propulsion technologies to dramatically increase performance as measured in fuel burn reduction that will enable reductions of carbon dioxide (CO_2) emissions. This is necessary

to address the potential climate impact of long-term aviation growth.

The seven projects that make up the UEET Program are the Propulsion Systems Integration and Assessment Project, the Emissions Reduction Project, the Highly Loaded Turbomachinery Project, the Materials and Structures for High Performance Project, the Propulsion-Airframe Integration

Project, the Intelligent Propulsion Controls Project, and the Integrated Component Technology Demonstrations Project. These projects are described briefly in the following paragraphs.

Propulsion Systems Integration and Assessment

The Propulsion Systems Integration and Assessment Project takes the component technologies being developed in the other projects, integrates them into total conceptual systems, and assesses the potential of those systems for meeting the UEET Program goals. These assessments will also provide overall program guidance and identify technology shortfalls. The Propulsion Systems Integration and Assessment Project has three key subprojects: Propulsion System Evaluation, Environmental Impact Assessment, and High Fidelity System Simulation.

Emissions Reduction

The Emissions Reduction Project will work with the U.S. aeropropulsion industry to develop combustion technologies to significantly reduce NO_x emissions with no increase in other emission constituents (carbon monoxide, smoke, and unburned hydrocarbons) and with comparable NO_x reduction during cruise operations. As in the past, new combustor concepts and technologies will be required to produce cleaner burning combustors to offset the increased NO_x produced by the future more fuel efficient engines with higher pressure ratios and temperatures. These new combustion concepts and technologies will include lean burning combustors with advanced controls and new high-temperature ceramic matrix composite materials that will reduce cooling air. Low-emission combustor concepts will be developed and evaluated to achieve major reductions in NO_x emissions for both large and regional engines.

Highly Loaded Turbomachinery

The Highly Loaded Turbomachinery Project of the UEET Program will provide revolutionary turbomachinery technologies for increased performance and efficiency. The technologies developed will be applicable to a wide range of applications, both in terms of flight speed and size class. This project will develop turbomachinery technologies for lighter weight, reduced-stage cores, low-pressure spools, and propulsors for high-performing, highly efficient, and environmentally compatible propulsion systems. Specifically, concepts for significantly increased aero loading, trailing-edge wake control, and higher cooling effectiveness will be developed and demonstrated through proof-of-concept tests. Fan technology development will reduce weight and increase efficiency while satisfying noise constraints.

Materials and Structures for High Performance

The Materials and Structures for High Performance project will develop and demonstrate advanced high-temperature materials to enable environmentally compatible propulsion systems with high performance and efficiency. Technologies to be developed in this project include ceramic matrix composite combustor liners and turbine vanes, advanced disk alloys, turbine airfoil material systems, high-temperature polymer matrix composites, and innovative lightweight materials and structures for static engine structures.

Propulsion-Airframe Integration

The Propulsion-Airframe Integration Project of the UEET Program will develop advanced technologies to yield lower drag propulsion system integration with the airframe for a wide range of vehicle classes. Decreasing drag improves air vehicle performance and efficiency, which reduces fuel burn to accomplish a particular mission, thereby reducing the CO_2 emissions. This project can be defined as the determination of optimum nacelle placement and optimum shaping to both the nacelle and the airframe to minimize drag. This objective is accomplished through both computational and experimental methods.

Intelligent Propulsion Controls

The rapid explosion of information technologies makes it possible to envision future autonomous propulsion system designs that allow the control system to, independent of pilot interaction, maximize performance across the particular mission profile while at the same time minimizing environmental impact. Such a control system could also adjust system characteristics to maximize the lives of individual components and, therefore, improve propulsion system life and safety. Currently, the overall Intelligent Propulsion Controls Project is being planned with the challenge to find the proper integration of information, propulsion, and integrated flight propulsion control technologies. The initial efforts will focus on (1) assessing systems for the projected payoffs of various technologies and (2) experimentally and analytically evaluating active combustion control approaches to support the program goal of landing and takeoff NO_x reduction.

Integrated Component Technology Demonstrations

Technology demonstration tests are a critical step in the technology development process. The Integrated Component Technology Demonstrations Project tests will reduce risk significantly by demonstrating that the technologies are still viable when integrated into an overall system. The results of these tests provide the necessary confidence to the aeropropulsion industry to incorporate the technologies in follow-on product insertion programs. The initial efforts in this project will focus on determining the most attractive, cost-effective approaches to conducting the needed tests. Many potential opportunities exist for NASA and DOD to collaborate on these tests through partnership efforts between the UEET and Integrated High Performance Turbine Engine Technology (IHPTET) programs. In addition, potential partnership efforts with the U.S. aeropropulsion industry are being evaluated. In all cases, it is desirable to make maximum use of existing engine hardware to allow for the most cost-effective tests.

Find out more about the UEET

Program: <http://www.ueet.nasa.gov/>

Glenn contacts:

Dr. Robert J. Shaw, 216-977-7135, Robert.J.Shaw@grc.nasa.gov; and
Lori A. Manthey, 216-433-2484, Lori.A.Manthey@grc.nasa.gov

Author: Lori A. Manthey

Headquarters program office: OAT

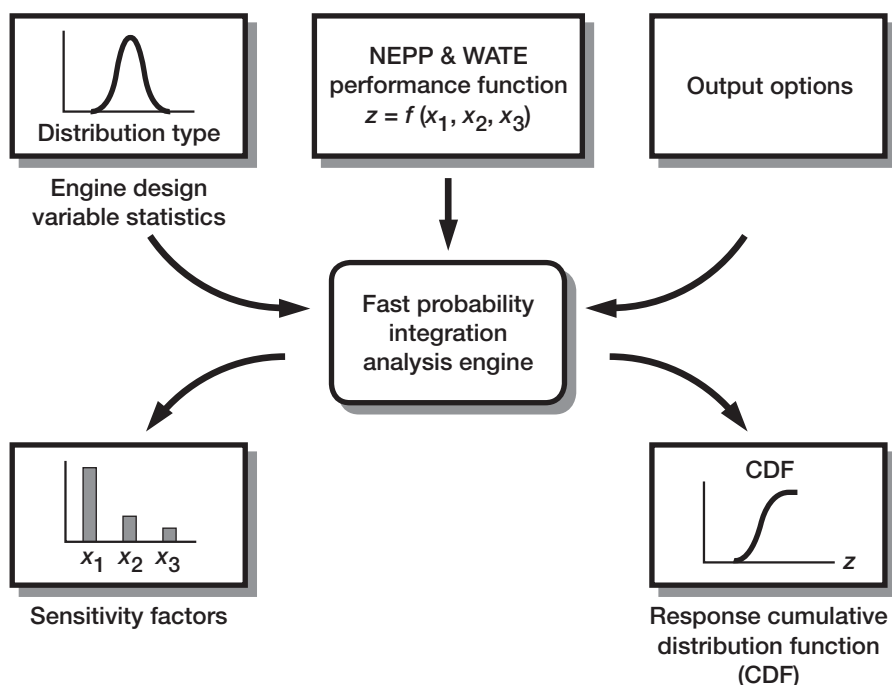
Programs/Projects: UEET, Propulsion Systems Integration and Assessment, Emissions Reduction, Highly Loaded Turbomachinery, Materials and Structures for High Performance, PAI, IPC, ICTD

Propulsion Systems Analysis

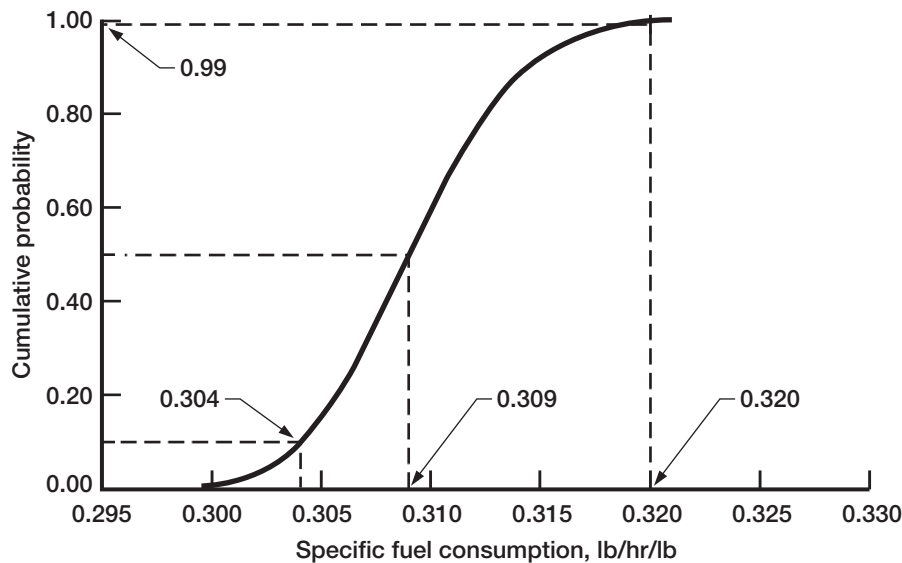
Probabilistic Risk-Based Approach to Aeropropulsion System Assessment Developed

In an era of shrinking development budgets and resources, where there is also an emphasis on reducing the product development cycle, the role of system assessment, performed in the early stages of an engine development program, becomes very critical to the successful development of new

aeropropulsion systems. A reliable system assessment not only helps to identify the best propulsion system concept among several candidates, it can also identify which technologies are worth pursuing. This is particularly important for advanced aeropropulsion technology development programs, which require an enormous amount of resources. In the current practice of deterministic, or point-design, approaches, the uncertainties of design variables are either unaccounted for or accounted for by safety factors. This could often result in an assessment with unknown and unquantifiable reliability. Consequently, it would fail to provide additional insight into the risks associated with the new technologies, which are often needed by decisionmakers to determine the feasibility and return-on-investment of a new aircraft engine.



Probabilistic approach.



Cumulative distribution function of specific fuel consumption.

In this work, an alternative approach based on the probabilistic method was described for a comprehensive assessment of an aeropropulsion system. The statistical approach quantifies the design uncertainties inherent in a new aeropropulsion system and their influences on engine performance. Because of this, it enhances the reliability of a system assessment. A technical assessment of a wave-rotor-enhanced gas turbine engine was performed to demonstrate the methodology. The assessment used probability distributions to account for the uncertainties that occur in component efficiencies and flows and in mechanical design variables. The approach taken in this effort was to integrate the thermodynamic cycle analysis embedded in the computer code NEPP (NASA Engine Performance Program) and the engine weight analysis embedded in the computer code WATE (Weight Analysis of Turbine Engines) with the fast probabil-

ity integration technique (FPI). FPI was developed by Southwest Research Institute under contract with the NASA Glenn Research Center.

The results were plotted in the form of cumulative distribution functions and sensitivity analyses and were compared with results from the traditional deterministic approach. The comparison showed that the probabilistic approach provides a more realistic and systematic way to assess an aeropropulsion system. The accompanying figures show sample results from the analyses. The current work addressed the application of the probabilistic approach to assess specific fuel consumption, engine thrust, and weight. Similarly, the approach can be used to assess other aspects of aeropropulsion system performance, such as cost, acoustic noise, and emissions.

Bibliography

Tong, Michael T.: A Probabilistic Approach to Aeropropulsion System Assessment. NASA/TM-2000-210334, 2000. <http://gltrs.grc.nasa.gov/GLTRS>

Glenn contact:

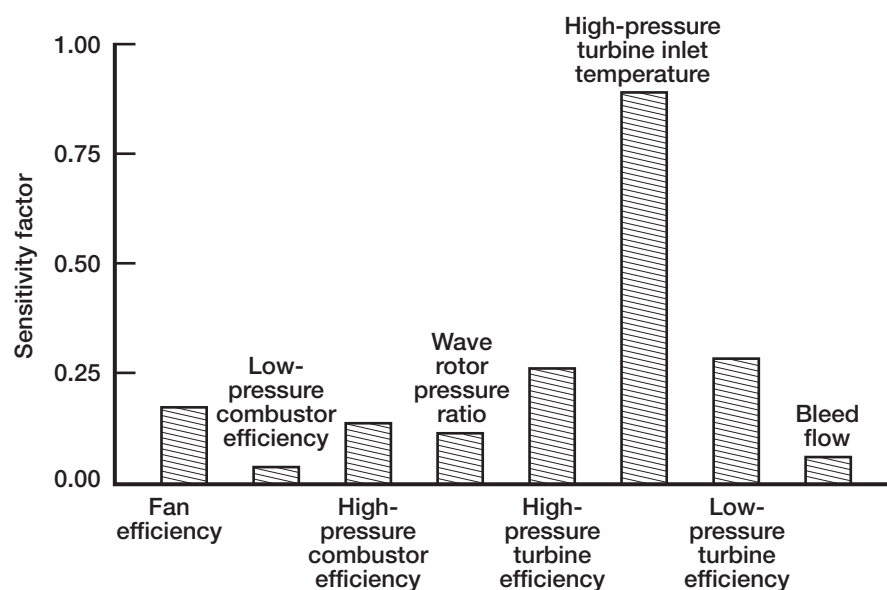
Michael T. Tong, 216-433-6739, Michael.T.Tong@grc.nasa.gov

Author: Michael T. Tong

Headquarters program office: OAT

Programs/Projects:

Power and Propulsion Base Program



Sensitivity of specific fuel consumption to the various engine design parameters.

Computing and Interdisciplinary Systems

EngineSim: Turbojet Engine Simulator Adapted for High School Classroom Use

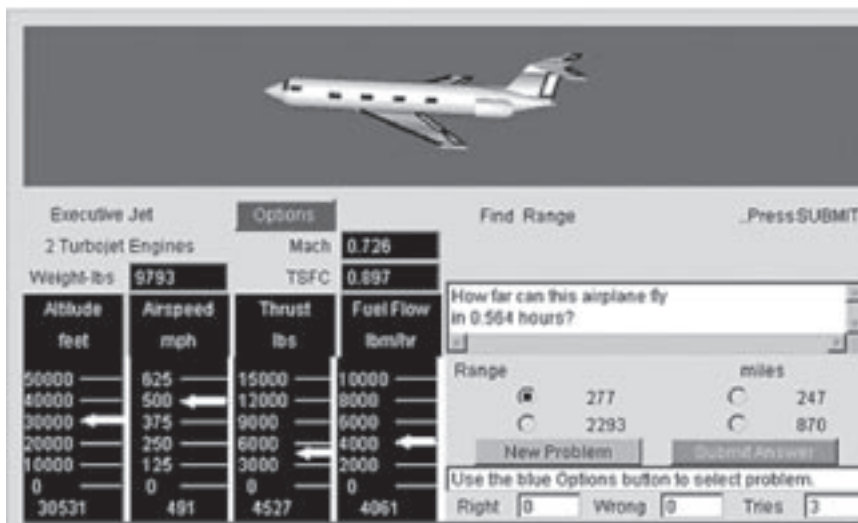
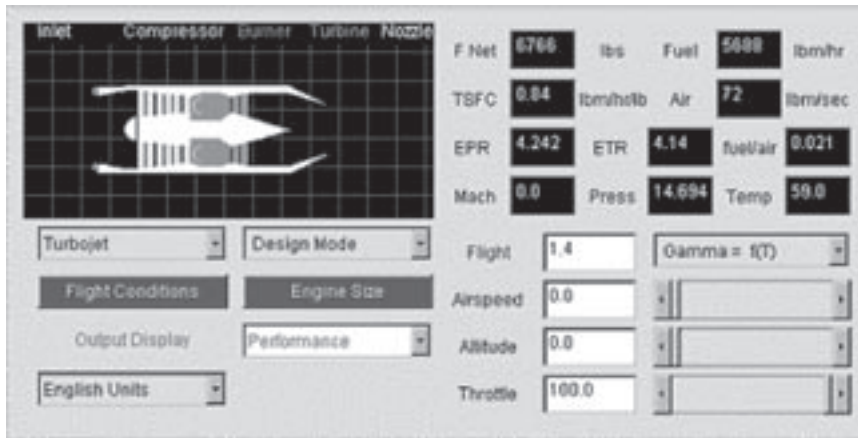
EngineSim is an interactive educational computer program that allows users to explore the effect of engine operation on total aircraft performance. The software is supported by a basic propulsion web site called the *Beginner's Guide to Propulsion*, which includes educator-created, web-based activities for the classroom use of EngineSim. In addition, educators can schedule videoconferencing workshops in which EngineSim's creator demonstrates the software and discusses its use in the educational setting. This software is a product of NASA Glenn Research Center's Learning Technologies Project, an educational outreach initiative within the High Performance Computing and Communications Program.

EngineSim consists of two parts: (1) a range program that includes rate and force problems of different levels of difficulty and (2) a design program that models the design and testing of jet engines.

EngineSim—Design calculates the one-dimensional thermodynamic performance of a simple turbojet engine, a turbojet with an afterburner, a two-spool turbofan engine, or a ramjet engine. It can be used to design an engine or to evaluate the engine's off-design performance. In the design mode, students can change design variables such as the flight conditions, the engine size, the inlet performance, the turbomachinery compressor and turbine performance, the combustors or burner performance, and the nozzle performance. The student's design can then be tested in Tunnel Test Mode, where the student can vary the flight conditions (airspeed, altitude, and throttle setting).

EngineSim—Range uses jet engines to present a variety of rate and force problems of different levels of difficulty. The rate problems deal with how far and how long an airplane can fly on a given amount of fuel, and the force problems deal with Newton's laws of motion on takeoff. Students can choose a play mode, a learn mode (in which the student's chances to determine the correct answer are limited), or an exam mode (in which the student gets one chance to determine the correct answer and the answer is recorded for the teacher). Graphical feedback is given for each answer choice.

EngineSim was created to illustrate an example of the research being conducted at Glenn and is designed to be an intuitive tool to supplement and enhance math and science curricula. It was



Top: EngineSim—Design. Bottom: EngineSim—Range.

originally written for college-level engineering students (VU-TURBO). Adjustment of the code to the high school level resulted in EngineSim, which was created and tested by a diverse team composed of NASA employees, contractors, and educators. Glenn's Learning Technologies Project participates in NASA's Learning Technologies Project, which is managed by the NASA Ames Research Center.

Learning Technologies Project: <http://learn.ivv.nasa.gov>

Glenn Learning Technologies Project: <http://www.grc.nasa.gov/WWW/K-12>

EngineSim—Range: <http://www.grc.nasa.gov/WWW/K-12/airplane/ngnsimr.html>

EngineSim—Design: <http://www.grc.nasa.gov/WWW/K-12/airplane/ngnsim.html>

Beginner's Guide to Propulsion:

<http://www.grc.nasa.gov/WWW/K-12/airplane/bgp.html>

Beginner's Guide to Propulsion Problem Sets:

<http://www.grc.nasa.gov/WWW/K-12/BGP/BGPindex.html>

Glenn contact:

Tom J. Benson, 216-433-5920,
Thomas.J.Benson@grc.nasa.gov

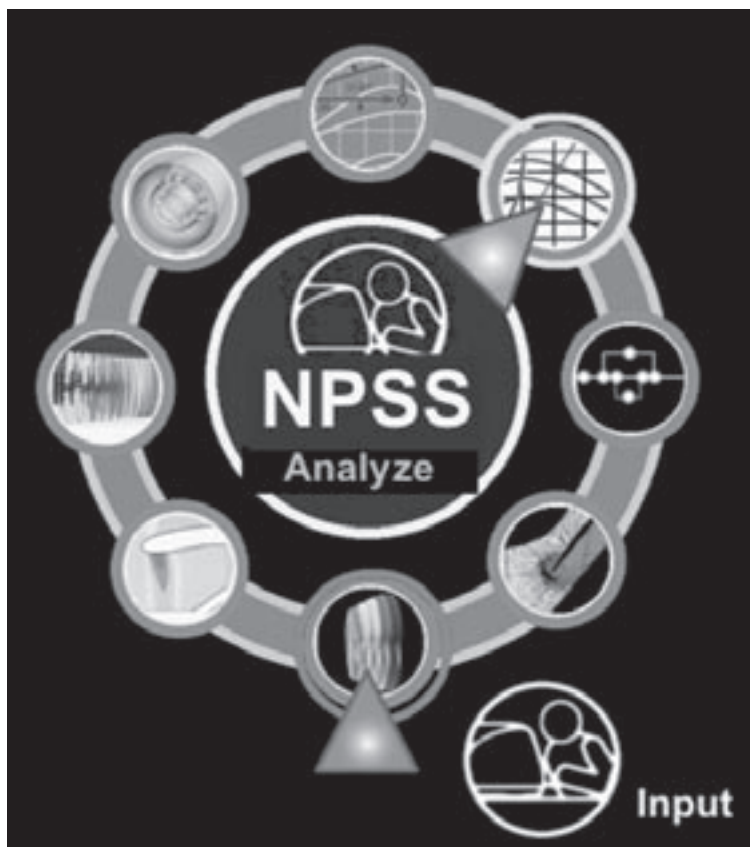
Author: Ruth A. Petersen

Headquarters program office: OAT

Programs/Projects: HPCCP, LTP

Numerical Propulsion System Simulation—A Common Tool for Aerospace Propulsion Being Developed

The NASA Glenn Research Center is developing an advanced multidisciplinary analysis environment for aerospace propulsion systems called the Numerical Propulsion System Simulation (NPSS). This simulation is initially being used to support aeropropulsion in the analysis and design of aircraft engines. NPSS provides increased flexibility for the user, which reduces the total development time and cost. It is currently being extended to support the Aviation Safety Program and Advanced Space Transportation. NPSS focuses on the integration of multiple disciplines such as aerodynamics, structure, and heat transfer with numerical zooming on component codes. Zooming is the coupling of analyses at various levels of detail. NPSS development includes using the Common Object Request Broker Architecture (CORBA) in the NPSS Developer's Kit to facilitate collaborative engineering. The NPSS Developer's Kit will provide the tools to develop custom components and to use the CORBA capability for zooming to higher fidelity codes, coupling to multidiscipline codes, transmitting secure data, and distributing simulations across different platforms. These powerful capabilities will extend NPSS from a zero-dimensional simulation tool to a multifidelity, multidiscipline system-level simulation tool for the full life cycle of an engine.



The ultimate goal of NPSS is to improve the quality and reduce the development time for aerospace propulsion systems. Currently, interdisciplinary design involves several different types of tools that are not designed to

work together. NPSS will streamline and improve this process by providing tighter integration of

NPSS COMPETITIVE ADVANTAGE

In the past, at each step in the cycle an expert operator was required to do the following:	With NPSS
<ol style="list-style-type: none"> 1. Read the results of the previous analysis. 2. Analyze the results and decide what changes to their own model are required. 3. Translate the data from the previous analysis for use in the current tool. 4. Manually enter the new input. 5. Run the current tool. 6. Feed the output to the next step or tool in the analysis cycle. 	<ol style="list-style-type: none"> 1. Results from the previous analysis are automatically available. 2. Results are analyzed, and model changes are made. 3. Data are automatically translated and available. 4. Any tool can run accessing data with output available.

various tools, with automated translation. This reduces development time and reduces errors due to the manual entry of data. NPSS accelerates the engine system design analysis and test phases, including integration with the airframe, which facilitates bringing the final product to market faster.

By providing an integrated framework within which the various tools can execute and communicate, the NPSS will significantly streamline the design and development process. This will, in turn, shorten the development cycle, giving NPSS users an advantage over other developers.

U.S. aircraft and airframe companies recognize NPSS as the future industry standard common analysis tool for aeropropulsion system modeling. The estimated potential payoff, if NPSS is adopted by the aeronautics industry, is a \$50 million/year savings through improved engineering productivity.

Through the NASA/Industry Cooperative Effort agreement, NASA Glenn and industry and Government partners are developing NPSS. The NPSS team consists of propulsion experts and software engineers from GE Aircraft Engines, Pratt & Whitney, the Boeing Company, Honeywell, Rolls-Royce Corporation, Williams International, Teledyne Ryan Aeronautical, Arnold Engineering Development Center, Wright-Patterson Air Force Base, and the NASA Glenn Research Center. Interest in using NPSS continues to broaden from aeropropulsion, both commercial and military, to space transportation and ground-based power systems. Formal software development processes, which are under ISO 9000 high control, are followed to facilitate technology transfer.

In fiscal year 2000, the major accomplishment of the NPSS team was the distribution of NPSS Version 1.0.0 on schedule. NPSS Version 1.0.0 can be used as an aerothermodynamic zero-dimensional cycle simulation tool. The capabilities include text-based input syntax, a sophisticated solver, steady-state and transient operation, report generation, a built-in object-oriented programming language for user-definable components and functions, support for distributed running of external codes via CORBA, test data reduction, interactive debug capability, and customer deck generation.

In fiscal year 2001, we plan to focus on enhancing the NPSS Developer's Kit (providing the initial Visual-Based Syntax (VBS) capability) and on supporting space transportation. NPSS Version 2.0.0 for aerospace is scheduled to be released in fiscal year 2001. NPSS is supported under NASA's High Performance Computing and Communications Program.

Find out more about High Performance Computing and Communications at Glenn:

<http://hpcc.grc.nasa.gov/hpcc2>

References

1. Follen, G.J.; and auBuchon, M.: Numerical Zooming Between the NPSS Version 1 and a 1-Dimensional Meanline Design Analysis Code. ISABE 99-7196, Proceedings of the 14th International Symposium on Air Breathing Engines, 1999.
2. Binder, M.: Numerical Propulsion System Simulation Introduction. Multimedia CD, 2000. Available from the NASA Glenn Computing and Interdisciplinary Systems Office.
3. Evans, A.L., et al.: Numerical Propulsion System Simulation's National Cycle Program. AIAA Paper 98-3113, 1998.
4. Ashleman, Russell H., Jr.: The National Cycle Program—A Flexible System Modeling Architecture for Aircraft Engine Simulation. AIAA Paper 98-3114, 1998.

Glenn contacts:

Gregory J. Follen, 216-433-5193, Gregory.J.Follen@grc.nasa.gov; and Cynthia G. Naiman, 216-433-5238, Cynthia.G.Naiman@grc.nasa.gov

Authors: Cynthia G. Naiman and Gregory J. Follen

Headquarters program office: OAT

Programs/Projects: HPCCP, Computational Aerospace Sciences Project

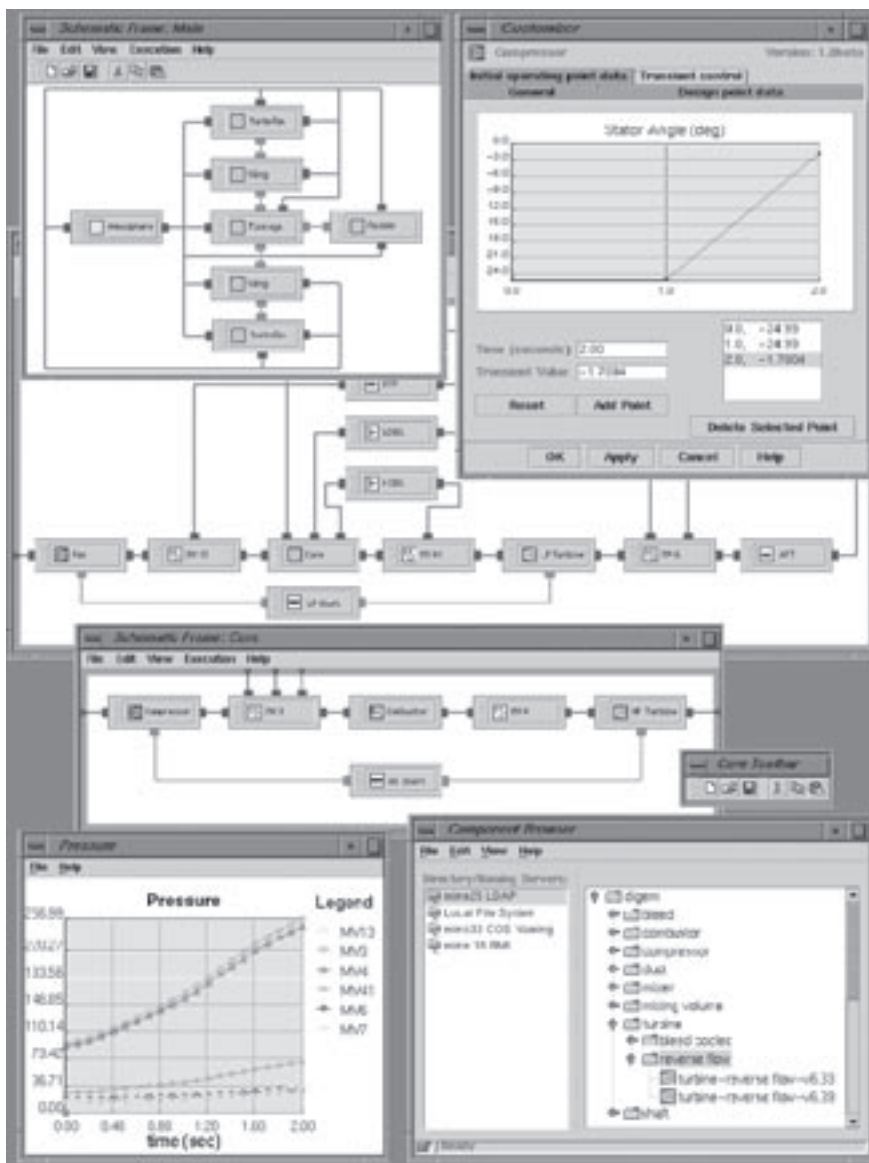
Onyx-Advanced Aeropropulsion Simulation Framework Created

The Numerical Propulsion System Simulation (NPSS) project at the NASA Glenn Research Center is developing a new software environment for analyzing and designing aircraft engines and, eventually, space transportation systems. Its purpose is to dramatically reduce the time, effort, and expense necessary to design and test jet engines by creating sophisticated computer simulations of an aerospace object or system (refs. 1 and 2). Through a university grant as part of that effort, researchers at the University of Toledo have developed *Onyx*, an extensible Java-based (Sun Microsystems, Inc.), object-oriented simulation framework, to investigate how advanced software design techniques can be successfully applied to aeropropulsion system simulation (refs. 3 and 4).

The design of Onyx's architecture enables users to customize and extend the framework to add new functionality or adapt simulation behavior as required. It exploits object-oriented technologies, such as design patterns, domain frameworks, and software components, to develop a modular system in which users can dynamically replace components with others having different functionality.

The accompanying figure shows a sample simulation session developed using Onyx's configurable Visual Assembly interface. Icons, representing available aerospace component models, are selected from a network repository and dragged into a model editor window. The icons are then interconnected to form a schematic diagram of the overall model. Customizing forms are provided for entering or editing data for each component, as well as for defining and controlling the numerical methods used to execute the simulation. Plotting capabilities, help browsers, text editors, and other user interface utilities are also included in the framework.

The component models represented in the Visual Assembly interface are defined by Onyx's Common Engineering Model (CEM). CEM is a hierarchical object model that forms the foundation for an integrated representation of an aerospace system, its components, subcomponents, and sub-assemblies. Using CEM, users can create primitive component models, and visually or programmatically combine them to form more complex models. In addition, CEM can accommodate models having differing fidelity and discipline. Higher order analysis methods,



Onyx Visual Assembly interface showing an example simulation model.

such as computational fluid dynamics or finite element analysis, can be integrated within a component object with a small amount of programming. This feature enables a more concurrent engineering approach by allowing users to select a particular analysis method based on the level of detail needed, the objective of the simulation, the available knowledge, and the given resources. A general mechanism is provided to handle data transformation when components of different disciplines and fidelities are connected.

The introduction of interdisciplinary models and models having differing levels of fidelity requires support for distributed computing as it cannot be assumed that the higher fidelity software will run efficiently (or at all) on the same computer platform as the rest of the system. Onyx supports distributed computing by using several common software distribution mechanisms, including Java's RMI (Remote Method Invocation) and CORBA (Common Object Request Broker Architecture). Using CORBA objects, one can integrate within the Onyx framework legacy software packages that must operate on specific architectures or operating systems and include them in a simulation mode.

Find out more about this research on the World Wide Web:

<http://memslab.eng.utoledo.edu/~jreed>

References

1. Claus, R.W., et al.: Numerical Propulsion System Simulation. *Comput. Syst. Eng.*, vol. 2, no. 4, 1991, pp. 357–364.
2. Evans, A.L., et al.: An Integrated Computing and Interdisciplinary Systems Approach to Aeropropulsion Simulation. *ASME Paper 97-GT-303*, 1998.
3. Reed, John A.; and Afjeh, Abdollah A.: Computational Simulation of Gas Turbines: Part I—Foundations of Component-Based Models. *J. Eng. Gas Turbines Power*, vol. 122, 2000, pp. 366–376.
4. Reed, John A.; and Afjeh, Abdollah A.: Computational Simulation of Gas Turbines: Part 2—Extensible Domain Framework. *J. Eng. Gas Turbines Power*, vol. 122, 2000, pp. 377–386.

Glenn contact:

Gregory J. Follen, 216–433–5193,
Gregory.J.Follen@grc.nasa.gov

Author: John A. Reed

Headquarters program office: OAT

Programs/Projects: HPCCP, CAS

Special recognition: Best Paper Award,
1999 ASME International Gas Turbine
Institute, Aircraft Engine Committee

Cost/Performance Ratio Achieved by Using a Commodity-Based Cluster

Researchers at the NASA Glenn Research Center acquired a commodity cluster based on Intel Corporation processors to compare its performance with a traditional UNIX cluster in the execution of aeropropulsion applications. Since the cost differential of the clusters was significant, a cost/performance ratio was calculated. After executing a propulsion application on both clusters, the researchers demonstrated a 9.4 cost/performance ratio in favor of the Intel-based cluster.

Within NASA's High Performance Computing and Communication (HPCC) program, Glenn is developing an environment for analyzing and designing propulsion engines called the Numerical Propulsion System Simulation (NPSS). NASA personnel are interested in computational simulations because of the potential for fielding improved air propulsion systems with lower development costs, greater fuel efficiency, and greater performance and reliability. One of the goals for NPSS is to create a "numerical test cell" enabling full engine simulations overnight on cost-effective computing platforms. In order to achieve this goal, NASA personnel at Glenn have been involved since the early 1990's in applying cluster-computing technology in solving aeropropulsion applications.

These researchers utilize the Aeroshark cluster as one of the primary testbeds for developing NPSS parallel application codes and system software. The Aeroshark cluster provides 64 Intel Pentium II 400-MHz processors, housed in 32 nodes. Recently, APNASA—a code developed by a Government/industry team for the design and analysis of turbomachinery systems—was used for a simulation on Glenn's Aeroshark cluster. APNASA has been used to evaluate new turbomachinery design concepts, from small compressors to large commercial aircraft engines. In this simulation, a single-stage fan was analyzed to



Commodity-based cluster "Aeroshark."

determine the noise levels associated with three different rotor geometries based on takeoff (100 percent), cutback (87.5 percent), and approach (61.7 percent) engine wheel speeds, each paired with three different vane geometries. This design matrix resulted in 9 (3 by 3) different configurations to be simulated in 24 CPU's.

After the application was executed on both the Aeroshark and on a Silicon Graphics Incorporated (SGI) Origin 2000 cluster, a performance factor of

2.36 was obtained in favor of the SGI. The cost of the SGI is 22.3 greater than that of the Intel-based cluster, therefore a cost/performance ratio of 9.4 in favor of the Aeroshark cluster was obtained.

Clearly, the commodity-based cluster has a tremendous potential for providing a computing platform on which detailed aeropropulsion simulations can be executed in a time compatible with the engine design cycle. In addition, the performance shown by the commodity-based cluster was impressive considering the cost differential between the two computing platforms.

Find out more about the Aeroshark cluster:

<http://hpcc.grc.nasa.gov/aeroshark>

Glenn contact:

Isaac Lopez, 216-433-5893,

Isaac.Lopez@grc.nasa.gov

Author: Isaac Lopez

Headquarters program office: OAT

Programs/Projects: HPCCP, CAS

NASA Research Being Shared Through Live, Interactive Video Tours

On June 2, 2000, the NASA Glenn Research Center Learning Technologies Project (LTP) coordinated the first live remote videoconferencing broadcast from a Glenn facility. The historic event from Glenn's Icing Research Tunnel featured wind tunnel technicians and researchers performing an icing experiment, obtaining results, and discussing the relevance to everyday flight operations and safety. After a brief overview of its history, students were able to "walk through" the tunnel, stand in the control room, and observe a live icing experiment that demonstrated how ice would grow on an airplane wing in flight through an icing cloud. The tour was interactive, with a spirited exchange of questions and explanations between the students and presenters.

The virtual tour of the oldest and largest refrigerated icing research tunnel in the world was the second of a series of videoconferencing connections with the AP Physics students at Bay Village High School, Bay Village, Ohio. The first connection, called Aircraft Safety and Icing Research, introduced the Tailplane Icing Program. In an effort to improve aircraft safety by reducing

the number of in-flight icing events, Glenn's Icing Branch uses its icing research aircraft to conduct flight tests. The presenter engaged the students in discussions of basic aircraft flight mechanics and the function of the horizontal tailplane, as well as the effect of ice on airfoil (wing or tail) surfaces. A brief video of actual flight footage provided a view of the pilot's actions and reactions and of the horizon during tailplane icing conditions. The event, which has been archived at <http://www.grc.nasa.gov/WWW/K-12/IRT>, includes online, interactive post-conference activities and assessment tools.

The conference was made possible through the cooperative efforts of Glenn's Icing Branch, Computer Services Division, Engineering Design and Analysis Division, and LTP. This videoconference demonstrates the tremendous potential of the NASA Glenn LTP distance learning program. In addition, because a network connection was successfully set up between the facility, a midpoint videoconference room at Glenn, and the school itself, the groundwork has been established for further virtual tours of Glenn's facilities. Other outreach groups can now use this demonstrated capability for a number of different functions, including celebrating the past 100 years of flight. Glenn's LTP is part of NASA's agencywide Learning Technologies Project, which is managed by the NASA Ames Research Center.

Learning Technologies Project: <http://learn.ivv.nasa.gov>

Glenn Learning Technologies Project:

<http://www.grc.nasa.gov/WWW/K-12>

Virtual Tour of the Glenn Icing Research Tunnel:

<http://www.grc.nasa.gov/WWW/K-12/IRT>

Integral Systems, Inc., contact:

Ruth A. Petersen, 216-433-9714, Ruth.A.Petersen@grc.nasa.gov

Authors: Ruth A. Petersen and Kathleen A. Zona

Headquarters program office: OAT

Programs/Projects: HPCCP, LTP



Left to right: Kurt Blankenship, Dr. Judy Van Zante, and Arlette Haeberle in the Icing Research Tunnel providing details on an icing experiment during the live video tour.

Coupled-Flow Simulation of HP-LP Turbines Has Resulted in Significant Fuel Savings

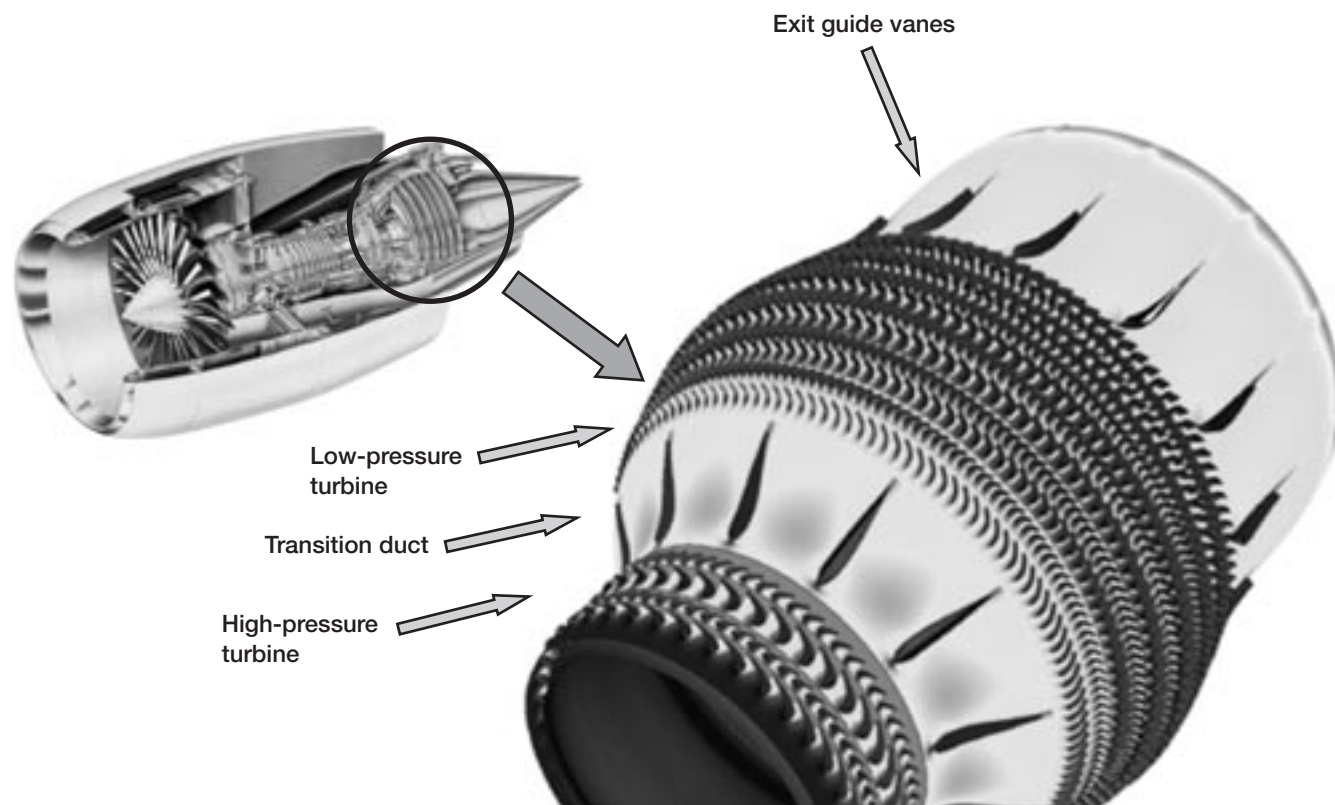
Our objective was to create a high-fidelity Navier-Stokes computer simulation of the flow through the turbines of a modern high-bypass-ratio turbofan engine. The simulation would have to capture the aerodynamic interactions between closely coupled high- and low-pressure turbines.

A computer simulation of the flow in the GE90 turbofan engine's high-pressure (HP) and low-pressure (LP) turbines was created at GE Aircraft Engines under contract with the NASA Glenn Research Center. The three-dimensional steady-state computer simulation was performed using Glenn's average-passage approach named APNASA. The areas upstream and downstream of each blade row mutually interact with each other during engine operation. The embedded blade row operating conditions are modeled since the average passage equations in APNASA actively include the effects of the adjacent blade rows. The turbine airfoils, platforms, and casing are actively cooled by compressor bleed air. Hot gas leaks around the tips of rotors through labyrinth seals. The flow exiting the high work HP turbines is partially transonic and, therefore, has a strong shock system in the transition region.

The simulation was done using 121 processors of a Silicon Graphics Origin 2000 (NAS 02K) cluster at the NASA Ames Research Center, with a parallel efficiency of 87 percent in 15 hr. The typical average-passage analysis mesh

size per blade row was 280 by 45 by 55, or ~700,000 grid points. The total number of blade rows was 18 for a combined HP and LP turbine system including the struts in the transition duct and exit guide vane, which contain 12.6 million grid points. Design cycle turnaround time requirements ran typically from 24 to 48 hr of wall clock time. The number of iterations for convergence was 10,000 at 8.0×10^{-5} sec/iteration/grid point (NAS 02K). Parallel processing by up to 40 processors is required to meet the design cycle time constraints.

This is the first-ever flow simulation of an HP and LP turbine. In addition, it includes the struts in the transition duct and exit guide vanes.



Modern high-bypass-ratio turbofan engine with closely coupled high- and low-pressure turbines.

The flow simulation of the closely coupled HP and LP turbines resulted in efficiency predictions that fall within 0.8 and 0.5 percent of data taken on component test rigs, and shock interaction loss was predicted within 0.5 percent. Analysis of the simulation has identified excessive turbine aerodynamic interaction losses that can be reduced by 50 percent. The reduction in turbine interaction losses will result in a \$3 million/year savings in fuel costs for a fleet of aircraft. The high parallel efficiency and accurate simulation now make APNASA practical to use in the design environment. This work is a major element of the Numerical Propulsion System Simulation (NPSS), and it supports the High Performance Computing and Communication Program Grand Challenge milestone: "Demonstrate Impact of Improved Engine Simulation Capability."

More information about the GE90 turbofan engine:
<http://hpcc.grc.nasa.gov/fy/99/ge90/>

Glenn contact:
Joseph P. Veres, 216-433-2436,
Joseph.P.Veres@grc.nasa.gov

Author: Joseph P. Veres

Headquarters program office: OAT

Programs/Projects: HPCCP, CAS



Research and Technology

Materials

Software Package Completed for Alloy Design at the Atomic Level

As a result of a multidisciplinary effort involving solid-state physics, quantum mechanics, and materials and surface science, the first version of a software package dedicated to the atomistic analysis of multicomponent systems was recently completed. Based on the BFS (Bozzolo, Ferrante, and Smith) method for the calculation of alloy and surface energetics, this package includes modules devoted to the analysis of many essential features that characterize any given alloy or surface system, including (1) surface structure analysis, (2) surface segregation, (3) surface alloying, (4) bulk crystalline material properties and atomic defect structures, and (5) thermal processes that allow us to perform phase diagram calculations. All the modules of this Alloy Design Workbench 1.0 (ADW 1.0) are designed to run in PC and workstation environments, and their operation and performance are substantially linked to the needs of the user and the specific application.

In response to the diverse needs of the scientific community, this tool, with the BFS method at its core, provides a simple and straightforward approach for gaining understanding of the properties of materials by increasing knowledge of the system behavior at the atomic level. In what constitutes a substantial improvement over alternative quantum approximate methods with comparable computational simplicity, the BFS method for alloys is free from most of the constraints on other techniques, such as limitations in the number and type of atomic species that can be accommodated or an inability to deal with arbitrary crystal structures. This results in a general, transferable, and accurate tool for examining the characteristics of multicomponent systems.

In the last few years, the BFS method for alloys, developed at the NASA Glenn Research Center, has been tested and applied to a large number of fundamental problems with consistent success (refs. 1 to 3). Because of the strong foundation of its general formulation, the simplicity of its implementation, and its computational economy, the method has proven to be a powerful and useful tool to aid in the process of alloy design and analysis. Although there are no limitations on the number of elements involved in the calculations, the crystal structure, or the input compositions, the current version of ADW is parameterized and can perform calculations with 15 elements in body-centered cubic form, 12 in face-centered cubic form, and 2 in the diamond structure. This data base is being updated constantly.

ADW 1.0 is available at Glenn for internal use by the Computational Materials Group. We envision that interaction with potential collaborators will help us to expand the scope and capability of this tool. Eventually, such collaborations and interactions with individuals and institutions will be instrumental in leading to a generally available software package.

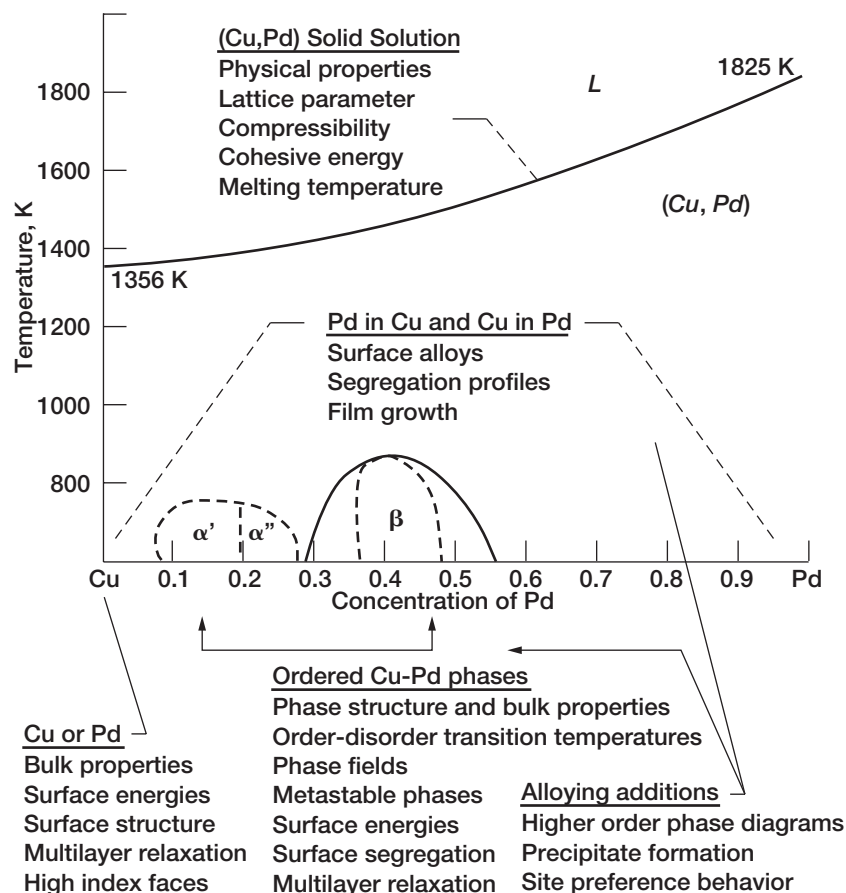
The BFS method is extremely economical in the input needed, which is completely provided by first-principles calculations (linearized augmented

plane wave method) without reference to any experimental data. Moreover, the small number of parameters needed (three for each single element, two for each element pair), together with the universal nature of these parameters (i.e., applicable, without adjustment, to any problem dealing with these elements in a given symmetry, even in the presence of additional elements), make the BFS-based predictions surprisingly general given the limited input and the severe transferability constraints imposed on the parameters.

The package includes tools for developing large-scale atomistic simulations using Monte Carlo methods, as well as tools for performing analytical calculations based on user-defined catalogues of specific atomic configurations, which provide insight into the basic features of a given system on an atom-by-atom basis.

The figure summarizes the type of information that has been determined using ADW 1.0 on an example binary system such as Cu-Pd (ref. 3).

- (1) Analyzing the bulk and surface properties of pure elements, including surface energies, surface structure, reconstruction, and multilayer relaxation
- (2) Forming surface alloys for any level of coverage, thin film structure and growth patterns, and interdiffusion into pure crystals
- (3) Identifying the segregating species and determining the



ADW 1.0 modules available for atomistic calculations of multicomponent metallic systems, illustrated by the applications related to the different regions of the Cu-Pd phase diagram (ref. 4).

driving mechanisms for segregation, surface segregation profiles, and their dependence on temperature, concentration and alloy crystal face, and alloy surface energies and structure

- (4) Determining bulk alloy crystal structure and properties including phase fields, order-disorder transitions, and critical temperatures
- (5) Determining the energetics of point and other atomic defects
- (6) Predicting and analyzing metastable structures
- (7) Determining physical properties such as lattice parameter, compressibility, and cohesive energy as a function of composition and temperature
- (8) Determining the role and behavior of ternary and higher order alloying additions, their site preference behavior, the formation of other phases, and the partitioning of the alloying additions to these phases

In summary, the first version of ADW, a software package dedicated to the atomistic analysis of multicomponent systems, was recently completed in response to the diverse needs of the scientific and engineering community.

References

1. Bozzolo, G., et al.: Surface Segregation in Multicomponent Systems: Modeling of Surface Alloys and Alloy Surfaces. *Comput. Mater. Sci.*, vol. 15, no. 2, 1999, pp. 169–195.
2. Bozzolo, G.; Noebe, R.D.; and Honey, F.: Modeling of Ternary Element Site Substitution in NiAl. *Intermetallics*, vol. 8, no. 1, 2000, pp. 7–18.
3. Garces, J.E.; Mosca, H.O.; and Bozzolo, G.H.: Atomistic Modeling of Pd/Cu(100) Surface Alloy Formation. *Surf. Sci.*, vol. 459, no. 3, 2000, pp. 365–389.
4. Hultgren, Ralph, et al.: Selected Values of the Thermodynamic Properties of Binary Alloys. American Society for Metals, Metals Park, OH, 1973.

Additional references are available via the World Wide Web:

http://www.grc.nasa.gov/WWW/SurfSci/bfs/bfs_index.html

Ohio Aerospace Institute contact:

Dr. Guillermo H. Bozzolo,
440–962–3103 or 216–433–5824,
Guillermo.H.Bozzolo@grc.nasa.gov

Glenn contacts:

Dr. Ronald D. Noebe, 216–433–2093,
Ronald.D.Noebe@grc.nasa.gov;
Dr. Phillip B. Abel, 216–433–6063,
Phillip.B.Abel@grc.nasa.gov; and
Dr. Brian S. Good, 216–433–6296,
Brian.S.Good@grc.nasa.gov

Authors: Dr. Guillermo H. Bozzolo,
Dr. Ronald D. Noebe, Dr. Phillip B. Abel,
and Dr. Brian S. Good

Headquarters program office: OAT

Programs/Projects: HOTPC

Special Recognition: Reference 1 was named Glenn Research Center's Distinguished Paper of the Year for 1999.

Thermodynamics of Titanium-Aluminum-Oxygen Alloys Studied

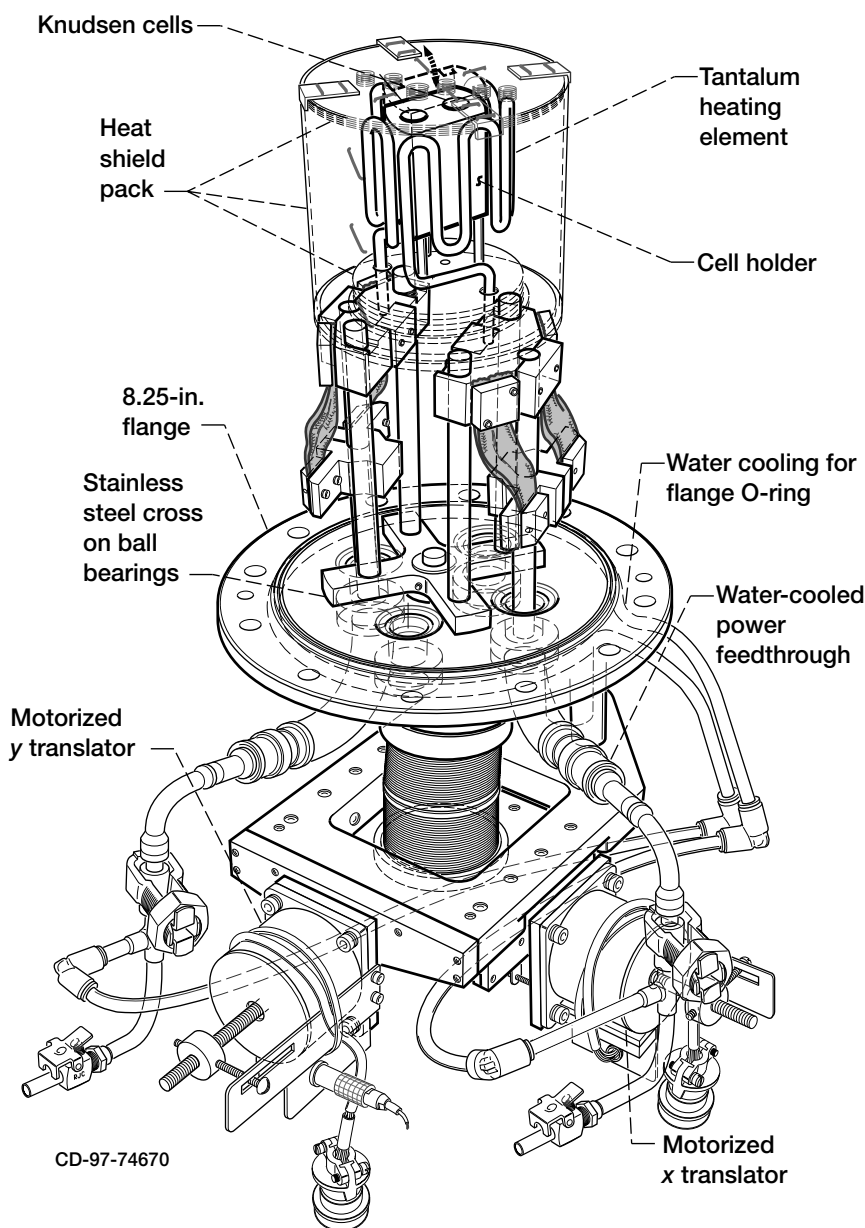
Titanium-aluminum alloys are promising intermediate-temperature alloys for possible compressor applications in gas-turbine engines. These materials are based on the α_2 -Ti₃Al + γ -TiAl phases. The major issue with these materials is high oxygen solubility in α_2 -Ti₃Al, and oxidation of unsaturated alloys generally leads to mixed nonprotective TiO₂+Al₂O₃ scales. From phase diagram studies, oxygen saturated α_2 -Ti₃Al(O) is in equilibrium with Al₂O₃ (ref. 1); however, oxygen dissolution has a detrimental effect on mechanical properties and cannot be accepted. To better understand the effect of oxygen dissolution, we examined the thermodynamics of titanium-aluminum-oxygen alloys.

A series of alloys near the α_2 -Ti₃Al phase field of varying oxygen content were prepared. The study involved (1) determining the precise phase and composition of each alloy at temperature and (2) determining the thermodynamic activities of titanium, aluminum, and oxygen for each alloy. Compositional and phase analysis was done via standard chemical analysis, x-ray diffraction, and microprobe techniques.

Thermodynamic measurements were conducted with a vapor pressure technique, using a unique double-cell system designed and fabricated at the NASA Glenn Research Center (ref. 2). This is illustrated in the figure. The Knudsen cell technique has been used for many years to give precise vapor pressures. In this technique, vapor pressures of a particular component in an alloy and those in a pure material are measured. The ratio of the two vapor pressures is the thermodynamic activity.

For accurate measurements to be obtained, a number of critical issues must be addressed. Precise measurement and uniformity of temperature in the cells is essential. Temperatures were measured with thermocouples touching the sides of the cells. Mixing of the molecular beams from each cell proved to be a major issue, so alternative materials were used, with appropriate corrections for the cross sections. Copper was used in place of aluminum; nickel was used in place of titanium.

In a mass spectrometer, vapor pressures P are related to intensity I by $P = kI/\sigma$. Here, k is the machine constant and σ is the



Double Knudsen cell flange with furnace and x-y translation.

ionization cross section. Initially, a second law heat was measured with the copper or nickel standard. Agreement with the tabulated values indicated that the temperature calibrations and ion intensity measurement system were functioning properly. From each standard data point, the quantity k/σ_{Cu} or k/σ_{Ni} was determined. The cross-section ratios $\sigma_{\text{Cu}}/\sigma_{\text{Al}}$ and $\sigma_{\text{Ni}}/\sigma_{\text{Ti}}$ were obtained from previous measurements of pure copper/pure aluminum and pure nickel/pure titanium. The standard provided a check of the system and an in situ value of k/σ_{Al} and k/σ_{Ti} that could then be used to calculate the vapor pressure of Al or Ti over the alloy.

Oxygen activities were measured from the $\text{Al}_2\text{O}(\text{g}) = \frac{1}{2} \text{O}_2(\text{g}) + \text{Al}(\text{in alloy})$ equilibria (ref. 3). The equilibrium constant for this reaction is well known (ref. 3). The values for $P(\text{Al}_2\text{O})$ and the activity of Al are measured and, hence, $P(\text{O}_2)$ could be determined. Oxygen partial pressures in the range of 10^{-30} can be reliably measured.

Initial measurements have been completed in the $\beta\text{-Ti} + \alpha_2\text{-Ti}_3\text{Al}$ and $\alpha_2\text{-Ti}_3\text{Al} + \gamma\text{-TiAl}$ two-phase fields. In the $\beta\text{-Ti} + \alpha_2\text{-Ti}_3\text{Al}$ two-phase field, oxygen decreases the titanium activity and increases the aluminum activity. In the $\alpha_2\text{-Ti}_3\text{Al} + \gamma\text{-TiAl}$ two-phase field, the activities of Al and Ti appear less dependent on oxygen. Further work is underway on additional alloys in this system.

References

1. Li, X.L., et al.: Reactions and Phase-Relations in the Ti-Al-O System. *Acta Metall. Mater.*, vol. 40, no. 11, 1992, pp. 3149–3157.
2. Jacobson, N.S.; Brady, M.P.; Mehrotra, G.M.: Thermodynamics of Selected Ti-Al and Ti-Al-Cr Alloys. *Oxid. Met.*, vol. 52, nos. 5–6, 1999, pp. 537–556.
3. Chase, Malcolm W., Jr.: NIST-JANAF Thermochemical Tables. Fourth ed., American Chemical Society, Washington, DC, 1998.

Glenn contacts:

Dr. Evan H. Copland, 216–433–3738, Evan.H.Copland@grc.nasa.gov; and Dr. Nathan S. Jacobson, 216–433–5498, Nathan.S.Jacobson@grc.nasa.gov

Authors: Dr. Evan H. Copland and Dr. Nathan S. Jacobson

Headquarters program office: OAT

Programs/Projects: DDF

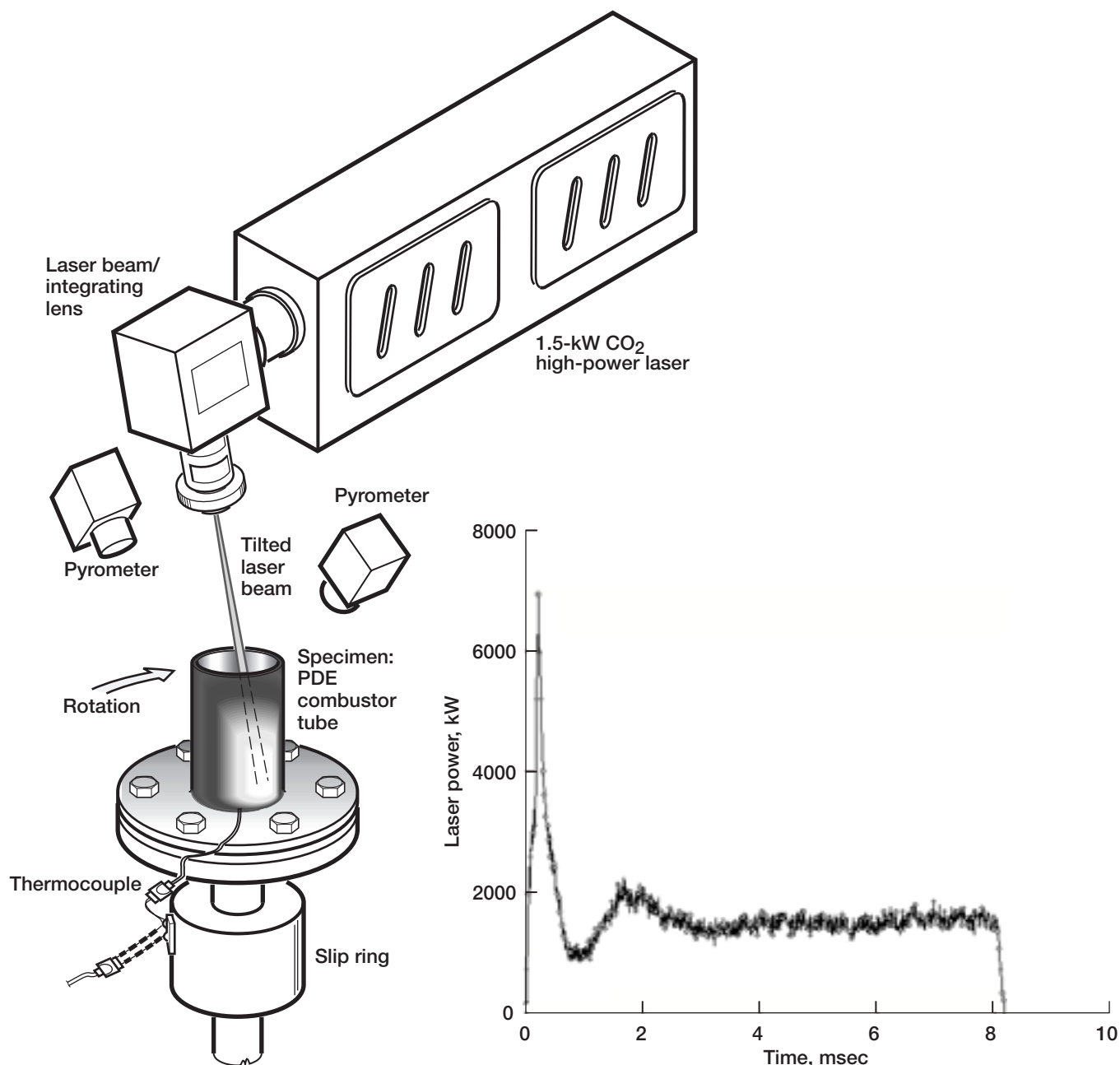
Laser High-Cycle Thermal Fatigue of Pulse Detonation Engine Combustor Materials Tested

Pulse detonation engines (PDE's) have received increasing attention for future aerospace propulsion applications. Because the PDE is designed for a high-frequency, intermittent-detonation combustion process, extremely high gas temperatures and pressures can be realized under the nearly constant-volume combustion environment. The PDE's can potentially achieve higher thermodynamic cycle efficiency and thrust density in comparison to traditional constant-pressure combustion gas turbine engines (ref. 1). However, the development of these engines requires robust design of the engine components that must endure harsh detonation environments. In particular, the detonation combustor chamber, which is designed to sustain and confine the detonation combustion process, will experience high pressure and temperature pulses with very short durations (refs. 2 and 3). Therefore, it is of great importance to evaluate PDE combustor materials and components under simulated engine temperatures and stress conditions in the laboratory.

In this study, a high-cycle thermal fatigue test rig was established at the NASA Glenn Research Center using a 1.5-kW CO_2 laser. The high-power laser, operating in the pulsed mode, can be controlled at various pulse energy levels and waveform distributions. The enhanced laser pulses can be used to mimic the time-dependent temperature and pressure waves encountered in a pulsed detonation engine. Under the enhanced laser

pulse condition, a maximum 7.5-kW peak power with a duration of approximately 0.1 to 0.2 msec (a spike) can be achieved, followed by a plateau region that has about one-fifth of the maximum power level with several milliseconds duration. The laser thermal fatigue rig has also been developed to adopt flat and rotating tubular specimen configurations for the simulated engine tests. More sophisticated laser optic systems can be used to simulate the spatial distributions of the temperature and shock waves in the engine.

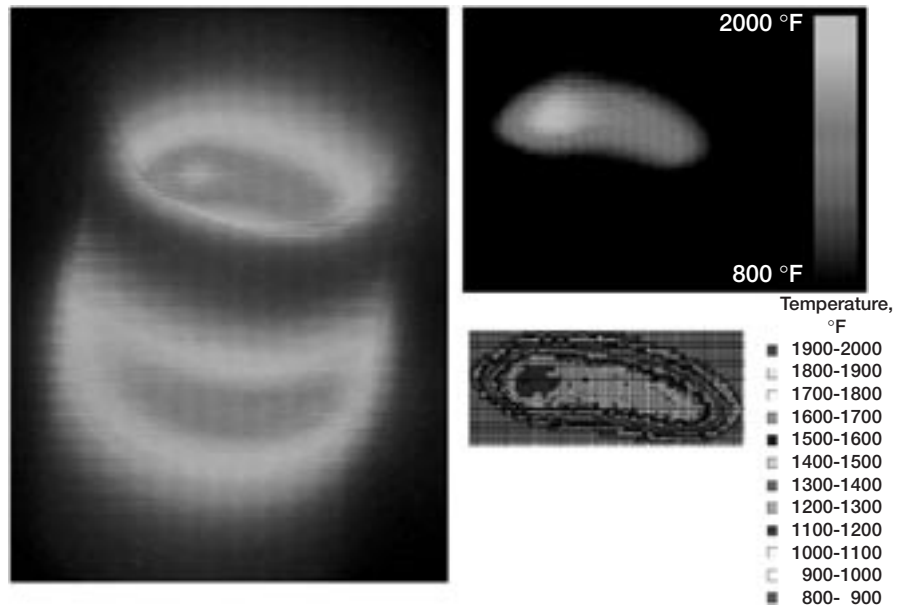
Pulse laser high-cycle thermal fatigue behavior has been investigated on a flat Haynes 188 alloy specimen, under the test condi-



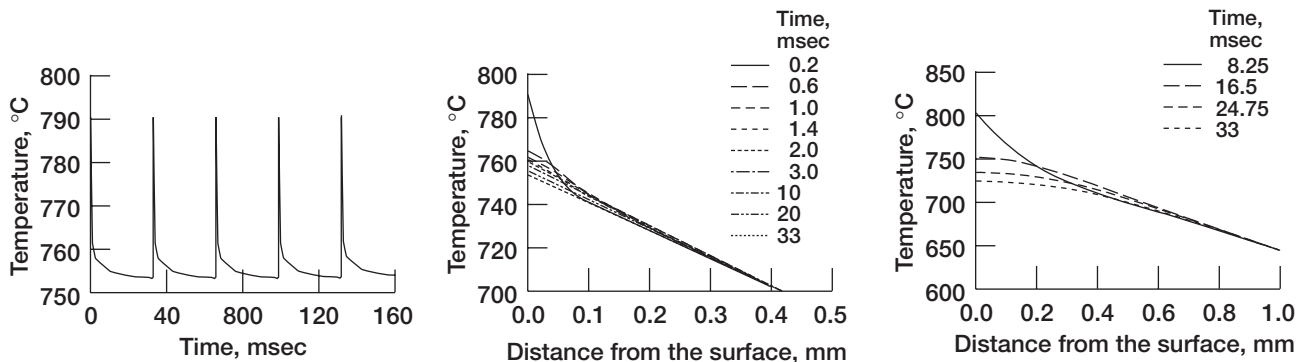
High-power CO₂ laser rig developed for testing PDE combustor materials and components under simulated engine temperature and stress conditions. The insert shown is a measured laser pulse waveform from the pulse signal of a 1.5-kW CO₂ laser using an oscilloscope. The laser pulse width is 8 msec, and a maximum laser power 7.5-kW can be achieved over about 0.2-msec duration at the pulse enhancement mode.

tion of 30-Hz cycle frequency (33-msec pulse period and 10-msec pulse width including a 0.2-msec pulse spike; ref. 4). Temperature distributions were calculated with one-dimensional finite difference models. The calculations show that the 0.2-msec pulse spike can cause an additional 40 °C temperature fluctuation with an interaction depth of 0.08 mm near the specimen surface region. This temperature swing will be superimposed onto the temperature swing of 80 °C that is induced by the 10-msec laser pulse near the 0.53-mm-deep surface interaction region.

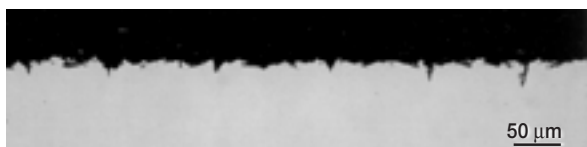
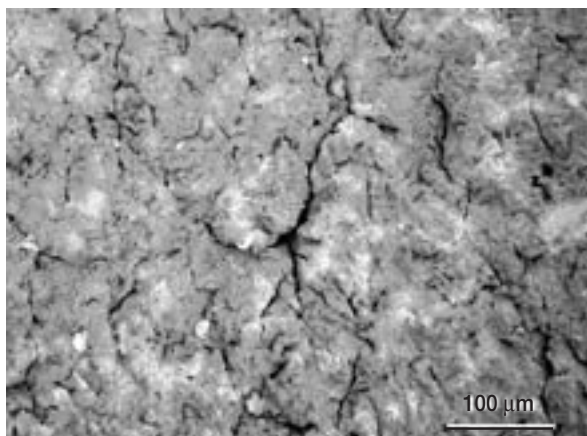
Specimen failure modes were also studied after the laser thermal fatigue testing. Extensive surface cracking with crack depths of approximately 30 μ m was observed on the flat and tubular specimens tested under enhanced laser pulses and thermal cycling.



A tubular Inconel 601 superalloy specimen is being tested in the pulsed-laser high-cycle thermal fatigue rig (100-Hz laser pulse frequency; 10-msec pulse period, 5-msec pulse width including a 0.2-msec pulse spike). Enhanced laser pulses and a rotating tubular configuration are used to mimic the time-dependent temperature and pressure waves in a pulsed detonation engine. Top: Laser testing of the rotating tubular specimen. Right: Temperature distributions of the specimen determined from infrared thermography during the laser testing. Maximum surface temperature, 1950 °F; maximum back temperature, 1550 °F. This figure appears in color in the online version of this article (<http://www.grc.nasa.gov/WWW/RT2000/5100/5100C-zhu.html>).



One-dimensional finite difference modeling results showing the temperature swings on a Haynes 188 specimen under the enhanced pulse condition (33-msec pulse period, 10-msec pulse width including 0.2-msec pulse spike). Left: Temperature pulses induced by the high-energy laser pulse spike. Center: Temperature swings due to the enhanced, 0.2-msec laser pulse spike. Right: Temperature fluctuations due to the regular 10-msec laser pulse.



Surface cracking patterns of the Haynes 188 superalloy after the enhanced laser pulses and thermal cycling (10.8 million 30-hr high-cycle fatigue cycles, and 200 30-min heating-cooling cycles). Striations on the alloy and crack surfaces may reveal high-cycle fatigue mechanisms under the intense laser pulse cyclic loads. Top: Surface cracking morphologies of the tested specimen. Bottom: Cross section of tested specimen showing surface cracking penetration into the alloy.

The laser-induced severe high-frequency thermal cycles are detrimental to the potential PDE combustor superalloy materials. Preliminary results suggest that surface oxidation, alloy inclusions, grain boundaries, and surface roughness have accelerated crack initiation and propagation under intense laser-pulse cyclic loads.

References

1. Eidelman, S.; Grossmann, W.; and Lottati, I.: Review of Propulsion Applications and Numerical Simulations of the Pulsed Detonation Engine Concept. *J. Propul.*, vol. 7, no. 6, 1991, pp. 857–865.
2. Bussing, T.; and Pappas, G.: An Introduction to Pulse Detonation Engines. AIAA Paper 94–0263, 1994.
3. Bussing, T.R.A.; Hinkey, J.B.; and Kaye, L.: Pulse Detonation Engine Preliminary Design Considerations. AIAA Paper 94–3220, 1994.
4. Zhu, D.; Fox, D.S.; and Miller, R.A.: Pulsed Laser Fatigue Behavior of Pulsed Detonation Engine Combustor Materials. To be published as a NASA TM, 2001. <http://gltrs.grc.nasa.gov/GLTRS>

Glenn contacts:

Dr. Dongming Zhu, 216–433–5422, Dongming.Zhu@grc.nasa.gov;
Dr. Dennis S. Fox, 216–433–3295, Dennis.S.Fox@grc.nasa.gov;
and Dr. Robert A. Miller, 216–433–3298,
Robert.A.Miller@grc.nasa.gov

Authors:

Dr. Dongming Zhu, Dr. Dennis S. Fox, and Dr. Robert A. Miller

Headquarters program office: OAT

Programs/Projects:

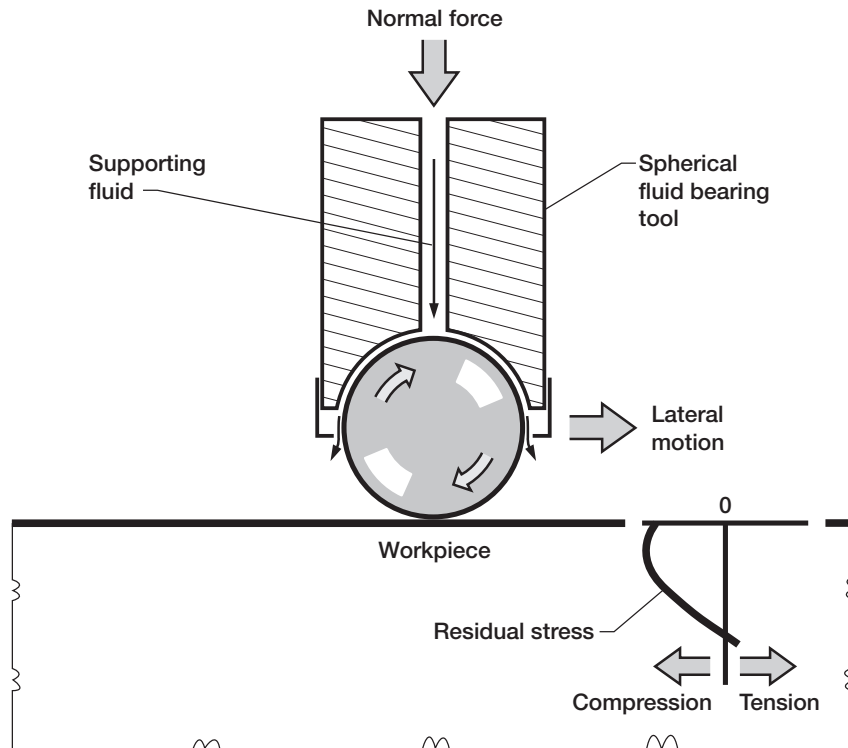
Propulsion Systems Base R&T, Pulse Detonation Technology

Improved Method Being Developed for Surface Enhancement of Metallic Materials

Surface enhancement methods induce a layer of beneficial residual compressive stress to improve the impact (FOD) resistance and fatigue life of metallic materials. A traditional method of surface enhancement often used is shot peening, in which small steel spheres are repeatedly impinged on metallic surfaces. Shot peening is inexpensive and widely used, but the plastic deformation of 20 to 40 percent imparted by the impacts can be harmful. This plastic deformation can damage the microstructure, severely limiting the ductility and durability of the material near the surface. It has also been shown to promote accelerated relaxation of the beneficial compressive residual stresses at elevated temperatures. Low-plasticity burnishing (LPB) is being developed as an improved method for the surface enhancement of metallic materials.

LPB is being investigated as a rapid, inexpensive surface enhancement method under NASA Small Business Innovation Research contracts NAS3–98034 and NAS3–99116, with supporting characterization work at NASA.

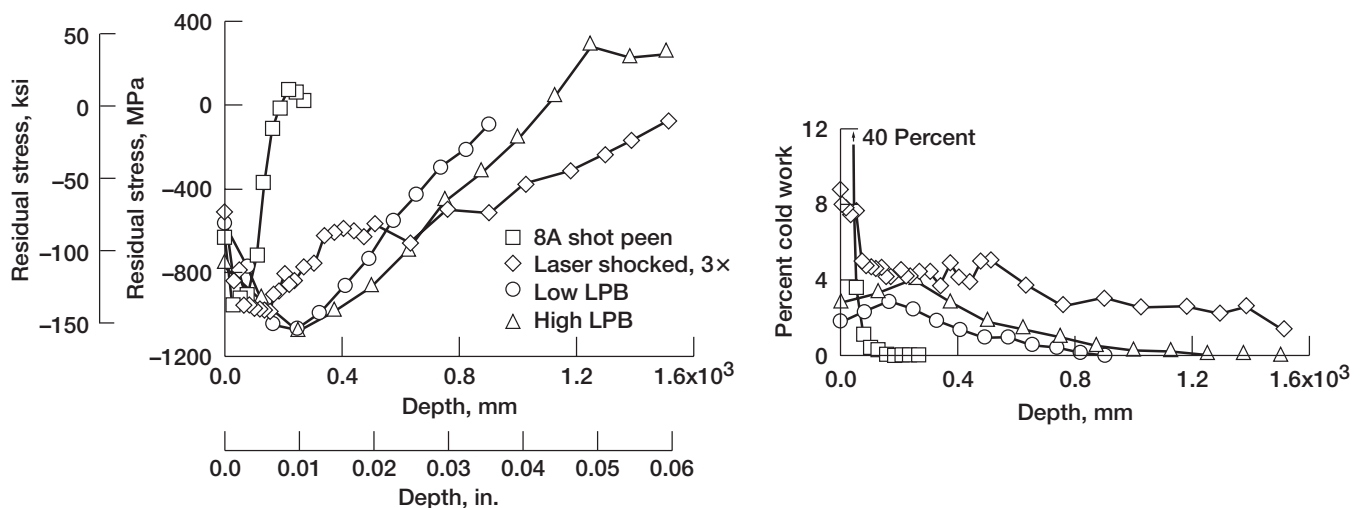
Previously, roller burnishing had been employed to refine surface finish. This concept was adopted and then optimized as a means of producing a layer of compressive stress of high magnitude and depth, with minimal plastic deformation (ref. 1). A simplified diagram of the developed process is given in the following figure. A single pass of a smooth, free-rolling spherical ball under a normal force deforms the surface of the material in tension, creating a compressive layer of residual stress. The ball is supported in a fluid with sufficient



Low-plasticity burnishing apparatus.

pressure to lift the ball off the surface of the retaining spherical socket. The ball is only in mechanical contact with the surface of the material being burnished and is free to roll on the surface. This apparatus is designed to be mounted in the conventional lathes and vertical mills currently used to machine parts. The process has been successfully applied to nickel-base superalloys by a team from the NASA Glenn Research Center, Lambda Research, and METCUT Research, as supported by the NASA Small Business Innovation Research Phase I and II programs, the Ultra Safe program, and the Ultra-Efficient Engine Technology (UEET) Program.

A comparison of the residual stresses and plasticity produced by shot peening and LPB on the nickel-base alloy IN718 is shown in the following figure. The residual stress and plasticity profiles were measured using x-ray diffraction peak shift and broadening after repeatedly electropolishing a material layer. LPB clearly can produce deeper compressive residual stresses with much less plasticity (percent cold work) than shot peening. The high-cycle fatigue resistance of this alloy increases with the application of this LPB treatment. Shot peen and LPB-treated high-cycle fatigue specimens were exposed at 600 °C for 10 hr and then tested at room temperature. LPB-treated specimens had 2 to 5 times longer lives, even when given surface scratches normal to the load axis to simulate foreign object damage. The shot-peened specimens failed at the scratches with reduced fatigue lives. Crack-growth specimens were notched, precracked, and LPB treated. The notch was then machined away before crack growth testing at room temperature. The LPB treatment was highly effective, completely arresting crack growth into the material. This LPB



Comparison of the residual stresses and percent cold work produced by shot peening, laser shock treatment, and low-plasticity burnishing (LPB) in IN718 (ref. 1). Top: Perpendicular residual stress distribution. Bottom: Percent cold work distribution.

process has been successfully applied to several nickel, titanium, and aluminum alloys (ref. 2) used in aerospace gas turbine engine and airframe applications. LPB has recently been shown surprisingly effective for treating corroded airframe materials after extended service, restoring fatigue lives to the unaged levels. LPB processing is now being extended to other alloys and applications.

References

1. Prevey, Paul S., et al.: FOD Resistance and Fatigue Crack Arrest in Low Plasticity Burnished IN718. Proceedings of the 5th National Turbine Engine High Cycle Fatigue Conference, Chandler, AZ, 2000.
2. Prevey, Paul S.; and Cammett, J.: Low Cost Corrosion Damage Mitigation and Improved Fatigue Performance of Low Plasticity Burnished 7075-T6. Proceedings of the 4th International Aircraft Corrosion Workshop, Solomons, MD, 2000.

Glenn contact:

Timothy P. Gabb, 216-433-3272,
Timothy.P.Gabb@grc.nasa.gov

Authors: Timothy P. Gabb,
 Jack Telesman, and Peter T. Kantzos

Headquarters program office: OAT

Programs/Projects:

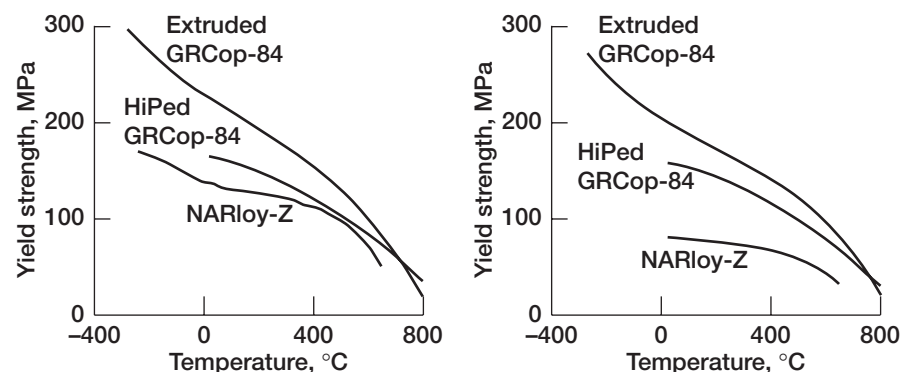
SBIR, Ultra Safe, UEET

GRCoP-84 Developed for Rocket Engines

GRCoP-84 (Cu-8 at.% Cr-4 at.% Nb) was developed at the NASA Glenn Research Center for use in regeneratively cooled rocket engines. This alloy possesses an excellent combination of conductivity, thermal expansion, strength, creep resistance, ductility, and low-cycle fatigue (LCF) life. In comparison to the currently used alloy, NARloy-Z (Cu-3 wt % Ag-0.5 wt % Zr), GRCoP-84's significantly better properties (refs. 1 and 2) give it the potential for significant gains in engine performance and reliability.

For GRCoP-84 to be safely used in a rocket engine, it is critical to develop a detailed data base of the important thermophysical and mechanical properties. Work has focused on five major properties: thermal conductivity, thermal expansion, tensile strength, creep resistance, and LCF life. The analysis went beyond simply measuring the data and reporting averages. A detailed statistical analysis was conducted that allowed regression of the data over the entire temperature range tested and establishment of design minimums. The design values were expressed as simple mathematical formulas that are highly amenable to use in computer codes such as in finite element analysis and related computer modeling work.

During 2000, work was completed for all five properties. The thermal expansion of GRCoP-84 was found to be at least 7 percent lower than for NARloy-Z. Lowering the thermal expansion lowers thermal stresses and increases liner life. The thermal conductivity of GRCoP-84, which is 70 to 83 percent the conductivity of copper, is slightly lower than that of NARloy-Z but is much higher than for most alloys with similar strengths. The yield strength of GRCoP-84 is approximately twice that of NARloy-Z over the temperature range tested. It also retains more of its strength following simulated brazing than NARloy-Z does, as can be seen in the following figure. The higher temperatures experienced during hot isostatic pressing (HIPing) somewhat degrade the properties, but HIPed GRCoP-84 still retains significant advantages over NARloy-Z. The modulus of GRCoP-84 is lower than that of pure copper. Lowering the modulus lowers the thermal stresses and again increases life.



Yield strength of extruded GRCoP-84. Left: As-produced. Right: Following a simulated braze cycle at 935 °C (1715 °F).



Hot fire testing of a GRCop-84 spool piece.

Creep and LCF lives are much greater than for NARloy-Z. Subjecting the material to a simulated braze cycle at 935 °C (1715 °F) did not adversely affect the LCF lives.

The ultimate test is to actually make a liner and test it in a rocket engine. Working with NASA Marshall Space Flight Center, two 15.2-cm- (6-in.-) long liners with inner diameters of approximately 5.1 cm (2 in.) were fabricated at the NASA Marshall Space Flight Center using vacuum plasma spraying (ref. 3) and tested at Glenn. Twenty-seven tests accumulating 482 sec of hot fire testing using fuel ratios up to 7:1 were conducted. The liners showed no signs of degradation following testing.

In addition to being able to be extruded, HIPed, and vacuum plasma sprayed, GRCop-84 has been shown to be highly workable at low to moderate temperatures (250 to 350 °C). Sheet product approximately 22.9 by 50.8 cm (9 by 20 in.) has been rolled to a thickness of 0.1 cm (0.040 in.).

Find out more at our Web sites:

<http://www.grc.nasa.gov/WWW/MDWeb/People/MSELLIS.html>

<http://www.grc.nasa.gov/WWW/MDWeb/People/MSYUN.html>

References

1. Ellis, David L.; and Michal, Gary M.: Mechanical and Thermal Properties of Two Cu-Cr-Nb Alloys and NARloy-Z. NASA CR-198529, 1996. <http://gltrs.grc.nasa.gov/GLTRS>
2. Ellis, David L.; and Keller, Dennis J.: Thermophysical Properties of GRCop-84. NASA CR-2000-210055, 2000. <http://gltrs.grc.nasa.gov/GLTRS>
3. Holmes, Richard; Ellis, David; and McKechnie, T.: Robust Low Cost Aerospike/RLV Combustion Chamber by Advanced Vacuum Plasma Process. Proceedings of the 36th Annual Space Conference, Cape Canaveral, FL, 1999.

Case Western Reserve University contact:

Dr. David L. Ellis, 216-433-8736,
David.L.Ellis@grc.nasa.gov

Glenn contact:

Dr. Michael V. Nathal, 216-433-9516,
Michael.V.Nathal@grc.nasa.gov

Authors: Dr. David L. Ellis, Hee Man Yun, Dr. Bradley A. Lerch, Dennis A. Keller, and Richard Holmes

Headquarters program office: OAT

Programs/Projects: RLV Focused Program (NRA 8-21 Task 7.3)

High-Flow PMR-Polyimide Composites Developed With Mechanical Properties Comparable to Other High-Temperature Systems

PMR polyimides, in particular PMR-15, are well known for their excellent high-temperature stability and performance, and solvent resistance. However, the processing of these materials is limited, for the most part, to prepreg-based methods, such as compression or autoclave processing. These methods involve substantial amounts of hand labor, and as a result, manufacturing costs for components made from PMR polyimides can be high. In cost-sensitive applications, these high manufacturing costs can make the use of PMR polyimide-based components cost prohibitive.

Lower cost manufacturing methods, such as resin transfer molding (RTM) and resin film infusion, have been demonstrated to reduce manufacturing costs by as much as 50 percent over prepreg-based methods. However, these processes are only amenable to materials with melt viscosities below 30 poise. Most PMR polyimides have melt viscosities on the order of 100 poise or higher. Recent efforts at the NASA Glenn Research Center have focused on chemical modifications to PMR polyimides to reduce their melt viscosity to the point where they could be processed by these low-cost manufacturing methods without adversely affecting their high-temperature properties and performance.

These efforts have led to a new family of PMR polyimides that have melt viscosities significantly lower than that of PMR-15. Reductions in melt viscosity are brought about through the introduction of molecular twists in the polymer backbone. Carbon fiber (T650-35) composites were prepared from one of these polyimides, designated PMR-Flex, by compression molding. The properties of these composites are presented below and compared with comparable composites made from PMR-15 and PETI-RTM, a new low-melt-viscosity polyimide.

PMR-Flex had the lowest minimum melt viscosity of the three resins reported in the table. Room-temperature properties (flexural strength and modulus, and short beam shear) of the PMR-Flex composites were comparable to those of the PMR-15 composites and slightly higher than those of the PETI-RTM-based system (possibly due to the lower number of plies in the later). Also, results of PMR-Flex composite testing at 232 °C were compared with comparable properties of PMR-15 laminates at 288 °C. The lower test temperatures for the PMR-Flex laminates were chosen because of the lower glass-transition temperature of those laminates relative to that of the PMR-15 composites. Flexural and short beam shear strengths of PMR-Flex laminates were slightly lower than those of the PMR-15 composites. Efforts are underway to further modify this chemistry to increase the glass-transition temperature and elevated-temperature properties of these materials.

COMPARISON OF VARIOUS PROPERTIES OF PMR-FLEX COMPOSITES WITH THOSE OF PMR-15 AND PETI-RTM-BASED COMPOSITES

	PMR-Flex ^a	PMR-15 ^a	PETI-RTM ^b
Glass transition temperature, °C	260	339	246
Flexural strength at room temperature, Mpa	1166±34	1001±68	889±59
Flexural modulus at room temperature, Gpa	75.6±1.2	70.1±1.0	43.3±2.4
Short beam shear at room temperature, Mpa	70.8±2.1	66.2±1.5	61.0±3.9
Flexural strength at elevated temperature, ^d MPa	555±56	704±18	---
Flexural modulus at elevated temperature, ^d GPa	70.9±1.4	70.9±1.2	---
Short beam shear at elevated temperature, ^d MPa	36.8±2.5	40.5±1.8	---
Minimum melt viscosity, P	34	~2500	600

^aLaminates were eight plies reinforced with 8-HS, T650-35 carbon fabric.

^bLaminates were four plies reinforced with 5-HS, IM-7 carbon fabric (data from ref. 1).

^cMeasured by DMA.

^dPMR-Flex tested at 232 °C; PMR-15 tested at 288 °C.

Find out more about the work of Glenn's Polymer Branch:

<http://www.grc.nasa.gov/WWW/MDWeb/5150/Polymers.html>

Reference

Criss, J.M., et al.: SAMPE J., vol. 36, 2000, p. 32.

Glenn contact:

Dr. Michael A. Meador, 216-433-9518, Michael.A.Meador@grc.nasa.gov

Author: Dr. Michael A. Meador

Headquarters program office: OAT

Programs/Projects: RLV Focused

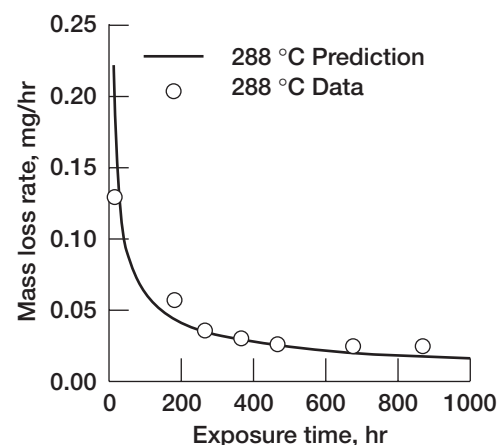
Long-Term Durability of a Matrix for High-Temperature Composites Predicted

Polymer matrix composites (PMC's) are being increasingly used in applications where they are exposed for long durations to harsh environments such as elevated temperatures, moisture, oils and solvents, and thermal cycling. The exposure to these environments leads to the degradation of structures made from these materials. This also affects the useful lifetimes of these structures. Some of the more prominent aerospace applications of polymer matrix composites include engine supports and cowlings, reusable launch vehicle parts, radomes, thrust-vectoring flaps, and the thermal insulation of rocket motors. This demand has led to efforts to develop lightweight, high-strength, high-modulus materials that have upper-use temperatures over 316 °C.

A cooperative program involving two grants to the Massachusetts Institute of Technology and in-house work at the NASA Glenn Research Center was conducted to identify the mechanisms and the measurement of mechanical and physical properties that are necessary to formulate a mechanism-based model for predicting the lifetime of high-temperature polymer matrix composites. The polymer that was studied was PMR-15 polyimide, a leading matrix resin for use in high-temperature-resistant aerospace composite structures such as propulsion systems. The temperature range that was studied was from 125 to 316 °C.

The diffusion behavior of PMR-15 neat resin was characterized and modeled. Thermogravimetric analysis (TGA) was also conducted in nitrogen, oxygen, and air to provide quantitative information on thermal and oxidative degradation reactions. A new low-cost technique was developed to collect chemical degradation data for isothermal tests lasting up to 4000 hr in duration. In the temperature range studied, results indicate complex behavior that was not observed by previous TGA tests, including the presence of weight-gain reactions. These were found to be significant in the initial periods of aging from 125 to 225 °C. Two types of weight loss reactions dominated at aging temperatures above 225 °C. One was concentrated at the surface of the polymer and was very active at temperatures above 225 °C. The second was observed to dominate in the latter stages of aging at temperatures below 260 °C. This three-reaction model satisfactorily explains past findings that the degradation mechanism of PMR-15 appears to change around 316 °C. It also indicates that the second weight gain mechanism is a significant factor at temperatures below 204 °C. On the basis of these results, a predictive model was developed for the thermal degradation of PMR-15 at 316 °C. A comparison of data generated by this model with actual experimental data is shown in the figure to the top right.

Tests were also conducted at Glenn to further elucidate the theory of a three-mechanism degradation model. PMR-15 specimens were aged in air at 204, 260, 288, and 316 °C for times as long as 4400 hr. Specimens of four different volume/surface areas were studied to evaluate



Comparison of model-generated and experimental data for the decomposition of PMR-15 at 316 °C

geometrical effects. Weight loss and dimensional changes were measured—3 length, 4 width, and 10 thickness measurements for each specimen. The surface layer thickness was measured at predetermined intervals. The study confirmed that a three-mechanism degradation model is appropriate. Also, it indicates that other mechanisms may be operating. The weight loss was shared by both the oxidizing surface and the thermally degrading central core material. The ratios were dependent on the test temperature. The surface loss diminished as the temperature was reduced, and the core loss remained about the same. Dimensional shrinkage partitioning between the surface and the bulk polymer followed the same course. The next figure presents the progression of shrinkage with aging time for different dimensions of PMR-15 neat resin specimens aged at 316 °C.

Thermo-oxidative aging produces a nonuniform degradation state in PMR-15. A surface layer, usually attributed to oxidative degradation, forms. This surface layer has different properties than the central core material. A set of material tests was designed to

separate the properties of the oxidized surface layer from the properties of the inner material. Test specimens were aged at 316 °C in either air or nitrogen for up to 800 hr. The thickness of the oxidized layer, the dimensional shrinkage, and the coefficient of thermal expansion were measured directly. The coefficient of thermal expansion data are shown in the final figure. The nitrogen-aged specimens were assumed to be representative of thermally aged PMR-15 and, therefore, have the same properties as the interior material in the air-aged specimens. Four-point bend tests were performed to measure the flexural modulus of both the surface layer and the inner material. Innovative bimetallic strip specimens were machined from thick aged specimens and tested to determine surface layer shrinkage and coefficient of thermal expansion.

Results show that the surface layer is under tension at the cure temperature and under compressive loading at room temperature. This confirms a previous report that showed that surface cracking of PMR-15 occurs while at elevated temperature and is not due to thermal cycling during specimen weighing operations. These physical properties are of valuable use in modeling the durability and lifetime of PMR-15 structural elements because they are not readily found in the literature.

The data gained from these studies present a new understanding of the degradation of all polyimide-type composite matrices. The results from this cooperative effort are of significant importance to the development of new composite materials for advanced aerospace propulsion systems.

Find out more at our Web site:

<http://www.grc.nasa.gov/WWW/MDWeb/5150/Polymers.html>

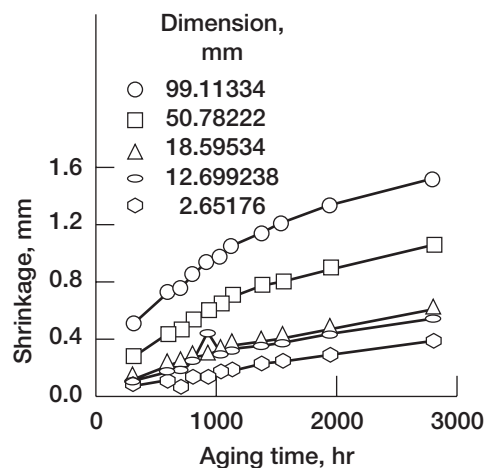
Glenn contact:

Dr. Kenneth J. Bowles, 216-433-3197,
Kenneth.J.Bowles@grc.nasa.gov

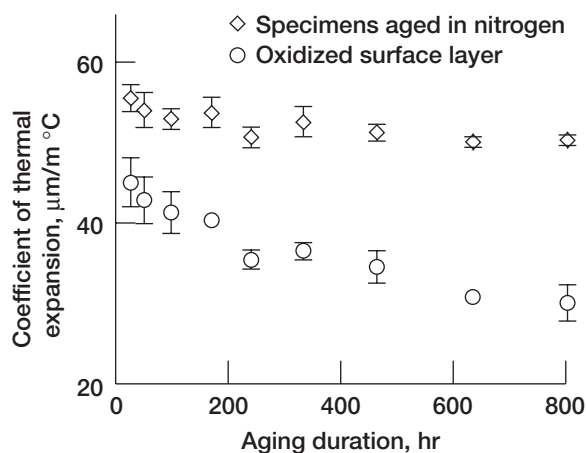
Author: Dr. Kenneth J. Bowles

Headquarters program office: OAT

Programs/Projects: UEET



Dimensional changes as a function of aging time and temperature for PMR-15 neat resin specimens during aging at 316 °C.

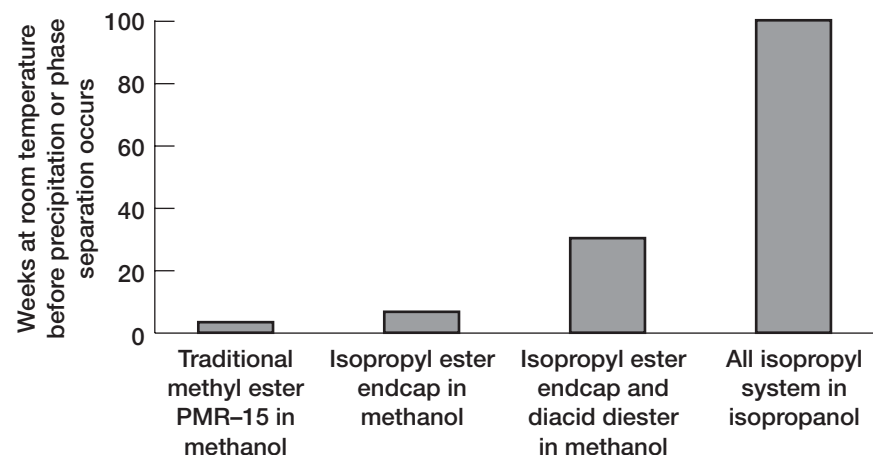


Effects of aging time on the coefficient of thermal expansion on the bulk and oxidized surface layer of PMR-15 neat resin.

PMR Extended Shelf Life Technology Given 2000 R&D 100 Award

An approach developed at the NASA Glenn Research Center for extending the shelf life of PMR polyimide solutions and prepreps received an R&D 100 Award this year. PMR polyimides, in particular PMR-15, have become attractive materials for a variety of aerospace applications because of their outstanding high-temperature stability and performance. PMR-15 can be used in components with exposures to temperatures as high as 290 °C, which leads to substantial reductions in weight, as much as 30 percent over metal components. PMR-15 composites are used widely in aerospace applications ranging from ducts and external components in aircraft engines to an engine access door for the Space Shuttle Main Engine. A major barrier to more widespread use of these materials is high component costs. Recent efforts at Glenn have addressed the various factors that contribute to these costs in an attempt to more fully utilize these lightweight, high-temperature materials.

During storage, standard PMR polyimide solutions and prepreps undergo chemical reactions that lead to the buildup of higher molecular weight species. These chemical changes affect processability and can lead to higher part rejection and scrap rates, ultimately resulting in higher component costs. The stability of PMR prepreps and solutions can be improved by refrigeration. However, this adds to shipping and storage costs, thereby increasing manufacturing costs.



Comparison of the storage lives of traditional and extended shelf-life PMR solutions. (Solution stability via time to precipitate.)

This new technology increases the storage life of PMR polyimide solutions by almost a factor of 30 over standard PMR resin chemistry (see the figure). Use of extended shelf life PMR solutions and prepreps can make processing more repeatable and can reduce manufacturing costs by reducing scrap rates and unnecessary storage and handling costs.

Find out more on the World Wide

Web: <http://www.grc.nasa.gov/WWW/MDWeb/5150/Polymers.html>

Glenn/U.S. Army Research Laboratory contact:

Dr. William B. Alston, 216-433-3220, William.B.Alston@grc.nasa.gov

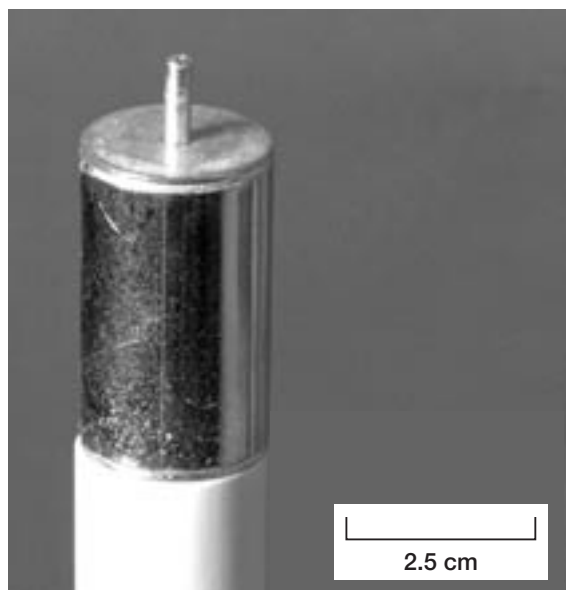
Author: Dr. Michael A. Meador

Headquarters program office: OAT

Programs/Projects: HOTPC

Special recognition: A Glenn-developed approach to extending the shelf life of PMR polyimide solutions and prepreps was a recipient of this year's R&D-100 Award.

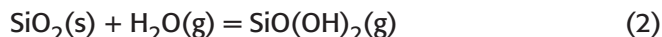
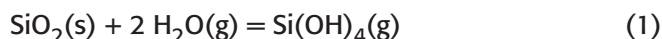
Thermodynamics of Volatile Silicon Hydroxides Studied



Pt-Rh transpiration cell.

Silicon-based ceramics are promising candidate structural materials for heat engines. The long-term stability of these materials to environmental degradation is dependent on the formation and retention of a protective SiO_2 layer. It is well known that SiO_2 forms stable volatile hydroxides in the presence of water vapor at elevated temperatures. Combustion conditions, which characteristically are at high velocities, contain significant water vapor pressures, and high temperatures tend to promote continuous formation of these hydroxides with resulting material degradation. For the degradation of silicon-based ceramics to be predicted, accurate thermodynamic data on the formation of silicon hydroxides are needed.

Three volatile silicon-hydroxide species have been proposed as being significant under combustion conditions:



Thermodynamic data on these species are limited (refs. 1 to 5). A transpiration apparatus was designed and constructed to measure thermodynamic quantities for these volatile hydroxides and add to the available data.

Volatile hydroxides are formed by flowing a carrier gas containing a controlled amount of water vapor over solid SiO_2 at temperatures above 800°C . The volatile species leave the transpiration cell, condense downstream on a cool collection tube, and are analyzed. Temperature, carrier gas flow rate, and water vapor pressure must be carefully controlled to ensure that equilibrium is obtained within the cell, to minimize diffusion

effects, and to completely collect the reaction products. The transpiration cell, which was based on a design of Hashimoto (ref. 1), was fabricated at Glenn from Pt-20%Rh (see the figure). Laser welding was used to ensure a leak-tight system. The cell can be used with both reactive and nonreactive carrier gases at temperatures up to 1773 K .

Initial studies at the NASA Glenn Research Center focused on experiments with an argon carrier gas containing high- (0.38-atm) and low- (0.15-atm) pressure water ($P(\text{H}_2\text{O})$) flowing over amorphous SiO_2 . The first series at high $P(\text{H}_2\text{O})$ was conducted at temperatures between 1073 and 1723 K and, according to reaction (1), gave $\Delta H_r = 49.8 \pm 1.8\text{ kJ/mole}$ and $\Delta S_r = -72.6 \pm 1.3\text{ J/mole}$. The second series of measurements at lower $P(\text{H}_2\text{O})$ were taken over the temperature range of 1450 to 1723 K . According to reaction (1), these results gave $\Delta H_r = 56.9 \pm 0.8\text{ kJ/mole}$ and $\Delta S_r = 66.9 \pm 0.5\text{ J/mole}$. The results show excellent agreement with recent data from Hashimoto (ref. 1) for the formation of $\text{Si}(\text{OH})_4(\text{g})$: $\Delta H_r = 56.7 \pm 1.7\text{ kJ/mole}$ and $\Delta S_r = -66.2 \pm 1.0\text{ J/mole}$ at an average temperature of 1600 K . The difference between the two data sets suggests $\text{SiO}(\text{OH})_2(\text{g})$ may be forming. Further work is underway to clarify this and obtain data for $\text{SiO}(\text{OH})_2(\text{g})$.

References

1. Hashimoto, A: The Effect of H_2O Gas on Volatilities of Planet-Forming Major Elements. 1—Experimental-Determination of Thermodynamic Properties of Ca-Hydroxide, Al-Hydroxide, and Si-Hydroxide Gas Molecules and Its Application to the Solar Nebula. *Geochim. Cosmochim.*

- Acta, vol. 56, no. 1, 1992, pp. 511–532.
2. Krikorian, O.H.: Thermodynamics of the Silica-Steam System. Symposium on Engineering With Nuclear Explosives. Vol. 1, 1970, pp. 481–492.
 3. Hildenbrand D.L.; and Lau, K.H.: Thermochemistry of Gaseous $\text{SiO}(\text{OH})$, $\text{SiO}(\text{OH})(2)$, SiO_2 . J. Chem. Phys., vol. 101, no. 7, 1994, pp. 6076–6079.
 4. Hildenbrand, D.L.; and Lau, K.H.: Thermochemistry of Gaseous $\text{SiO}(\text{OH})$, $\text{SiO}(\text{OH})(2)$, SiO_2 . J. Chem. Phys., vol. 108, no. 15, 1998, pp. 6535.
 5. Allendorf, M.D., et al.: Theoretical-Study of the Thermochemistry of Molecules in the Si-O-H System. J. Phys. Chem., vol. 99, no. 41, 1995, pp. 15285–15293.

Glenn contacts:

Dr. Evan H. Copland, 216–433–3738, Evan.H.Copland@grc.nasa.gov; and
Dr. Nathan S. Jacobson, 216–433–5498, Nathan.S.Jacobson@grc.nasa.gov

Cleveland State University contact:

Dr. Elizabeth J. Opila, 216–433–8904,
Elizabeth.J.Opila@grc.nasa.gov

Authors: Dr. Evan H. Copland,
Dr. Elizabeth J. Opila, and Dr. Nathan S.
Jacobson

Headquarters program office: OAT

Programs/Projects:

Silicon-based ceramics

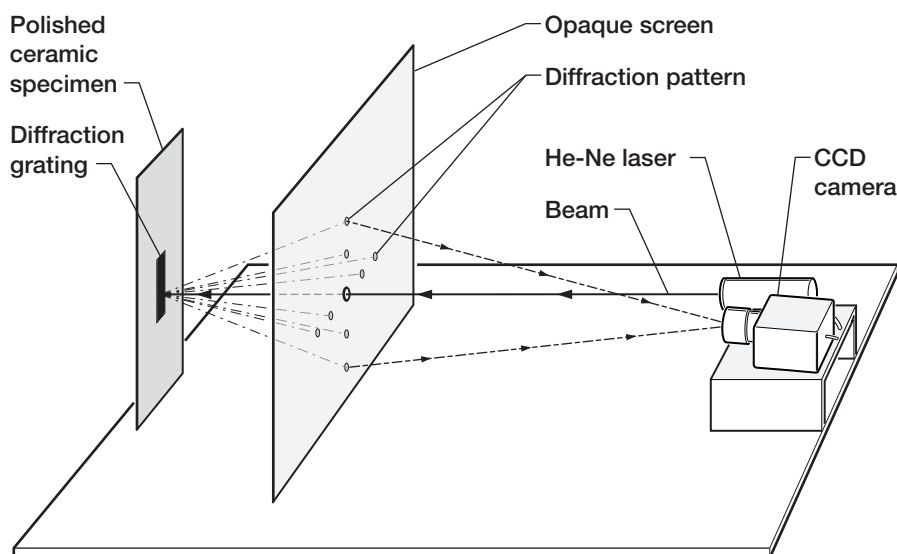
Remote, Noncontact Strain Sensing by Laser Diffraction Developed

A system was developed at the NASA Glenn Research Center for continually monitoring, in real time, the in-plane strain tensor in opaque solids during high-temperature, long-term mechanical testing. The simple, non-contacting, strain-sensing methodology should also be suitable for measurement in hostile environments. This procedure has obvious advantages over traditional, mechanical, contacting techniques, and it is easier to interpret than moiré and speckle interferometric approaches.

A two-dimensional metallic grid of micrometer dimensions is applied to a metallographically prepared gauge section on the surface of a tensile test specimen by a standard photolithographic process. The grid on the fixtured specimen is interrogated by an He-Ne laser, and the resulting diffraction pattern is projected backwards onto a translucent screen. A charge-coupled

device (CCD) camera is used to image the first-order diffraction peaks from the translucent screen. A schematic representation of the system is shown in the figure.

When the specimen is heated in a furnace, changes to the diffraction pattern can be detected. From the location of the new diffraction peaks in comparison with the initial image at the same point on the grid, all four components of the inplane deformation tensor: longitudinal, transverse and shear strain, and rigid body rotation can be calculated. In this way, bidirectional thermal expansion coefficients can be calculated. Subsequent application of the load to the specimen at a high temperature results in additional changes to the diffraction pattern. These changes are recorded and used to calculate bidirectional strain as a function of time (i.e., creep). Continuous translation of the laser to discrete spots covering the entire area of the grid on the specimen during the test period yields a real-time “map” of localized two-dimensional strain over time.



Remote, noncontact strain-sensing system.

This method was developed to measure strain in relatively small, flat test specimens under controlled conditions. Modifications to the current methodology, including miniaturization, have been considered to encompass strain sensing of complex and/or curved surfaces. Further development would be required to provide in situ strain monitoring of aerosurfaces during manufacturing and use.

Glenn contact: Marc R. Freedman, 216-433-3284 or 216-433-5544, Marc.R.Freedman@grc.nasa.gov

Author: Marc R. Freedman

Headquarters program office: OAT

Program/Projects: Propulsion and Power Systems (R&T Base), HITEMP

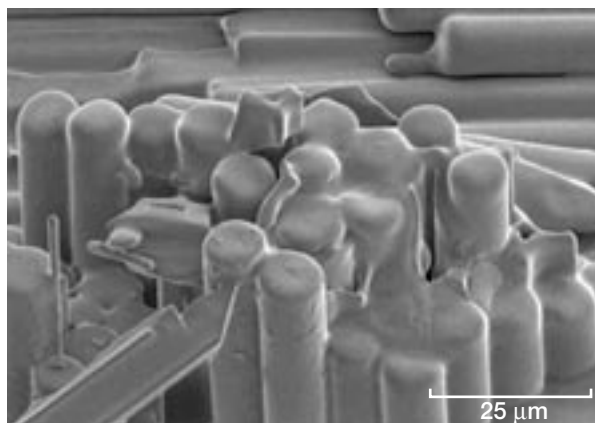
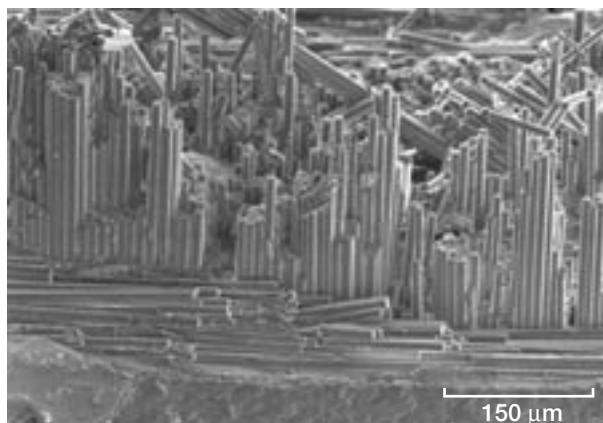
Creep/Rupture Behavior of Melt-Infiltrated SiC/SiC Composites Being Investigated

The failure behavior of melt-infiltrated SiC/SiC ceramic matrix composites is under investigation at the NASA Glenn Research Center as part of NASA's Ultra-Efficient Engine Technology Program. This material was originally developed under the High Speed Research Office's Enabling Propulsion Materials Program. Creep and rupture data provide accelerated testing information to predict material behavior under engine use situations (1500 to 2400 °F). This information gives insights into various material development paths to improve composites as well as improve understanding of failure mechanisms.

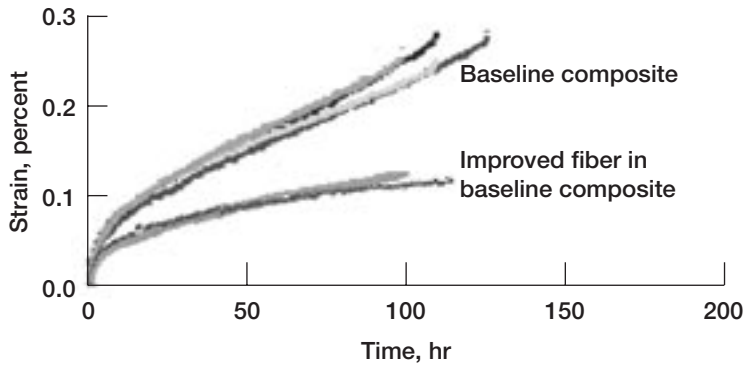
The left figure shows the fracture surface of a CMC material following over 200 hr of testing at 2400 °F. This surface demonstrates the kind of fibrous pullout desirable for maximum crack deflection, hence nonbrittle failure. Microscopy suggests that creep and rupture of these materials can best be considered as a probabilistic property, rather than a material property. Fiber failure occurs first in isolated regions, while stronger adjacent fibers remain intact. The right figure shows a region where oxide deposits blur and round the fiber images. Because the oxidation kinetics of SiC are well understood, this oxide scale can be used as a measure of the length of time various

regions of the composites have been exposed to the environment, hence providing vital information regarding the sequence of failure. The oxide scale in the right figure indicates an early failure of this tow of fibers, whereas adjacent tows remain oxide free, suggesting failure much later in time. The path of various cracks can be followed throughout the composite in this manner, suggesting failure mechanisms.

Most CMC applications require stringent dimensional tolerance. In addition, excessive amounts of creep strain have been shown to degrade material strength. Current



Remote, noncontact strain-sensing system. Left: Typical fibrous fracture surface of a nonbrittle composite. Right: Isolated oxide scale formed during creep.



Improved creep and rupture behavior can be achieved by altering the reinforcing fiber phase. Temperature, 1315 °C; pressure, 15 ksi.

work has demonstrated that improvements to the reinforcing fiber have been shown to dramatically improve creep behavior as shown in the graph.

Creep and rupture testing are providing guidance for ongoing improvements to the high-temperature thermomechanical behavior of SiC/SiC composites as well as fundamental understanding of the failure mechanisms involved in these materials.

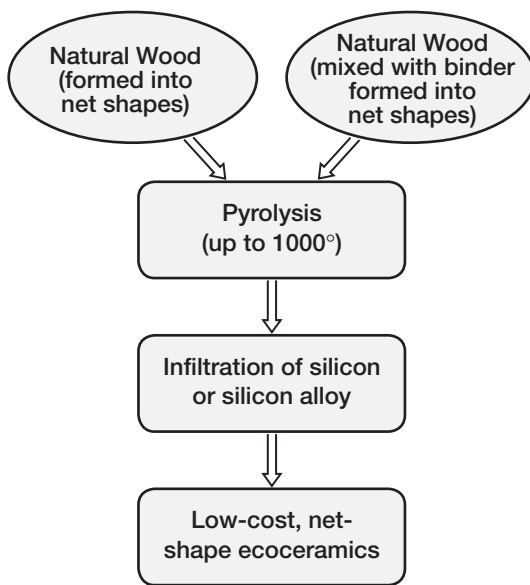
Glenn contact: Janet B. Hurst, 216-433-3286 or 216-433-5544, Janet.B.Hurst@glenn.nasa.gov

Author: Janet B. Hurst

Headquarters program office: OAT

Programs/Projects: UEET

Environment-Conscious Ceramics (Ecoceramics)



Fabrication process for ecoceramics.

Since the dawn of human civilization, there has always been a delicate balance between expanding human frontiers and coexisting with the ecosystem. In the new millennium, it will be extremely important to develop various materials, products, and processes to sustain a healthy life in harmony with nature that allow us to minimize any harmful effects.

Environment-conscious ceramics (ecoceramics) are a new class of materials that can be produced with renewable resources (wood and wood wastes (wood

sawdust). Wood is one of the best and most intricate engineering materials created by nature. Natural woods of various types are available throughout the world. In addition, wood sawdusts are generated in abundant quantities by sawmills. Environment-conscious ceramic materials, fabricated via the pyrolysis and infiltration of natural wood-derived preforms with silicon have tailorable properties with numerous potential applications.

Silicon carbide-based ecoceramics have been fabricated at the NASA Glenn Research Center by the reactive infiltration of wood-derived carbonaceous preforms with molten silicon or silicon-refractory metal alloys (see the figure). These carbonaceous preforms are fabricated by pyrolysis of solid wood bodies up to 1000 °C. The pyrolysis is carried out in a flowing nitrogen atmosphere. Melt infiltration is then carried out at temperatures above

the melting point of silicon or the silicon alloy. The microstructure and mechanical properties (flexural strength and compressive strength) of a wide variety of SiC-based ecoceramics have been measured. Ecoceramics have tailorable properties and behave like ceramic materials manufactured by conventional approaches. The wood-derived carbonaceous preforms have been shown to be quite useful in producing porous or dense materials with different microstructures and compositions. Detailed thermomechanical characterization of a wide variety of silicon-carbide-based ecoceramics is underway.

Find out more from Glenn's Ceramic Branch and Commercial Technology Office: <http://www.grc.nasa.gov/WWW/Ceramics/homepage.htm>
<http://cto.grc.nasa.gov>

Dynacs Engineering Corporation, Inc., contact:

Dr. Mrityunjay Singh, 216-433-8883, Mrityunjay.Singh@grc.nasa.gov

Author: Dr. Mrityunjay Singh

Headquarters program office: OAT

Programs/Projects: CTO

Feasibility of Actively Cooled Silicon Nitride Airfoil for Turbine Applications Demonstrated

Nickel-base superalloys currently limit gas turbine engine performance. Active cooling has extended the temperature range of service of nickel-base superalloys in current gas turbine engines, but the margin for further improvement appears modest. Therefore, significant advancements in materials technology are needed to raise turbine inlet temperatures above 2400 °F to increase engine specific thrust and operating efficiency. Because of their low density and high-temperature strength and thermal conductivity, in situ toughened silicon nitride ceramics have received a great deal of attention for cooled structures. However, the high processing costs and low impact resistance of silicon nitride ceramics have proven to be major obstacles for widespread applications. Advanced rapid prototyping technology in combination with conventional gel casting and sintering can reduce high processing costs and may offer an affordable manufacturing approach.

Researchers at the NASA Glenn Research Center, in cooperation with a local university and an aerospace company, are developing actively cooled and functionally graded ceramic structures. The objective of this program is to develop cost-effective manufacturing technology and experimental and analytical capabilities for environmentally stable, aerodynamically efficient, foreign-object-damage-resistant, in situ toughened silicon nitride turbine nozzle vanes, and to test these vanes under simulated engine conditions.

Starting with computer aided design (CAD) files of an airfoil and a flat plate with internal cooling passages, the permanent and removable mold components for gel casting ceramic slips were made by stereolithography and Sanders machines, respectively. The gel-cast part was dried and sintered to final shape. Several in situ toughened silicon nitride generic

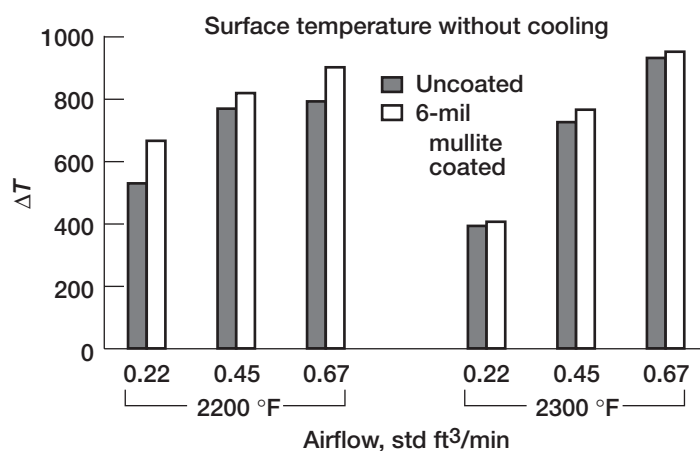
airfoils with internal cooling passages have been fabricated. The uncoated and thermal-barrier-coated airfoils and flat plates were burner rig tested for 30 min without and with air cooling. Without cooling, the surface temperature of the flat plate reached ~2350 °F. With cooling, the surface temperature decreased to ~1910 °F—a drop of ~440 °F (see the figure). This preliminary study demonstrates that a near-net-shape silicon nitride airfoil can be fabricated and that silicon nitride can sustain severe thermal shock and the thermal gradients induced by cooling and, thus, is a viable candidate for cooled components.

Glenn contact: Dr. Ramakrishna T. Bhatt, 216-433-5513,
Ramakrishna.T.Bhatt@grc.nasa.gov

Author: Dr. Ramakrishna T. Bhatt

Headquarters program office: OAT

Programs/Projects:
Propulsion and Power Systems R&T



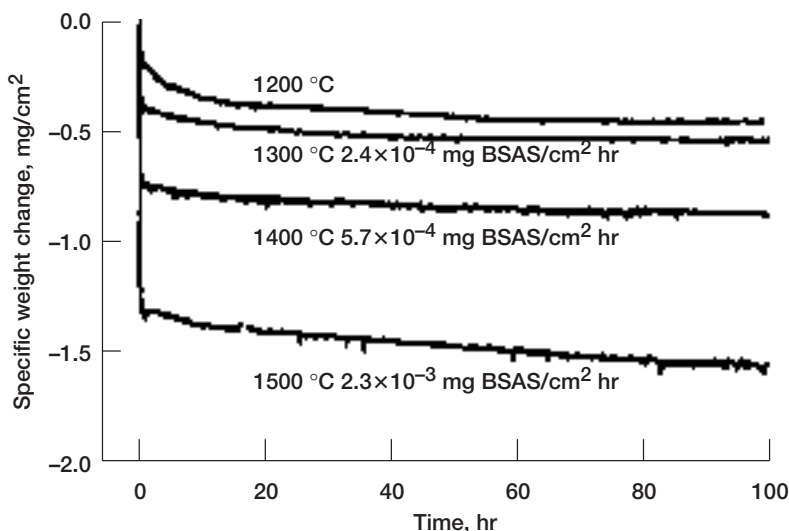
Variation of ΔT (surface temperature minus maximum internal temperature) with cooling airflow for an uncoated and a thermal-barrier-coated silicon nitride plate with cooling holes.

Upper Temperature Limit of Environmental Barrier Coatings for Enabling Propulsion Materials Established

Silicon-based ceramics, such as SiC/SiC composites and Si_3N_4 , are the prime candidates for hot section structural components of next-generation gas turbines. A key barrier to such an application is the rapid recession of silicon-based ceramics in combustion environments because of the volatilization of silica scale by water vapor (refs. 1 and 2). Environmental barrier coatings (EBC's) were developed to prevent recession in the High Speed Research—Enabling Propulsion Materials (HSR—EPM) Program (refs. 3 and 4). An investigation under the Ultra-Efficient Engine Technology Program was undertaken at the NASA Glenn Research Center to establish the upper temperature limit of the EPM EBC.

The EPM EBC consists of three layers: a silicon bond coat, a mullite ($3\text{Al}_2\text{O}_3 \cdot 2\text{SiO}_2$) or mullite-based bond coat, and a barium-strontium-aluminum silicate (BSAS: $\text{BaO}_x \cdot \text{SrO}_{1-x} \cdot \text{Al}_2\text{O}_3 \cdot 2\text{SiO}_2$) topcoat. Volatility and environmental/chemical stability of the EBC in water vapor were the key criteria in establishing the upper temperature limit in this study.

The volatility was investigated by exposing monolithic hot-pressed BSAS coupons in 50 vol % H_2O /balance O_2 at 1200 to 1500 °C while continuously monitoring the weight change using a microbalance. The following graph plots weight change versus time for hot-pressed BSAS in water vapor. The rapid initial weight loss is an artifact of the experimental procedure. A linear weight loss was observed, with the rate increasing with temperature. In the table, the weight loss rate is converted to a recession rate in a simulated combustion environment (pressure, 6 atm; gas velocity, 25 m/sec; $p\text{H}_2\text{O}$, 0.6 atm). The recession rate of BSAS determined in a high-pressure burner rig at 1300 °C agreed with the converted recession rate in the table, within a factor of two, supporting the validity of the conversion. The high recession rate at $T > 1400$ °C can become an issue, especially for thin EBC's (<100 μm).

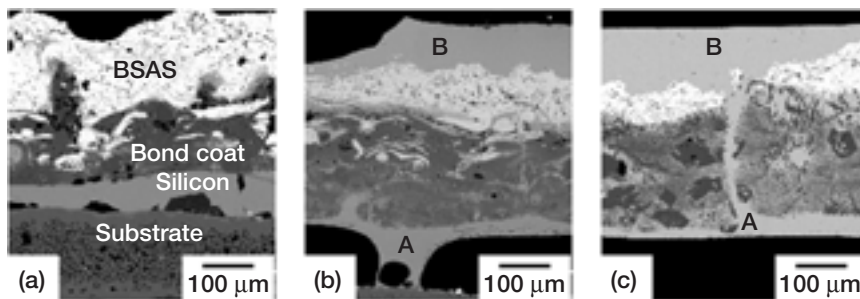


Weight change versus time for hot-pressed BSAS in 50 vol % H_2O /balance O_2 .

TABLE I.—RECESSION OF BSAS
[1000 hr, 6 atm; gas velocity, 25 m/sec;
 $p\text{H}_2\text{O}$, 0.6 atm]

Temperature, °C	1300	1400	1500
Recession, μm	7.5	17.8	72

For our environmental/chemical stability study, EBC-coated silicon-based ceramic coupons were exposed to 90 vol % H_2O /balance O_2 at 1300 to 1480 °C under thermal cycling. Each cycle consists of 1 hr at high temperature and 20 min at room temperature. The exposed coupons were subsequently prepared metallographically and the environmental/chemical degradation was characterized using scanning electron microscopy and energy dispersive spectroscopy. The images on the next page show the cross sections of EBC-coated silicon-based ceramics after 100 hr at 1400, 1440, and 1480 °C, respectively. Silicon was not applied on coupons exposed to 1440 and 1480 °C to avoid melting it (melt temperature, 1410 °C). The EBC cross section at 1400 °C remained similar to the as-processed state, except for some limited oxidation at the silicon/mullite-based bond coat interface. In contrast, a severe reaction developed at 1440 and 1480 °C: a thick scale formed at the silicon/mullite-based bond coat interface (area A in parts (b) and (c)), a new layer formed on top of the BSAS (area B), and an extensive reaction occurred between mullite and BSAS within the bond coat. X-ray diffraction indicates that the new top layer is a glass, which energy dispersive spectroscopy analysis shows has the same composition as the interface scale. According to the $\text{BaO-SiO}_2\text{-Al}_2\text{O}_3$ phase diagram, BSAS and silica form a low melting (1296 °C) silicate phase. It is therefore suggested



Cross section of EBC-coated silicon-based ceramics after 100 hr in 90 vol % H_2O /balance O_2 , showing the progress of the environmental/chemical reaction with temperature. (a) 1400 °C. (b) 1440 °C. (c) 1480 °C.

that the glass phase is a reaction product between the silica (grown on SiC as a result of oxidation) and the BSAS. The glass moved to the EBC surface, presumably due to capillary forces or the low surface energy of the glass phase. The significant thinning of the BSAS topcoat at $T > 1440$ °C and the channel that developed between the interface scale and the top glass layer (part (c)), supports this suggestion. The presence, and therefore the formation, of a low melting glass must be avoided because it leads to the spallation of the EBC.

Based on the foregoing results, one may conclude that the upper temperature limit of EPM EBC should be set at 1400 °C for a targeted 1000-hr life.

References

1. Robinson, R.C.; and Smialek, J.L.: SiC Recession Caused by SiO_2 Scale Volatility Under Combustion Conditions: I, Experimental Results and Empirical Model. J. Am. Ceram. Soc., vol. 82, no. 7, 1999, pp. 1817–1825.
2. Opila, E.J., et al.: SiC Recession Caused by SiO_2 Scale Volatility Under Combustion Conditions. Part II—Thermodynamics and Gaseous Diffusion Model. J. Am. Ceram. Soc., vol. 82, no. 7, 1999, pp. 1826–1834.

Cooled Ceramic Matrix Composite Panel Successfully Tested in Rocket Exhaust

Actively cooled ceramic matrix composite (CMC) components are enabling or enhancing for a broad range of hypersonic and reusable launch vehicle propulsion systems. Teaming with other NASA centers, the Air Force, and industry, the Glenn Ceramics Branch has successfully tested multiple cooled CMC panel concepts in high-heat-flux, high-pressure, flowing rocket engine combustion gas environments. Subelement components survived multiple cycles and the severe thermal gradients imposed by combustion gas temperatures in excess of 5500 °F and cryogenic hydrogen or ambient temperature water internal coolants. These demonstrations are critical for the continued development of this class of materials, and the research is expected to continue with additional concepts and increasingly larger and more complex geometries being fabricated and tested in a broad range of engine operating conditions.

Glenn contact: Dr. Andrew J. Eckel, 216–433–8185, Andrew.J.Eckel@grc.nasa.gov

3. Lee, K.N.: Current Status of Environmental Barrier Coatings for Si-Based Ceramics. Surface and Coatings Technology, vol. 133–134, nos. 1–7, 2000.
4. Lee, K.: Effect of Impurities and Coating Design on the Durability of EBC for Silicon-Based Ceramics. Proceedings of the Per Kofstad Memorial Symposium on High Temperature Corrosion and Materials Chemistry, Michael McNallan, ed., Electrochemical Society, Pennington, NJ, 2000, pp. 417–428.

Cleveland State University contact:

Dr. Kang N. Lee, 216–433–5634, Kang.N.Lee@grc.nasa.gov

Glenn contact:

Dr. Dennis S. Fox, 216–433–3295, Dennis.S.Fox@grc.nasa.gov

Dynacs Engineering Corporation, Inc., contact:

R. Craig Robinson, 216–433–5547, Raymond.C.Robinson@grc.nasa.gov

Authors: Dr. Kang N. Lee, Dr. Dennis S. Fox, and R. Craig Robinson

Headquarters program office: OAT

Programs/Projects: UEET



Actively cooled ceramic matrix composite panel under test in hydrogen-oxygen flame.

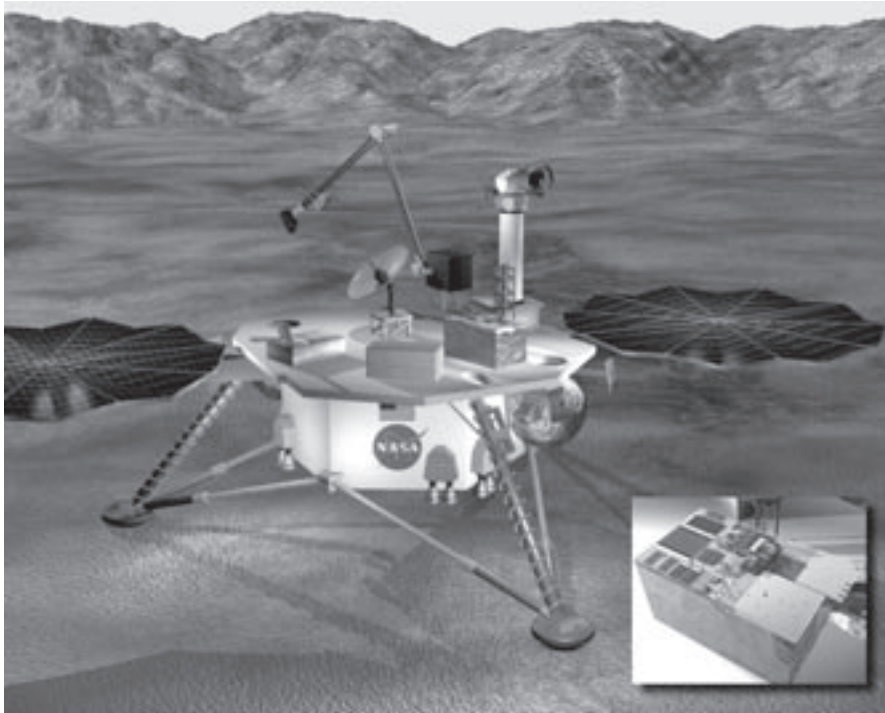
Author: Dr. Andrew J. Eckel

Headquarters program office: OAT

Programs/Projects: Propulsion Systems R&T, STR

Power and On-Board Propulsion Technology

DART: Instrument Package Developed for Investigating Atmospheric Dust on Mars



Artist's conception of Mars-2001 Surveyor Lander, with an inset showing the DART experiment package.

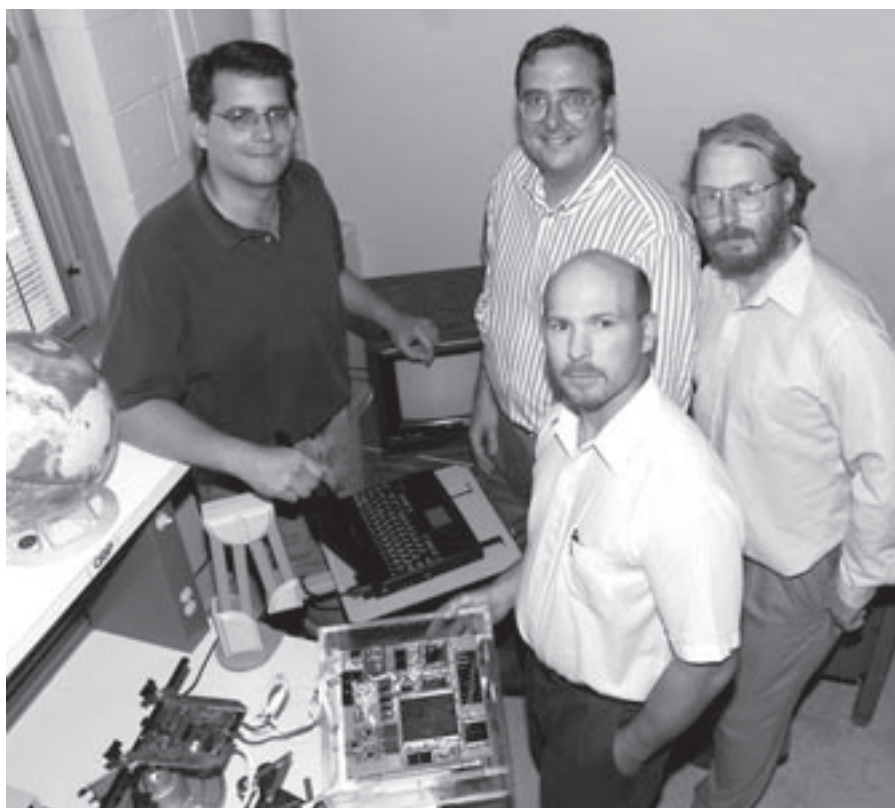
Mars' dust-filled atmosphere could be a significant problem for photovoltaic array operation during long missions on the surface of Mars. Measurements made by Pathfinder showed a 0.3-percent loss of solar array performance per day due to dust obscuration. Thus, dust deposition is the limiting factor in the lifetime of solar arrays for Martian power systems, and developing design tools to mitigate this deposition is important for long missions.

Despite the fact that dust deposition will severely degrade solar arrays, few details are known about the physical properties of Mars dust. The Dust Accumulation and Removal Test (DART) instrument was designed to gather this needed information: to quantify dust deposition, to measure the properties of the settled dust and its effect on array performance, and to test several ways to mitigate the effect of settled dust on a solar array. Although DART's purpose is to gather information critical to the design of future power systems on the surface of Mars, it will also provide significant scientific data on the properties of settled atmospheric dust through its dust characterization instrumentation. Two instruments will characterize dust: the dust microscope and the materials adherence experiment (MAE) commandable dust cover. In addition, two dust-mitigation tests will be conducted: tilted cell tests and an electrostatic dust-repulsion test.

DART's fixed-focus microscope is intended to furnish information about the size distribution of the settled dust. As atmospheric dust settles on DART's transparent glass settling plate, it will be imaged from below through a $\times 40$ objective that focuses onto a 512- by 512-pixel CMOS focal plane array. The microscope's resolution is about $0.5 \mu\text{m}$, and its total mass is 200 g. Since settled dust may be different in character from the dust that remains suspended in the atmosphere, this information is of considerable interest in the design of dust-mitigation strategies. For larger particles, the DART microscope will also yield shape information.

The MAE dust cover, which is based on the experiment flown on Pathfinder, consists of a transparent plate onto which dust settles. This plate is located above three small solar cells used in short-circuit current mode to measure solar intensity in three wavelength bands. A mechanism allows the cover to be rotated away from the cells. Comparison of the cell output with the dust-covered plate in position and removed measures the dust coverage independently of other changes in the cell performance or the atmosphere. By taking a spectrum of the sunlight through the MAE settling plate, we can also obtain a transmission spectrum of the settled dust.

Measurements of the camera window on the Viking lander showed no dust adhering to the vertical surface. Observations of the thermal shell of the Viking landers



DART Experiment flight hardware prepares for testing. The experiment team poses with the test hardware. Clockwise from upper left: John Lekki—Glenn, software engineer; Phillip Jenkins—Ohio Aerospace Institute, lead engineer for DART; Geoffrey A. Landis—Glenn, principal investigator for DART; and David Scheiman—Ohio Aerospace Institute, principal investigator for MATE.

seemed to show that dust also did not build up on tilted surfaces. Unfortunately, no quantitative measurement of the accumulation could be made. A high priority is, therefore, to see whether tilted solar cells avoid dust accumulation, and to find what angle is required to avoid dust coverage. The tilted cell measurement consists of solar cells tilted at 30°, 45°, and 60°; a horizontal control; and another solar cell tilted at 30° with a low friction (diamondlike carbon) coating.

The Martian atmospheric dust is expected to be charged. The electrostatic experiment will use a high-voltage solar cell to provide a potential of about 80 V to a transparent conductor on the front surface of the solar cell cover-glass. It will test three configurations—a positive potential applied to the cell cover, a negative potential applied to the cell, and a transverse field applied across the cell—to determine whether electrostatic fields can be used to mitigate the deposition of dust on solar arrays. These configurations will be compared with the control cell with no applied potential.

DART's sensors will provide both scientific information and important engineering data on the operation of solar power systems on Mars. DART will measure the dust accumulation rate and the transmitted spectrum of

the dust, and it will image individual settled particles to determine the size distribution and the particle shape, as well as gather information on electrostatic properties. DART was developed to fly as part of the MIP experiment on the (now postponed) Mars-2001 Surveyor Lander. The flight hardware was designed, built, and qualified for flight at the NASA Glenn Research Center, and it is ready to go to Mars.

Find out more about DART:

<http://powerweb.grc.nasa.gov/pvsee/publications/mars/Mars99.html>
<http://powerweb.grc.nasa.gov/pvsee/publications/wcpec2/DART.html>

References

1. Jenkins, P.P., et al.: Status of the Dust Accumulation and Removal Technology Experiment for the Mars 2001 Surveyor Lander. The Fifth International Conference on Mars. Lunar and Planetary Institute, Houston, TX, 1999.
2. Landis, G.A.; and Jenkins, P.P.: Measurement of the Settling Rate of Atmospheric Dust on Mars by the MAE Instrument on Mars Pathfinder. *J. Geoph. Res. Planets*, vol. 105, no. E1, 2000, pp. 1855-1857.

Ohio Aerospace Institute contact:

Phillip P. Jenkins, 216-433-2233,
Phillip.P.Jenkins@grc.nasa.gov

Glenn contacts:

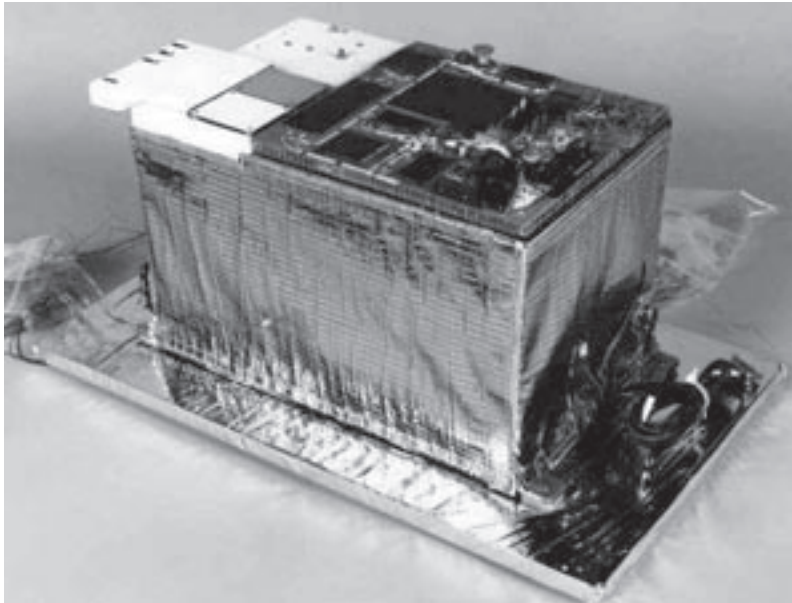
Dr. Geoffrey A. Landis, 216-433-2238,
Geoffrey.A.Landis@grc.nasa.gov;
 Cosmo R. Baraona, 216-433-5301,
Cosmo.R.Baraona@grc.nasa.gov; and
 Michael J. Krasowski, 216-433-3729,
Michael.J.Krasowski@grc.nasa.gov

Author: Dr. Geoffrey A. Landis

Headquarters program office: OSF

Programs/Projects: Mars Surveyor

Mars Array Technology Experiment Developed to Test Solar Arrays on Mars



MATE Experiment flight hardware.

Solar arrays will be the power supply for future missions to the planet Mars, including landers, rovers, and eventually human missions to explore the Martian surface. Until Mars Pathfinder landed in July 1997, no solar array had been used on the surface. The MATE package is intended to measure the solar energy reaching the surface, characterize the Martian environment to gather the baseline information required for designing power systems for long-duration missions, and to quantify the performance and degradation of advanced solar cells on the Martian surface.

To measure the properties of sunlight reaching the Martian surface, MATE incorporates two radiometers and a visible/NIR spectrometer. The radiometers consist of multiple thermocouple junctions using thin-film technology. These devices generate a voltage proportional to the solar intensity. One radiometer measures the global broadband solar intensity, including both the direct and scattered sunlight, with a field of view of approximately 130°. The second radiometer incorporates a slit to measure the direct (unscattered) intensity radiation. The direct radiometer can only be read once per day, with the Sun passing over the slit.

The spectrometer measures the global solar spectrum with two 256-element photodiode arrays, one Si sensitive in the visible range (300 to 1100 nm), and a second InGaAs sensitive to the near infrared (900 to 1700 nm). This range covers 86 percent of the total energy from the Sun, with approximately 5-nm resolution. Each photodiode array has its own fiber-optic feed and grating.

Although the purpose of the MATE is to gather data useful in designing solar arrays for Mars surface power systems, the radiometer and spectrometer measurements are expected to also provide important scientific data

for characterizing the properties of suspended atmospheric dust. In addition to measuring the solar environment of Mars, MATE will measure the performance of five different individual solar cell types and two different solar cell strings, to qualify advanced solar cell types for future Mars missions.

The MATE instrument, designed for the Mars-2001 Surveyor Lander mission, contains a capable suite of sensors that will provide both scientific information as well as important engineering data on the operation of solar power systems on Mars. MATE will characterize the intensity and spectrum of the solar radiation on Mars and measure the performance of solar arrays in the Mars environment. MATE flight hardware was built and tested at the NASA Glenn Research Center and is ready for flight.

Find out more about MATE:

<http://powerweb.grc.nasa.gov/pvsee/publications/wcpec2/mate2001.html>

Bibliography

Scheiman, D., et al.: Mars Array Technology Experiment (MATE). The 28th IEEE Photovoltaic Specialist Conference. Anchorage, Alaska, Sep. 2000.

Ohio Aerospace Institute contact:

David A Scheiman, 216-433-6756, David.A.Scheiman@grc.nasa.gov

Glenn contacts:

Dr. Geoffrey A. Landis, 216-433-2238, Geoffrey.A.Landis@grc.nasa.gov; Cosmo R. Baraona, 216-433-5301, Cosmo.R.Baraona@grc.nasa.gov; and Michael J. Krasowski, 216-433-3729, Michael.J.Krasowski@grc.nasa.gov

Author: Dr. Geoffrey A. Landis

Headquarters program office: OSS

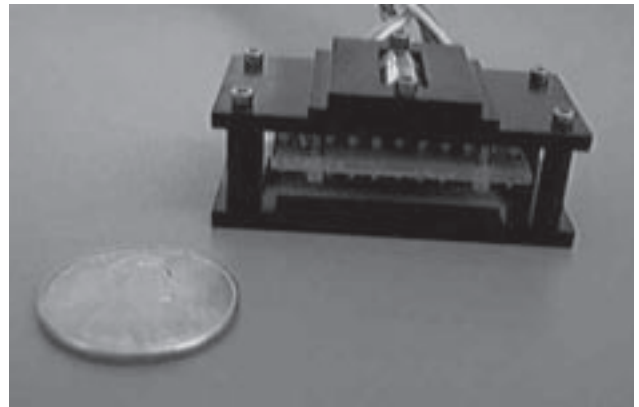
Programs/Projects: Mars Surveyor

Lightweight Sun-Position Sensor Developed

An orbiting spacecraft needs to be able to accurately locate the position of the Sun so that the solar arrays can be pointed toward the Sun. This not only maximizes the production of power, but it also helps the arrays find their orientation in space so that they can accurately point antennae at ground stations.

As part of the work on the (now postponed) Mars-2001 Surveyor Lander, NASA Glenn Research Center engineers developed a new Sun sensor that is far lighter and simpler than earlier designs. This sensor uses the technology of a linear photodiode array to find the position of the Sun in one axis. Two of these sensors, used together, can locate the x and y coordinates of the Sun relative to the spacecraft. These sensors have a mass of only 18 g each, nearly an order of magnitude lighter than earlier designs. (This mass does not include the electronic circuit to read the photodiode output, which is on the experiment microcontroller.) Near the center of the field of view, the Sun position can be found to 0.15° .

The heart of each sensor is a cylindrical lens focusing light onto a 512-element linear photodiode array. An OD8 ND filter is used to reduce the intensity of the sunlight to avoid saturating the detectors. Although the primary purpose of these sensors is to allow solar cell measurements to be referenced to the true Sun position relative to the solar cells, they will also provide scientific data in the form of one-dimensional scans of the sunlight intensity across the sky. The sensor has been tested to operate at Mars daytime temperatures as low as 40° below zero, and it has passed flight certification tests such as vibration, thermal vacuum operation, and pyrotechnic shock. For the Mars experiment, two Sun sensors were used to locate the x (N-S) and y (E-W) position of the Sun near noon, and a



Lightweight Sun-position sensor.

third Sun sensor measured the height of the Sun at low elevations. This sensor for Sun position was also baselined as part of the Photovoltaic Engineering Testbed, where it will be used to accurately position a solar cell measurement platform to point at the Sun.

Sensors of this type can be used on many future satellites, including NASA space probes and communications and weather satellites. Similar sensors could be used for terrestrial applications as well, for example, as a part of a control system to steer future solar arrays to face directly into the Sun.

Find out more about Glenn's experiments on the Mars Surveyor Lander:
<http://powerweb.grc.nasa.gov/pvsee/experiments/2003.html>

Glenn contacts:

David M. Wilt, 216-433-6293,
David.M.Wilt@grc.nasa.gov; and
Dr. Geoffrey A. Landis, 216-433-2238,
Geoffrey.A.Landis@grc.nasa.gov

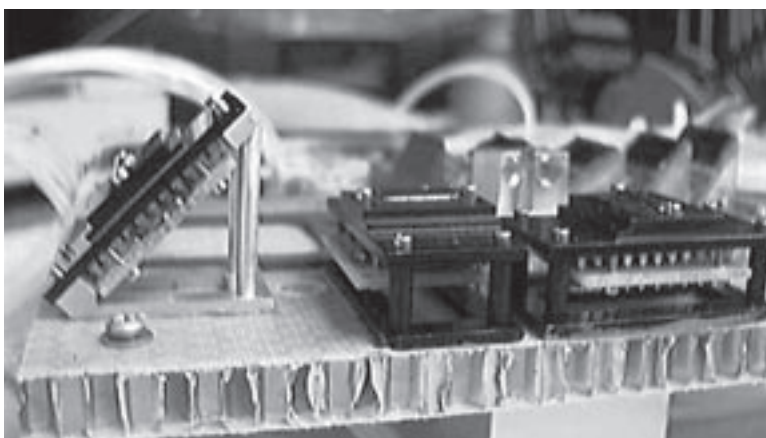
Ohio Aerospace Institute contact:

Phillip P. Jenkins, 216-433-2233,
Phillip.P.Jenkins@grc.nasa.gov

Author: Dr. Geoffrey A. Landis

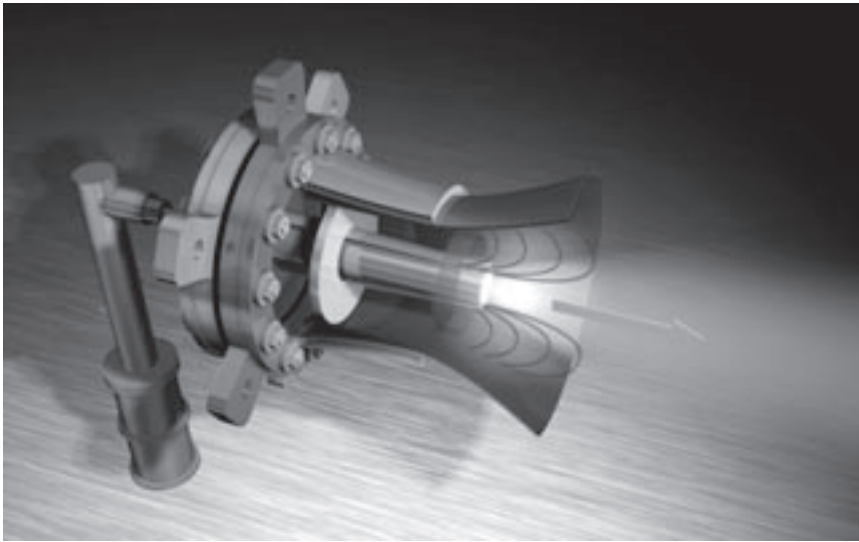
Headquarters program office: OSS

Programs/Projects: PET, Mars Surveyor



Three Sun sensors mounted on the honeycomb Dust Accumulation and Removal Test (DART) experiment plate for the Mars-2001 Surveyor Lander. Left: Sun sensor tilted at 45° to measure the height of the Sun at low Sun angles. Center and right: two Sun sensors mounted to view the Sun overhead and measure its x and y position near zenith.

High-Power Magnetoplasmadynamic Thruster Being Developed



Self-field MPD thruster.

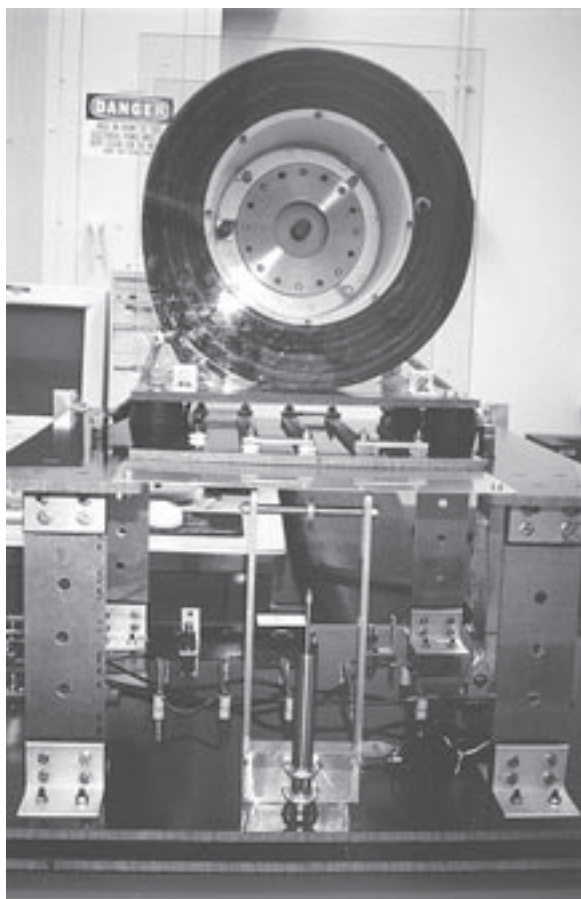
High-power electromagnetic thrusters have been proposed as primary in-space propulsion options for several of the bold new interplanetary and deep space missions envisioned by the Human Exploration and Development of Space (HEDS) Strategic Enterprise. As the lead center for electric propulsion, the NASA Glenn Research Center is actively involved in the design, development, and testing of high-power electromagnetic technologies to meet these demanding mission requirements.

One concept of particular interest is the magnetoplasmadynamic (MPD) thruster, shown schematically in the figure above. In its basic form, the MPD thruster consists of a central cathode surrounded by a concentric cylindrical anode. A high-current arc is struck between the anode and cathode, which ionizes and accelerates a gas (plasma) propellant. In the self-field version of the thruster, an azimuthal magnetic field generated by the current returning through the cathode interacts with the radial discharge current flowing through the plasma to produce an axial electromagnetic body force, providing thrust. In applied field-versions of the thruster, a magnetic field coil surrounding the anode is used to provide additional radial and axial magnetic fields that can help stabilize and accelerate the plasma propellant.

The following figure shows an experimental megawatt-class MPD thruster developed at Glenn. The MPD thruster is fitted inside a magnetic field coil, which in turn is mounted on a thrust stand supported by thin metal flexures. A calibrated position transducer is used to determine the force provided by the thruster as a function of thrust stand displacement. Power to the thruster is supplied by a 250-kJ capacitor bank, which provides up to 30-MW to the thruster for a period of 2 msec. This short period of time is

sufficient to establish thruster performance similar to steady-state operation, and it allows a number of thruster designs to be quickly and economically evaluated. In concert with this experimental research, Glenn is also developing and using advanced numerical simulations to predict the performance of self-field and applied-field MPD thrusters. The pulsed high-power test facility serves as a testbed to validate the numerical thruster simulations, and the numerical simulations are, in turn, used to provide more efficient thruster designs. In addition, Glenn is currently refurbishing a megawatt-class steady-state thruster facility that will be used for extensive life testing of the optimized thruster designs developed from the numerical simulations and high-power pulsed MPD thruster experiments.

The ultimate goal of the high-power MPD thruster program is to provide an efficient, megawatt-class electromagnetic thruster capable of several thousand hours of continuous operation. Because of the high exhaust velocity inherent in electric propulsion thrusters, these devices can meet the most demanding mission applications with significantly less propellant than chemical rockets. For a given spacecraft launch mass, the reduction in propellant mass will allow more payload to be carried into orbit, requiring fewer launches and less cost for a total mission mass. Alternatively, the lower propellant mass requirements can be used to reduce the total spacecraft mass at launch, with a corresponding



Experimental megawatt-class MPD thruster.

reduction in launch vehicle class and associated launch costs. Providing robust and economical in-space transportation, Glenn is leading the way to develop these high-power plasma thrusters of the future.

Ohio Aerospace Institute contact: Dr. Michael R. LaPointe, 216-433-6192, Michael.R.Lapointe@grc.nasa.gov

Author: Dr. Michael R. LaPointe

Headquarters program office: OAT

Programs/Projects: ASTP

1000 Hours of Testing Completed on 10-kW Hall Thruster

Between the months of April and August 2000, a 10-kW Hall effect thruster, designated T-220, was subjected to a 1000-hr life test evaluation. Hall effect thrusters are propulsion devices that electrostatically accelerate xenon ions to produce thrust. Hall effect propulsion has been in development for many years, and low-power devices (1.35 kW) have been used in space for satellite orbit maintenance. The T-220, shown in the photo, produces sufficient thrust to enable efficient orbital transfers, saving hundreds of kilograms in propellant over conventional chemical propulsion systems. This test is the longest operation ever achieved on a high-power Hall thruster (greater than 4.5 kW) and is a key milestone leading to the use of this technology for future NASA, commercial, and military missions.



T-220 Hall effect thruster during operation.

The T-220 was developed by the NASA Glenn Research Center, TRW, and Space Power Incorporated under the NASA Advanced Space Transportation Program. The thruster provides over 500 mN of thrust at a specific impulse of 2450 sec and 59-percent total efficiency with 10 kW of input power. The 1000-hr test was conducted at Glenn's Electric Propulsion Laboratory, in Vacuum Facility 12. The T-220 performed well throughout the test with discharge current oscillations and propellant utilization improving over time. Thrust, specific impulse, and efficiency measurements taken at periodic intervals during the test showed less than 2-percent variation.

A key objective of the test was to characterize the amount of material erosion occurring on the ceramic discharge chamber. Material erosion results from the collision of high-energy ions on the annular chamber near the thruster exit plane. The erosion causes a chamfering effect on the corners of the chamber walls, which can lead to ion beam divergence, performance degradation, and potentially thruster failure. Correlated Solutions Incorporated and Glenn developed two methods for erosion measurement employing laser profilometry and video correlation. One method required removal of the thruster from the vacuum chamber and installation on a rotatable stand permitting full circumferential surveys of

the inner and outer rings in 1° increments with 0.01-mm accuracy. The other method accommodated more frequent, in situ erosion measurements of two discrete locations on the discharge chamber with 0.2-mm accuracy. The erosion data taken during this test will assist researchers in the design and development of longer life thrusters.

Glenn contacts:

Lee S. Mason, 216-977-7106,
Lee.S.Mason@grc.nasa.gov; and
Robert S. Jankovsky, 216-977-7515,
Robert.S.Jankovsky@grc.nasa.gov

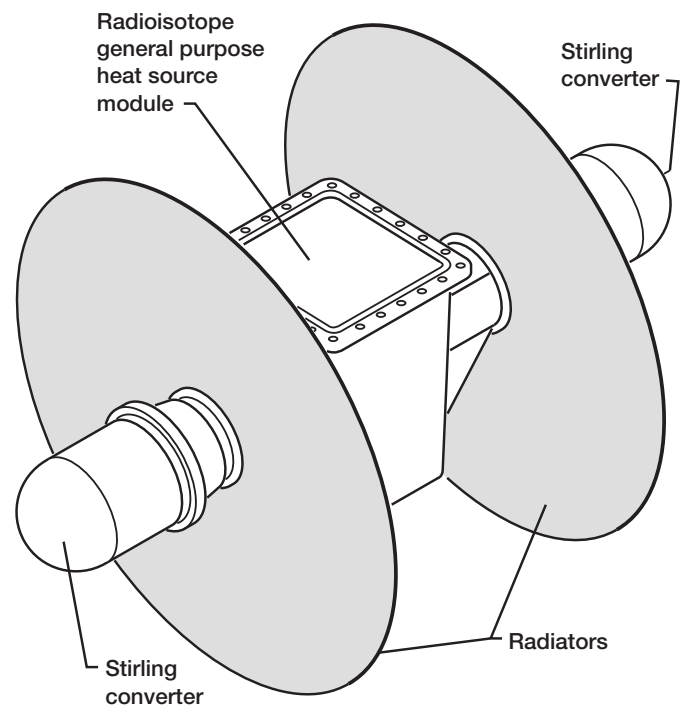
Author: Lee S. Mason

Headquarters program office: OAT

Programs/Projects: ASTP

Lightweight Radiators Being Developed for Advanced Stirling Radioisotope Power Systems

The thermodynamic heat-to-electric power conversion efficiency of Stirling systems is 3 to 5 times higher than that of thermoelectric converters. Hence for unmanned deep space probes, Stirling advanced radioisotope power systems (ARPS) could deliver up to 5 times as much power as radioisotope thermoelectric generators for the same amount of radioisotope, or they could require one-third to one-fifth as much isotope inventory for the same power output. However, Stirling power systems reject unconverted heat at much lower temperatures than radioisotope thermoelectric generators. Normally, this requires larger and heavier heat-rejection subsystems because of the greater radiator areas, which are proportional to the first power of the heat rejected and the fourth power of the absolute heat-rejection temperature, as specified by the Stefan-Boltzmann radiation heat transfer law. The development of directly coupled disk radiators using very high conductivity encapsulated thermopyrolytic graphite materials represents a significant advance in Stirling ARPS space heat-rejection subsystem technology. A conceptual Stirling ARPS with two engines coupled to a radioisotope general-purpose heat source (GPHS) is shown in the illustration.



Stirling ARPS with high-conductivity disk radiators.

The direct mounting of the disk on the engine “cold” end will practically eliminate heat transport temperature drop. The high thermal conductivity (over 3 times that of copper) will result in much lower temperature drops between the inner diameter and the outer rim of the disk radiators. Consequently, the radiators will operate at higher average temperatures and thus require smaller surface areas. At the same time, the low density of the material will lead to lower weight. Since the radiators are impervious to micrometeoroid impacts, their survivability and reliability over multiyear deep space missions will be superior to those of radiator systems that use heat-transfer fluids.

Fabrication of thermopyrolytic graphite disk radiators that could be used on a Stirling ARPS will be undertaken under a Phase II SBIR contract with k Technologies Corporation. A design code developed in house at the NASA Glenn Research Center, GPHRAD, will aid in the radiator designs. The relative simplicity of the design, without liquid transport lines, or heat pipes, should also lead to low fabrication and assembly costs, once the proper manufacturing procedures have been worked out during this contract.

Bibliography

Juhasz, Albert J.; Tew, Roy C.; and Thieme, Lanny G.: Design and Analysis Code for Heat Pipe Radiators of Stirling Power Systems Applicable to Deep Space Probes. 11th International Heat Pipe Conference, Musashinoshi, Tokyo, 1999.

Juhasz, Albert J.; Tew, Roy C.; and Thieme, Lanny G.: Parametric Study of Radiator Concepts for a Stirling Radioisotope Power System Applicable to Deep Space Missions. NASA/TP-2000-209676, 2000. <http://gltrs.grc.nasa.gov/GLTRS>

Glenn contacts:

Albert J. Juhasz, 216-433-6134, Albert.J.Juhasz@grc.nasa.gov;
Roy C. Tew, 216-433-8471, Roy.C.Tew@grc.nasa.gov; and
Lanny G. Thieme, 216-433-6119, Lanny.G.Thieme@grc.nasa.gov

Authors: Albert J. Juhasz, Roy C. Tew, and Lanny G. Thieme

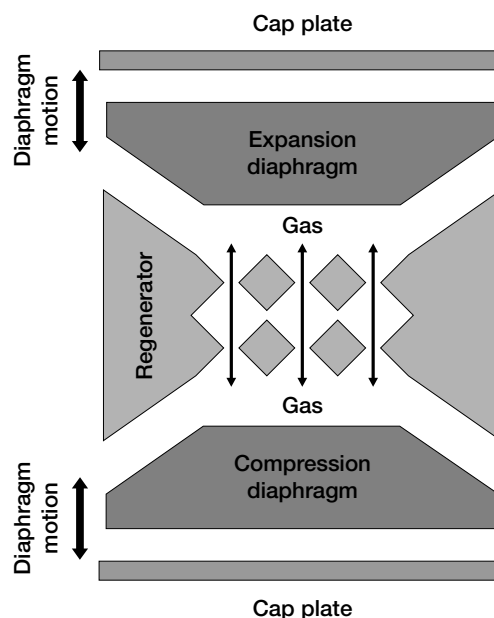
Headquarters program office: OSS

Programs/Projects:

Stirling technology, SBIR

MEMS Device Being Developed for Active Cooling and Temperature Control

High-capacity cooling options remain limited for many small-scale applications such as microelectronic components, miniature sensors, and microsystems. A microelectromechanical system (MEMS) is currently under development at the NASA Glenn Research Center to meet this need. It uses a thermodynamic cycle to provide cooling or heating directly to a thermally loaded surface. The device can be used strictly in the cooling mode, or it can be switched between cooling and heating modes in milliseconds for precise temperature control. Fabrication and assembly are accomplished by wet etching and wafer bonding techniques routinely used in the semiconductor processing industry. Benefits of the MEMS cooler include scalability to fractions of a millimeter, modularity for increased capacity and staging to low temperatures, simple interfaces and limited failure modes, and minimal induced vibration.



Cross-sectional view of one cell of the MEMS Stirling cooler.

The MEMS cooler has potential applications across a broad range of industries: biomedical, computer, automotive, and aerospace. The basic capabilities it provides can be categorized into four key areas:

- (1) Extended environmental temperature range in harsh environments
- (2) Lower operating temperatures for electronics and other components
- (3) Precision spatial and temporal thermal control for temperature-sensitive devices
- (4) The enabling of microsystem devices that require active cooling and/or temperature control

Stirling cycle coolers have been used for decades to produce cooling temperatures down to the cryogenic range for a variety of applications. Historically, these machines have been made using pistons, mechanical linkages, and other standard engine components along with traditional materials and fabrication methods. More recently, the need for smaller-scale coolers has pushed the limits of these traditional components and assembly techniques. However, available coolers are still too large for many applications including certain electronic components, sensors, and MEMS devices.

Rapidly expanding capabilities of semiconductor processing in general, and microsystems packaging in particular, present a new opportunity to extend Stirling cycle cooling to the MEMS domain. The comparatively high capacity and efficiency possible with a MEMS Stirling cooler provides a level of active cooling that is currently impossible at the micro scale with current state-of-the-art techniques. The MEMS cooler technology builds on decades of research on Stirling cycle machines performed at Glenn, while capitalizing on Glenn's emerging microsystems capabilities.

The MEMS cooler device is composed of numerous Stirling-cycle cells arranged in parallel and/or in series. The expansion and compression diaphragms, which are the only moving parts in the device, are deflected toward and away from the regenerator region in phase-shifted sinusoidal fashion to produce the Stirling cycle. Expansion of the working gas directly beneath the expansion diaphragm in each cycle creates a cold end for extracting heat, while compression at the other end creates a hot region for dissipating heat. Heat is transferred to and from the working gas as it is forced through the regenerator region by the moving diaphragms.

The slanted geometries of the diaphragm and regenerator surfaces are characteristic of the wet etching process used to create the structure and advantageously increase the swept volume in the expansion and compres-

sion regions. A thin-film temperature sensor deposited on the surface of the cap plate provides control feedback. This sensor, along with the ability to switch hot and cold ends by altering the cycle with control software, permits the device to be used for precise thermal control as well as cooling.

Preliminary analysis of the MEMS cooler has been completed and indicates a theoretical performance that is an order-of-magnitude improvement over existing state-of-the-art techniques for cooling small-scale components. Detailed analysis and design optimization is planned for the MEMS cooler followed by fabrication of a prototype device for performance testing. All research on the MEMS cooler has been conducted at the NASA Glenn Research Center, and a patent application has been prepared for this technology.

Bibliography

Moran, Matthew E.: Multidisciplinary Analysis of a Microsystem Device for Thermal Control. Prepared for the 11th Thermal & Fluids Analysis Workshop, Cleveland, OH, 2000.

Glenn contact:

Matthew E. Moran, 216-433-8324,
Matthew.E.Moran@grc.nasa.gov

Author: Matthew E. Moran

Headquarters program office:
OAT (CTD)

Programs/Projects:
CTO, Space Power Technology

Flywheel Energy Storage Technology Being Developed

A flywheel energy storage system was spun to 60,000 rpm while levitated on magnetic bearings. This system is being developed as an energy-efficient replacement for chemical battery systems. Used in groups, the flywheels can have two functions—providing attitude control for a spacecraft in orbit as well as providing energy storage. The first application for which the NASA Glenn Research Center is developing the flywheel is the International Space Station, where a two-flywheel system will replace one of the nickel-hydrogen battery strings in the space station's power system. The 60,000-rpm development rotor is about one-eighth the size that will be needed for the space station (0.395 versus 3.07 kW-hr).

The flywheel system is composed of a composite outer rim around an aluminum hub. This hub/rim assembly is connected to a shaft that uses a motor/generator to put energy into or take energy out of the flywheel. The shaft also has laminations to conduct the flux generated by the magnetic bearing actuators. This spinning portion of the system is contained in a housing that holds the motor stator, the magnetic bearing actuator circuits, and the backup mechanical bearings. The motor stator generates the magnetic fields to spin the motor rotor and the flywheel shaft; the magnetic bearing actuators generate and direct the flux to apply forces to the flywheel to keep it levitated. The back-up mechanical bearings capture the flywheel if the magnetic bearing fails. The housing provides structural support for all the systems and serves as a vacuum chamber to eliminate aerodynamic heating of the spinning flywheel.

One of the primary technical challenges to achieving the 60,000-rpm milestone was to develop the control algorithm for the magnetic bearings. Glenn worked with Texas A & M University to develop a multi-input, multi-output algorithm that controls the rotor modes (forward whirl, backward whirl, forward conical, and backward conical) of the flywheel using minimum control input. This is critical to demonstrating the efficiency and long life of the flywheel storage system.

Another primary technical challenge was to design and build the hub/rim system with sufficient stress margins to meet the safety standards of the space community. Glenn used a combination of analysis from finite element analysis programs and spin testing of assembled rotors to 110 percent to ensure the integrity of the flywheel design. In addition, a nondestructive evaluation test program is being developed by Glenn to analyze subsequent rotors for flight flywheel systems.



Development unit flywheel module that achieved 60,000 rpm.

Glenn contact:

James F. Soeder, 216-433-5328,
James.F.Soeder@grc.nasa.gov

Author: Frederick J. Wolff

Headquarters program office: OSF

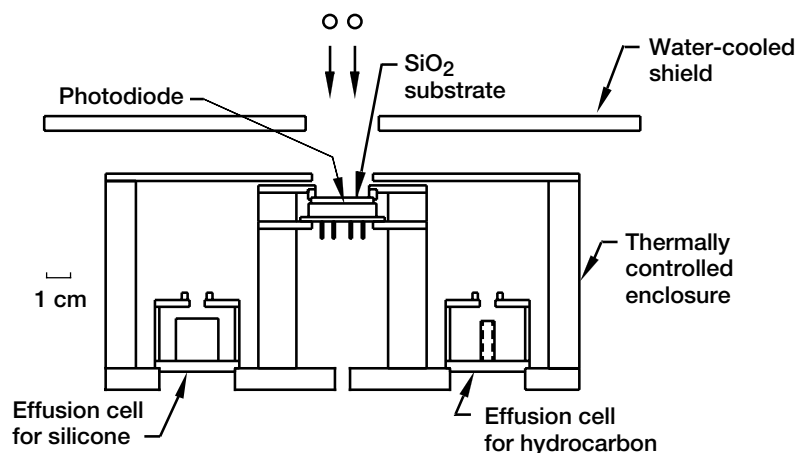
Programs/Projects: ISS

Atomic Oxygen Interactions With Silicone Contamination on Spacecraft in Low Earth Orbit Studied

Silicones have been widely used on spacecraft as potting compounds, adhesives, seals, gaskets, hydrophobic surfaces, and atomic oxygen protective coatings. Contamination of optical and thermal control surfaces on spacecraft in low Earth orbit (LEO) has been an ever-present problem as a result of the interaction of atomic oxygen with volatile species from silicones and hydrocarbons onboard spacecraft. These interactions can deposit a contaminant that is a risk to spacecraft performance because it can form an optically absorbing film on the surfaces of Sun sensors, star trackers, or optical components or can increase the solar absorptance of thermal control surfaces. The transmittance, absorptance, and reflectance of such contaminant films seem to vary widely from very transparent SiO_x films to much more absorbing SiO_x -based films that contain hydrocarbons.

At the NASA Glenn Research Center, silicone contamination that was oxidized by atomic oxygen has been examined from LEO spacecraft (including the Long Duration Exposure Facility and the Mir space station solar arrays) and from ground laboratory LEO simulations. The findings resulted in the development of predictive models that may help explain the underlying issues and effects. Atomic oxygen interactions with silicone volatiles and mixtures of silicone and hydrocarbon volatiles produce glassy SiO_x -based contaminant coatings. The addition of hydrocarbon volatiles in the presence of silicone volatiles appears to cause much more absorbing (and consequently less transmitting) contaminant films than when no hydrocarbon volatiles are present. On the basis of the LDEF and Mir results, conditions of high atomic oxygen flux relative to low contaminant flux appear to result in more transparent contaminant films than do conditions of low atomic oxygen flux with high contaminant flux. Modeling predictions indicate that the deposition of contaminant films early in a LEO flight should depend much more on atomic oxygen flux than it does later in a mission.

Find out more from Glenn's Electro-Physics Branch:
<http://www.grc.nasa.gov/WWW/epbranch/ephome.htm>



Ground laboratory system for simulation of atomic oxygen interaction with combined silicone and hydrocarbon contamination on SiO_2 windows.



1 cm

*Top: LDEF SiO_x -based contaminant streaks.
 Bottom: SiO_x -based contamination on Mir solar cell optical solar reflector.*

Glenn contacts:

Bruce A. Banks, 216-433-2308,
Bruce.A.Banks@grc.nasa.gov;
 Sharon K. Miller, 216-433-2219,
Sharon.K.Miller@grc.nasa.gov; and
 Aaron Snyder, 216-433-5918,
Aaron.Snyder@grc.nasa.gov;
 Kim K. de Groh, 216-433-2297,
Kim.K.deGroh@grc.nasa.gov; and
 Dr. David J. Brinker, 216-433-2236,
David.J.Brinker@grc.nasa.gov

Dynacs Engineering Company, Inc., contacts:

Edward A. Sechkar, 216-433-2299,
Edward.A.Sechar@grc.nasa.gov; and
 Thomas J. Stueber, 216-433-2218,
Thomas.J.Stueber@grc.nasa.gov

Author: Bruce A. Banks

Headquarters program office:
 OSS (ATMS)

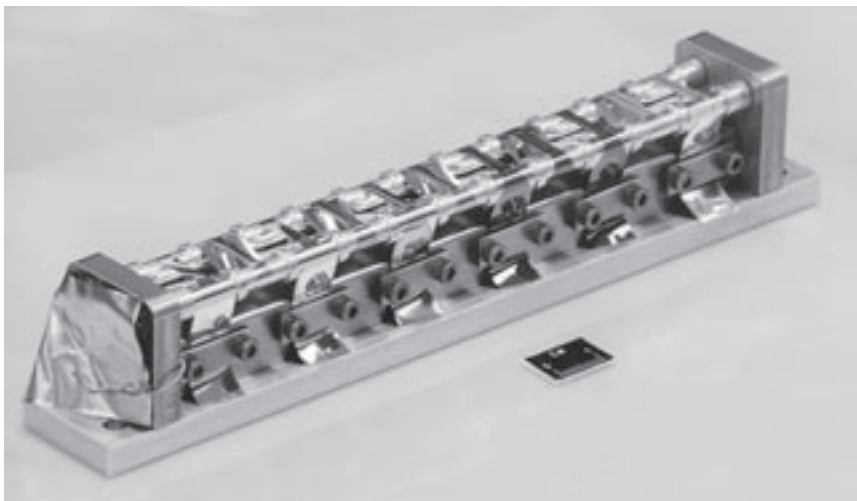
Programs/Projects:
 Space Power Technology

Specimens Prepared for Materials International Space Station Experiment

The Materials International Space Station Experiment (MISSE) is a materials flight experiment sponsored by the Materials and Manufacturing Directorate of the Air Force Research Laboratory at Wright-Patterson Air Force Base and the NASA Space Environmental Effects Program at the NASA Marshall Space Flight Center. MISSE is a cooperative effort among the Air Force, several NASA field centers, and industry. The experiment package will be placed on the exterior of the International Space Station in the summer of 2001. Approximately half of the specimens will be exposed to the space environment for 1 year, and the other half will be exposed for 3 years.

The Electro-Physics Branch at the NASA Glenn Research Center has prepared and delivered over 150 specimens to be included in MISSE. Specimens include (1) double-coated polyimide Kapton to compare mass loss from in-space atomic oxygen undercutting erosion to ground-laboratory atomic oxygen undercutting erosion for predicting in-space durability, (2) silicones to study changes in surface hardness and optical properties after combined atomic oxygen-ultraviolet radiation exposure for predicting in-space durability, (3) 41 different polymers to accurately measure their atomic oxygen erosion yields, (4) scattering chambers to study atomic oxygen scattering characteristics that are relevant to the degradation found in spacecraft with exterior openings, (5) thin polymer film disks and tensile specimens to study the effects of radiation on their optical properties and mechanical properties, (6) lightweight intercalated graphite epoxy composites to study electromagnetic interference shielding performance, and (7) polymer-based materials utilizing new atomic oxygen protection concepts to study their durability.

For more information, visit Glenn's Electro-Physics Branch:
<http://www.grc.nasa.gov/WWW/epbranch/ephome.htm>



Thin polymer film tensile specimens installed in MISSE flight hardware.



Disk specimens installed in MISSE flight hardware.

Glenn contacts:

Bruce A. Banks, 216-433-2308,
Bruce.A.Banks@grc.nasa.gov;
Kim K. de Groh, 216-433-2297,
Kim.K.deGroh@grc.nasa.gov;
Joyce A. Dever, 216-433-6294,
Joyce.A.Dever@grc.nasa.gov;
Dr. Donald A. Jaworske,
216-433-2312,
Donald.A.Jaworske@grc.nasa.gov;
Sharon K. Miller, 216-433-2219,
Sharon.K.Miller@grc.nasa.gov; and
Aaron Snyder, 216-433-5918,
Aaron.Snyder@grc.nasa.gov

Dynacs Engineering Company, Inc., contact:

Edward A. Sechkar, 216-433-2299,
Edward.A.Sechkar@grc.nasa.gov

Authors: Bruce A. Banks, Kim K. de Groh, Joyce A. Dever, Dr. Donald A. Jaworske, Sharon K. Miller, Aaron Snyder, and Edward A. Sechkar

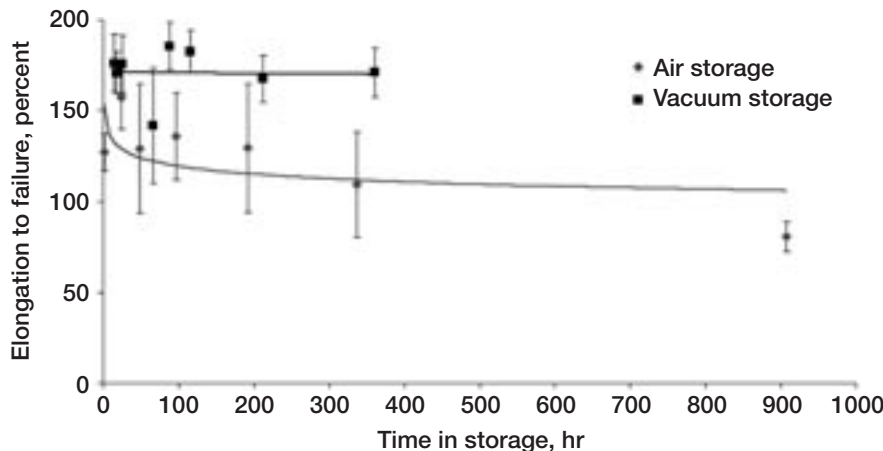
Headquarters program office:
OSS (ATMS)

Programs/Projects: ISS

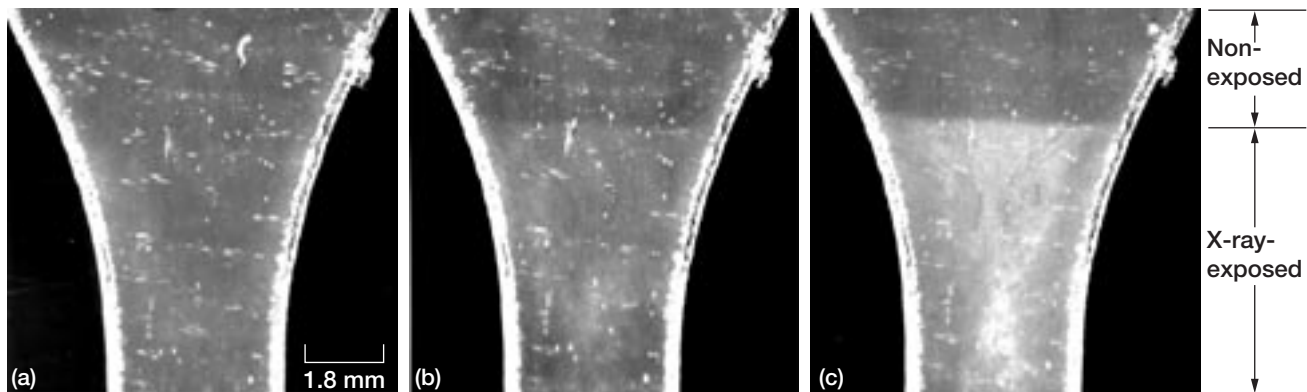
Effect of Air and Vacuum Storage on the Degradation of X-Ray-Exposed Aluminized-Teflon Investigated

Metalized Teflon FEP (fluorinated ethylene propylene, DuPont), a common thermal control material, has been found to degrade in the low-Earth-orbit space environment. The aluminized-FEP (Al-FEP) exterior layer on the Hubble Space Telescope has become extremely embrittled, with extensive cracking occurring on all sides of the telescope. This embrittlement has been primarily attributed to radiation exposure (x-rays from solar flares, electron/proton radiation, and possibly near-ultraviolet radiation) combined with thermal cycling. Limited samples of FEP tested after long-term exposure to low Earth orbit on the Hubble Space Telescope and on the Long Duration Exposure Facility indicated that there might be continued degradation in tensile properties over time. An investigation was conducted at the NASA Glenn Research Center to evaluate the effect of air and vacuum storage on the mechanical properties of x-ray-exposed FEP.

Aluminized-FEP (5-mil-thick) tensile samples were x-ray exposed with 15.3-kV copper x-rays for 2 hr, reducing the percent elongation to failure by approximately 50 percent in comparison to that for pristine Al-FEP. X-ray-exposed samples were stored in air or under vacuum for various time periods to see the effect of storage on tensile properties. Tensile results indicated that samples stored in air had larger decreases in tensile properties than samples stored under vacuum had, as seen in the graph. Samples stored under vacuum (for up to 400 hr) showed no further decrease in tensile properties over time, whereas samples stored in air (for up to 900 hr) appeared to show decreases in tensile properties over time. X-ray-exposed samples stored in air developed a hazy appearance in the exposed area, as seen in the graphs. When the source of the haziness was evaluated using scanning electron microscopy and atomic force microscopy, it was found to reside at the Al/FEP interface as witnessed by an increased surface roughness of the aluminized side



Percent elongation to failure for x-ray-exposed Al-FEP samples stored in air and under vacuum.



Development of hazy appearance in an x-ray-exposed Al-FEP sample after various durations of air storage. (a) 25 min. (b) 27 hr. (c) 118 hr.

of the material and a dramatic decrease in the adhesion between the Al and FEP. Optical properties of air-stored irradiated samples showed an increase in the diffuse reflectance, which is consistent with observed roughening that was characterized by AFM. These findings indicate that air exposure helps degrade x-ray-irradiated FEP. These results indicate that proper sample handling and storage is necessary with space-retrieved materials and with those exposed to ground-based irradiation simulation exposures.

Find out more from Glenn's Electro-Physics branch:
<http://www.grc.nasa.gov/WWW/epbranch/ephhome.htm>

Glenn contact:

Kim K. de Groh, 216-433-2297,
Kim.K.deGroh@grc.nasa.gov

Authors: Kim K. de Groh and
 Jonathan D. Gummow

Headquarters program office: OSS

Programs/Projects: HST, ISS

Effects of Vacuum Ultraviolet Radiation on Thin Polyimide Films Evaluated

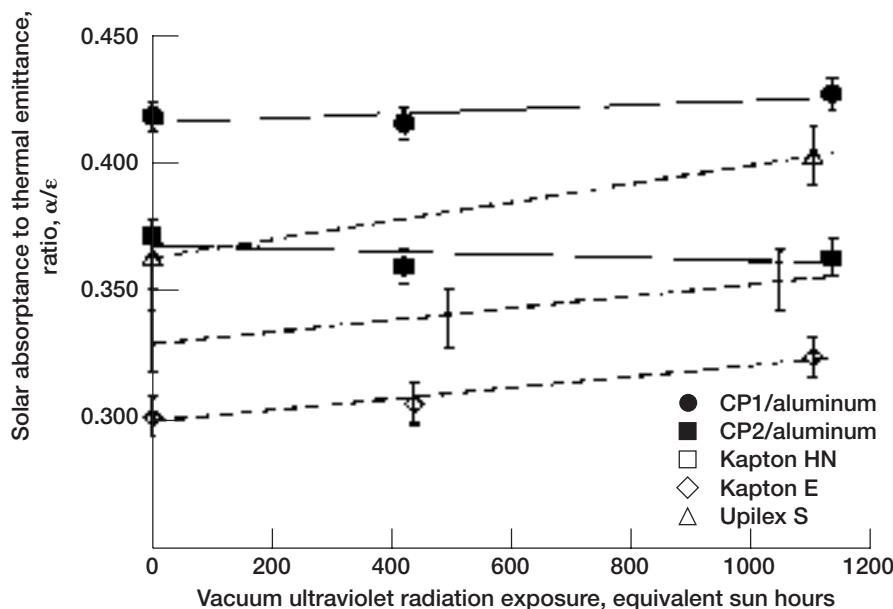
NASA anticipates launching the Next Generation Space Telescope (NGST) mission—whose purpose is to examine the origins of our universe by making measurements in the infrared portion of the spectrum—in 2009. So that the telescope can operate at very low temperatures (less than 100 K), a halo orbit about the second Lagrangian point (L2) is being considered because it is far from Earth and its reflected sunlight. The Sun-Earth L2 point is located 1.5×10^6 km from the Earth in the direction away from the Sun (ref. 1).

This mission presents new challenges in many areas of technology, including the development of a multilayer insulation sunshield for the telescope. This sunshield is required to be large (proposed dimensions of approximately 33 by 14 m), storable, deployable, and lightweight (ref. 1). In addition, its polymer film layers must be seamable, foldable, and resistant to tearing and creep, with low outgassing (ref. 1). The sunshield must

maintain its structural integrity and its Sun-facing side must maintain a low solar absorptance to thermal emittance ratio (α/ϵ) over the planned 10-yr mission duration including over 80,000 hr facing constant sunlight.

One possible configuration for the NGST sunshield uses a polymer film as thin as 12 μm , metalized on the backside, as the outermost (space-facing) layer. This outer layer will be most vulnerable to the effects of the space environment, which can degrade polymers (ref. 2). A program has been established by the NASA Goddard Space Flight Center to use ground testing to evaluate space environmental effects on candidate sunshield materials for NGST. The effects being evaluated include electron and proton radiation, vacuum ultraviolet (VUV) radiation, and micrometeoroid impacts.

The NASA Glenn Research Center is evaluating the VUV durability of the sunshield outer membrane candidate materials. Polyimide films (Kapton HN, Kapton E, and Upilex S) and fluorinated polyimide films (CP1 and CP2) being considered for the Sun-facing layer of the NGST sunshield were exposed to up to 1100 equivalent sun hours of VUV radiation. At various exposure



Solar absorptance to thermal emittance ratio for polyimide films with exposure to VUV radiation.

levels, samples were measured for changes in optical and mechanical properties. Kapton HN, Kapton E, and Upilex S all showed increases in solar absorptance and the α/ϵ ratio (see the figure), although emittance changes were not significant. In addition, all samples tested showed decreases in spectral reflectance in the ultraviolet-to-visible wavelength range, indicative of changes to the polymer chemistry even at this low exposure level that represented only approximately 1 percent of the planned 10-year NGST mission. For exposures up to 1100 equivalent sun hours of VUV radiation, no significant changes were observed in ultimate tensile strength and elongation at failure for these materials. Longer-term VUV exposure testing being conducted at Glenn will help to validate these trends and to predict the long-term performance of these materials for the NGST sunshield.

Find out more on the World Wide Web:

Glenn's Electro-Physics Branch:

<http://www.grc.nasa.gov/WWW/epbranch/ephhome.htm>

Next Generation Space Telescope: <http://ngst.gsfc.nasa.gov>

References

1. Perrygo, Charles, et al.: Passive Thermal Control of the NGST; Next Generation Space Telescope. Space Telescopes and Instruments, vols. 25–28, Pierre Y. Bely and James B. Breckinridge, eds., SPIE, Bellingham, WA, 1998.
2. Tribble, Alan C.: The Space Environment: Implications for Spacecraft Design. Princeton University Press, Princeton, NJ, 1995.

Glenn contact:

Joyce A. Dever, 216–433–6294,
Joyce.A.Dever@grc.nasa.gov

Authors: Joyce A. Dever, Russell K. Messer, Charles Powers, Jacqueline A. Townsend, and Eve Wooldridge

Headquarters program office: OSS

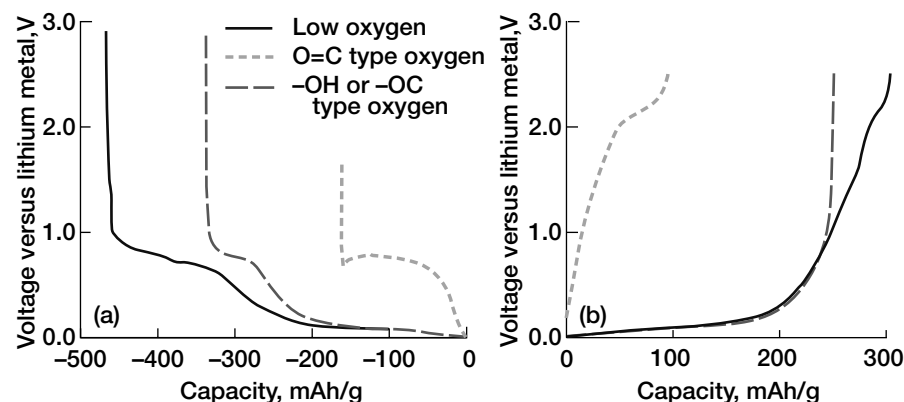
Programs/Projects: NGST

Chemical State of Surface Oxygen on Carbon and Its Effects on the Capacity of the Carbon Anode in a Lithium-Ion Battery Investigated

In a lithium-ion battery, the lithium-storage capacity of the carbon anode is greatly affected by a surface layer formed during the first half cycle of lithium insertion and release into and out of the carbon anode. The formation of this solid-electrolyte interface, in turn, is affected by the chemistry of the carbon surface. A study at the NASA Glenn Research Center examined the cause-and-effect relations. Information obtained from this research could contribute in designing a high-capacity lithium-ion battery and, therefore, small, powerful spacecraft.

In one test, three types of surfaces were examined: (1) a surface with low oxygen content (1.5 at.%) and a high concentration of active sites, (2) a

surface with 4.5 at.% –OH or –OC type oxygen, and (3) a surface with 6.5 at.% O=C type oxygen. The samples were made from the same precursor and had similar bulk properties. They were tested under a constant current of 10 mA/g in half cells that used lithium metal as the counter electrode and 0.5 M lithium iodide in 50/50 (vol %) ethylene carbonate and dimethyl carbonate as the electrolyte.



Voltage of carbon anodes (with different surfaces) versus lithium metal. Left: During the first half cycle of lithium insertion. Right: During the first half cycle of lithium release.

For the first cycle of the electrochemical test, the graph describes the voltage of the carbon anode versus the lithium metal as a function of the capacity (amount of lithium insertion or release). From these data, it can be observed that the surface with low oxygen and a high concentration of active sites could result in a high irreversible capacity. Such a high irreversible capacity could be prevented if the active sites were allowed to react with oxygen in air, producing –OH or –OC type

TABLE I.—CAPACITIES OF LITHIUM INSERTION AND RELEASE FOR CARBON
WITH DIFFERENT SURFACES AND SIMILAR BULK STRUCTURE

Sample	Surface oxygen		Active sites concentration	Irreversible capacity, mAh/g	Reversible capacity, mAh/g	
	Chemical state	Content, at. %			Capacity contributed by intercalation, <i>I</i>	Capacity not contributed by intercalation, <i>NI</i>
A	—OH or —OC	1.5	High	163	169	135
B	—OH or —OC	4.5	Low	85	174	78
C	O=C	6.5	Low	66	0	95

oxygen. The O=C type oxygen, on the other hand, could greatly reduce the capacity of lithium intercalation and, therefore, needs to be avoided during battery fabrication.

Glenn contact:

Dr. Ching-cheh Hung, 216–433–2302, Ching-Cheh.Hung@grc.nasa.gov

Author: Dr. Ching-cheh Hung

Headquarter program office:
OSS (ATMS)

Programs/Projects:
Space Power Technology

Surface Texturing Investigated for a High Solar Absorptance Low Infrared Emittance Solar Collector

The objective of this work was to design, build, and vacuum test a high solar absorptance, low infrared emittance solar collector for heat engine and thermal switching applications. Minisatellites proposed by the Applied Physics Laboratory for operation in environments that are subject to radiation threat may utilize a heat engine for power and a thermal bus for thermal control. To achieve this goal, a surface having high solar absorptance and low infrared emittance is needed. At the NASA Glenn Research Center, one concept being pursued to achieve this goal is texturing high thermal conductivity graphite epoxy composites using a directed atomic oxygen beam and then coating the textured surface with a reflective metallic coating.

Coupons were successfully textured, coated, and evaluated. A variety of texturing conditions were explored, and textures were documented by scanning electron microscopy. Copper, gold, silver, iridium, and aluminum coatings were applied, and the highest solar absorptance to infrared emittance ratio was found to be 1.3. A full-sized solar collector was manufactured with this ratio, and the amount of heat collected was observed using an Inconel calorimeter installed in a bench-top vacuum chamber equipped with a solar simulator. Results to date indicate good heat flow through the system, with 9 W of heat flow measured by the calorimeter.

For more information, visit Glenn's Electro-Physics Branch:
<http://www.grc.nasa.gov/WWW/epbranch/ephhome.htm>



Water-cooled Inconel 718 calorimeter and atomic-oxygen-textured solar collector.

Glenn contacts: Dr. Donald A. Jaworske, 216–433–2312,
Donald.A.Jaworske@grc.nasa.gov

Author: Dr. Donald A. Jaworske
Headquarters program office:
OSS (ATMS)

Programs/Projects: SRF

International Test Program for Synergistic Atomic Oxygen and Vacuum Ultraviolet Radiation Exposure of Spacecraft Materials

The components and materials of spacecraft in low Earth orbit can degrade in thermal and optical performance through interaction with atomic oxygen and vacuum ultraviolet (VUV) radiation, which are predominant in low Earth orbit. Because of the importance of low Earth orbit durability and performance to manufacturers and users, an international test program for assessing the durability of spacecraft materials and components was initiated. Initial tests at the NASA Glenn Research Center consisted of exposure of samples representing a variety of thermal control paints, multilayer insulation materials, and Sun sensors that have been used in space. Materials donated from various international sources were tested alongside materials whose performance is well known, such as Teflon FEP, Kapton H, or Z-93-P white paint. The optical, thermal, or mass loss data generated during the tests were then provided to the participating material suppliers. Data were not published unless the participant donating the material consented to publication. The test program is intended to give spacecraft builders and users a better understanding of degradation processes and effects so that they can improve their predictions of spacecraft performance.

Glenn contacts:

Sharon K. Miller, 216-433-2219, Sharon.K.Miller@grc.nasa.gov;
Bruce A. Banks, 216-433-2308, Bruce.A.Banks@grc.nasa.gov; and
Joyce A. Dever, 216-433-6294, Joyce.A.Dever@grc.nasa.gov

Author: Sharon K. Miller

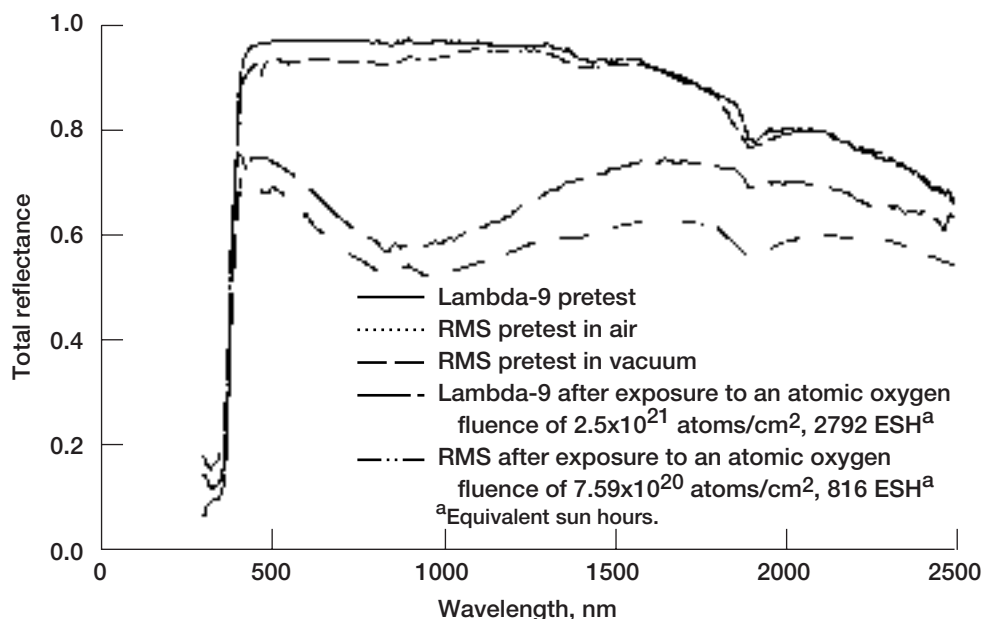
Headquarters program office: OAT

Programs/Projects:

ISS, other low-Earth-orbit satellites

Find out more from Glenn's Electro-Physics Branch:

<http://www.grc.nasa.gov/WWW/epbranch/ephome.htm>



Example of reflectance data generated for a PSB silicate white paint from France.

Electronics for Low-Temperature Space Operation Being Evaluated

Electronic components and systems capable of low-temperature operation are needed for many future NASA missions where it is desirable to have smaller, lighter, and cheaper (unheated) spacecraft. These missions include Mars (-20 to -120 °C) orbiters, landers, and rovers; Europa (-150 °C) oceanic exploratory probes and instrumentation; Saturn (-183 °C) and Pluto (-229 °C) interplanetary probes.

At the present, most electronic equipment can operate down to only -55 °C. It would be very desirable to have electronic components that expand the operating temperature range down to -233 °C. The successful development of these low-temperature components will eventually allow space probes and onboard electronics to operate in very cold environments (out as far as the planet Pluto). As a result, radioisotope heating units, which are used presently to keep space electronics near room temperature, will be reduced in number or eliminated. The new cold electronics will make spacecraft design and operation simpler, more flexible, more reliable, lighter, and cheaper.

Researchers at the NASA Glenn Research Center are evaluating potential commercial off-the-shelf devices and are developing new electronic components that will tolerate operation at low temperatures down to -233 °C. This work is being carried out mainly in-house and also through university grants and commercial contracts. The components include analog-to-digital converters, semiconductor switches, capacitors, dielectric and packaging material, and batteries. For example, the effect of low temperature on the capacitance of three different types of capacitors is shown in the graph. Using these advanced components, system products will be developed,

including dc/dc converters, battery charge/discharge management systems, digital control electronics, transducers, and sensor instrumentation.

The Low Temperature Electronics Program at Glenn collaborates with other Government agencies, industrial and aerospace companies, and academia. It supports missions and development programs at the Jet Propulsion Laboratory, the NASA Goddard Space Flight Center, and the NASA Langley Research Center.

To find out more, visit us on the World Wide Web:

<http://www.grc.nasa.gov/WWW/epbranch/ephome.htm>

Glenn contact:

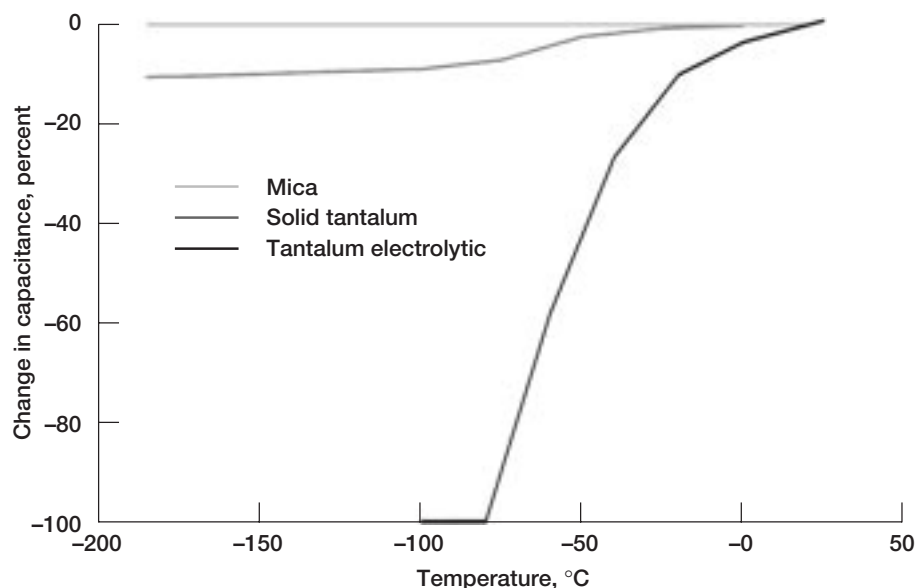
Richard L. Patterson, 216-433-8166,
Richard.L.Patterson@grc.nasa.gov

Authors: Richard L. Patterson and
Ahmad Hammoud

Headquarters program office: CETDP

Programs/Projects:

Galex, NGST, CloudSat, CETDP



Change in capacitance due to low temperature for mica, solid tantalum, and liquid electrolytic tantalum capacitors.

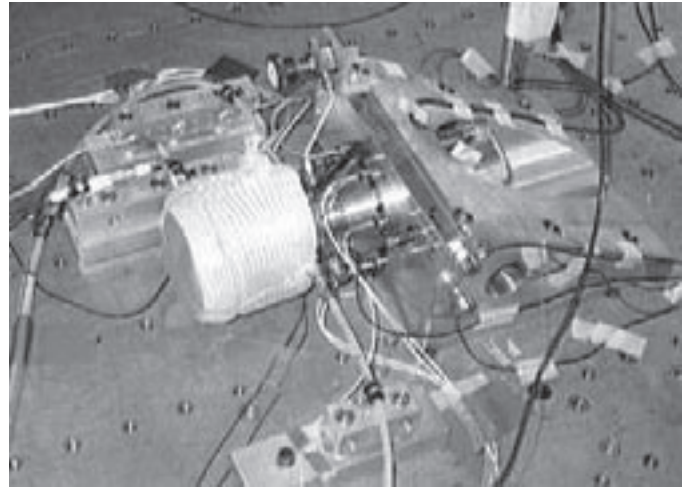
Assessment of Stirling Technology Has Provided Critical Data Leading Toward Flight Readiness of the Stirling Converter

The NASA Glenn Research Center is supporting the development of a Stirling converter with the Department of Energy (DOE, Germantown, Maryland) for an advanced Stirling Radioisotope Power System (SRPS) to provide spacecraft onboard electric power for NASA space science missions. A key technology assessment completed by Glenn and DOE has led to the SRPS being identified as a high-efficiency power source for such deep space missions as the Europa Orbiter and the Solar Probe. In addition, the Stirling system is now being considered for unmanned Mars rovers, especially where mission profiles may exclude the use of photovoltaic power systems, such as exploration at high Martian latitudes or for missions of long duration.

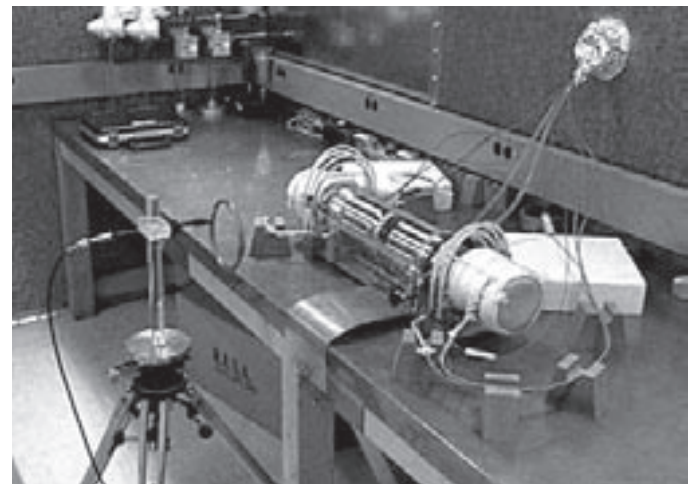
The SRPS efficiency of over 20 percent will reduce the required amount of radioisotope by more than a factor of 3 in comparison to current radioisotope thermoelectric generators. This significantly reduces radioisotope cost, radiological inventory, and system cost, and it provides efficient use of scarce radioisotope resources.

In support of this technology assessment, Glenn conducted a series of independent evaluations and tests to determine the technology readiness of a 55-We Stirling converter developed by Stirling Technology Company (Kennewick, Washington) and DOE. Key areas evaluated by Glenn included (1) radiation tolerance of materials, (2) random vibration testing of the Stirling converter in Glenn's Structural Dynamics Lab to simulate operation in the launch environment, (3) electromagnetic interference and compatibility (EMI/EMC) of the converter operating in Glenn's EMI lab, (4) independent failure modes, effects, and criticality analysis, and life and reliability assessment, and (5) SRPS cost estimate. The data from these evaluations were presented to NASA Headquarters and the Jet Propulsion Laboratory mission office by a joint industry/Government team consisting of DOE, Glenn, and Lockheed Martin Astronautics. This team concluded that there are no technical reasons that would rule out using the Stirling converter for deep space missions.

As a direct result of the successful testing at Glenn, the DOE/Stirling Technology Company 55-We Stirling converter has been baselined for the SRPS. Glenn is now continuing an in-house project to assist in developing the Stirling converter for readiness for space qualification and mission implementation. As part of this effort, the Stirling converter will be further characterized under launch environment random vibration testing, methods to reduce converter EMI will be developed, and an independent performance verification will be completed. Converter life assessment and permanent



Launch environment testing of Stirling converter.



Stirling converter EMI/EMC characterization.

magnet aging characterization tasks are also underway. Substitute organic materials for the linear alternator and piston bearing coatings for use in a high-radiation environment have been identified and have now been incorporated in Stirling converters built by Stirling Technology Company for Glenn. Electromagnetic and thermal finite element analyses for the alternator are also being conducted.

Find out more about this research on the World Wide Web:

Glenn's Thermo-Mechanical Systems Branch:

<http://www.grc.nasa.gov/WWW/tmsb>

Glenn's Structural Dynamics Laboratory:

<http://www.grc.nasa.gov/WWW/SDL/Home.html>

References

1. Furlong, Richard; and Shaltens, Richard: Technology Assessment of DoE's 55-We Stirling Technology Demonstrator Convertor (TDC). AIAA Paper 2000-3018 (NASA/TM-2000-210509, <http://gltrs.grc.nasa.gov/GLTRS>), 2000.
2. Thieme, Lanny G.; and Schreiber, Jeffrey G.: NASA GRC Technology Development Project for a Stirling Radioisotope Power System. AIAA Paper 2000-2840, 2000.
3. Goodnight, T.W.; Hughes, W.O.; and McNelis, M.E.: Dynamic Capability of an Operating Stirling Convertor. AIAA Paper 2000-2839 (NASA/TM-2000-210527, <http://gltrs.grc.nasa.gov/GLTRS>), 2000.

Glenn contacts:

Richard K. Shaltens, 216-433-6138, Richard.K.Shaltens@grc.nasa.gov;
Jeffrey G. Schreiber, 216-433-6144, Jeffrey.G.Schreiber@grc.nasa.gov; and
Lanny G. Thieme, 216-433-6119, Lanny.G.Thieme@grc.nasa.gov

Author: Lanny G. Thieme

Headquarters program office: OSS

Programs/Projects: Stirling Radioisotope Power System, Outer Planets/Solar Probe Project, Mars Rover

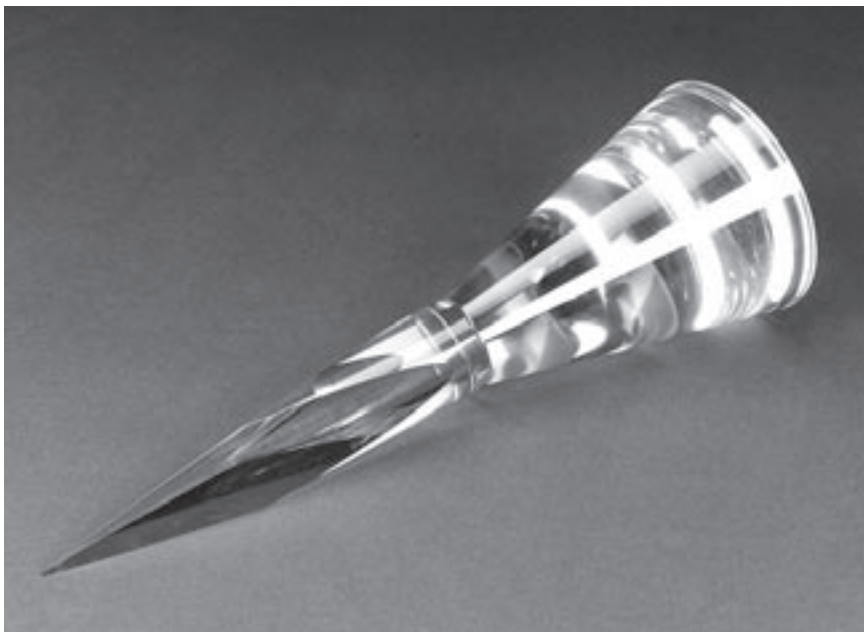
High-Efficiency Solar Thermal Vacuum Demonstration Completed for Refractive Secondary Concentrator

Common to many of the space applications that utilize solar thermal energy—such as electric power conversion, thermal propulsion, and furnaces—is a need for highly efficient, solar concentration systems. An effort is underway at the NASA Glenn Research Center to develop the refractive secondary concentrator, which uses refraction and total internal reflection to efficiently concentrate and direct solar energy. When used in combination with advanced lightweight primary concentrators, the refractive secondary concentrator enables very high system concentration ratios (10,000 to 1) and very high temperatures (>2000 K).

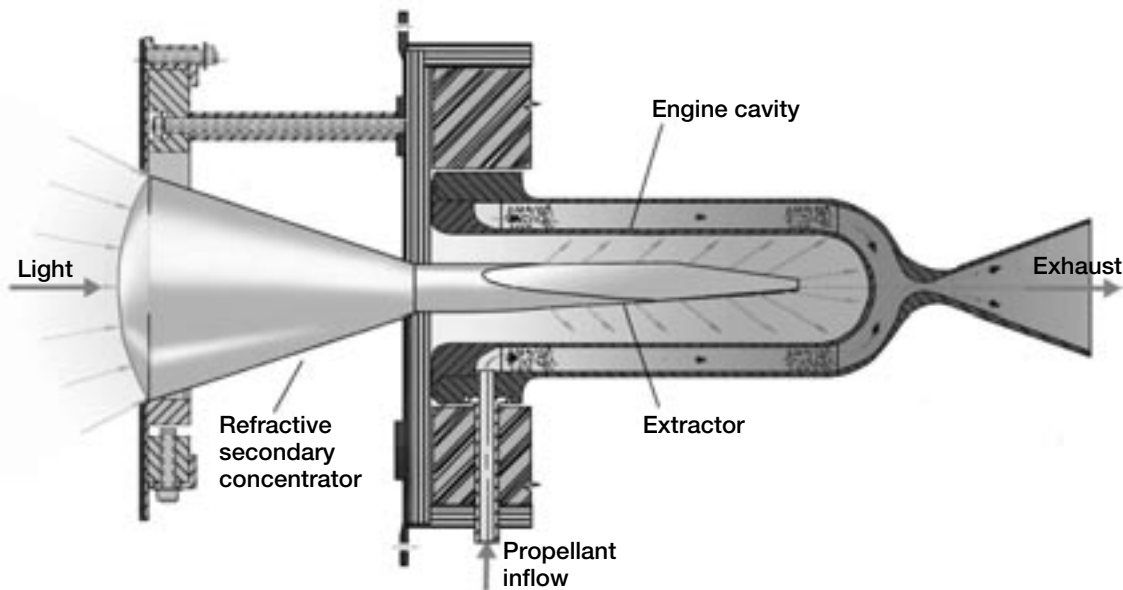
The innovative refractive secondary concentrator offers significant advantages over all other types of secondary concentrators. The refractive secondary offers the highest throughput efficiency, provides for flux tailoring, requires no active cooling, relaxes the pointing and tracking requirements of the primary concentrator, and enables very high system concentration ratios. This technology has broad applicability to any system that requires the conversion of solar energy to heat. Glenn initiated the development of the refractive secondary concentrator in support of Shooting Star, a solar thermal propulsion flight experiment, and continued the development in support of Space Solar Power.

Glenn's Thermo-Mechanical Systems Branch has completed a performance evaluation of a prototype refractive secondary concentrator in Glenn's Tank 6 solar thermal vacuum facility

using a low-temperature liquid-cooled calorimeter. The effort involved the design and fabrication of a sapphire refractive secondary concentrator, design and fabrication of a calorimeter and its support systems, calibration of the calorimeter, on-sun vacuum testing of the refractive secondary, and comparing the test results with modeling predictions.



The sapphire refractive secondary concentrator enables high-temperature solar power and propulsion applications.



The refractive secondary concentrator provides efficient delivery of solar energy to a solar thermal propulsion engine.

The prototype refractive secondary concentrator, measuring 3.5 in. in diameter and 11.2 in. long, was designed for the Tank 6 facility and the existing primary concentrator/solar simulator system. Ray trace optics software was used to model the secondary concentrator, resulting in a predicted efficiency of 90 percent without an antireflective coating. For the test, input power to the refractive secondary ranged between 400 to 1200 W. Test results indicate an average throughput efficiency of 87 percent, which agrees well with the modeling predictions. We anticipate that using an antireflective coating to reduce the reflection loss at the inlet surface of the concentrator would result in a secondary concentrator throughput efficiency of approximately 93 percent. Potential future activities to further develop the technology include high-temperature, high-power throughput tests, antireflective coating tests, and additional material characterization and interaction tests.

**Find out more about Glenn's
Secondary Solar Concentrators:**

<http://www.grc.nasa.gov/WWW/tmsb/secondconc.html>

Glenn contact:

Wayne A. Wong, 216-433-6318,
Wayne.A.Wong@grc.nasa.gov

Author: Wayne A. Wong

Headquarters program office: OSF

Programs/Projects: SERT, ASTP

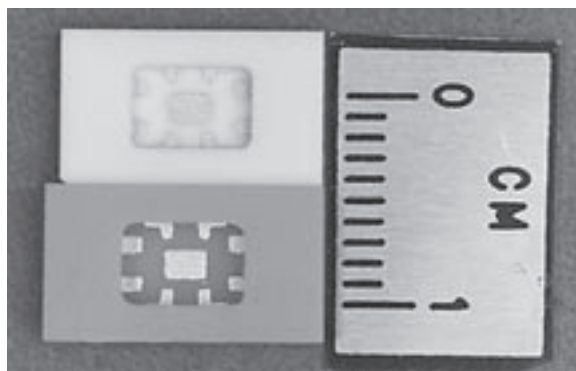
Instrumentation and Controls

Packaging Technology Developed for High-Temperature Silicon Carbide Microsystems

High-temperature electronics and sensors are necessary for harsh-environment space and aeronautical applications, such as sensors and electronics for space missions to the inner solar system, sensors for in situ combustion and emission monitoring, and electronics for combustion control for aeronautical and automotive engines. However, these devices cannot be used until they can be packaged in appropriate forms for specific applications. Suitable packaging technology for operation temperatures up to 500 °C and beyond is not commercially available. Thus, the development of a systematic high-temperature packaging technology for SiC-based microsystems is essential for both in situ testing and commercializing high-temperature SiC sensors and electronics.

In response to these needs, researchers at Glenn innovatively designed, fabricated, and assembled a new prototype electronic package for high-temperature electronic microsystems using ceramic substrates (aluminum nitride and aluminum oxide) and gold (Au) thick-film metallization (see the figure). Packaging components include a ceramic packaging frame, thick-film metallization-based interconnection system, and a low-electrical-resistance SiC die-attachment scheme. Both the materials and fabrication process of the basic packaging components have been tested with an in-house-fabricated SiC semiconductor test chip in an oxidizing environment at temperatures from room temperature to 500 °C for more than 1000 hr. These test results set lifetime records for both high-temperature electronic packaging and high-temperature electronic device testing.

As required, the thick-film-based interconnection system demonstrated low (2.5 times of the room-temperature resistance of the Au conductor) and stable (decreased 3 percent in 1500 hr of continuous testing) electrical resistance at 500 °C in an oxidizing environment. Also as required, the electrical isolation impedance between printed wires that were not electrically joined by a wire bond remained high ($>0.4 \text{ G}\Omega$) at 500 °C in air. The attached SiC diode demonstrated low ($< 3.8 \text{ }\Omega/\text{mm}^2$) and relatively consistent dynamic resistance from room temperature to 500 °C. These results indicate that the prototype package and the compatible die-attach scheme meet the initial design standards for high-temperature, low-power, and long-term operation. This technology will be further developed and evaluated, especially with more mechanical tests of each packaging element for operation at higher temperatures and longer lifetimes.



Prototype high-temperature electronic package composed of ceramic substrates and Au thick-film metallization being developed for SiC microsystems with sensors and electronic devices.

Find out more about this research:
<http://www.grc.nasa.gov/WWW/sensors/>

A.Y.T. Corporation contact:
Dr. Liang-Yu Chen, 216-433-6458,
Liangyu.Chen@grc.nasa.gov

Glenn contact:
Dr. Gary W. Hunter, 216-433-6459,
Gary.W.Hunter@grc.nasa.gov

Glenn/U.S. Army Research Laboratory contact:
Dr. Jih-Fen Lei, 216-433-6328,
Jih-Fen.Lei@grc.nasa.gov

Authors: Dr. Liang-Yu Chen, Dr. Gary W. Hunter, and Dr. Philip G. Neudeck

Headquarters program office:
OAT, OSS

Programs/Projects: GMI, NEPP

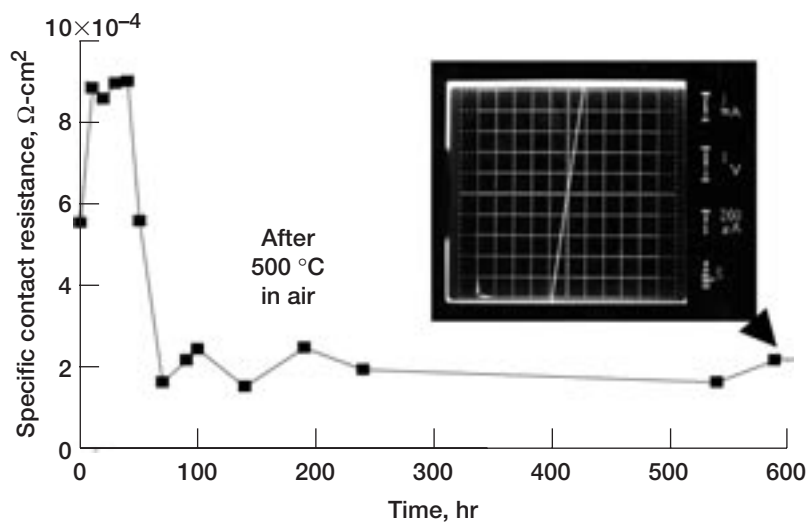
Thermally Stable Ohmic Contacts on Silicon Carbide Developed for High-Temperature Sensors and Electronics

The NASA aerospace program, in particular, requires breakthrough instrumentation inside the combustion chambers of engines for the purpose of, among other things, improving computational fluid dynamics code validation and active engine behavioral control (combustion, flow, stall, and noise). This environment can be as high as 600 °C, which is beyond the capability of silicon and gallium arsenide devices. Silicon-carbide- (SiC-) based devices appear to be the most technologically mature among wide-bandgap semiconductors with the proven capability to function at temperatures above 500 °C. However, the contact metalization of SiC degrades

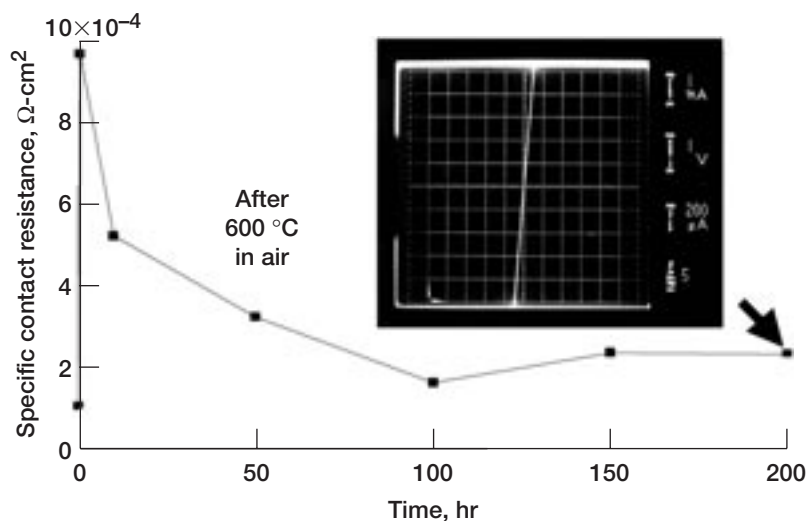
severely beyond this temperature because of factors such as the interdiffusion between layers, oxidation of the contact, and compositional and microstructural changes at the metal/semiconductor interface. These mechanisms have been proven to be device killers. Very costly and weight-adding packaging schemes that include vacuum sealing are sometimes adopted as a solution.

Research work at the Sensors and Electronics Branch of NASA Glenn Research Center's Instrumentation and Controls Division has demonstrated thermally stable I-V characteristics and contact resistance of Ti(100nm)/TaSi₂(200nm)/Pt(300nm) ohmic contact metalization on n-type 6H-SiC after 500 °C and 600 °C treatment in air for over 600 hr (top figure) and over 200 hr (bottom figure), respectively. Auger electron spectroscopy and high-resolution transmission electron microscopy were used to analyze the metal and semiconductor interfaces to understand the prevailing reactions. The thermal stability of the ohmic contact in air is believed to be due to the formation of silicides and carbides of titanium after being initially annealed at 600 °C in N₂ for 30 min. Most importantly, the oxidation of silicon species is proposed to be the critical diffusion barrier mechanism that prevents further oxygen penetration into the metalization.

These results had an immediate impact on ongoing research in SiC sensors and electronics projects. Real operating environment testing of SiC devices with this metalization scheme is planned. This contact scheme is expected to have



Specific contact resistance of Ti/TaSi₂/Pt on an n-type SiC epilayer measured after a 500 °C treatment in air. The inset shows the corresponding I-V characteristics after 640 hr, showing excellent linear behavior.



Specific contact resistance of Ti/TaSi₂/Pt on an n-type SiC measured after a 600 °C treatment in air. The inset shows the corresponding I-V characteristics after 200 hr, showing excellent linear behavior.

the following attributes: (1) ohmic contact with reasonably low contact resistance relative to the bulk epilayer, (2) long-term contact stability in the harsh environment, (3) compatibility with SiC large-scale integrated fabrication technology, (4) good wirebond strength, and (5) compatibility with high-temperature interconnect and packaging technology.

Glenn contact:

Dr. Robert S. Okojie, 216-433-6522,
Robert.S.Okojie@grc.nasa.gov

Author: Dr. Robert S. Okojie

Headquarters program office: OSS

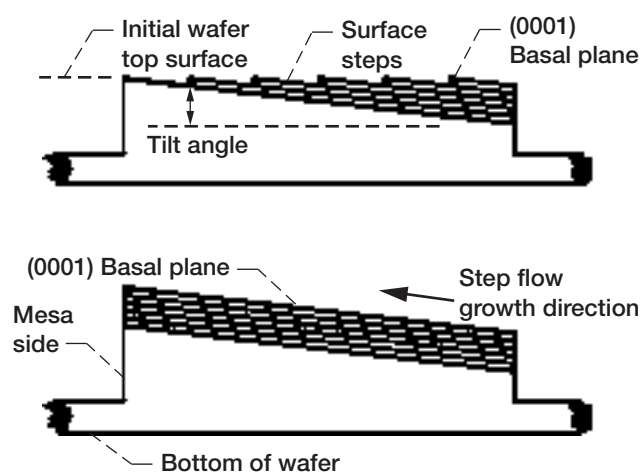
Programs/Projects: GMI

Atomically Flat Surfaces Developed for Improved Semiconductor Devices

New wide bandgap semiconductor materials are being developed to meet the diverse high-temperature, -power, and -frequency demands of the aerospace industry. Two of the most promising emerging materials are silicon carbide (SiC) for high-temperature and high-power applications and gallium nitride (GaN) for high-frequency and optical (blue-light-emitting diodes and lasers) applications. This past year Glenn scientists implemented a NASA-patented crystal growth process for producing arrays of device-size mesas whose tops are atomically flat (i.e., step-free). It is expected that these mesas can be used for fabricating SiC and GaN devices with major improvements in performance and lifetime.

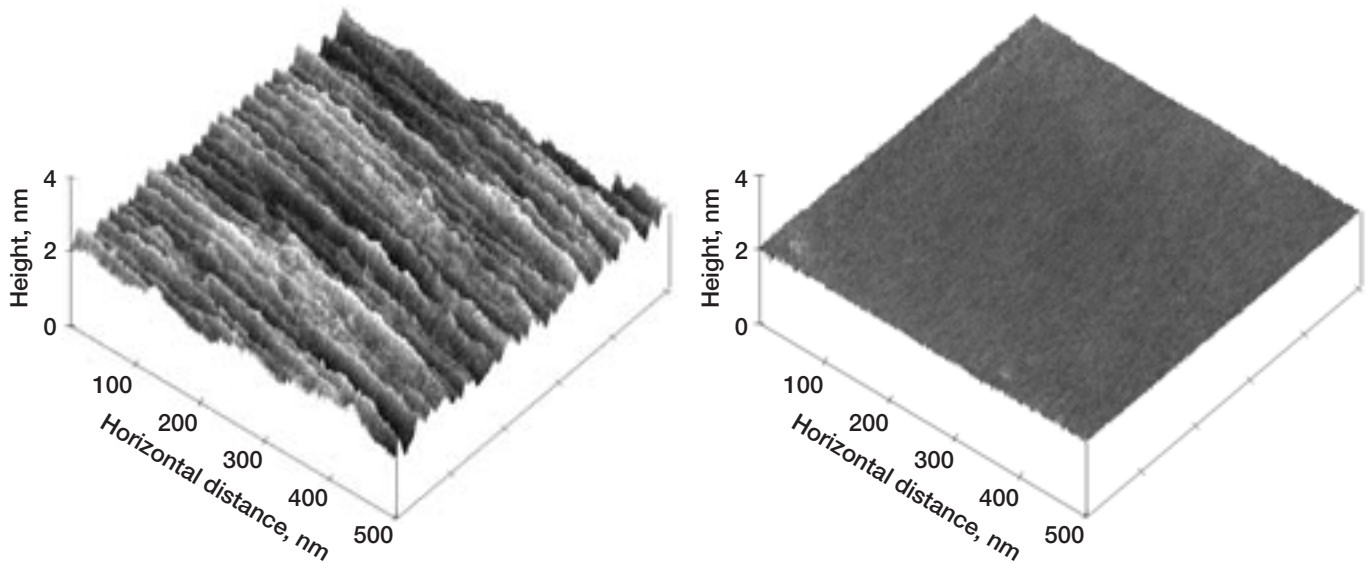
The promising new SiC and GaN devices are fabricated in thin-crystal films (known as epi films) that are grown on commercial single-crystal SiC wafers. At this time, no commercial GaN wafers exist. Crystal defects, known as screw defects and micropipes, that are present in the commercial SiC wafers propagate into the epi films and degrade the performance and lifetime of subsequently fabricated devices. The new technology isolates the screw defects in a small percentage of small device-size mesas on the surface of commercial SiC wafers. This enables atomically flat surfaces to be grown on the remaining defect-free mesas. We believe that the atomically flat mesas can also be used to grow GaN epi films with a much lower defect density than in the GaN epi films currently being grown. Much improved devices are expected from these improved low-defect epi films. Surface-sensitive SiC devices such as Schottky diodes and field effect transistors should benefit from atomically flat substrates. Also, we believe that the atomically flat SiC surface will be an ideal surface on which to fabricate nanoscale sensors and devices.

The preceding figure illustrates the process for achieving atomically flat surfaces. The top part illustrates the surface steps present on the “as-received” commercial SiC wafer because of the small tilt angle between the crystal “basal” plane and the polished wafer surface. These steps are used in normal SiC epi film growth in a process known as step-flow growth to produce material for device fabrication. In the new process,



Growth of atomically flat mesas. Top: Before growth, the initial mesa surface (parallel to the bottom of the wafer surface) contains steps due to the tilt of the basal plane with respect to the polished wafer surface. Bottom: After growth, steps have been grown out of existence, leaving a step-free mesa surface parallel to the basal plane (i.e., tilted with respect to the initial surface).

the first step is to etch an array of mesas on the SiC wafer top surface. Then, epi film growth is carried out in the step flow fashion until all steps have grown themselves out of existence on each defect-free mesa. If the size of the mesas is sufficiently small (about 0.1 by 0.1 mm), then only a small percentage of the mesas will contain an undesired screw defect. Mesas with screw defects supply steps during the growth process, allowing a rough surface with unwanted hillocks to form on the mesa.



Atomic force microscope images of two epi-layer surfaces on 4H-SiC wafers. Left: Typical commercial SiC epi-layer surface. Right: Atomically flat (step-free) epi-layer surface grown at Glenn.

The figure above illustrates the improvement in SiC epi surface morphology achievable with the new technology. The left figure is an atomic force microscope image of a typical SiC commercial epi-layer surface. The right figure is a similar image of an SiC atomically flat epi surface grown in a Glenn laboratory. With the current screw defect density of commercial wafers (about 5000 defects/cm²), the yield of atomically free 0.1 by 0.1 mm mesas is expected to be about 90 percent. This is large enough for many types of electronic and optical devices. The implementation of this new technology was recently published in *Applied Physics Letters*.

This work was initially carried out in-house under a Director's Discretionary Fund project and is currently being further developed under the Information Technology Base Program.

Find out more about this research on the World Wide Web:
<http://www.grc.nasa.gov/WWW/SiC/SiC.html>

Bibliography

Powell, J.A.; et al.: Growth of Step-Free Surfaces on Device-Size (0001) SiC Mesas. *Appl. Phys. Letters*, vol. 77, no. 10, 2000, pp. 1449–1451.

Powell, J. Anthony, et al.: Method for Growth of Crystal Surfaces and Growth of Heteroepitaxial Single Crystal Films Thereon. U.S. Patent 5,915,194, June 1999.

Glenn contact:

J. Anthony Powell, 216–433–3652,
J.A.Powell@grc.nasa.gov

Author: J. Anthony Powell

Headquarters program office:
 Funded through Glenn's DDF

Program/Projects: ISCO, IT Base

Borescope Imaging System Developed for Luminescent Paint Measurements

The luminescent paint measurement technique utilizes a coating that is applied to a test article, allowing the air pressure or temperature of a surface to be measured. These coatings are commonly referred to as pressure- or temperature-sensitive paints.

These paints are excited with short wavelength light and emit light at a longer wavelength. By measuring the change of intensity of the emitted light from a known reference condition, researchers can determine the pressure or temperature.

The technique of measuring full-field surface pressure and temperatures using luminescent coatings has required a direct line-of-sight from the camera to the surface under study. In most experiments that have used pressure- or temperature-sensitive paints, the test surfaces are mounted so it is straightforward to position the camera and excitation source. In other cases, the luxury of having optical access through a window is not available or even possible. We developed a borescope imaging system to gain optical access in these confined areas.

The commercially available 10-mm-diameter rigid borescope contains relay optics to transmit the detected light to a charge-coupled device (CCD) camera as well as an internal fiber-optic light guide to provide the excitation source for the luminescent coatings. The coupled light source can be continuous for the intensity method but also can be pulsed or have a variable intensity for a newer method of acquisition that measures the decay or phase lag of the emitted light. This type of borescope focuses the image directly on the CCD chip without using a fiber-optic relay, eliminating unwanted honeycomb patterns that are typical of fiber-optic type borescopes. This produces images of much higher clarity and uniformity, which are critical for acquiring accurate measurements from the luminescent coatings.

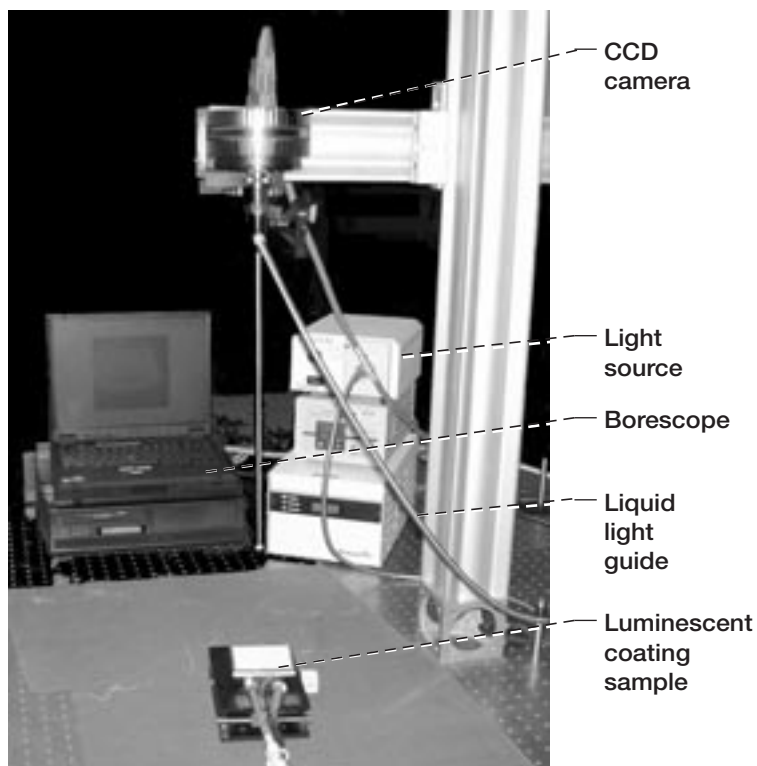
Find out more about Glenn's work with pressure-sensitive paints: <http://www.grc.nasa.gov/WWW/OptInstr/psp.html>

Glenn contact: Timothy J. Bencic, 216-433-5690, Timothy.J.Bencic@grc.nasa.gov

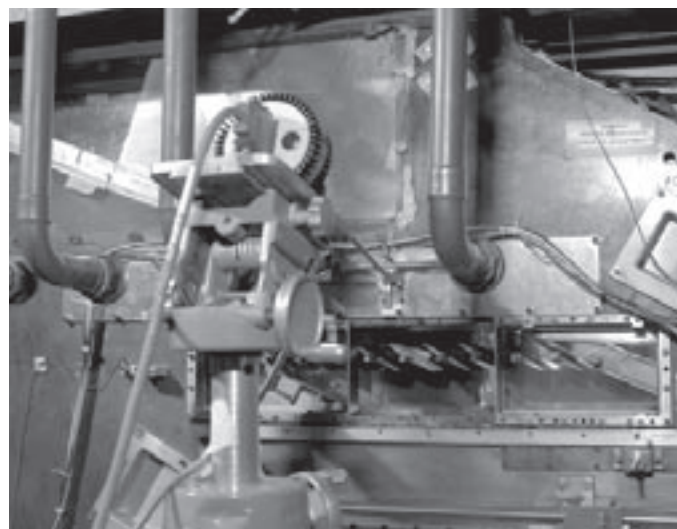
Author: Timothy J. Bencic

Headquarters program office: OAT

Programs/Projects: IT Base



Borescope imaging system configured for making intensity-based pressure-sensitive paint measurements.



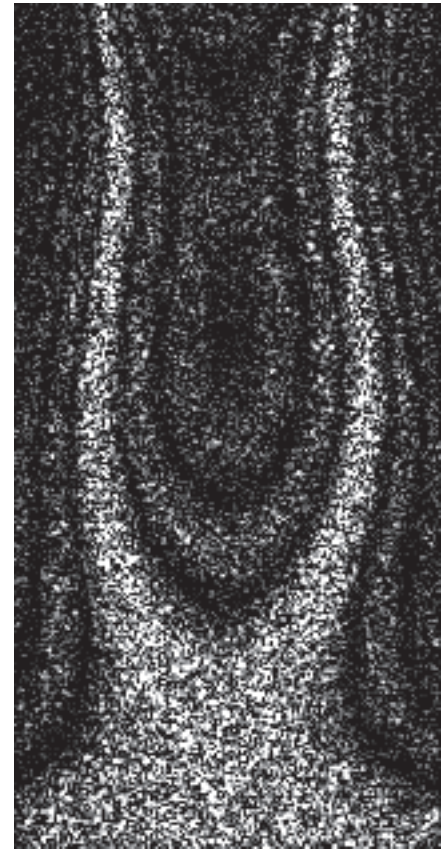
Borescope imaging system being used to gain a full perpendicular view to the painted blade surface in a Glenn research rig.

Training Data Optimized and Conditioned to Learn Characteristic Patterns of Vibrating Blisks and Fan Blades

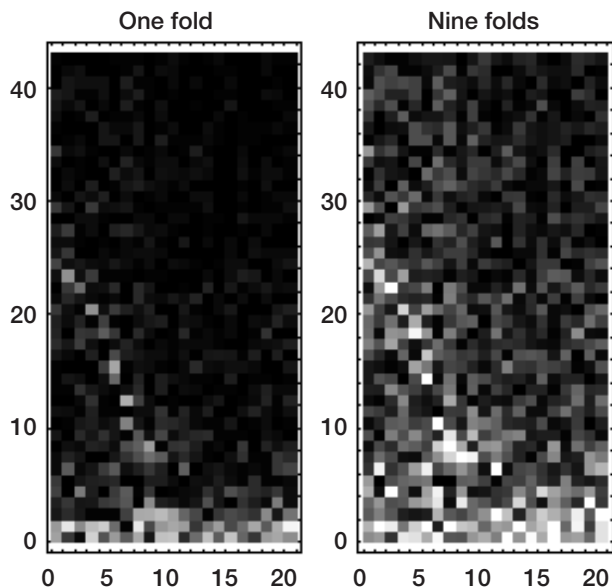
At the NASA Glenn Research Center, we have been training artificial neural networks to interpret the characteristic patterns (see the image to the right) generated from electronic holograms of vibrating structures. These patterns not only visualize the vibration properties of structures, but small changes in the patterns can indicate structural changes, cracking, or damage (refs. 1 and 2). Neural networks detect these small changes well. Our objective has been to adapt the neural-network, electronic-holography combination for inspecting components in Glenn's Spin Rig.

This project has generated an excellent beginning for answering a very important question for NASA's growing involvement with intelligent systems: Given any technology or process such as an artificial neural network, how do you impose a useful intelligence on that technology in an optimum manner? Artificial neural networks are trained by example, using a so-called training set, and training-set-educated systems are popular in general. Optimum training means that the technology learns the training set quickly, learns to distinguish small, but significant, variations in the input patterns, learns to handle noisy data, does not overtrain (overfit the training data), and learns, consequently, to generalize (correctly interpret patterns not in the original training set). Electronic holography of structures is especially useful for testing approaches for training, since models can be used to generate statistically realistic, although far from perfect (ref. 3), training sets.

Two questions must be answered in preparing training data for any technology: How do you condition the data optimally for the particular technology, and how do you generate statistically optimum training sets in general? We have developed a technique called folding for conditioning characteristic patterns for optimum training of feedforward neural net-



Characteristic pattern or mode shape of a vibrating blade. Note that the laser speckle effect causes a large intensity fluctuation about the local average.



Finite-element-resolution characteristic patterns before and after folding.

works. For image processing using feedforward neural networks, the data are usually normalized so that each input node covers the same range. A common practice is to use a minimum-maximum table, where the data for each pixel are scaled into the range -1 to 1 . Neural networks trained in this way learn more quickly, but they are prone to overfit the data. Folding, by contrast, divides the data into intensity ranges, and it scales each range into the full input range of the neural network. The laser speckle effect (the noise covering the image above) has a considerable variation about the average

intensity, which ensures that all the positions on the image participate in all folding ranges, whereas the minimum-maximum table imposes an image-position-dependent scaling. The folding-trained networks learn more quickly, are better able to distinguish between damaged and undamaged blades, and generalize better. The figure at the bottom of the previous page shows a finite-element-resolution node pattern for a blade vibrating in its first mode before and after folding. The final figure shows the training and test errors as a function of the number of folds.

The discovery of hardware that can emulate intelligent behavior is expected to be fortuitous. The discovery of effective, if not optimum, training procedures for specific kinds of data will provide the practical challenge. Neural-network processing of speckled fringe patterns from vibrating structures provides an excellent theoretical and experimental testbed for this work.

Find out more about this research:

<http://nesb.larc.nasa.gov/NNWG/VOL7.2/TASKS/GRC/grc722.html>

References

1. Decker, Arthur J. et al.: Vibrational Analysis of Engine Components Using Neural-Net Processing and Electronic Holography. AGARD-CP-598, 1997, pp. 33-1-33-6.
2. Decker, Arthur J.; Melis, Matthew E.; and Weiland, Kenneth E.: Inspection of Space Station Cold Plate Using Visual and Automated Holographic Techniques. NASA/TM-1999-209388, 1999. <http://gltrs.grc.nasa.gov/GLTRS>
3. Mahajan, Ajay: Intelligent Sensor Models With Learning Capabilities. Chapt. 7.1, Automation, Miniature Robotics and Sensors for Nondestructive Testing and Evaluation, vol. 4, Yoseph Bar-Cohen, ed., 2000, pp. 281-299.

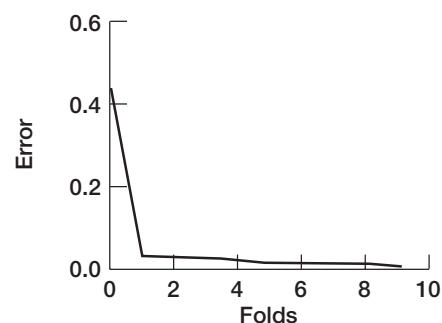
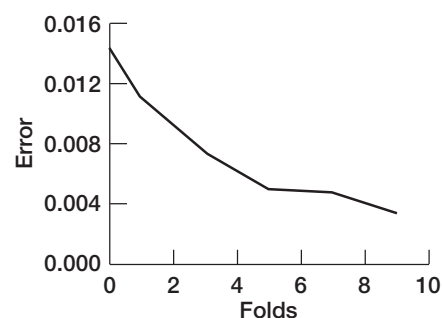
Glenn contact: Dr. Arthur J. Decker, 216-433-3639, Arthur.J.Decker@grc.nasa.gov

Author: Dr. Arthur J. Decker

Headquarters program office: OSMA

Programs/Projects:

ISS, ASTP, UEET, Aerospace Propulsion and Power Base



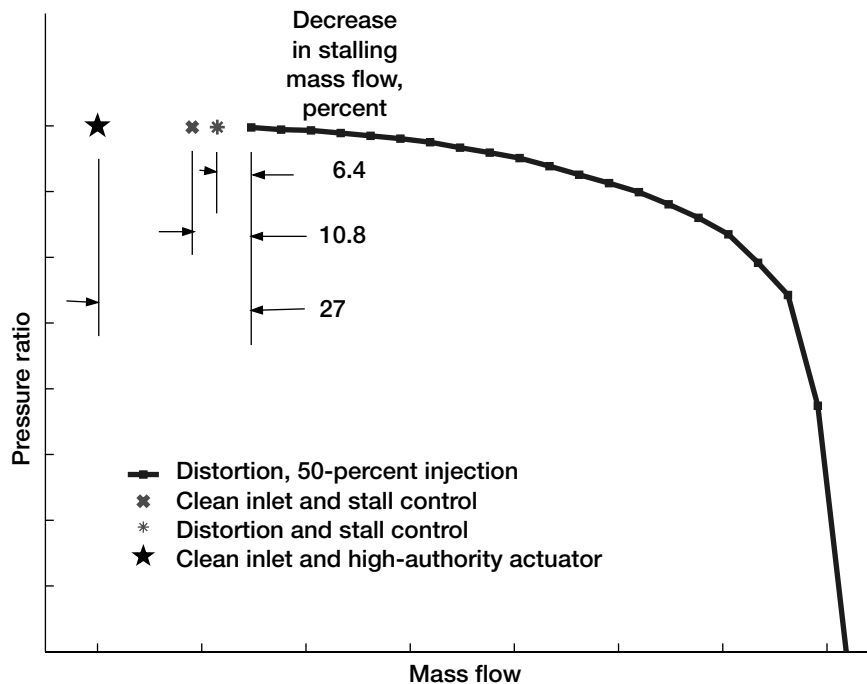
Root mean square error as a function of the number of intensity folds in the neural net training patterns. Top: Training error. Bottom: Test error.

Active Control of Rotating Stall Demonstrated for a Multistage Compressor With Inlet Distortion

Aircraft compressors can suffer debilitating consequences as a result of rotating stall and surge events caused by inlet distortions. This is particularly true of aircraft during takeoff, when the compressor is operating at peak performance close to the surge line. Significant research has been conducted by the NASA Glenn Research Center in the area of compressor stability enhancement through active and passive control methods (refs. 1 to 4). Most recently, an experiment was conducted at the Wright Patterson Air Force Base Research Laboratory on a two-stage fan with inlet guide vanes and inlet distortion.

In this joint Small Business Innovation Research effort between Scientific Systems and Glenn, control of rotating stall was demonstrated in a multistage transonic fan. This two-stage fan with inlet guide vanes was tested under clean and distorted inlet conditions. The compressor was also

configured with a circumferential distortion screen capable of 180° of distortion and with 14 high-velocity injectors upstream of the first rotor. Twelve of these injectors could oscillate up to frequencies of 450 Hz. The additional two injectors were located next to each other and were used in concert with each other as a single, on/off, high-authority actuator.



Stabilized compressor characteristics with and without active stall control.

In a first test of injection in this multistage environment, 12 of the valves were opened 50 percent of their full stroke to assess steady injection through the compressor. This baseline injection is shown in the compressor characteristic of the following figure, and stall margin improvements are tracked from this baseline condition. The compressor was then tested with clean inlet conditions using 12 injectors and active control. Pressure disturbances were tracked before rotating stall, and a constant gain control scheme reduced the stalling mass flow by 10.8 percent over the baseline. With the distortion screen present in the inlet, a pole-zero cancellation control scheme was used to achieve a 6.4-percent decrease in stalling mass flow. These improvements also are shown in the figure.

In a final experiment, actively controlled, high-frequency injection from the 12 valves was used in conjunction with the high-authority actuators. In this test, the stalling mass flow of the compressor was reduced by 27 percent as indicated in the graph. These results were obtained by injecting less than 2 percent of the total compressor throughflow into the rotor tip region via 14 injection ports. These results mark the first successful demonstration of actively controlled air injection as a stall-control strategy for multistage compressors operating at speeds typical of an actual gas turbine engine.

A goal of continuing research is to determine the combination of air-injection parameters and control strategies that are most effective in providing stall control for both clean and distorted inlet flow conditions for multistage environments. Other goals include the demonstration of stall control at many locations along the core compressor and development and application of active stall control strategies that will be integral flightworthy components of onboard engine hardware.

References

1. Bright, M.M., et al.: Stall Precursor Identification in High-Speed Compressor Stages Using Chaotic Time Series Analysis Methods. ASME J. Turbomachinery, vol. 119, no. 3, 1997, pp. 491–499.
2. Bright, M.M.; Qammar, H.K.; and Wang, L.Z.: Investigation of Pre-stall Mode and Pip Inception in High-Speed Compressors Through the Use of Correlation Integral. ASME J. Turbomachinery, vol. 121, no. 4, 1999, pp. 743–750.
3. Spakovszky, Z.S., et al.: Rotating Stall Control in a High-Speed Stage With Inlet Distortion. I—Radial Distortion. ASME Paper 98–GT–264, 1999.
4. Spakovszky, Z.S., et al.: Rotating Stall Control in a High-Speed Stage With Inlet Distortion. II—Circumferential Distortion. ASME Paper 98–GT–265, 1999.

Glenn contact:

Michelle M. Bright, 216–433–2304,
Michelle.M.Bright@grc.nasa.gov

Authors: Christian Van Schalkwyk,
 Michelle M. Bright, Dr. Kenneth L.
 Suder, Dr. Anthony J. Strazisar, and
 Scott A. Thorp

Headquarters program office: OAT

Programs/Projects: Aerospace
 Propulsion and Power Base,
 Turbomachinery Combustion Technol-
 ogy, SBIR Phase II, Base Propulsion R&T

Pulse Detonation Engine Modeled

Pulse Detonation Engine Technology is currently being investigated at Glenn for both air-breathing and rocket propulsion applications. The potential for both mechanical simplicity and high efficiency due to the inherent near-constant-volume combustion process, may make Pulse Detonation Engines (PDE's) well suited for a number of mission profiles.

Assessment of PDE cycles requires a simulation capability that is both fast and accurate. It should capture the essential physics of the system, yet run at speeds that allow parametric analysis. A quasi-one-dimensional, computational-fluid-dynamics-based simulation has been developed that may meet these requirements. The Euler equations of mass, momentum, and energy have been used—along with a single reactive species transport equation, and submodels to account for dominant loss mechanisms (e.g., viscous losses, heat transfer, and valving)—to successfully simulate PDE cycles. A high-resolution numerical integration scheme was chosen to capture the discontinuities associated with detonation, and robust boundary condition procedures were incorporated to accommodate flow reversals that may arise during a given cycle.

The accompanying graphs compare experimentally measured and computed performance over a range of operating conditions for a particular PDE. Experimental data were supplied by Fred Schauer and Jeff Stutrud from the Air Force Research Laboratory at Wright-Patterson AFB and by Royce Bradley from Innovative Scientific Solutions, Inc. The left graph shows thrust and specific impulse, I_{sp} , as functions of equivalence ratio for a PDE cycle in which the tube is completely filled with a detonable hydrogen/air mixture. The right graph shows thrust and specific impulse as functions of the fraction of the tube that is filled with a stoichiometric mixture of hydrogen and air. For both figures, the operating frequency was 16 Hz. The agreement between measured and computed values is quite

good, both in terms of trend and magnitude. The error is under 10 percent everywhere except for the thrust value at an equivalence ratio of 0.8 in the left figure, where it is 14 percent.

The simulation results shown were made using 200 numerical cells. Each cycle of the engine, approximately 0.06 sec, required 2.0 min of CPU time on a Sun Ultra2. The simulation is currently being used to analyze existing experiments, design new experiments, and predict performance in propulsion concepts where the PDE is a component (e.g., hybrid engines and combined cycles).

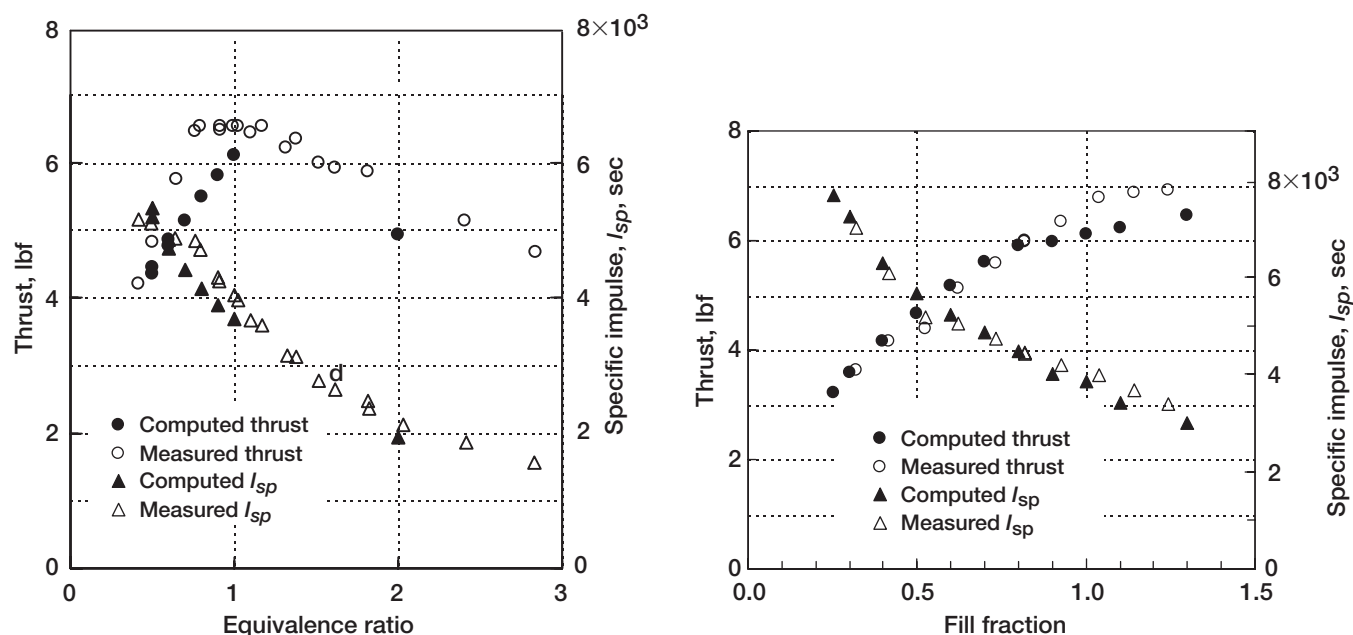
Glenn contact:

Dr. Daniel E. Paxson, 216-433-8334,
Daniel.E.Paxson@grc.nasa.gov

Author: Dr. Daniel E. Paxson

Headquarters program office: OAT

Programs/Projects: Aerospace
Propulsion and Power Base, PDE



Measured and computed thrust and specific thrust. Left: As functions of equivalence ratio for a 100-percent fill, 50-percent purge, 16-Hz PDE cycle. Right: As functions of fill fraction in a 50-percent purge, 16-Hz stoichiometric PDE cycle.

Accurate Time-Dependent Traveling-Wave Tube Model Developed for Computational Bit-Error-Rate Testing

The phenomenal growth of the satellite communications industry has created a large demand for traveling-wave tubes (TWT's) operating with unprecedented specifications requiring the design and production of many novel devices in record time. To achieve this, the TWT industry heavily relies on computational modeling. However, the TWT industry's computational modeling capabilities need to be improved because there are often discrepancies between measured TWT data and that predicted by conventional two-dimensional helical TWT interaction codes. This limits the analysis and design of novel devices or TWT's with parameters differing from what is conventionally manufactured. In addition, the inaccuracy of current computational tools limits achievable TWT performance because optimized designs require highly accurate models.

To address these concerns, a fully three-dimensional, time-dependent, helical TWT interaction model was developed using the electromagnetic particle-in-cell code MAFIA (Solution of MAXwell's equations by the Finite-Integration-Algorithm) (refs. 1 and 2). The model includes a short section of helical slow-wave circuit with excitation fed by radiofrequency input/output couplers, and an electron beam contained by periodic permanent magnet focusing. A cutaway view of several turns of the three-dimensional helical slow-wave circuit with input/output couplers is shown in the figure. This has been shown to be more accurate than conventionally used two-dimensional models (ref. 3).

The growth of the communications industry has also imposed a demand for increased data rates for the transmission of large volumes of data. To achieve increased data rates, complex modulation and multiple access techniques are employed requiring minimum distortion of the signal as it is passed through the TWT. Thus, intersymbol interference (ISI) becomes a major consideration, as well as suspected causes such as reflections within the TWT. To experimentally investigate effects of the physical TWT on ISI would be prohibitively expensive, as it would require manufacturing numer-

ous amplifiers, in addition to acquiring the required digital hardware. As an alternative, the time-domain TWT interaction model developed here provides the capability to establish a computational test bench where ISI or bit error rate can be simulated as a function of TWT operating parameters and component geometries. Intermodulation products, harmonic generation, and backward waves can also be monitored with the model for similar correlations.

The advancements in computational capabilities and corresponding potential improvements in TWT performance may prove to be the enabling technologies for realizing unprecedented data rates for near real time transmission of the increasingly larger volumes of data demanded by planned commercial and Government satellite communications applications.

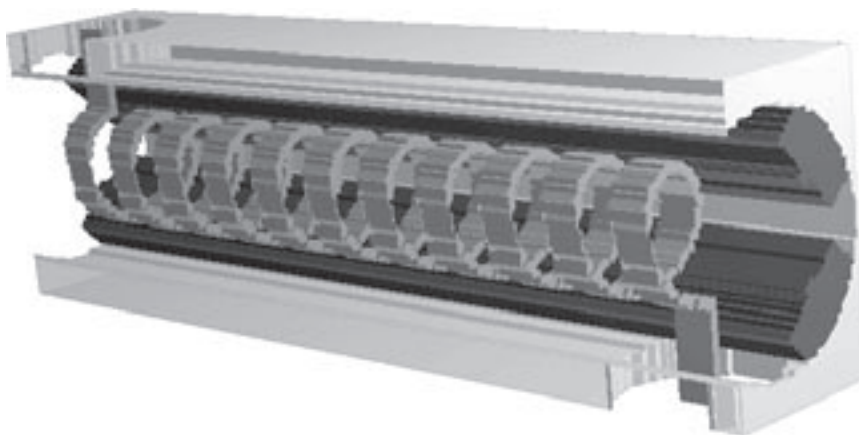
This work is in support of the Cross Enterprise Technology Development Program in Headquarters' Advanced Technology & Mission Studies Division and the Air Force Office of Scientific Research Small Business Technology Transfer programs.

Find out more about this research:

<http://ctd.grc.nasa.gov/5620/5620.html>

References

1. Weiland, Thomas: On the Numerical Solution of Maxwell's Equations and Applications in the Field of Accelerator Physics. Part. Accel., vol. 15, no. 4, 1984, pp. 245-292.
2. Weiland, T.: On the Unique Numerical Solution of Maxwellian Eigenvalue Problems in Three Dimensions. Part. Accel., vol. 17, nos. 3-4, 1985, pp. 227-242.



Cutaway of several turns of the helical slow-wave circuit with input/output couplers. This figure appears in color in the online version of this article (<http://www.grc.nasa.gov/WWW/RT2000/5600/5620kory.html>).

3. Kory, Carol L.: Three-Dimensional Simulations of PPM Focused Helical Traveling-Wave Tubes. Doctor of Engineering Dissertation, Cleveland State Univ., 2000.

Analex contact: Carol L. Kory, 216-433-3512, Carol.L.Kory@grc.nasa.gov

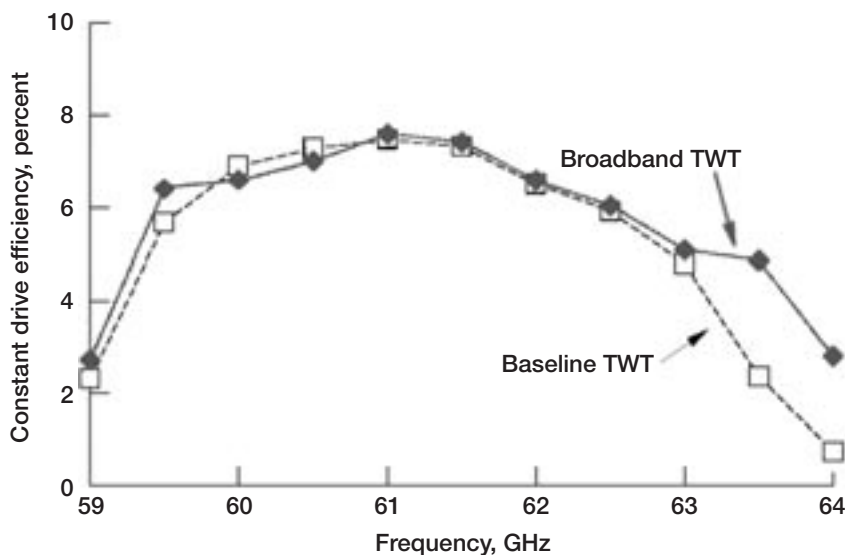
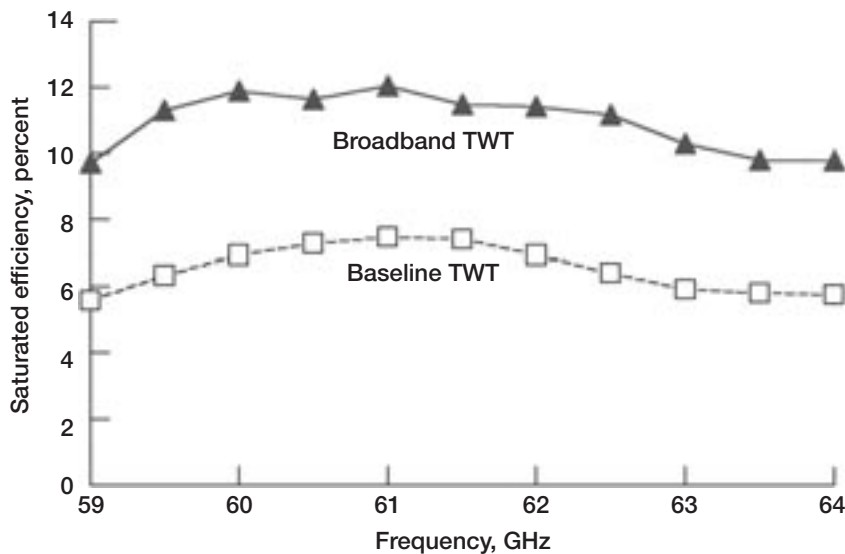
Glenn contact: Alan N. Downey, 216-433-3508, Alan.Downey@grc.nasa.gov

Author: Carol L. Kory

Headquarters program office:
OSS (ATMS)

Programs/Projects: CETDP, Air Force
Office of Scientific Research Small
Business Technology Transfer

Power and Efficiency Optimized in Traveling-Wave Tubes Over a Broad Frequency Bandwidth



Top: Computed saturated power efficiency for a TWT designed with the first broadband design algorithm compared with that for the baseline Hughes 961HA TWT. Bottom: Computed power efficiency with constant input drive power for a TWT designed with the second broadband design algorithm compared with that for the baseline Hughes 961HA TWT.

A traveling-wave tube (TWT) is an electron beam device that is used to amplify electromagnetic communication waves at radio and microwave frequencies. TWT's are critical components in deep space probes, communication satellites, and high-power radar systems.

Power conversion efficiency is of paramount importance for TWT's employed in deep-space probes and communication satellites. A previous effort was very successful in increasing efficiency and power at a single frequency (ref. 1). Such an algorithm is sufficient for narrow bandwidth designs, but for optimal designs in applications that require high radiofrequency power over a wide bandwidth, such as high-density communications or high-resolution radar, the variation of the circuit response with respect to frequency must be considered. This work at the NASA Glenn Research Center is the first to develop techniques for optimizing TWT efficiency and output power over a broad frequency bandwidth (ref. 2).

The techniques are based on simulated annealing, which has the advantage over conventional optimization techniques in that it enables the best possible solution to be obtained (ref. 3). Two new broadband simulated annealing algorithms were developed that optimize (1) minimum saturated power efficiency over a frequency

bandwidth and (2) simultaneous bandwidth and minimum power efficiency over the frequency band with constant input power. The algorithms were incorporated into the NASA coupled-cavity TWT computer model (ref. 4) and used to design optimal phase velocity tapers using the 59- to 64-GHz Hughes 961HA coupled-cavity TWT as a baseline model. In comparison to the baseline design, the computational results of the first broadband design algorithm show an improvement of 73.9 percent in minimum saturated efficiency (see the top graph). The second broadband design algorithm (see the bottom graph) improves minimum radiofrequency efficiency with constant input power drive by a factor of 2.7 at the high band edge (64 GHz) and increases simultaneous bandwidth by 500 MHz.

References

1. Wilson, J.D.: A Simulated Annealing Algorithm for Optimizing RF Power Efficiency in Coupled-Cavity Traveling-Wave Tubes. *IEEE Trans. Electron Devices*, vol. 44, no. 12, 1997, pp. 2295–2299.
2. Wilson, J.D.: Design of High-Efficiency Wide-Bandwidth Coupled-Cavity Traveling-Wave Tube Phase Velocity Tapers With Simulated Annealing Algorithms. *IEEE Trans. Electron Devices*, vol. 48, no. 1, 2001, pp. 95–100.
3. Kirkpatrick, S., Gelatt, C.D.; and Vecchi, M.P.: Optimization by Simulated Annealing. *SCI*, vol. 220, no. 4598, 1983, pp. 671–680.
4. Wilson, J.D.: Revised NASA Axially Symmetric Ring Model for Coupled-Cavity Traveling-Wave Tubes. NASA TP-2675, 1987.

Find out more about Glenn's vacuum electronics program and facilities:

<http://spacecom.grc.nasa.gov/technologies/electron/wavetube.asp>
<http://ctd.grc.nasa.gov/Facilities/vacuum.html>

Glenn contact:

Dr. Jeffrey D. Wilson, 216–433–3513,
Jeffrey.D.Wilson@grc.nasa.gov

Author: Dr. Jeffrey D. Wilson

Headquarters program office:
 OSS (ATMS)

Programs/Projects: CETDP

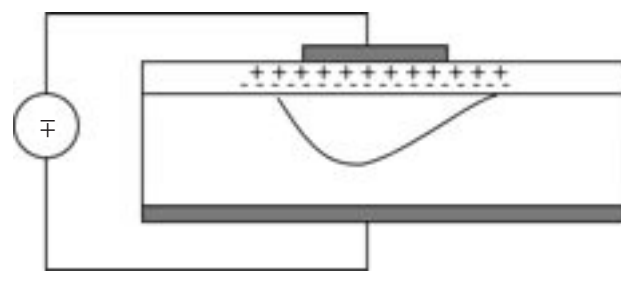
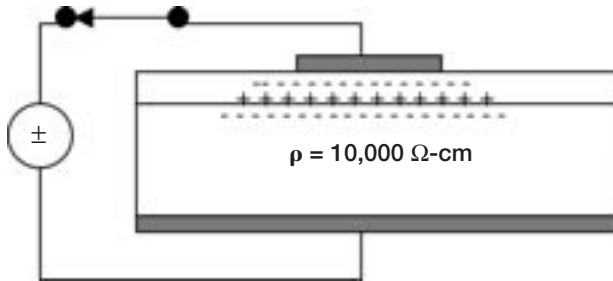
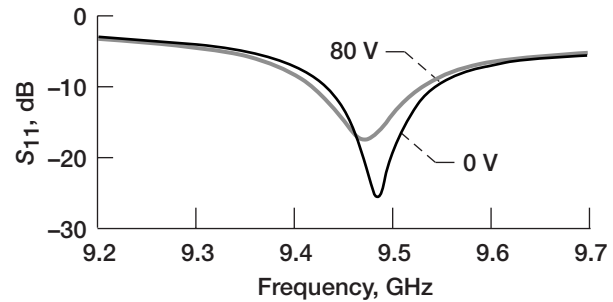
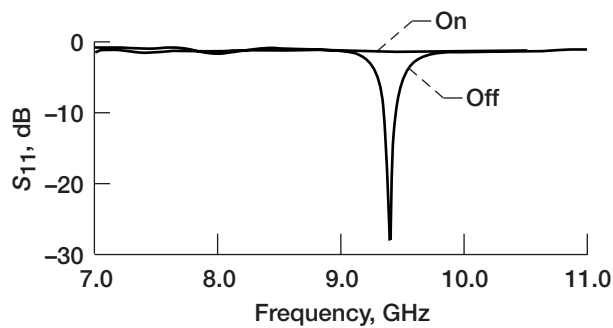
Ferroelectric/Semiconductor Tunable Microstrip Patch Antenna Developed

A lithographically printed microwave antenna that can be switched and tuned has been developed. The structure consists of a rectangular metallic “patch” radiator patterned on a thin ferroelectric film that was grown on high-resistivity silicon. Such an antenna may one day enable a single-phased array aperture to transmit and receive signals at different frequencies, or it may provide a simple way to reconfigure fractal arrays for communications and radar applications.

Modern aircraft are riddled with antennas to accommodate such needs as communications, navigation, and weather radar. For economic and safety reasons, there is a strong desire to bundle as many functions as possible into a single aperture. This is especially true in the case of small commercial and fighter aircraft. The problem will become more severe as consumers demand more access to information en route and as improved safety features such as microwave landing systems proliferate. The designs for spacecraft antennas are even more stringent because of mass and volume constraints. Phased-array antennas—antennas that steer a beam electronically rather than mechanically—are desirable for spacecraft because they are vibration free. But conventional arrays operate only over a single narrow band of frequencies.

The NASA Glenn Research Center has devised a prototype frequency agile antenna based on thin ferroelectric films and semiconductor substrates. The 350-nm $\text{Ba}_{0.5}\text{Sr}_{0.5}\text{TiO}_3$ film was grown by pulsed laser ablation on

10,000- $\Omega\text{-cm}$ 300- μm -thick silicon using a 50-nm $\text{Bi}_4\text{Ti}_3\text{O}_{12}$ /50 nm yttria-stabilized zirconia buffer layer. The antenna corresponding to the figure measured 0.675 by 0.45 cm and resonated at about 9.5 GHz in the TM_{01} mode. The left side shows the antenna behavior when the radiator has a positive bias with respect to the ground plane. When the switch is closed, electrons are swept from the silicon to the ferroelectric/semiconductor interface. This sea of electrons, or plasma, forms a virtual ground resonance plane near the interface. An electron density of about $10^{19}/\text{cm}^3$ extinguishes the antenna. When the switch is opened, the radiator behaves more or less as a conventional patch antenna. The measured far-field E- and H-plane radiation patterns were normal. By reversing the



Reflection coefficient of the antenna. Left: Forward-biased radiator. Right: Reverse-biased radiator.

polarity, as in the right side of the figure, electrons were swept to the natural ground plane and a depletion region formed under the patch in the silicon. In this configuration, the antenna was tuned about 25 MHz with 80 V applied. Operating the antenna in a higher order odd mode produced a second useful frequency of operation, and the ferroelectric effect was used for vernier tuning. The tuning range is ultimately limited by the formation of an inversion layer, or generation of higher order modes because of the electrical thickness of the stratified device.

Most startling is the current/voltage (I/V) relationship of the device. The structure exhibits discontinuities in the I/V curves, and at certain temperatures regions of negative differential resistance are encountered. This phenomenon is believed to be due to a tunneling process that may be enhanced by the polarization of the ferroelectric layer. Future work includes the redesign of the antenna to permit broader tuning and investi-

gation of the I/V characteristics for alternative device applications. The antenna design and testing were conducted by Glenn, and the ferroelectric films were grown by the University of Maryland.

Glenn contact: Dr. Robert R. Romanofsky, 216-433-3507, Robert.R.Romanofsky@grc.nasa.gov

Author: Dr. Robert R. Romanofsky

Headquarters program office: OAT

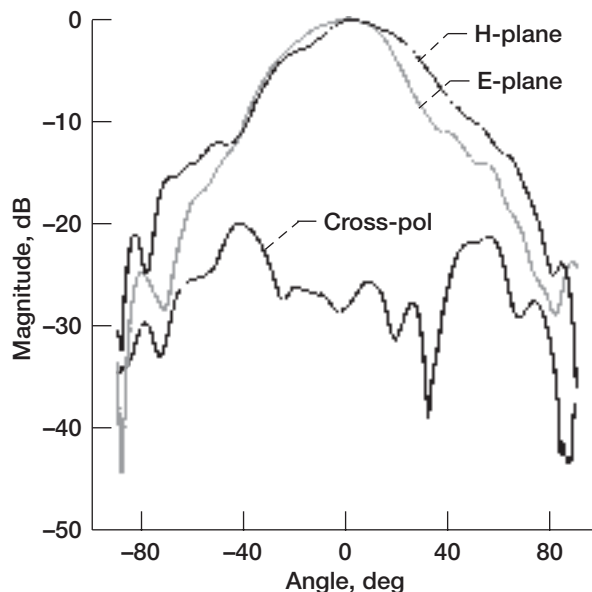
Programs/Projects:
SRF, Earth Science, HEDS

High-Efficiency Wide-Band Suspended Patch Antenna Array Demonstrated

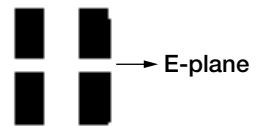
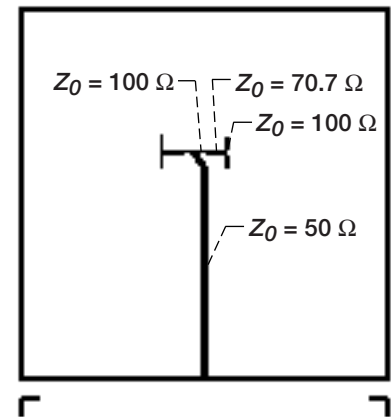
A four-element, suspended patch antenna array that has a parasitic patch layer on top and is electromagnetically coupled to an inverted microstrip feed for linear polarization was demonstrated at K-band frequencies. The layout of the array is shown in the figure to the right. The antenna has the following advantages over conventional microstrip antennas:

- (1) The inverted microstrip has lower losses, which result in higher gain and efficiency.
- (2) The inverted microstrip is easier to fabricate, because the strip width is wider for a given characteristic impedance.
- (3) A conventional proximity-coupled patch antenna requires a substrate for the feed and a superstrate for the patch. However, the inverted microstrip-fed patch antenna makes use of a single substrate and, hence, is lightweight and inexpensive.
- (4) Electromagnetic coupling results in a wider bandwidth.

The measurements show that the array is very well matched to the 50-W feed and has a 2:1 voltage standing wave ratio (VSWR) bandwidth of 5.4 percent for the initial experiments, which are K-band frequencies. The array radiates with a linear polarization perpendicular to the feed. The measured E- and H-plane radiation patterns and cross-polarization level for the array are shown in the following graph. The measured gain of the array in comparison to a standard-gain horn antenna is estimated to be about 10.0 dB. The efficiency of the array is about 59 percent.



Measured co-pol and cross-pol radiation patterns at 22.5 GHz.



Mask layout of four-element K-band suspended patch antenna array. Top: Feed network. Bottom: Patch array.

Glenn contact:

Dr. Felix A. Miranda, 216-433-6589,
Felix.A.Miranda@grc.nasa.gov

Author: Dr. Rainee N. Simons

Headquarters program office:

OSS (ATMS)

Programs/Projects: CETDP

Microelectromechanical Systems (MEMS) Actuator for Reconfigurable Patch Antenna Demonstrated

A microstrip patch antenna with two contact actuators along the radiating edges for frequency reconfiguration was demonstrated at K-band frequencies. The layout of the antenna is shown in the following figure. This antenna has the following advantages over conventional semiconductor varactor-diode-tuned patch antennas: (1) By eliminating the semiconductor diode and its nonlinear I-V characteristics, the antenna minimizes intermodulation signal distortion. This is particularly important in digital wireless systems, which are sensitive to intersymbol interference caused by intermodulation products. (2) Because the MEMS actuator is an electrostatic device, it does not draw any current during operation and, hence, requires a negligible amount of power for actuation. This is an important advantage for hand-held, battery-operated, portable wireless systems since the battery does not need to be charged frequently. (3) The MEMS actuator does not require any special epitaxial layers as in the case of diodes and, hence, is cost effective.

The measured return loss of the patch antenna with and without the actuator is shown in part (d). This figure shows that the antenna can be tuned over a frequency range of several gigahertz at K-band frequencies.

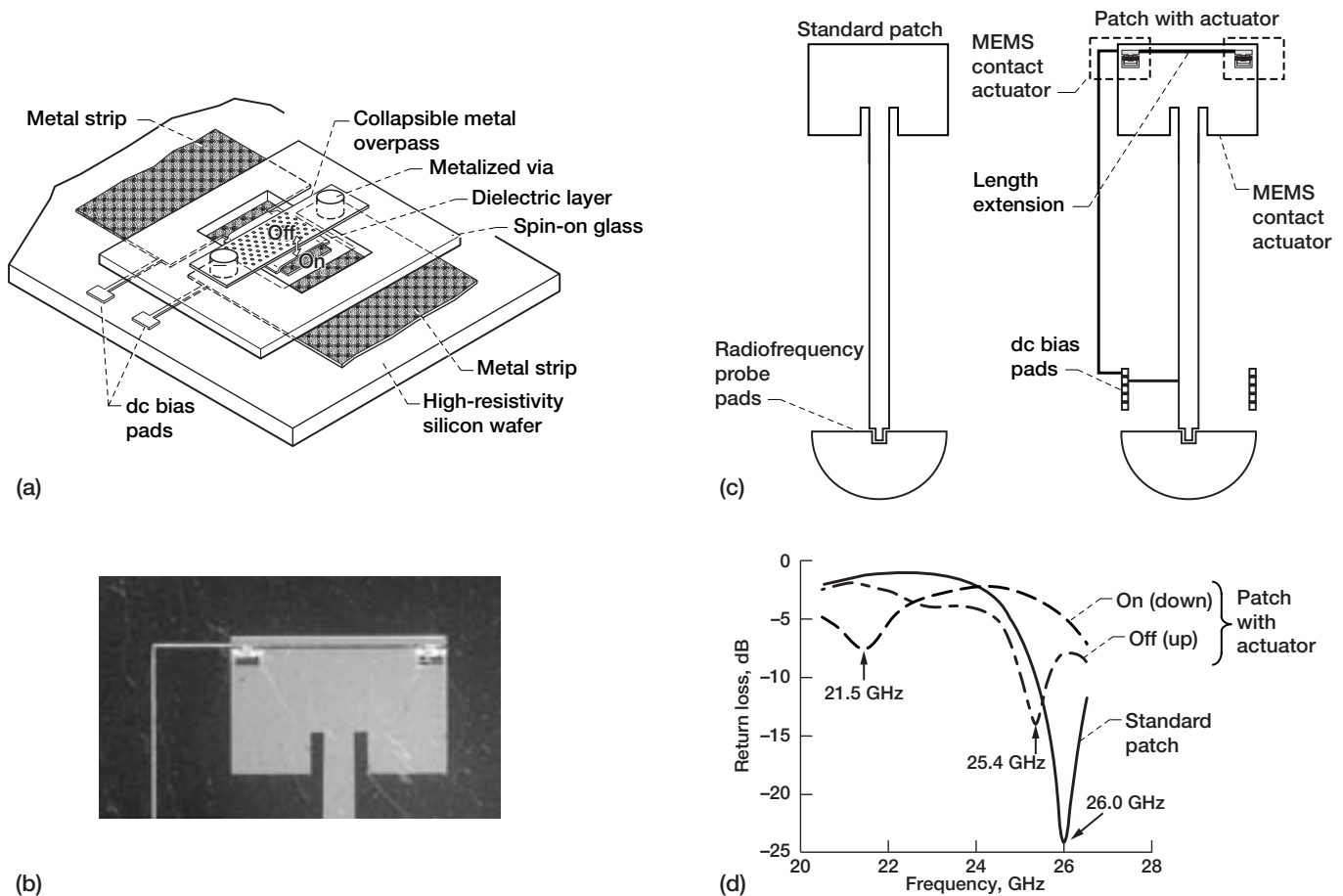
Glenn contact:

Dr. Felix A. Miranda, 216-433-6589,
Felix.A.Miranda@grc.nasa.gov

Author: Dr. Rainee N. Simons

Headquarters program office:
 OSS (ATMS)

Programs/Projects: CETDP



MEMS contact-actuator-based frequency-reconfigurable patch antenna. (a) MEMS contact actuator. (b) MEMS contact actuator integrated with patch antenna. (c) Standard patch and patch with actuator. (d) Reconfigurable patch antenna characteristics.

Turbomachinery and Propulsion Systems

Complex Flow Separation Pattern on Transonic Fan Airfoils Revealed by Flow Visualization

Modern turbofan engines employ a highly loaded fan stage with transonic or low-supersonic velocities in the blade-tip region. The fan blades are often prone to flutter at off-design conditions. Flutter is a highly undesirable and dangerous self-excited mode of blade oscillations that can result in high-cycle fatigue blade failure. The origins of blade flutter are not fully understood yet. The latest view is that the blade oscillations are triggered by high-frequency changes in the extent of the partially separated area on the airfoil suction side. There is a lack of experimental data describing the separated flow characteristics of modern airfoils for transonic fans.

It is very difficult to determine the presence and extent of the separated flow zone from only static pressure measurements on the airfoil surface. Therefore, two visualization experimental techniques were used to determine flow behavior on the suction side of an airfoil: (1) surface flow visualization using dye oils and (2) shadowgraph flow visualization. Surface flow visualization techniques are based on a dye being smeared over the surface by flow. Droplets of colored oil are deposited on the test surface, and the facility is started. Requirements for reliable surface flow data are a very short facility startup time and a dye-oil mixture of suitable viscosity in conjunction with small dye-oil marks on the test surface. The tests were carried out in the Transonic Flutter Cascade Facility at the NASA Glenn Research Center. Data were acquired for steady-state conditions at a high flow incidence of 10° .

For a subsonic inlet Mach number of 0.8, the flow exhibits a large separated region that starts immediately at the leading edge and extends, at midspan, down to 52 percent of the blade chord. The separation pattern for a low supersonic Mach number of 1.18 is completely different as seen

in the picture on the right. First, starting from the leading edge, the flow is attached to the blade surface down to approximately 32 percent of the chord. Then, there is a separated flow region in which air moves in the direction against the inlet flow. Finally, at 62 percent of the blade chord, the flow attaches back to the blade surface. The adjacent shadowgraph (left) helps depict this complex flow pattern. The excellent agreement of these two methods is clearly demonstrated here.

The experimental results are being used to verify computational code. The prediction of flow separation for the supersonic inlet conditions agrees qualitatively with experimental results. It appears that the separation bubble in the calculations starts closer to the leading edge than is seen in the experimental data.

Find out more about turbomachinery analysis codes:

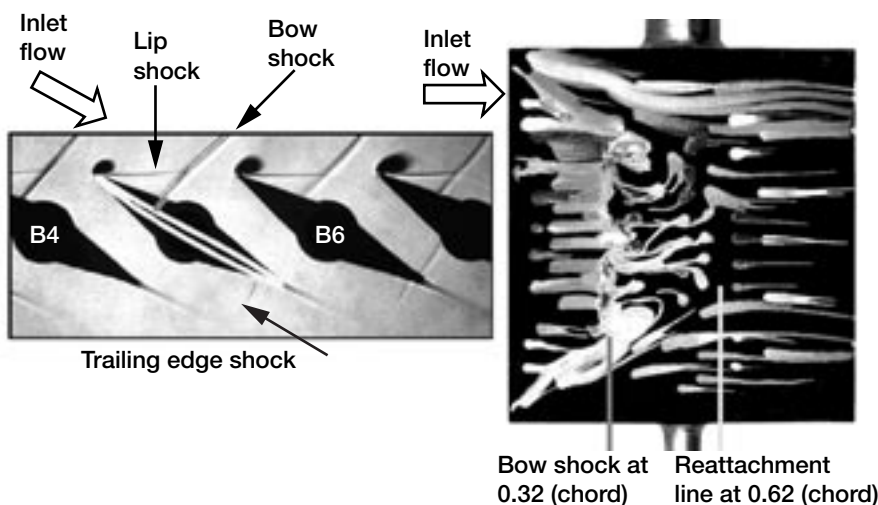
<http://www.grc.nasa.gov/WWW/5810/webpage/rvc.htm>

Bibliography

Lepicovsky, J., et al.: On Flow Periodicity in the NASA Transonic Flutter Cascade, Part I—Experimental Study. NASA/TM—2000-209934 (ASME-2000-GT-0572-Pt-2), 2000. <http://gltrs.grc.nasa.gov/GLTRS>

Chima, Rodrick V., et al.: On Flow Periodicity in the NASA Transonic Flutter Cascade, Part 2—Numerical Study. NASA/TM—2000-209933, 2000. <http://gltrs.grc.nasa.gov/GLTRS>

Lepicovsky, J., et al.: Investigation of Flow Separation in a Transonic-Fan Cascade Using Visualization Methods. NASA/TM—2000-210521, 2000. <http://gltrs.grc.nasa.gov/GLTRS>



Surface flow pattern for supersonic inlet flow; Mach number of inlet flow, 1.18. Left: Shadowgraph of cascade (side view). Right: Surface flow visualization of blade B5 (top view).

Dynacs contact:

Dr. Jan Lepicovsky, 216-977-1402, Jan.Lepicovsky@grc.nasa.gov

Glenn contacts:

Dr. Eric R. McFarland, 216-433-5915, Eric.R.McFarland@grc.nasa.gov; and
Dr. Rodrick V. Chima, 216-977-5919, Rodrick.V.Chima@grc.nasa.gov

Author: Dr. Jan Lepicovsky

Headquarters program office: OAT

Programs/Projects:

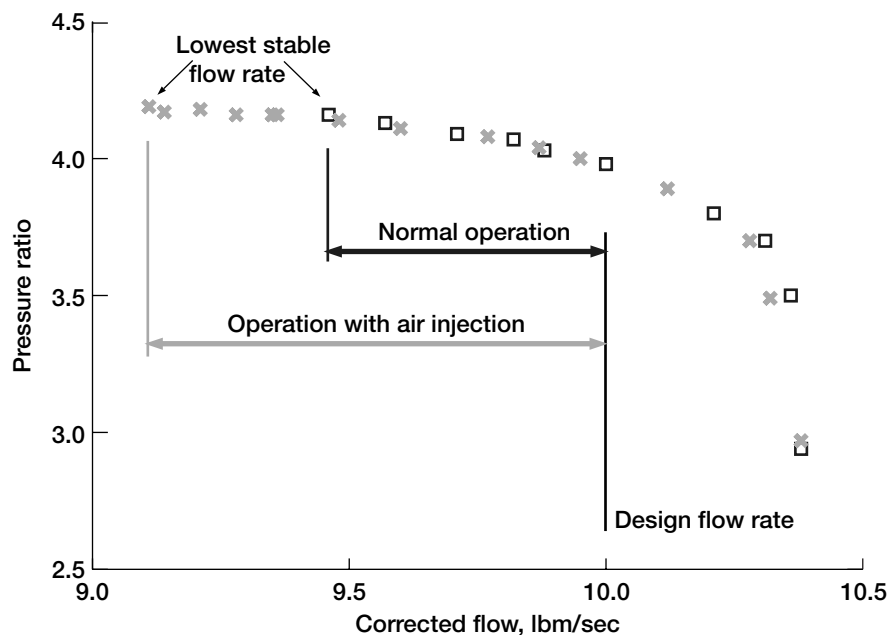
Propulsion Systems R&T, TCT

Flow Range of Centrifugal Compressor Being Extended

General Aviation will benefit from turbine engines that are both fuel-efficient and reliable. Current engines fall short of their potential to achieve these attributes. The reason is compressor surge, which is a flow stability problem that develops when the compressor is subjected to conditions that are outside of its operating range. Compressor surge can occur when fuel flow to the engine is increased, temporarily back pressuring the compressor and pushing it past its stability limit, or when the compressor is subjected to inlet flow-field distortions that may occur during takeoff and landing.

Compressor surge can result in the loss of an aircraft. As a result, engine designers include a margin of safety between the operating line of the engine and the stability limit line of the compressor. Unfortunately, the most efficient operating line for the compressor is usually closer to its stability limit line than it is to the line that provides an adequate margin of safety. A wider stable flow range will permit operation along the most efficient operating line of the compressor, improving the specific fuel consumption of the engine and reducing emissions.

The NASA Glenn Research Center is working to extend the stable flow range of the compressor. Significant extension has been achieved in axial compressors (ref. 1) by injecting air upstream of the compressor blade rows. Recently, the technique was successfully applied to a 4:1 pressure ratio centrifugal compressor by injecting streams of air into the diffuser (see the graph). Both steady and controlled unsteady injection were used to inject air through the diffuser shroud surface and extend the range. Future work will evaluate the effect of air injection through the diffuser hub surface and diffuser vanes with the goal of maximizing the range extension while minimizing the amount of injected air that is required.



Stable flow range extension achieved in a 4:1 pressure ratio centrifugal compressor using steady and controlled unsteady air injection.

Reference

1. Suder, Kenneth L, et al.: Compressor Stability Enhancement Using Discrete Tip Injection. The 45th ASME International Gas Turbine & Aero-engine Congress, Exposition and Users Symposium, 2000-GT-0650, 2000.

U.S. Army Vehicle Technology Center at Glenn contact:

Gary J. Skoch, 216-433-3396,
Gary.J.Skoch@grc.nasa.gov

Glenn contacts:

Dr. Anthony J. Strazisar, 216-433-5881,
Anthony.J.Strazisar@grc.nasa.gov; and
Michelle M. Bright, 216-433-2304,
Michelle.M.Bright@grc.nasa.gov

Author: Gary J. Skoch

Headquarters program office: OAT

Programs/Projects:

Propulsion Systems R&T, TCT

Compressor Stall Recovery Through Tip Injection Assessed

Aerodynamic stability is a fundamental limit in the compressor design process. The development of robust techniques for increasing stability has several benefits: enabling higher loading and fewer blades, increasing safety throughout a mission, increasing tolerance to stage mismatch during part-speed operation and speed transients, and providing an opportunity to match stages at the compressor maximum efficiency point, thus reducing fuel burn.

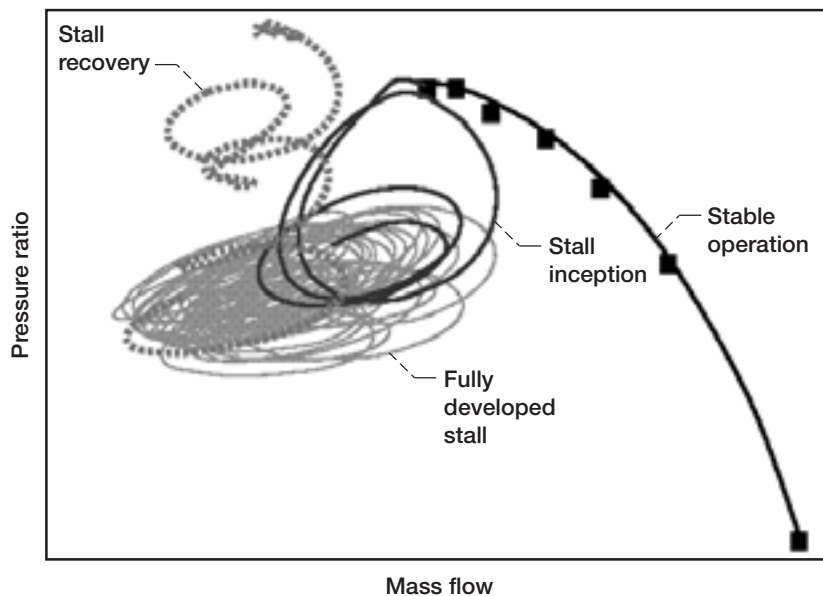
Mass injection upstream of the tip of a high-speed axial compressor rotor is a stability enhancement approach known to be effective in suppressing stall in tip-critical rotors (ref. 1) if the injection is activated before stall occurs. This approach to stall suppression requires that a reliable stall warning system be available. Tests have recently been performed to assess whether steady injection can also be used to recover from fully developed stall (ref 2). If mass injection is effective in recovering from stall quickly enough to avoid structural damage or loss of engine power, then a stall warning system may not be required.

The stall recovery tests were performed on a transonic compressor rotor at its design tip speed of 1475 ft/sec using four injectors evenly spaced around the compressor case upstream of the rotor. The injectors were connected to an external air source. In an actual engine application, the injected air would be supplied with compressor bleed air. The injectors were isolated from the air source by a fast-acting butterfly valve. With the injectors turned off, the compressor was throttled into stall. Air injection was then activated with no change in throttle setting by opening the butterfly valve. The compressor recovered from stall at a fixed throttle setting with the aid of tip injection.

The unsteady operating characteristic of the rotor was measured during these tests using high-response pressure sensors located upstream and downstream of the rotor. The figure shows the results, where the unsteady pressure and massflow are superimposed on the steady operating characteristic. The total injected massflow was equal to 1.3 percent of the compressor flow. The solid line with no solid squares on it denotes the operating point during the beginning of throttle closure and the initial drop into stall. The gray traces denote the operating point during an additional throttle closure that occurred over the next 1200 rotor revolutions (4 sec). The dashed line denotes the recovery from stall that occurred during 90 rotor revolutions (0.3 sec) after the injectors were activated with no change in throttle setting. Tip injection not only recovers the compressor from stall, but also restores the compressor to its pre-stall level of pressure rise. In contrast, standard stall recovery schemes such as compressor bleed, stator vane actuation, or engine throttle modulation result in a loss of pressure rise across the compressor, which results in a loss of engine power.

References

1. Weigl, H.J., et al.: Active Stabilization of Rotating Stall and Surge in a Transonic Single-Stage Axial Compressor. ASME J. Turbomachinery, vol. 120, no. 4, 1998, pp. 625–636.
2. Suder, Kenneth L, et al.: Compressor Stability Enhancement Using Discrete Tip Injection. The 45th ASME International Gas Turbine & Aero-engine Congress, Exposition and Users Symposium, 2000–GT-0650, 2000.



Unsteady compressor operating point at design speed during stall inception and stall recovery. Stall recovery at a fixed throttle setting (dashed lines) occurs 0.3 sec after tip injection is activated. This figure is shown in color in the online version of this article (<http://www.grc.nasa.gov/WWW/RT2000/5000/5810suder.html>).

Glenn contacts:

Dr. Ken L. Suder, 216-433-5899, Kenneth.L.Suder@grc.nasa.gov;
Scott A. Thorp, 216-433-8013, Scott.A.Thorp@grc.nasa.gov;
Dr. Anthony J. Strazisar, 216-433-5881, Anthony.J.Strazisar@grc.nasa.gov; and
Michelle M. Bright, 216-433-2304, Michelle.M.Bright@grc.nasa.gov

Glenn contact: Dr. Michael D. Hathaway, 216-433-6250,
Michael.D.Hathaway@grc.nasa.gov

Author: Dr. Ken L. Suder

Headquarters program office: OAT

Programs/Projects:
Propulsion Systems R&T

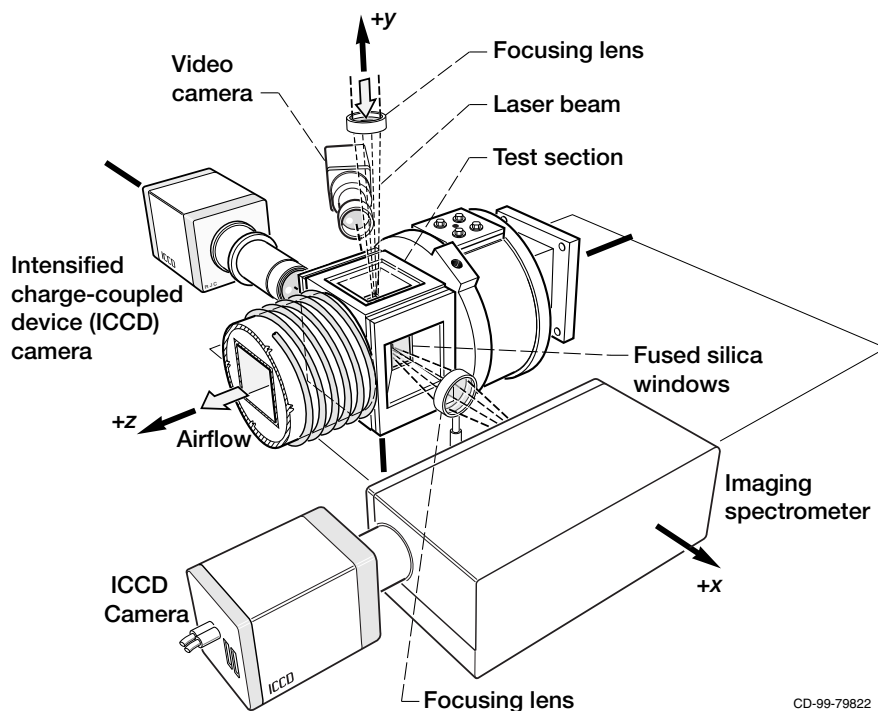
One-Dimensional Spontaneous Raman Measurements Made in a Gas Turbine Combustor

The NASA Glenn Research Center and the aerospace industry are designing and testing low-emission combustor concepts to build the next generation of cleaner, more fuel efficient aircraft powerplants. These combustors will operate at much higher inlet temperatures and at pressures that are up to 3 to 5 times greater than combustors in the current fleet. From a test and analysis viewpoint, there is an increasing need for measurements from these combustors that are nonintrusive, simultaneous, multipoint, and more quantitative. Glenn researchers have developed several unique test facilities (refs. 1 and 2) that allow, for the first time, optical interrogation of combustor flow fields, including subcomponent performance, at pressures ranging from 1 to 60 bar (1 to 60 atm).

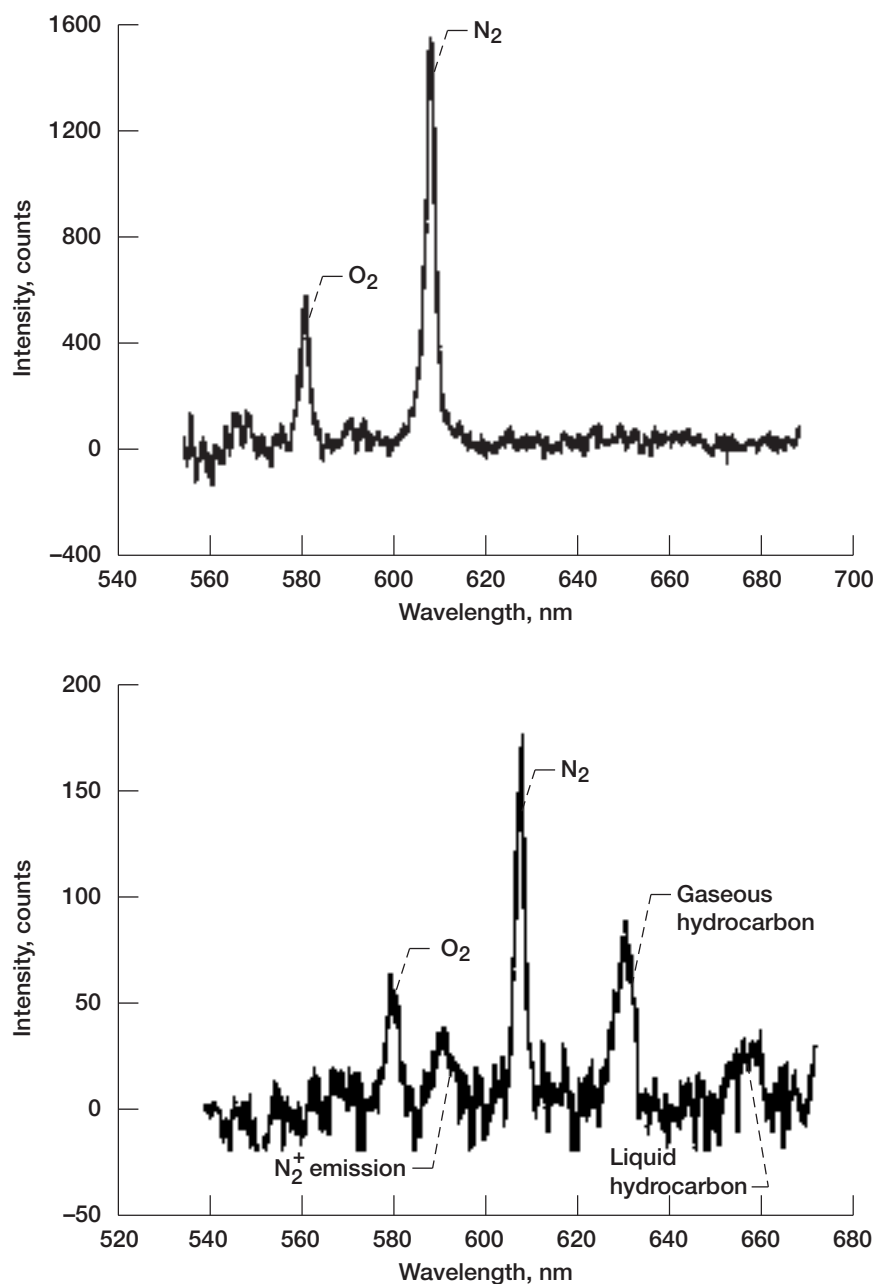
Experiments conducted at Glenn are the first application of a visible laser-pumped, one-dimensional, spontaneous Raman-scattering technique to analyze the flow in a high-pressure, advanced-concept fuel injector at pres-

ures thus far reaching 12 bar (12 atm). This technique offers a complementary method to the existing two- and three-dimensional imaging methods used, such as planar laser-induced fluorescence. Raman measurements benefit from the fact that the signal from each species is a linear function of its density, and the relative densities of all major species can be acquired simultaneously with good precision. The Raman method has the added potential to calibrate multidimensional measurements by providing an independent measurement of species number-densities at known points within the planar laser-induced fluorescence images. The visible Raman method is similar to an ultraviolet-Raman technique first tried in the same test facility (ref. 3). However, the visible method did not suffer from the ultraviolet technique's fuel-born polycyclic aromatic hydrocarbon fluorescence interferences.

The figure to the left shows a schematic of the Raman diagnostic setup. The visible laser beam enters vertically through a window at the top of the combustor. Raman scattering is measured normal to both the incident laser beam and to the direction of its electric vector, the latter in order to maximize the Raman signal.



One-dimensional, visible Raman setup and the optically accessible combustor test section.



Top: Comparison of the averaged spectrum of high-pressure air in the combustor at 400 °F and 12 bar. Average over 200 single-shot spectra; spectrometer slit, 100 μ m; laser energy, 47 mJ/pulse (output). Bottom: Comparison of the averaged spectrum of fuel injected in air at 900 °F and 10 bar. Spectrometer slit, 100 μ m; average of 2606 laser pulses; laser energy, 50 mJ/pulse.

At the measurement location, Jet-A fuel is partially evaporated and generates a strong hydrocarbon signal in addition to nitrogen and oxygen signals. Single-shot and averaged spectra and images of the combustor speciation were obtained—with oxygen, nitrogen, gaseous, and liquid hydrocarbons clearly visible—with acceptable resolution over a wide range of engine cycle conditions.

The figure above shows a 200-shot average spectrum of air at a pressure of 12 bar and a temperature of 400 °F (top) and a 2600-shot average

spectrum of air with injected fuel inside the combustor at 900 °F and 10 bar (bottom). The ratio of oxygen versus nitrogen peak height in the fuel-injected case is the same as for the pure air, which indicates that no reaction has taken place. A large number of peaks in addition to the oxygen and nitrogen lines seen in both cases are identified in the top figure as hydrocarbon fuel components and fragments. In addition, a broader peak appears in the top figure, slightly below the predicted location of water. This peak is substantially more pronounced at lower temperatures and is attributed to Raman scattering of liquid alcohol compounds (OH-vibration) in the fuel (ref. 4). Further applications and refinements of this technique to the harsh environment within advanced liquid-fueled, gas turbine combustors should lead to a better understanding of the physical and chemical processes of these combusting flow fields.

References

1. Locke, R.J., et al.: Optical Fuel Injector Patterning Measurements in Advanced Liquid Fueled, High Pressure, Gas Turbine Combustors. *Combust. Sci. Technol.*, vol. 138, nos. 1–6, 1998, pp. 297–311.
2. Hicks, Yolanda R.; Locke, Randy J.; and Anderson, Robert C.: Optical Measurement and Visualization in High-Pressure, High-Temperature, Aviation Gas Turbine Combustors. NASA/TM–2000-210377, 2000. <http://gltrs.grc.nasa.gov/GLTRS>
3. Gu, Yongwei, et al.: 1-D, UV-Raman Imaging From a High-Pressure, Jet-A Fueled Gas Turbine Combustor. AIAA Paper 2000-0773, 2000.
4. Mewes, Bernd; Bauer, Gerd; and Brueggemann, Dieter: Fuel Vapor Measurements by Linear Raman Spectroscopy Using Spectral Discrimination From Droplet Interferences. *Applied Optics*, vol. 38, no. 6, Feb. 20, 1999.

Dynacs Engineering Company, Inc., contacts:

Dr. Wilhelmus A. DeGroot, 216-977-7485, Wilhelmus.A.DeGroot@grc.nasa.gov; and
Dr. Randy J. Locke, 216-433-6110, Randy.J.Locke@grc.nasa.gov

Glenn contact: Dr. Yolanda R. Hicks, 216-433-3410, Yolanda.R.Hicks@grc.nasa.gov

Authors: Dr. Wilhelmus A. DeGroot, Dr. Yolanda R. Hicks, Dr. Randy J. Locke, and
Robert C. Anderson

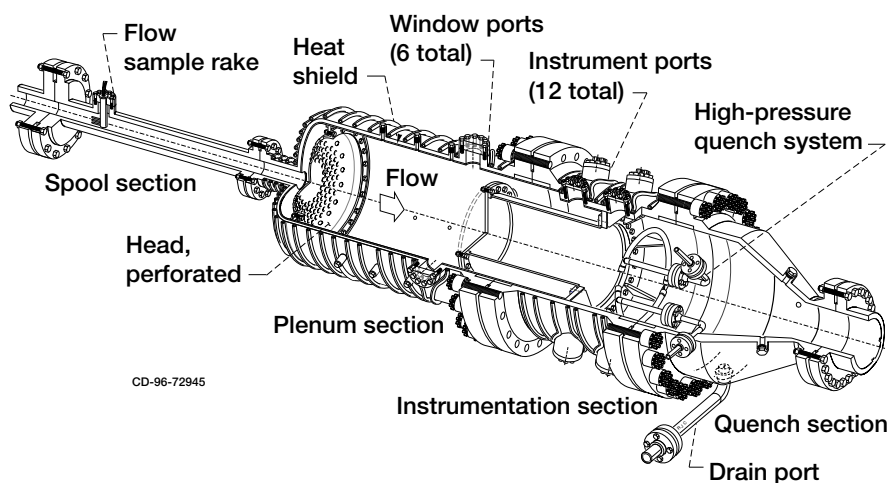
Headquarters program office: OAT

Programs/Projects: UEET

Optical Diagnosis of Gas Turbine Combustors Being Conducted

Researchers at the NASA Glenn Research Center, in collaboration with industry, are reducing gas turbine engine emissions by studying visually the air-fuel interactions and combustion processes in combustors (refs. 1 to 2). This is especially critical for next-generation engines that, in order to be more fuel-efficient, operate at higher temperatures and pressures than the current fleet engines.

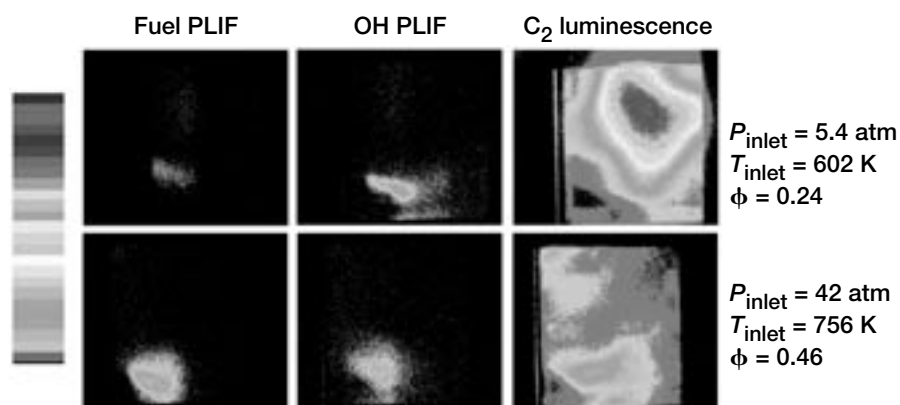
Optically based experiments were conducted in support of the Ultra-Efficient Engine Technology program in Glenn's unique, world-class, advanced subsonic combustion rig (ASCR) facility. The ASCR can supply air and jet fuel at the flow rates, temperatures, and pressures that simulate the conditions expected in the combustors of high-performance, civilian aircraft engines (ref. 3). In addition, this facility is large enough to support true sectors ("pie" slices of a full annular combustor). Sectors enable one to test true shapes rather than rectangular approximations of the actual hardware. Therefore, there is no compromise to actual engine geometry. The following figure shows a schematic drawing of the sector test stand. The test hardware is mounted just upstream of the instrumentation section. The test stand can accommodate hardware up to 0.76-m diameter by 1.2 m long; thus sectors or small full annular combustors can be examined in this facility.



ASCR sector combustor pressure shell. Flow passes from left to right. The inner vessel that contains the actual combustor hardware bolts onto the instrumentation section.

Planar (two-dimensional) imaging using laser-induced fluorescence and Mie scattering, chemiluminescence, and video imagery were obtained for a variety of engine cycle conditions. The hardware tested was a double annular sector (two adjacent fuel injectors aligned radially) representing approximately 15° of a full annular combustor. The next figure shows an example of the two-dimensional data obtained for this configuration. The fluorescence data show the location of fuel and hydroxyl radical (OH) along the centerline of the fuel injectors. The chemiluminescence data show C_2 within the total observable volume. The top row of this figure shows images obtained at an engine low-power condition, and the bottom row shows data from a higher power operating point. The data show distinctly the differences in flame structure between low-power and high-power engine conditions, in both location and amount of species produced (OH, C_2) or consumed (fuel).

The unique capability of the facility coupled with its optical accessibility helps to eliminate the need for high-pressure performance extrapolations. Tests such as described here have been used successfully to assess the performance of fuel-injection concepts and to modify those designs, if needed.



Comparisons of fuel planar laser-induced fluorescence (PLIF), OH PLIF, and C_2 chemiluminescence. Images are scaled per species. Conditions are as noted per row. Fuel-to-air equivalence ratio, ϕ . This figure is shown in color in the online version of this article (<http://www.grc.nasa.gov/WWW/RT2000/5000/5830hicks.html>).

References

1. Hicks, Yolanda R.; Locke, Randy J.; and Anderson, Robert C.: Optical Measurement and Visualization in High-Pressure, High-Temperature, Aviation Gas Turbine Combustors. Optical Diagnostics for Industrial Applications, Neil A. Halliwell, ed., vol. 4076, 2000, pp. 66–77. (Also NASA/TM–2000-210377, <http://gltrs.grc.nasa.gov/GLTRS>)

2. Locke, R.J., et al.: Progress in Species and Flowfield Mapping in Advanced Liquid-Fueled Gas Turbine Combustors. AIAA Paper 2000–0774, 2000.

Glenn contacts:

Dr. Yolanda R. Hicks, 216–433–3410, Yolanda.R.Hicks@grc.nasa.gov; and Robert C. Anderson, 216–433–3643, Robert.C.Anderson@grc.nasa.gov

Dynacs Engineering Company, Inc., contact:

Dr. Randy J. Locke, 216–433–6110, Randy.J.Locke@grc.nasa.gov

Authors: Dr. Yolanda R. Hicks, Dr. Randy J. Locke, Robert C. Anderson, and Dr. Wilhelmus A. DeGroot

Headquarters program office: OAT

Programs/Projects: UEET

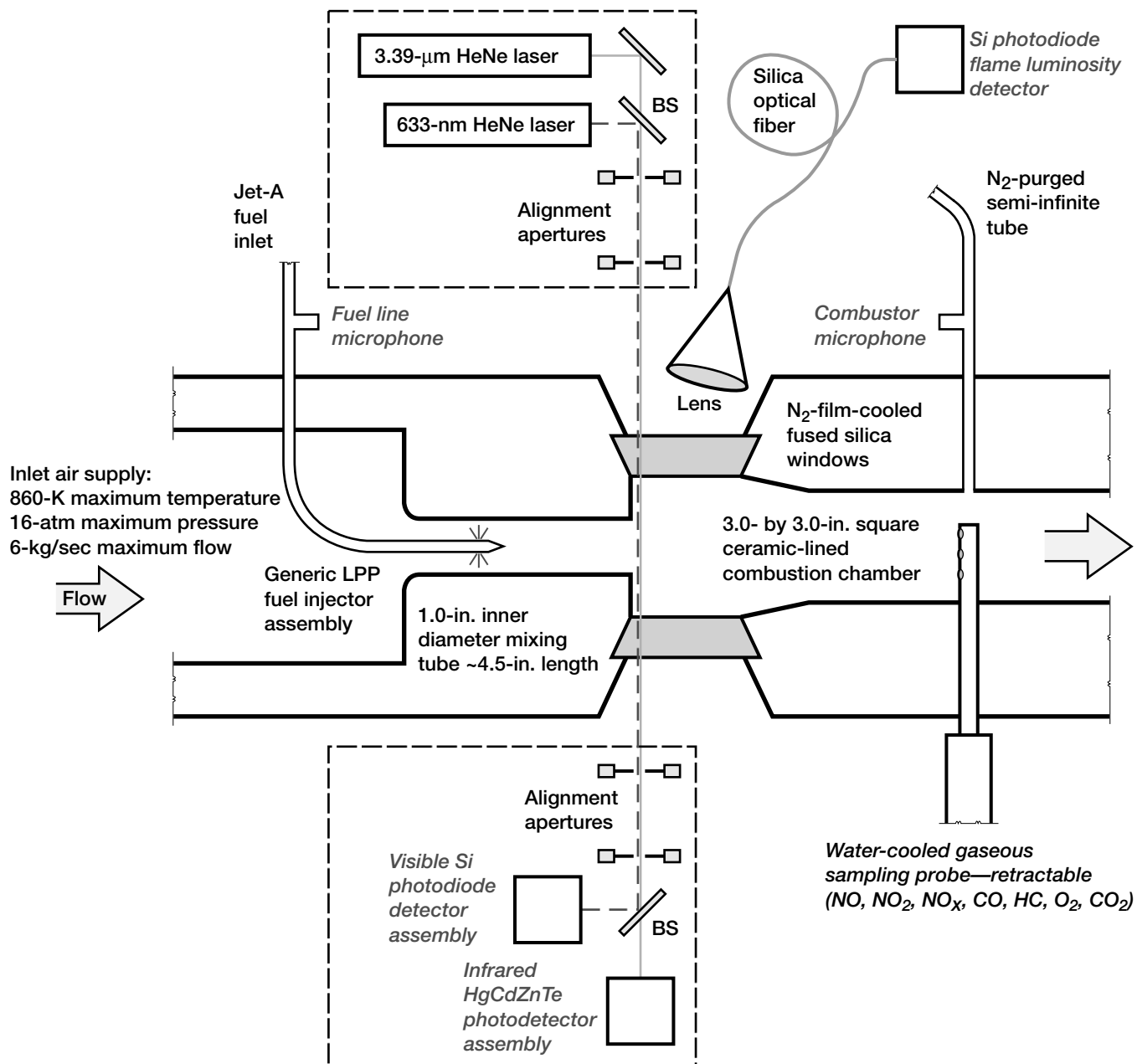
Laser Absorption Measurements of Equivalence Ratios Studied Along With Their Coupling to Pressure Fluctuations in Lean Premixed Prevaporized (LPP) Combustion

Concerns about damaging the Earth's ozone layer as a result of high levels of nitrogen oxides (known collectively as NO_x) from high-altitude, high-speed aircraft have prompted the study of lean premixed prevaporized (LPP) combustion in aircraft engines. LPP combustion reduces NO_x emissions principally by reducing the peak flame temperatures inside an engine. Recent advances in LPP technologies have realized exceptional reductions in pollutant emissions (single-digit ppm NO_x for example). However, LPP combustion also presents major challenges: combustion instability and dynamic coupling effects between fluctuations in heat-release rate, dynamic pressure, and fuel pressure. These challenges are formidable and can literally shake an engine apart if uncontrolled.

To better understand this phenomenon so that it can be controlled, we obtained real-time laser absorption measurements of the fuel vapor concentration (and equivalence ratio) simultaneously with the dynamic pressure, flame luminosity, and time-averaged gaseous emissions measurements in a research-type jet-A-fueled LPP combustor. The measurements were obtained in NASA Glenn Research Center's CE–5B optically accessible flame tube facility. A schematic of the experiment and the

optical diagnostic system is shown in the following figure. The CE–5B facility provides inlet air temperatures and pressures similar to the actual operating conditions of real aircraft engines. The laser absorption measurements were performed using an infrared 3.39- μm HeNe laser in conjunction with a visible HeNe laser for liquid droplet scattering compensation (ref. 1).

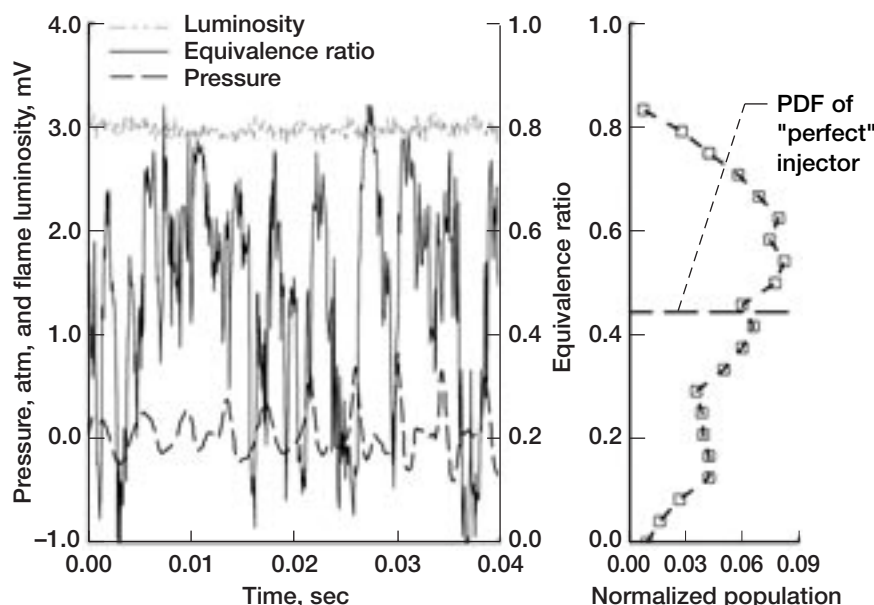
The second figure shows data from a "generic" LPP injector developed specifically for this study. The left side of the figure shows the real-time equivalence ratio, the dynamic combustion pressure, and the combustion flame luminosity over



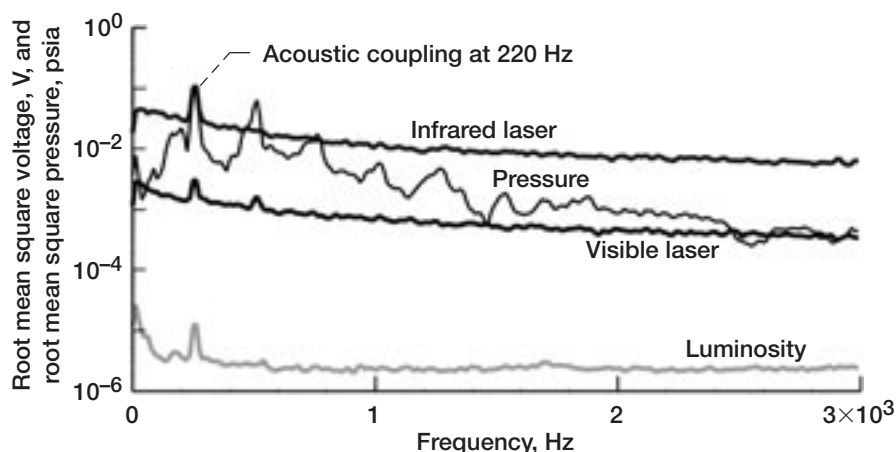
Experimental facility located in test cell CE-5B (Stand 2) in Glenn's Engine Research Building. The laser absorption diagnostic system is portable and is mounted on two small optical breadboards shown by the dashed boxes. *Italicized text denotes real-time data-producing components of the experiment.* The dynamic pressure data are acquired with piezoresistive microphone transducers mounted in a semi-infinite tube arrangement for optimal pressure-signal fidelity. The time-averaged gaseous emissions measurements are obtained using a standard suite of online gas bench analyzers. This figure appears in color in the online version of this article (<http://www.grc.nasa.gov/WWW/RT2000/5000/5830nguyen.html>).

a period of 40 msec. The right side shows a histogram, or probability density function (PDF), of the equivalence ratio for this injector, which indicates how much "time" an injector spends at a given equivalence ratio. Well-designed injectors have very narrow PDF's, which translate to lower NO_x emissions and quieter operation. The bottom figure on the next page shows the frequency spectrum of the fluctuations in the dynamic combus-

tion pressure. These fluctuations drive fluctuations in both the infrared and visible laser signals (at 220 Hz). The final figure shows the amplitude and phase relationship between the combustion



Data from a "generic" LPP injector operating at 16.7 atm, 754 K, and an equivalence ratio of 0.542. Left: Time-resolved data collected at a rate of 12 kHz. Equivalence mean, 0.532; equivalence standard deviation, 0.240. Right: Probability density function (PDF) of the equivalence ratio at this operating condition. Note that this injector is far from perfect in that it has a very wide PDF.



Power spectral density plot of signals acquired in the previous figure, showing the data in frequency space. The spectrum shows a moderate acoustic coupling at 220 Hz that corresponds to the fundamental (organ pipe) mode of the combustion rig.

pressure, the fuel line pressure, and the flame luminosity for a low inlet temperature condition. The frequency spectrum shows a very strong correlation between all the measured quantities and indicates that the dynamic combustion pressure modulates the fuel line pressure and, hence, the flow rate.

These are the first measurements of their kind that show a direct correlation between the quantitative fuel vapor fluctuations, dynamic pressure, fuel pressure, and flame luminosity at actual operating conditions. The measurements show that all the measured time-varying quantities are highly correlated in time and frequency—indicating that there is a basis for actively controlling combustion instabilities and noise normally associated with LPP combustion systems. Furthermore, the real-time data provide additional valuable information, such as the measured PDF of the equivalence ratio, which allows us to predict the emissions performance of new injector designs without resorting to expensive testing.

Find out more about research in Glenn's Combustion Branch:

<http://www.grc.nasa.gov/WWW/combustion/projects.html>

Reference

1. Nguyen, Quang-Viet; Mongia, Rajiv K.; and Dibble, Robert W.: Real-Time Optical Fuel-to-Air Ratio Sensor for Gas Turbine Combustors. NASA/TM-1999-209041, 1999.
<http://gltrs.grc.nasa.gov/GLTRS>

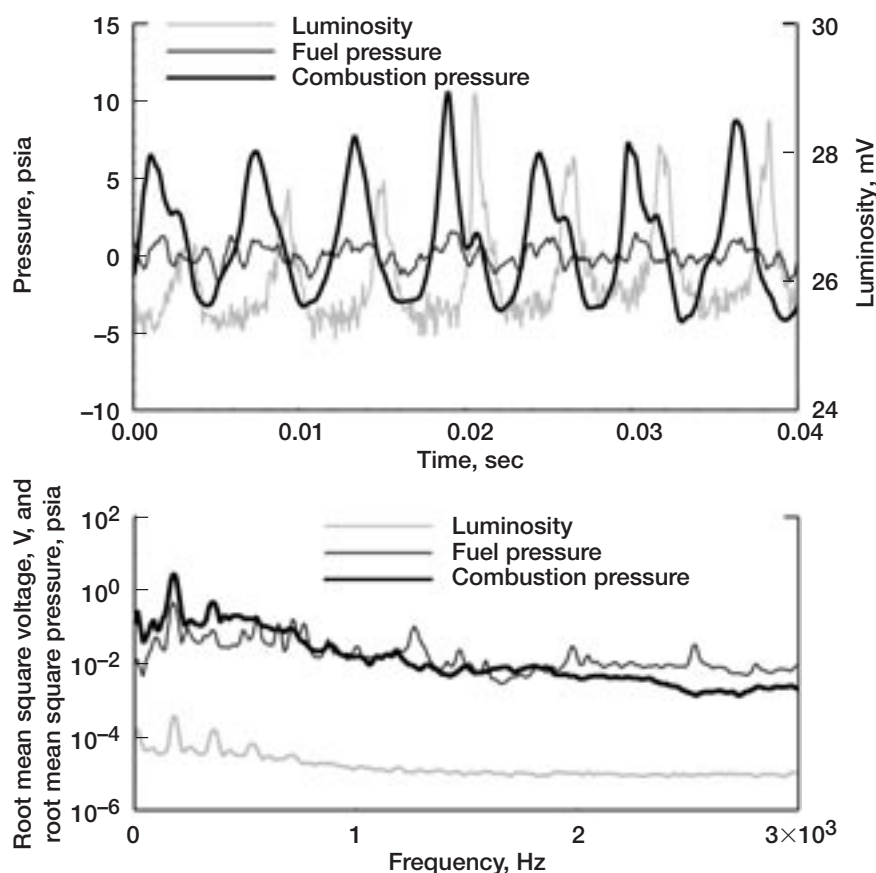
Glenn contact:

Dr. Quang-Viet Nguyen, 216-433-3574,
Quang-Viet.Nguyen@grc.nasa.gov

Author: Dr. Quang-Viet Nguyen

Headquarters program office: OAT

Programs/Projects: UEET



Example of strong acoustic coupling between dynamic combustion pressure, fuel line pressure, and bulk flame luminosity. The upper graph shows the time-varying signals over a 40-msec period. Note the luminosity in this case is almost pulselike and is out of phase with the pressure. The lower graph shows these signals in frequency space. The acoustic coupling between all the signals is clearly evident at about 200 Hz and even has substantially higher frequency harmonics.

Solid Hydrogen Particles Analyzed for Atomic Fuels

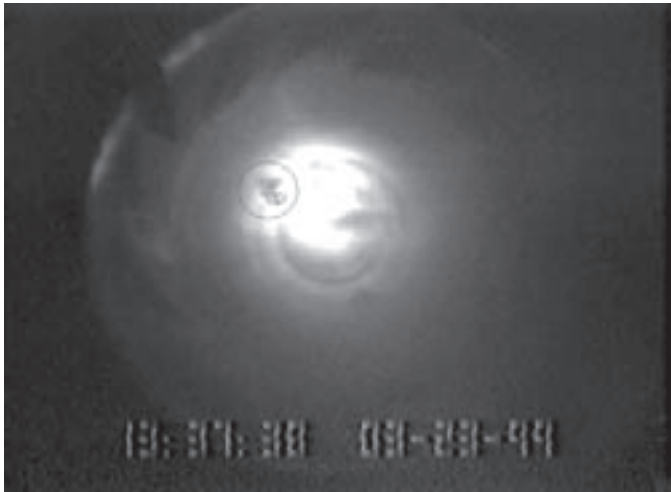
Solid hydrogen particles have been selected as a means of storing atomic propellants in future launch vehicles (refs. 1 to 2). In preparation for this, hydrogen particle formation in liquid helium was tested experimentally.

These experiments were conducted to visually characterize the particles and to observe their formation and molecular transformations (aging) while in liquid helium. The particle sizes, molecular transformations, and agglomeration times were estimated from video image analyses.

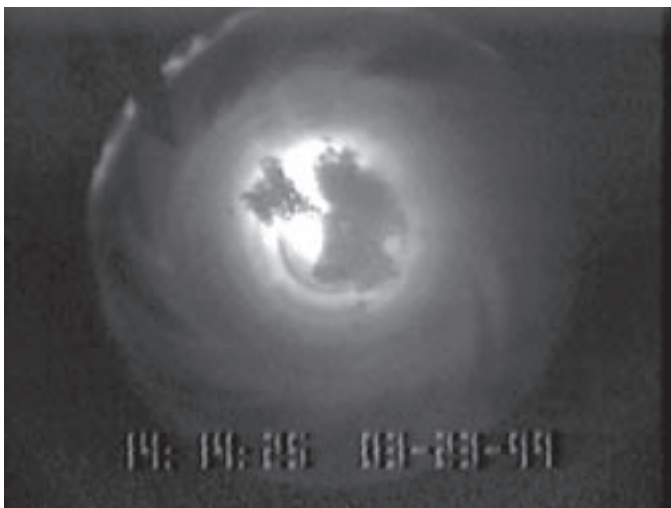
The experiments were conducted at the NASA Glenn Research Center in the Supplemental Multilayer Insulation Research Facility (SMIRF, ref. 3). The facility has a vacuum tank, into which the experimental setup was placed. The vacuum tank prevented heat leaks and subsequent boiloff of the liquid

helium, and the supporting systems maintained the temperature and pressure of the liquid helium bath where the solid particles were created.

As the operation of the apparatus was developed, the hydrogen particles were easily visualized. The figures (ref. 1) show images from the experimental runs. The first image shows the initial particle freezing, and the second image



Solid hydrogen particles floating on the surface of a liquid helium bath. A small number of frozen particles have clumped together.



Solid hydrogen particles after they have all clumped together. The particle clumping process took up to 11 min.

shows the particles after the small particles have agglomerated. The particles finally all clump, but stick together loosely. The solid particles tended to agglomerate within a maximum of 11 min, and the agglomerate was very weak. Because the hydrogen particles are buoyant in the helium, the agglomerate tends to compact itself into a flat pancake on the surface of the helium. This pancake agglomerate is easily broken apart by reducing the pressure above the liquid. The weak agglomerate implies that the particles can be used as a gelling agent for the liquid helium, as well as a storage medium for atomic boron, carbon, or hydrogen.

The smallest particle sizes that resulted from the initial freezing experiments were about 1.8 mm. About 50 percent of the particles formed were between 1.8 to 4.6 mm in diameter. These very small particle sizes are encouraging for future formation experiments, where simpler operations will reduce the costs of production.

The particle freezing process was completed almost immediately after the hydrogen fell onto the liquid helium surface, and the molecular structure of the hydrogen tended to change from a face-centered-cubic to a hexagonal-close-packed structure within 1 min. This transition must be controlled to allow the deposition of atoms into the solid particles. Further analysis of the images is needed to more fully understand the particle formation and to better understand the structural transition in such small particles.

Find out more about our research with fuels and space propellants:

<http://www.grc.nasa.gov/WWW/TU/launch/foctopsb.htm>

References

1. Palaszewski, Bryan: Solid Hydrogen Experiments for Atomic Propellants. AIAA Paper 2000-3855, 2000.
2. Palaszewski, Bryan: Launch Vehicle Performance for Bipropellant Propulsion Using Atomic Propellants With Oxygen. AIAA Paper 99-2837, 1999.
3. Dempsey, P.J.; and Stochl, R.J.: Supplemental Multilayer Insulation Research Facility. NASA/TM-106991, 1995. <http://gltrs.grc.nasa.gov/GLTRS>

Glenn contact:

Bryan A. Palaszewski, 216-977-7493, Bryan.A.Palaszewski@grc.nasa.gov

Author: Bryan A. Palaszewski

Headquarters program office: OAT

Programs/Projects: ASTP, STR

Safer Aircraft Possible With Nitrogen Generation

A system named On-Board Inert Gas Generation System/On-Board Oxygen Generation System (OBIGGS/OBOGS) was studied with Boeing (ref. 1). The study established the requirements for nitrogen purge (for fuel tank inerting and cargo compartment fire suppression) and oxygen (for passengers and crew). The nitrogen would be used for suppressing fires and fuel tank explosions on the aircraft, and the oxygen would be used for breathing gas during high-altitude or emergency operations.

In the vision of the Aviation Safety Program, a nitrogen-generation system might be used in a combined suppression system. Halon gas or a water spray would be used for initial fire suppression; then nitrogen would blanket the burned materials, assuring that a fire would not reignite.

The following figure shows the nitrogen required for fire suppression aboard several commercial aircraft: 737 through 777. The nitrogen volume required grows significantly with the higher requirements for nitrogen percentage in the cargo compartment atmosphere. The figure on the next page depicts the related requirements for oxygen generation aboard the 777 aircraft. Additional data for many aircraft types were created.

The study provided the initial information for sizing the fuel tank inerting systems using ground-based and aircraft-based OBIGGS/OBOGS. Other important results in the study were the requirements and timing for aircraft operations, and timing for airport operations to support OBIGGS/OBOGS.

A number of technologies for inerting and oxygen production were suggested. These technologies included hollow fiber membrane and air liquefaction. The study fostered coordination with Boeing designers and technology planners, allowing for easier transition to flight certification and future test flights.

The study was also coordinated with the Federal Aviation Administration Technical Center (Atlantic City, NJ), whose contacts with numerous working groups allow for a diverse multipronged international research program.

NASA Glenn sponsored this work as part of the Accident Mitigation aspects of Fire Prevention under the NASA Aviation Safety Program. A follow-on study to assess the current and future state of the art is being conducted with Boeing/FAA.

Reference

1. Reynolds, Thomas L., et al.: Onboard Inert Gas Generation System/ Onboard Oxygen Gas Generation System (OBIGGS/OBOGS) Study (Subtask 1). Aircraft and Spacecraft Guidance and Controls Research Task Order 11, Boeing Commercial Airplane Group, Seattle, WA, June 30, 2000.

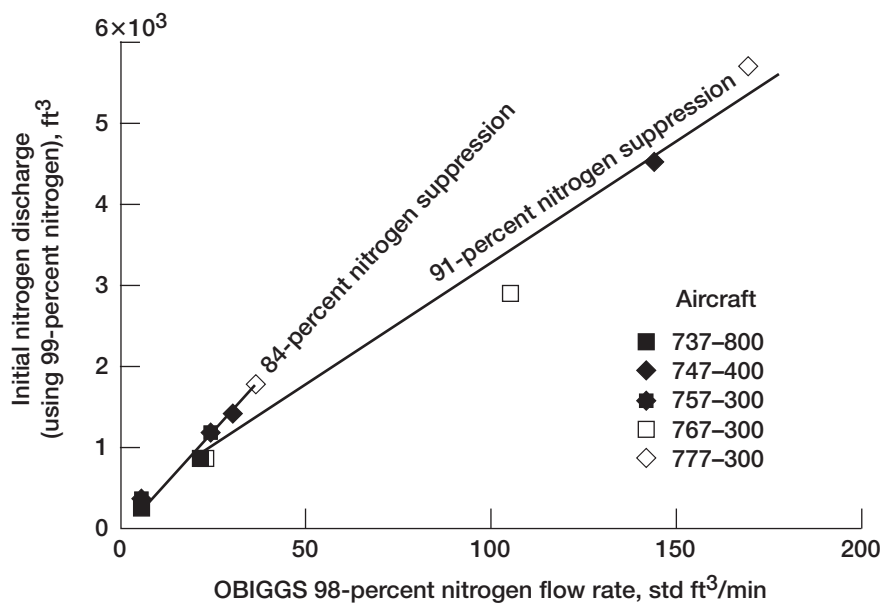
Find out more about this research:

Aviation safety:

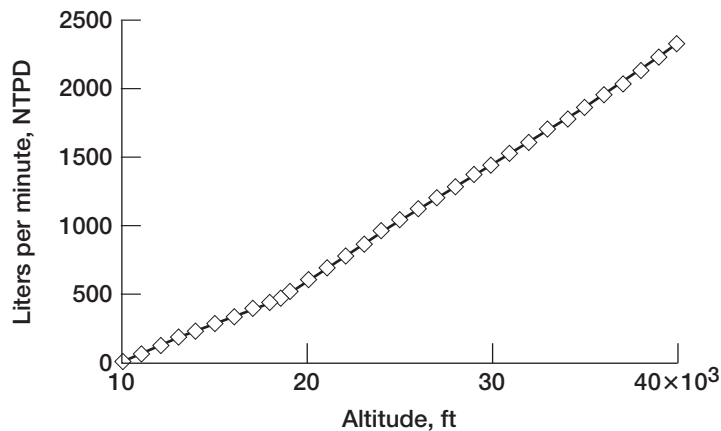
<http://www.aero-space.nasa.gov/goals/safety.htm>

Aviation safety at Glenn:

<http://www.grc.nasa.gov/WWW/grcavsp>



Nitrogen-generation requirements for existing transport aircraft.



Oxygen-generation requirements for existing transport aircraft.
NTPD, normal pressure and temperature dry.

Glenn contacts:

Bryan A. Palaszewski, 216-977-7493,
Bryan.A.Palaszewski@grc.nasa.gov; and
Douglas A. Rohn, 216-433-3325,
Douglas.A.Rohn@grc.nasa.gov

Author: Bryan A. Palaszewski

Headquarters program office: OAT

Programs/Projects: AvSP (Fire
Prevention, Accident Mitigation)

Safer Aviation Materials Tested

A series of thermally stable polymer samples were tested. These materials are called low heat release materials and are designed for aircraft interior decorative materials. The materials are designed to give off a minimum amount of noxious gases when heated, which increases the possibility that people can escape from a burning aircraft.

New cabin materials have suitably low heat release so that fire does not spread, toxic chemicals are not given off, and the fire-emergency escape time for crew and passengers is lengthened. These low heat-release materials have a variety of advantages and applications: interiors for ground-based facilities, interiors of space vehicles, and many commercial fire-protection environments.

A microscale combustion calorimeter at the Federal Aviation Administration's (FAA) Technical Center tested NASA Langley Research Center materials samples. The photo shows the calorimeter.

A sharp, quantitative, and reproducible heat-release-rate peak is obtained in the microscale heat-release-rate test. The newly tested NASA materials significantly reduced the heat-release capacity and total heat release.

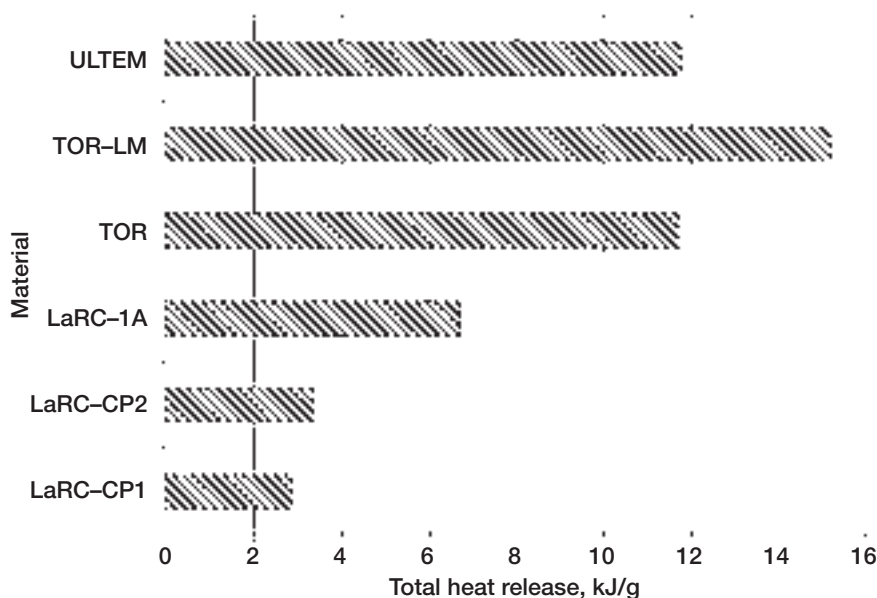
The thermal stability and flammability behavior of the samples was very good. The new materials demonstrated a factor of 4 reduction in total heat release over ULTEM (a currently used material). This information is provided in the following barchart. In other tests, the materials showed greater than a factor 9 reduction in heat-release capacity over ULTEM. The newly tested materials were developed for low dielectric constant, low color, and good solubility.



Calorimeter testing rig at FAA Technical Center.

A scale up of the material samples is needed to determine the repeatability of the performance in larger samples. Larger panels composed of the best candidate materials will be tested in a larger scale FAA Technical Center fire facility.

The NASA Glenn Research Center, Langley (Jeff Hinkley), and the FAA Technical Center (Richard Lyon) cooperatively tested these materials for the Accident Mitigation aspects of Fire Prevention under NASA's Aviation Safety Program.



Material (total heat release) properties for NASA samples newly tested as part of the FAA ultralow heat-release materials project.

Find out more about this research on the World Wide Web:

Aviation safety: <http://www.aero-space.nasa.gov/goals/safety.htm>

Aviation safety research at Glenn: <http://www.grc.nasa.gov/WWW/grcavsp>

FAA fire research: <http://www.fire.tc.faa.gov>, see "Materials Group"

Glenn contacts:

Bryan A. Palaszewski, 216-977-7493, Bryan.A.Palaszewski@grc.nasa.gov; and Douglas A. Rohn, 216-433-3325, Douglas.A.Rohn@grc.nasa.gov

Author: Bryan A. Palaszewski

Headquarters program office: OAT

Programs/Projects: AvSP
(Fire Prevention, Accident Mitigation)

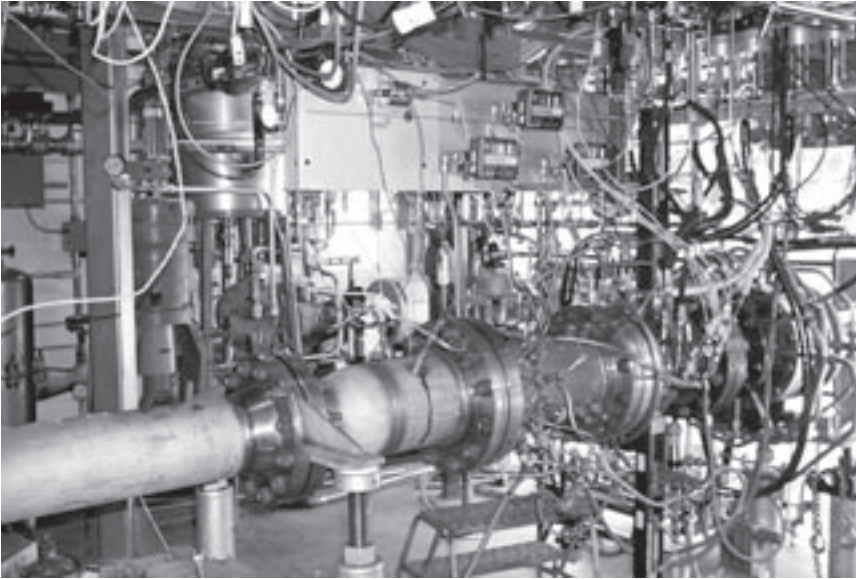
Hydrogen/Air Fuel Nozzle Emissions Experiments

The use of hydrogen combustion for aircraft gas turbine engines provides significant opportunities to reduce harmful exhaust emissions. Hydrogen has many advantages (no CO₂ production, high reaction rates, high heating value, and future availability), along with some disadvantages (high current cost of production and storage, high volume per BTU, and an unknown safety profile when in wide use). One of the primary reasons for switching to hydrogen is the elimination of CO₂ emissions. Also, with hydrogen, design challenges such as fuel coking in the fuel nozzle and particulate emissions are no longer an issue. However, because it takes place at high temperatures, hydrogen-air combustion can still produce significant levels of NO_x emissions. Much of the current research into conventional hydrocarbon-fueled aircraft gas turbine combustors is focused on NO_x-reduction methods. The Zero CO₂ Emission Technology (ZCET) hydrogen combustion project will focus on meeting the Office of Aerospace Technology goal 2 within pillar one for Global Civil Aviation—reducing the emissions of future aircraft by a factor of 3 within 10 years and by a factor of 5 within 25 years.

Recent advances in hydrocarbon-based gas turbine combustion components have expanded the horizons for fuel nozzle development. Both new fluid designs and manufacturing technologies have led to the devel-

opment of fuel nozzles that significantly reduce aircraft emissions. The goal of the ZCET program is to mesh the current technology of Lean Direct Injection and rocket injectors to provide quick mixing, low emissions, and high-performance fuel nozzle designs.

An experimental program is planned to investigate the fuel nozzle concepts in a flametube test rig. Currently, a hydrogen system is being installed in cell 23 at NASA Glenn Research Center's Research Combustion Laboratory. Testing will be conducted on a variety of fuel nozzle concepts up to combustion pressures of 350 psia and inlet air temperatures of 1200 °F. Computational fluid dynamics calculations, with the



Hydrogen flametube rig located in cell 23 of Glenn's Research Combustion Laboratory.

Glenn-developed National Combustor Code, are being performed to optimize the fuel nozzle designs.

Glenn contact:

Timothy D. Smith, 216-977-7546,
Timothy.D.Smith@grc.nasa.gov

Author: Timothy D. Smith

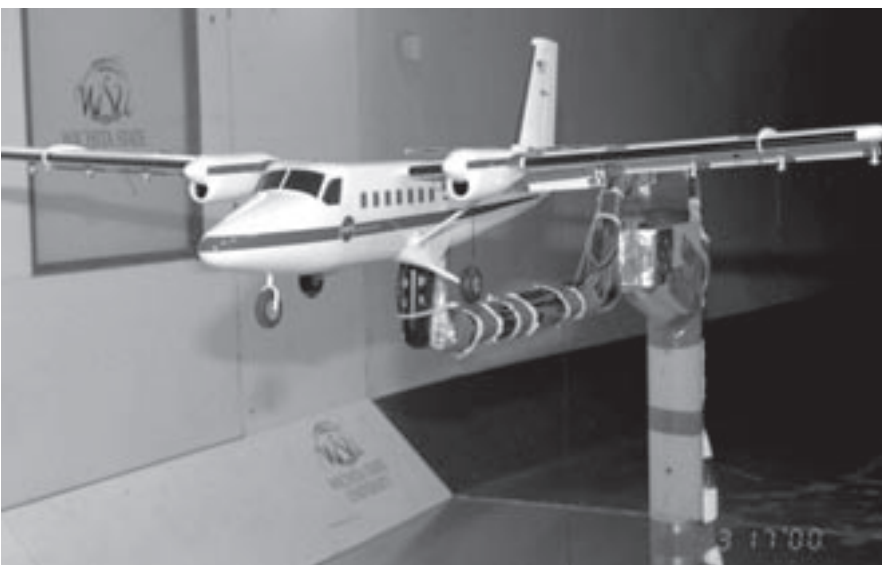
Headquarters program office: OAT

Programs/Projects: ZCET

Wind Tunnel Tests Conducted to Develop an Icing Flight Simulator

As part of NASA's Aviation Safety Program goals to reduce aviation accidents due to icing, NASA Glenn Research Center is leading a flight simulator development activity to improve pilot training for the adverse flying characteristics due to icing. Developing flight simulators that incorporate the aerodynamic effects of icing will provide a critical element in pilot

training programs by giving pilots a pre-exposure of icing-related hazards, such as ice-contaminated roll upset or tailplane stall. Integrating these effects into training flight simulators will provide an accurate representation of scenarios to develop pilot skills in unusual attitudes and loss-of-control events that may result from airframe icing.

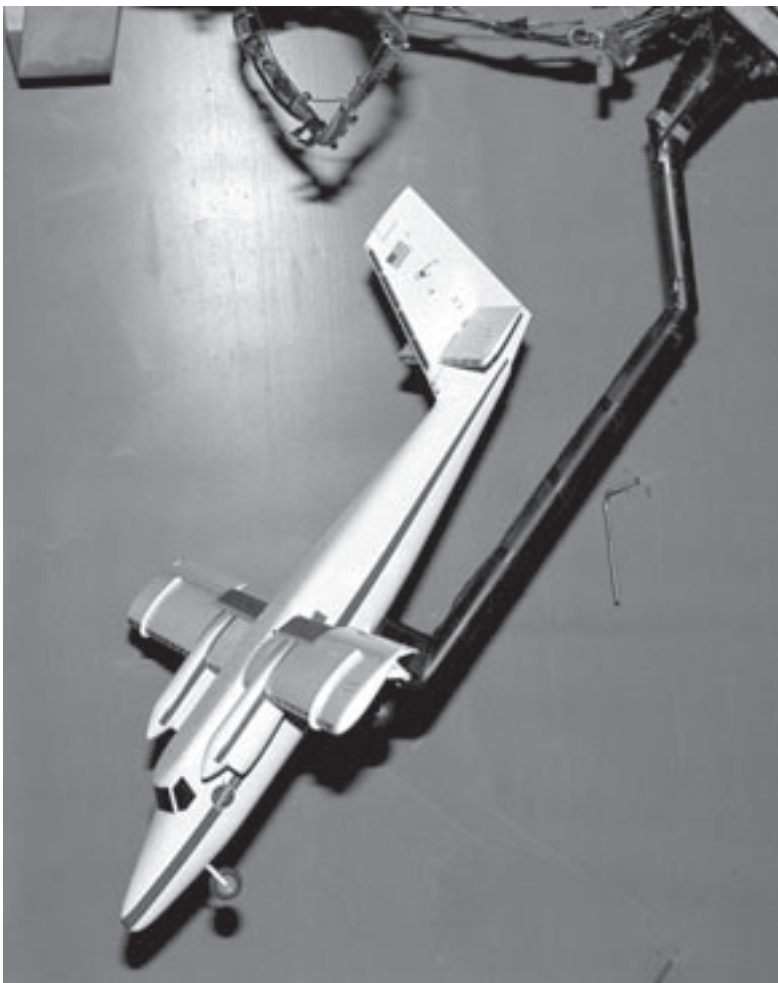


6.5-percent-scale Twin Otter model in the Wichita State University 7- by 10-ft wind tunnel for static testing.

In order to achieve a high level of fidelity in the flight simulation, a series of wind tunnel tests have been conducted on a 6.5-percent-scale Twin Otter aircraft model. These wind tunnel tests were conducted at the Wichita State University 7- by 10-ft wind tunnel and Bihle Applied Research's Large Amplitude Multiple Purpose Facility in Neuburg, Germany. The Twin Otter model was tested without ice (baseline), and with two ice configurations: (1) ice on the



Simulated ice shape on leading edge of the horizontal tail.



6.5-percent-scale Twin Otter model in Bihrlle Applied Research vertical wind tunnel for dynamic testing.

horizontal tail only and (2) ice on the wing, horizontal tail, and vertical tail. These wind tunnel tests resulted in data bases of aerodynamic forces and moments as functions of angle of attack; sideslip; control surface deflections; forced oscillations in the pitch, roll, and yaw axes; and various rotational speeds. A limited amount of wing and tail surface pressure data were also measured for comparison with data taken at Wichita State and with flight data. The data bases from these tests will be the foundation for a PC-based Icing Flight Simulator to be delivered to Glenn in fiscal year 2001.

Validation flight tests are planned to be conducted with the NASA Twin Otter Icing Research Aircraft equipped with similar artificial ice shapes in fiscal year 2001. Pilot training scenarios will be developed in cooperation with flight training experts, and the methodology of the development process documented in NASA technical reports.

Find out more about icing research at Glenn: <http://icebox.grc.nasa.gov>

Glenn contact:

Thomas P. Ratvasky, 216-433-3905, Thomas.P.Ratvasky@grc.nasa.gov; and Thomas H. Bond, 216-433-3900, Thomas.H.Bond@grc.nasa.gov

Author: Thomas P. Ratvasky

Headquarters program office: OAT

Program/Projects: AvSP (SWAP)

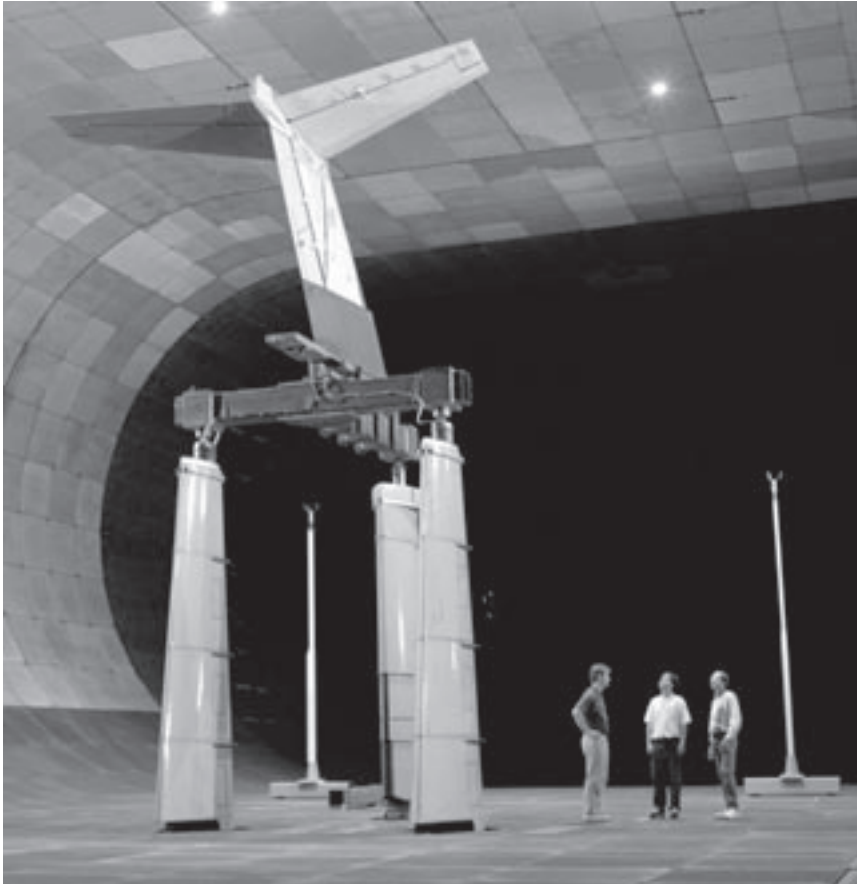
Icing Effects on a Full-Scale Business Jet Empennage

Recent safety findings have identified ice-contaminated tailplane stall as the cause of a significant number of aviation accidents that have occurred over the past three decades. The NASA Glenn Research Center, the Federal

Aviation Administration, industry, and academia have collaborated in research efforts to better understand the ice-contaminated tailplane stall phenomena and to improve test techniques and design tools to reduce this hazard. An initial research effort, called the NASA/FAA Tailplane Icing Program (TIP), focused on a commuter aircraft configuration. A follow-on program was developed (TIP 2) to examine the tailplane icing effects on a modern business jet configuration with the goals of developing improved test techniques and data bases for similitude and code validation.

To attain these goals, full-scale and subscale tests were required. Glenn's Icing Branch collaborated with the Wichita State University and Learjet, Inc., to conduct icing aeroperformance effect research on three models of a business jet, including a full-scale business jet empennage. The full-scale business jet empennage was tested in NASA Ames Research Center's 40- by 80-ft wind tunnel to obtain aeroperformance data for the clean (no-ice baseline) and ice-contaminated tail. The ice contamination consisted of nine variations of artificial ice shapes that included several LEWICE ice shapes, spoilers, sandpaper roughness, and a casting developed in an Icing Research Tunnel test. Force and moment measurements were made over a range of Reynolds numbers, angle of attack, sideslip, and elevator positions for each ice contamination. Likewise, surface pressure and boundary layer measurements, and some flow visualization were accomplished to aid in code development.

The full-scale data base is being analyzed and will be reported in



Full-scale business jet empennage model inside NASA Ames's 40- by 80-ft wind tunnel.



Simulated ice shape on the leading edge of the business jet's horizontal tail.



NASA Glenn icing researcher inspecting an ice casting mounted to the business jet's horizontal tail.

fiscal year 2001 with comparisons to results from a previous test of a 25-percent-scale business jet empennage model. Also, a 15-percent-scale model of a complete business jet aircraft will be tested with ice on the

horizontal tail. This research will provide improved test methodologies for aerodynamically scaling ice contamination and will provide the data bases to serve as valuable resources for designers and code developers as they validate tools for predicting aeroperformance effects with ice contamination. These tools will be highly beneficial to airframe manufacturers by reducing the time and cost of certification for icing conditions.

Find out more about icing research at Glenn: <http://icebox.grc.nasa.gov>

Glenn contacts:

Thomas P. Ratvasky, 216-433-3905, Thomas.P.Ratvasky@grc.nasa.gov; and Julius A. Giriunas, 216-433-3794, Julius.A.Giriunas@grc.nasa.gov

Author: Thomas P. Ratvasky

Headquarters program office: OAT

Programs/Projects: AOS

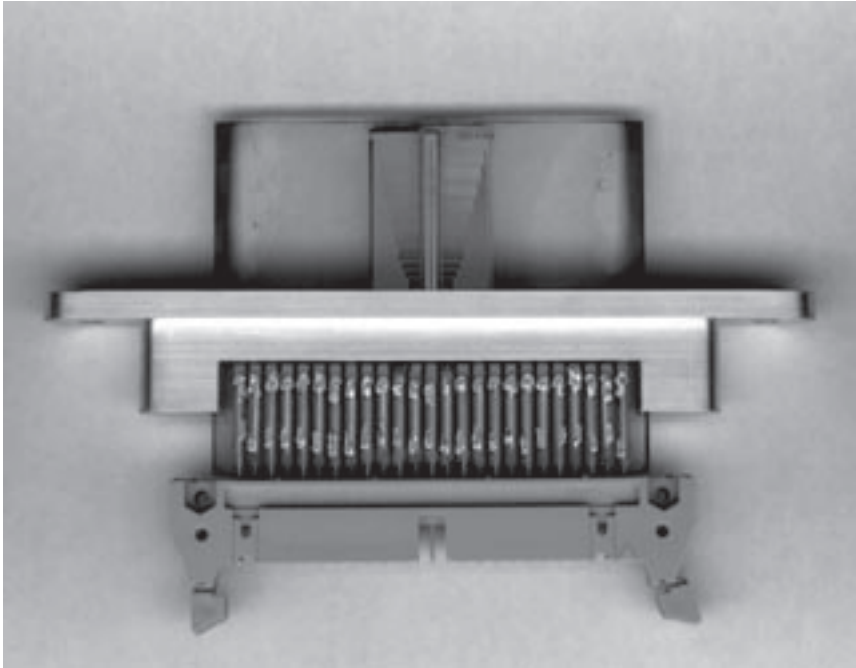
Thermocouple Rakes for Measuring Boundary Layer Flows Extremely Close to Surface

Of vital interest to aerodynamic researchers is precise knowledge of the flow velocity profile next to the surface. This information is needed for turbulence model development and the calculation of viscous shear force. Though many instruments can determine the flow velocity profile near the surface, none of them can make measurements closer than approximately 0.01 in. from the surface. The thermocouple boundary-layer rake can measure much closer to the surface than conventional instruments can, such as a total pressure boundary layer rake, hot wire, or hot film.

By embedding the sensors (thermocouples) in the region where the velocity is equivalent to the velocity ahead of a constant thickness strut, the boundary-layer flow profile can be obtained. The present device fabricated at the NASA Glenn Research Center microsystem clean room has a heater made of platinum and thermocouples made of platinum and gold. Equal numbers of thermocouples are placed both upstream and downstream of the heater, so that the voltage generated by each pair at the same distance from the surface is indicative of the difference in temperature between the upstream and downstream thermocouple locations. This voltage differential is a function of the flow velocity, and like the conventional total pressure rake, it can provide the velocity profile. In order to measure flow

extremely close to the surface, the strut is made of fused quartz with extremely low heat conductivity. A large size thermocouple boundary layer rake is shown in the following photo.

The latest medium size sensors already provide smooth velocity profiles well into the boundary layer, as close as 0.0025 in. from the surface. This is about 4 times closer to the surface than the previously used total pressure rakes. This device also has the advantage of providing the flow profile of separated flow and also it is possible to measure simultaneous turbulence levels within the boundary layer.



Large thermocouple boundary layer rake.

Bibliography

Hwang, Danny P.: Miniature Boundary-Layer Airfoil With Embedded Hot Wires. NASA Tech Briefs, vol. 21, no. 5, May 1997, p. 60.

Hwang, Danny P.; Will, Herbert A.; and Fralick, Gustave C.: Thermocouple Rakes for Measuring Boundary-Layer Flows. NASA Tech Brief LEW-16999-1, Aug. 10, 2000.

Find out more about this research:

<http://www.grc.nasa.gov/www/microblowing>

Glenn contacts:

Dr. Danny P. Hwang, 216-433-2187, Danny.P.Hwang@grc.nasa.gov; and Gustave C. Fralick, 216-433-3645, Gustave.C.Fralick@grc.nasa.gov

Authors:

Dr. Danny P. Hwang, Gustave C. Fralick, Lisa C. Martin, and Charles A. Blaha

Headquarters program office: OAT

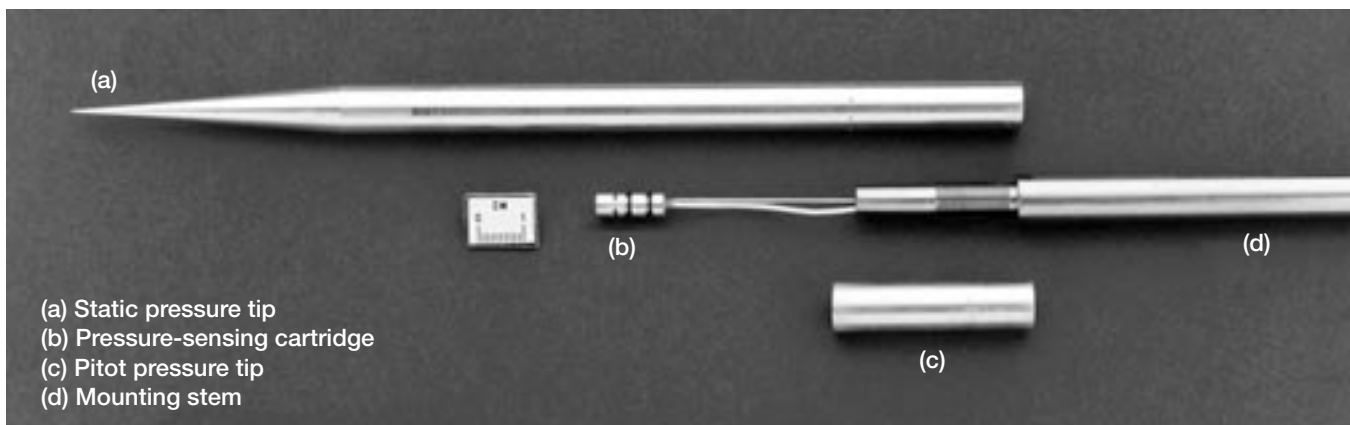
Programs/Projects: SRF

Special recognition: Patent pending

Dynamic Pressure Probes Developed for Supersonic Flow-Field Measurements

Current trends in supersonic propulsion research tend to focus more on analyzing transient fluid flow phenomena. Steady-state data, although valuable and informative, may not give a true characterization of the flow field in question. What may appear to be a benign steady-state flow may have some undesirable transient characteristics that do not come to light because of the time-averaged nature of steady-state data acquisition. In the case of supersonic propulsion systems, recent analyses show that the instantaneous dynamic flow distortion at the inlet/engine interface plane is a more reliable predictor of impending engine compressor surge and stall

than the steady-state flow distortion is. Also, fast-acting transients, such as an inlet unstart and subsequent engine compressor stall, occur on a millisecond time scale and cannot be adequately characterized with steady-state instrumentation.



Flow-field pressure probe components.

A series of dynamic flow-field pressure probes were developed for use in large-scale supersonic wind tunnels at the NASA Glenn Research Center. These flow-field probes include pitot and static pressure probes that can capture fast-acting flow-field pressure transients occurring on a millisecond timescale. The pitot and static probes can be used to determine local Mach number time histories during a transient event. A photograph of the flow-field pressure probe is shown on the preceding page. The probe design contains four major components: (1) a static pressure aerodynamic tip, (2) a pressure-sensing cartridge assembly, (3) a pitot pressure aerodynamic tip, and (4) a mounting stem. This modular design allows for a variety of probe tips to be used for a specific application. Here, the focus is on flow-field pressure measurements in supersonic flows, so we developed a cone-cylinder static pressure tip and a pitot pressure tip. Alternatively, probe tips optimized for subsonic and transonic flows could be used with this design. The pressure-sensing cartridge assembly allows the simultaneous measurement of steady-state and transient pressure which allows continuous calibration of the dynamic pressure transducer. The transient frequency response is nominally 800 Hz when the static pressure probe tip is used and 1900 Hz when the pitot pressure probe tip is used.

These probes were designed, developed, and tested at NASA Glenn. They were also used in a NASA Glenn Research Center 10- by 10-Foot Supersonic Wind Tunnel test program, where they successfully acquired flow-

field pressure data in the vicinity of a propulsion system during an engine compressor stall and inlet unstart transient event (ref. 1).

Reference

1. Porro, A.R.: Inlet Unstart Propulsion Integration Wind Tunnel Test Program Completed for High-Speed Civil Transport. Research & Technology 1999, NASA/TM-2000-209639, 2000, p. 87.
<http://www.grc.nasa.gov/WWW/RT1999/5000/5850porro.html>

Glenn contact:

A. Robert Porro, 216-433-5921,
Alvin.R.Porro@grc.nasa.gov

Author: A. Robert Porro

Headquarters program office: OAT

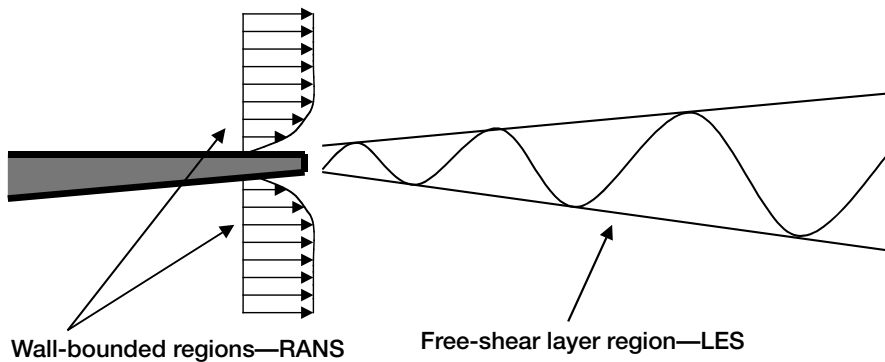
Programs/Projects: HSSO

Development of a Hybrid RANS/LES Method for Turbulent Mixing Layers

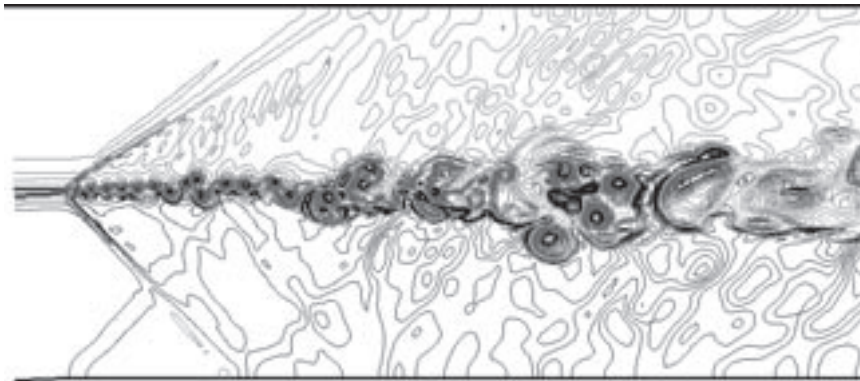
Significant research has been underway for several years in NASA Glenn Research Center's nozzle branch to develop advanced computational methods for simulating turbulent flows in exhaust nozzles. The primary efforts of this research have concentrated on improving our ability to calculate the turbulent mixing layers that dominate flows both in the exhaust systems of modern-day aircraft and in those of hypersonic vehicles under development. As part of these efforts, a hybrid numerical method was recently developed to simulate such turbulent mixing layers. The method developed here is intended for configurations in which a dominant structural feature provides an unsteady mechanism to drive the turbulent development in the mixing layer.

Interest in Large Eddy Simulation (LES) methods have increased in recent years, but applying an LES method to calculate the wide range of turbulent scales from small eddies in the wall-bounded regions to large eddies in the mixing region is not yet possible with current computers. As a result, the hybrid method developed here uses a Reynolds-averaged Navier-Stokes (RANS) procedure to calculate wall-bounded regions entering a mixing section and uses a LES procedure to calculate the mixing-dominated

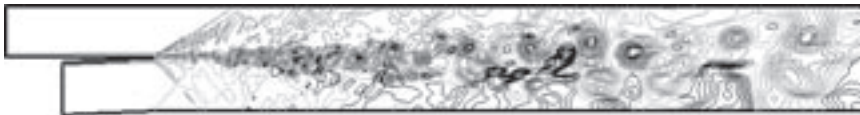
regions. A numerical technique was developed to enable the use of the hybrid RANS-LES method on stretched, non-Cartesian grids. With this technique, closure for the RANS equations is obtained by using the Cebeci-Smith algebraic turbulence model in conjunction with the wall-function approach of Ota and Goldberg. The LES equations are closed using the Smagorinsky subgrid scale model. Although the function of the Cebeci-Smith model to replace all of the turbulent stresses is quite different from that of the Smagorinsky subgrid model, which only replaces the small subgrid turbulent stresses, both are eddy



Mixing layer illustrating the hybrid RANS-LES approach.



Instantaneous density contours for the entire mixing section.



Instantaneous density contours near the beginning of the mixing section.

viscosity models and both are derived at least in part from mixing-length theory. The similar formulation of these two models enables the RANS and LES equations to be solved with a single solution scheme and computational grid.

The hybrid RANS-LES method has been applied to a benchmark compressible mixing layer experiment in which two isolated supersonic streams, separated by a splitter plate, provide the flows to a constant-area mixing section. Although the configuration is largely two dimensional in nature, three-dimensional calculations were found to be necessary to enable disturbances to develop in three spatial directions and to transition to turbulence. The flow in the initial part of the mixing section consists of a periodic vortex shedding downstream of the splitter plate trailing edge. This organized vortex shedding then rapidly transitions to a turbulent structure, which is very similar to the flow development observed in the experiments. Although the qualitative nature of the large-scale turbulent development in the entire mixing section is captured well by the LES part

of the current hybrid method, further efforts are planned to directly calculate a greater portion of the turbulence spectrum and to limit the subgrid scale modeling to only the very small scales. This will be accomplished by the use of higher accuracy solution schemes and more powerful computers, measured both in speed and memory capabilities.

Glenn contact:

Nicholas J. Georgiadis, 216-433-3958,
Nicholas.J.Georgiadis@grc.nasa.gov

Authors: Nicholas J. Georgiadis,
J. Iwan D. Alexander, and Eli Reshotko

Headquarters program office: OAT

Programs/Projects:
Propulsion Systems R&T

Restraint of Liquid Jets by Surface Tension in Microgravity Modeled

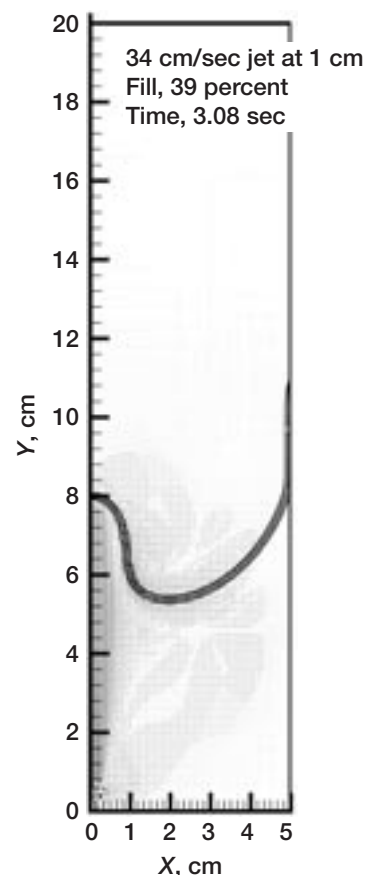
Microgravity poses many challenges to the designer of spacecraft tanks. Chief among these are the lack of phase separation and the need to supply vapor-free liquid or liquid-free vapor to the spacecraft processes that require fluid. One of the principal problems of phase separation is the creation of liquid jets. A jet can be created by liquid filling, settling of the fluid to one end of the tank, or even closing a valve to stop the liquid flow. Anyone who has seen a fountain knows that jets occur in normal gravity also. However, in normal gravity, the gravity controls and restricts the jet flow. In microgravity, with gravity largely absent, jets must be contained by surface tension forces. Recent NASA experiments in microgravity (Tank Pressure Control Experiment, TPCE, and Vented Tank Pressure Experiment, VTRE) resulted in a wealth of data about jet behavior in microgravity. VTRE was surprising in that, although it contained a complex geometry of baffles and vanes, the limit on liquid inflow was the emergence of a liquid jet from the top of the vane structure. Clearly understanding the restraint of liquid jets by surface tension is key to managing fluids in low gravity.

To model this phenomenon, we need a numerical method that can track the fluid motion and the surface tension forces. The fluid motion is modeled with the Navier-Stokes equation formulated for low-speed incompressible flows. The quantities of velocity and pressure are placed on a staggered grid, with velocity being tracked at cell faces and pressure at cell centers. The free surface is tracked via the introduction of a color function that tracks liquid as $1/2$ and gas as $-1/2$. A phase model developed by Jacqmin (ref. 1) is used. This model converts the discrete surface tension force into a barrier function that peaks at the free surface and decays rapidly. Previous attempts at this formulation have been criticized for smearing the interface. However, by sharpening the phase function, double gridding the fluid function, and using a higher order solution for the fluid function, interface smearing is avoided. These equations can be rewritten as two coupled Poisson equations that also include the velocity. The method of solution is as follows: first, the phase equations are solved from this solution, a velocity field is generated, then a successive overrelaxation scheme is used to solve for a pressure field consistent with the velocity solution.

After the code was implemented in axisymmetric form and verified by several test cases, the drop tower runs of Aydelott (ref. 2) were modeled. The model handled the free-surface deformation quite nicely, even to the point of modeling geyser growth in the regime where the free surface was no longer restrained. A representative run is shown in the graph.

References

1. Jacqmin, D.: Calculation of Two-Phase Navier-Stokes Flows Using Phase-Field Modeling. *J. Computational Physics*, vol. 155, 1999, pp. 96–127.
2. Aydelott, J.C.: Modeling of Space Vehicle Propellant Mixing. NASA TP–2107, 1983.



Computer simulation of submerged liquid jet striking the free surface in microgravity. Jet of 34 cm/sec at 1 cm; fill, 39 percent; time, 3.08 sec; reference vector, 10 cm/sec.

Glenn contacts:

Dr. David J. Chato, 216–977–7488, David.J.Chato@grc.nasa.gov; and
Dr. David A. Jacqmin, 216–433–5853, David.A.Jacqmin@grc.nasa.gov

Author: Dr. David J. Chato

Headquarters program office: OAT

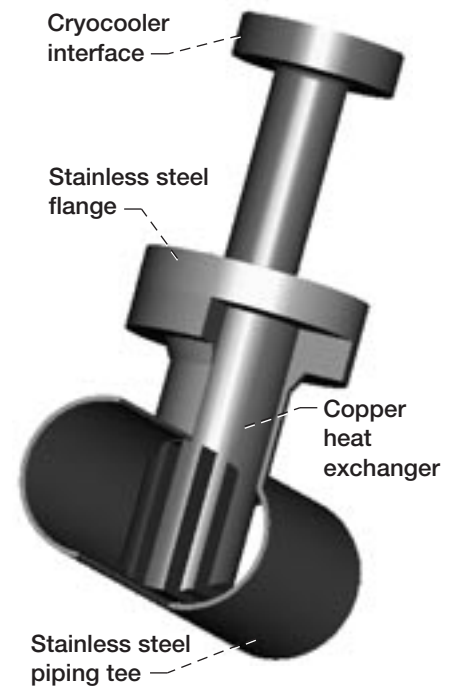
Programs/Projects: HEDS, ASTP

Zero-Boiloff Cryogenic Storage Cryocooler Integration Test

Developments in NASA Glenn Research Center's Centaur work have led to an exciting new cryogenic storage concept being considered for future NASA space missions. With long-duration cryogenic storage, propellants will boil off because of the environmental heating of the tank. To accommodate these losses, extra propellant is required along with larger propellant tanks. Analyses of space transportation concepts show that space-transfer cryogenic stages with the zero boiloff (ZBO) cryogenic storage concept reduce the stage mass for missions longer than approximately 45 days in low Earth orbit. The ZBO system consists of an active cryocooling system using a cryocooler in addition to traditional passive thermal insulation.

Engineers at Glenn analyzed, designed, built, and bench tested a heat exchanger and integration hardware for a large-scale ZBO demonstration for the NASA Marshall Space Flight Center. The heat exchanger, which transfers the heat that enters the tank from the fluid to the cryocooler, must limit the temperature difference across it to limit the cryocooler size and power requirements. With a low temperature difference, the system efficiency is improved.

For that temperature difference to be reduced, the thermal conductivity must be as high as possible at liquid hydrogen temperatures, around 25 K (-248°C). In addition, it is important for the heat exchanger to be welded to a stainless steel flange and have enough strength to accommodate piping stress. High-conductivity copper was selected and fabricated, then integrated with the stainless steel piping tee as shown in the cut-away representation. Literature showed that this conductivity might range from 2 to 100 W/cm/K but that is was likely to be around 13 W/cm/K. Unexpectedly, this conductivity was measured to be 23 W/cm/K, which limited the temperature increase along the heat exchanger to just 2 K. This limited temperature increase, compared with the predicted difference of 3.5 K, improves the overall system efficiency by 7.4 percent and limits the expected integration losses to a projected 4 percent with a flight design for liquid hydrogen storage. These results improve the cryocooler integration concept by allowing the cryocooler to operate at a lower input power, or by potentially permitting a smaller cryocooler to be selected.



Zero-boiloff heat exchanger concept.

Glenn contact:

David W. Plachta, 216-977-7126,
David.W.Plachta@grc.nasa.gov

Author: David W. Plachta

Headquarters program office: OAT

Programs/Projects:

Space Transfer Technologies

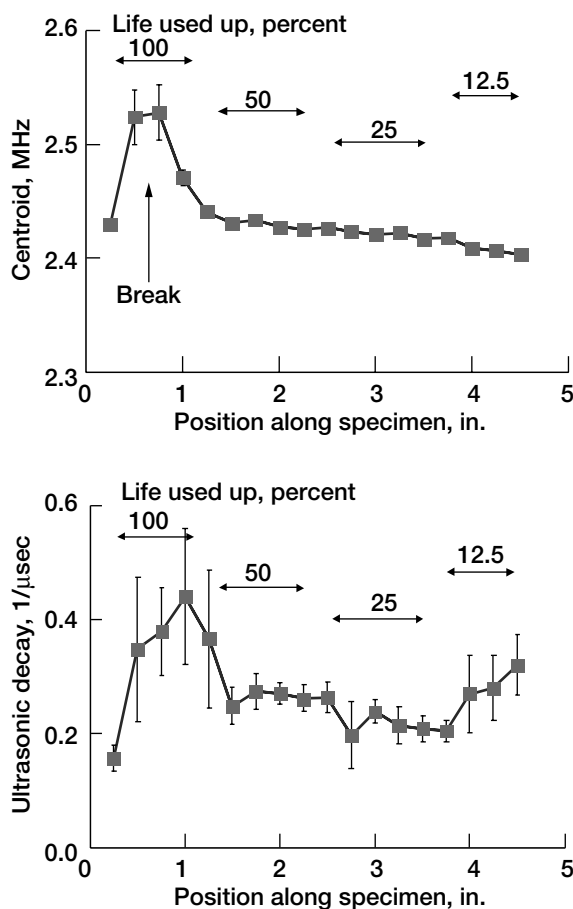
Structures and Acoustics

Damage Assessment of Creep Tested and Thermally Aged Metallic Alloys Using Acousto-Ultrasonics

In recent years emphasis has been placed on the early detection of material changes experienced in turbine powerplant components. During the scheduled overhaul of a turbine, the current techniques of examination of various hot section components aim to find flaws such as cracks, wear, and erosion, as well as excessive deformations. Thus far, these localized damage modes have been detected with satisfactory results. However, the techniques used to find these flaws provide no information on life until the

flaws are actually detected. Major improvements in damage assessment, safety, as well as more accurate life prediction could be achieved if nondestructive evaluation (NDE) techniques could be utilized to sense material changes that occur prior to the localized defects mentioned.

Because of elevated temperatures and excessive stresses, turbine components may experience creep behavior. As a result, it is desirable to monitor and access the current condition of such components. Research at the NASA Glenn Research Center involves developing and utilizing an NDE technique that discloses distributed material changes that occur prior to the localized damage detected by the current methods of inspection. In a recent study, creep processes in a nickel-base alloy were the life-limiting condition of interest, and the NDE technique was acousto-ultrasonics (AU). AU is an NDE technique that utilizes two ultrasonic transducers to interrogate the condition of a test specimen. The sending transducer introduces an ultrasonic pulse at a point on the surface of the specimen while a receiving transducer detects the signal after it has passed through the material. The goal of the method is to correlate certain parameters of the detected waveform to characteristics of the material between the two transducers. Here, the waveform parameter of interest is the attenuation due to internal damping for which information is being garnered from the frequency domain. The parameters utilized to indirectly quantify



Plots of the centroid of the power spectrum and ultrasonic decay rate as functions of position on a multistep specimen. The levels of used-up creep life are 100, 50, 25, and 12.5 percent for each of the four gauge widths, respectively. The specimen was creep tested at 1350 °F for 1395 hr.

the attenuation are the ultrasonic decay rate as well as various moments of the frequency power spectrum. A new, user-friendly, graphical interface AU system was developed at NASA Glenn. This system is an all-inclusive, multifunction system that controls the sending and receiving ultrasonic transducers as well as all posttest signal analysis. The system's postprocessing software calculates the multiple parameters used to study the material of interest.

The newly developed AU system was employed to monitor the state of damage due to creep testing in the nickel-base alloy, Udimet 520. A stepped specimen (i.e., varying cross-sectional area) was employed, which allowed for a post mortem NDE analysis of the various levels of used-up creep life. The AU method was able to detect material changes (i.e., distributed damage prior to the formation of localized cracks) as a function of used-up creep life. The AU parameters that displayed a functional dependence on used-up creep life were the centroid of the power spectrum and the ultrasonic decay rate (see the figure). With further research, confidence can be achieved and a protocol developed for utilizing AU as an early damage detection tool for turbine components that are exposed to various stress and temperature environments.

References

Gyekenyesi, A.L., et al.: Damage Assessment of Creep Tested and Thermally Aged Udimet 520 Using Acousto-Ultrasonics. Submitted to ASME Turbo Expo 2001, New Orleans, Louisiana, June, 2001.

Ohio Aerospace Institute contact: Dr. Andrew L. Gyekenyesi, 216-433-8155, Andrew.L.Gyekenyesi@grc.nasa.gov;

Glenn contacts:

Harold E. Kautz, 216-433-6015, Harold.E.Kautz@grc.nasa.gov; and Dr. George Y. Baaklini, 216-433-6016, George.Y.Baaklini@grc.nasa.gov

Authors:

Dr. Andrew L. Gyekenyesi, Harold E. Kautz, and Dr. George Y. Baaklini

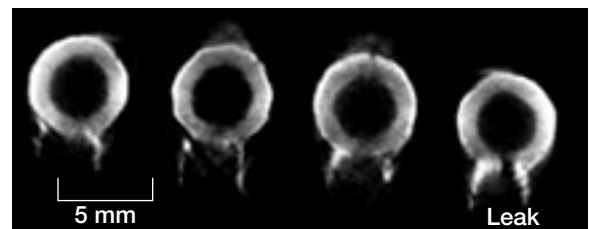
Headquarters program office: OAT

Programs/Projects: AvSP

Rapid Prototyping Integrated With Nondestructive Evaluation and Finite Element Analysis

Most reverse engineering approaches involve imaging or digitizing an object then creating a computerized reconstruction that can be integrated, in three dimensions, into a particular design environment. Rapid prototyping (RP) refers to the practical ability to build high-quality physical prototypes directly from computer aided design (CAD) files. Using rapid prototyping, full-scale models or patterns can be built using a variety of materials in a fraction of the time required by more traditional prototyping techniques (refs. 1 and 2).

Many software packages have been developed and are being designed to tackle the reverse engineering and rapid prototyping issues just mentioned. For example, image processing and three-dimensional reconstruction visualization software such as Velocity² (ref. 3) are being used to carry out the construction process of three-dimensional volume models and the subsequent generation of a stereolithography file that is suitable for CAD applications. Producing three-dimensional models of objects from computed tomography (CT) scans is becoming a valuable nondestructive evaluation methodology (ref. 4). Real components can be rendered and subjected to temperature and stress tests using structural engineering software codes. For this to be achieved, accurate high-resolution images have to be obtained via CT scans and then processed, converted into a traditional file format, and translated into finite element models.



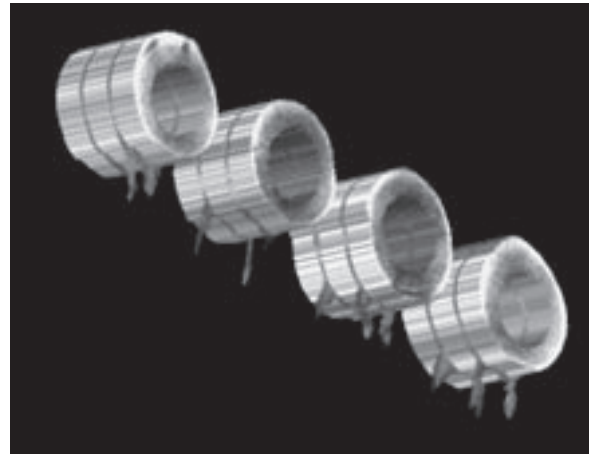
Top: Selected CT slice of the cooling panel. Bottom: Preprocessed and filtered image of the CT slice shown in the top part of this figure.

Prototyping a three-dimensional volume of a composite structure by reading in a series of two-dimensional images generated via CT and by using and integrating

commercial software (e.g. Velocity², MSC/PATRAN (ref. 5), and Hypermesh (ref. 6)) is being applied successfully at the NASA Glenn Research Center. The building process from structural modeling to the analysis level is outlined in reference 7. Subsequently, a stress analysis of a composite cooling panel under combined thermomechanical loading conditions was performed to validate this process.

The preceding figure shows a representative CT scan slice of a composite material cooling panel that has four metal tubes that were brazed to it by a brazing alloy. The bottom part of this figure shows an aligned, preprocessed, filtered image of the CT scan shown in the top part. The figure to the right represents the three-dimensional volume rendering of a set of 50 of the two-dimensional filtered CT slices shown in the top part of the first figure. The panel underwent a broad test matrix investigating its thermal performance, thermal shock performance, and thermomechanical life cycle.

The finite element analyses were performed on the cooling panel under elastic conditions and combined thermomechanical loading using the MARC code (ref. 8). High-pressure coolant injected through the cooling holes and a temperature were the applied loads considered. The next figure shows the stress distribution reported in one tube section of the cooling panel using a CT-scan-developed model. The maximum stress location is at the metal tube inside wall, which was expected. Furthermore, the brazing material deformation is clearly noted

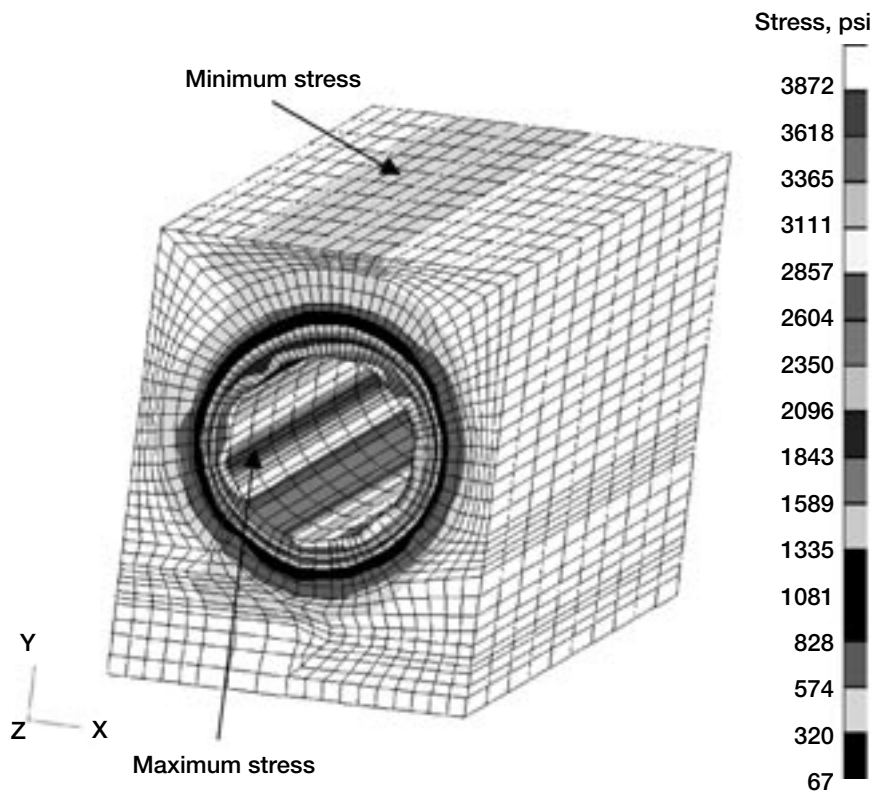


Three-dimensional volume rendering of a set of 50 two-dimensional filtered CT slices.

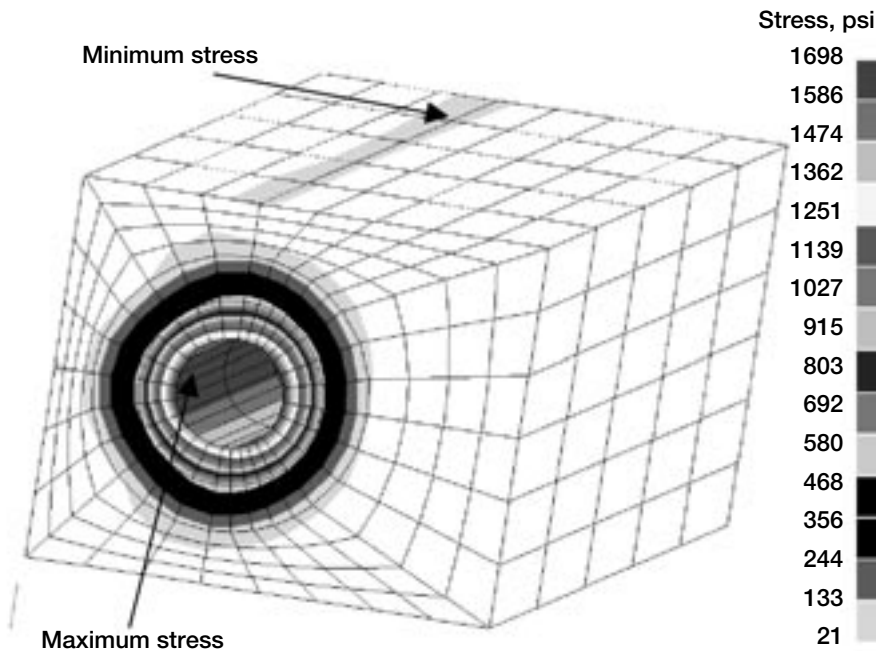
because of the high pressure of the cooling gas. Such data were noticed in the CT scan, and interpretation of the information collected confirmed failure and leaking at the metal-wall-brazing material interface. Similar results are reported in the final figure, a model generated manually with MSC/PATRAN. This confirms that the NDE and the finite element findings are in good agreement. However, the advantage of analyzing an NDE-produced model is that it offers more details than a CAD model concerning deformities and structural abnormalities, which can assist greatly in the structural evaluation of tested components. In contrast, in CAD modeling, all the flaws have to be artificially modeled.

References

1. Griffin, A.; McMillin, S.; and Knox, C.: Practical Examples: Using Scan Data for Reverse Engineering. Technical Papers from the Society of Manufacturing Engineers Autofact Conference, Detroit, MI, 1998.
2. Yancey, R., et al.: Integration of Reverse Engineering, Solidification Modeling, and Rapid Prototyping Technologies for the Production of Net Shape Investment Cast Tooling. Advanced Research and Applications Corporation, Dayton, OH, 1996.



Von Mises stress distribution for tube A and surrounding based on CT data.



Von Mises stress distribution for tube A and surrounding based on MSC/PATRAN data.

3. Velocity² Pro™ Image Processing and 3D Reconstruction Visualization Software, ver. 2.0. Image3, LLC, Salt Lake City, UT, July 1998.
4. Baaklini, George Y.: Engine Materials Characterization and Damage Monitoring by Using X-Ray Technologies. NASA TP-3328, 1993.

5. MSC/PATRAN Graphics and Finite Element Package. Vols. I and II, The MacNeal-Schwendler Corporation, Costa Mesa, CA, 1997.
6. Altair HyperMesh. Ver. 3.1, Altair Engineering, Inc., Troy, MI, 1999.
7. Abdul-Aziz, Ali, et al.: Challenges in Integrating Nondestructive Evaluation and Finite Element Methods for Realistic Structural Analysis. NASA/TM-2000-209952, 2000. <http://gltrs.grc.nasa.gov/GLTRS>
8. MARC General Purposes Finite Element Analysis Program. Vol. A: User Information Manual; Vol. F: Theoretical Manual. MARC Analysis Research Corporation, Palo Alto, CA, 1996.

Cleveland State University contact:

Dr. Ali Abdul-Aziz, 216-433-6729,
Ali.Abdul-aziz@grc.nasa.gov

Authors: Dr. Ali Abdul-Aziz and
Dr. George Y. Baaklini

Headquarters program office: OAT

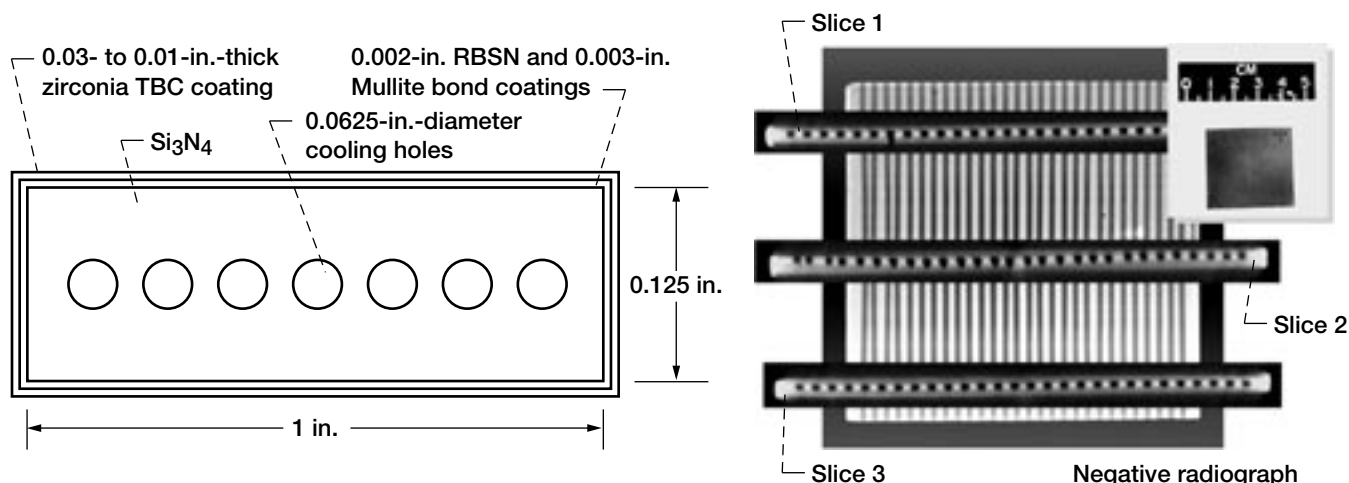
Programs/Projects:

HOTPC, FESS, RSL, AvSP

Silicon Nitride Plates for Turbine Blade Application: FEA and NDE Assessment

Engine manufacturers are continually attempting to improve the performance and the overall efficiency of internal combustion engines. The thermal efficiency is typically improved by raising the operating temperature of essential engine components in the combustion area. This reduces the heat loss to a cooling system and allows a greater portion of the heat to be used for propulsion. Further improvements can be achieved by diverting part of the air from the compressor, which would have been used in the combustor for combustion purposes, into the turbine components. Such a process is called active cooling. Increasing the operating temperature, decreasing the cooling air, or both can improve the efficiency of the engine. Furthermore, lightweight, strong, tough high-temperature materials are required to complement efficiency improvement for next-generation gas turbine engines that can operate with minimum cooling.

Because of their low-density, high-temperature strength, and thermal conductivity, ceramics are being investigated as potential materials for replacing ordinary metals that are currently used for engine hot section components. Ceramic structures can withstand higher operating temperatures and other harsh environmental factors. In addition, their low densities relative to metals helps condense component mass (ref. 1).

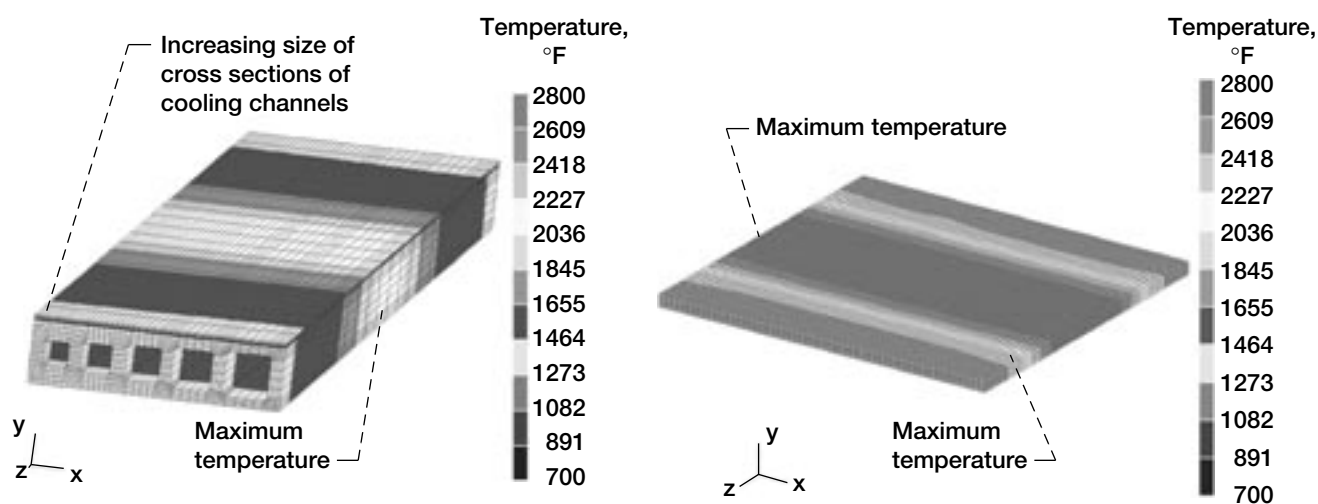


Left: Cooling plate configuration, showing circular cooling channels. Cross section of cooled monolithic silicon nitride (Si_3N_4) plates; test specimen size, 6 by 1 by 0.125 in. Right: Computed tomography of cooled silicon nitride plate. Location and shape of channels vary in the middle CT slice.

The objectives of this program at the NASA Glenn Research Center are to develop manufacturing technology, a thermal barrier coating/environmental barrier coating (TBC/EBC), and an analytical modeling capability to predict thermomechanical stresses, and to do minimal burner rig tests of silicon nitride (Si_3N_4) and SiC/SiC turbine nozzle vanes under simulated engine conditions. Furthermore, and in support of the latter objectives, an optimization exercise using finite element analysis and nondestructive evaluation (NDE) was carried out to characterize and evaluate silicon nitride plates with cooling channels.

The preceding figure on the left shows the geometric configuration of the plate with cooling channels, illustrating the dimensions including the TBC layers layout. The figure on the right represents a typical computed tomog-

raphy of the silicon nitride plate with three different cross sections of the cooling channels. The figure indicates NDE analysis, which shows uniformity and spacing of the cooling channels as well as the processing defects such as pores, cracks, and other geometric abnormalities. The figures below show temperature distributions generated via finite element analysis with the ANSYS code (ref. 2) and MSC/PATRAN (ref. 3) for two



Left: Steady-state temperature distribution of cooling plate with increasing cross-section cooling channel configurations. Right: Steady-state temperature distribution experienced by the cooling plate shown in the second figure.

different cooling channel configurations. Convective flame impingement was imposed over one quarter of the top of the plate, while convective cooling was imposed at the bottom of the plate and inside the cooling channels (ref. 4). The temperature plots were generated under noncooling boundary conditions.

The results indicate that the maximum temperature is at the middle section of the plate as anticipated, and the influence of the cooling channel configuration is clearly noticed by the temperature difference exhibited between the two plates. A temperature drop of 573 °F is reported. This is due to the difference in the cooling channel configurations, which shows that cooling channel size and shape are a major factor in optimizing a desired thermal profile. Furthermore, this confirms that the material temperature is highly dependent on the cooling channel configuration and the boundary conditions applied. Additional details regarding this work can be found in reference 5.

References

1. Bhatt, Ramakrishna T., et al.: Minimally Cooled Ceramics and Fiber Reinforced Ceramic Matrix Composite Turbine Components: A Progress Report. HITEMP Review 1999, NASA/CP-1999-208915, 1999. Available from the Subsonic Systems Office, NASA Glenn Research Center.
2. MSC/PATRAN Graphics and Finite Element Package. Vols. I and II, The MacNeal-Schwendler Corporation, Costa Mesa, CA, 1997.

3. ANSYS Finite Element Program. ANSYS Release 5.4. ANSYS, Inc., Canonsburg, PA, 1997.
4. Wolf, Helmut: Heat Transfer. Harper & Row, New York, 1983.
5. Abdul-Aziz, A.; Baaklini, G.Y.; and Bhatt, R.T.: Design Evaluation of Cooled Silicon Nitride Plates for Turbine Blade Application Using Finite Element. NASA/TM-2001-210819, 2001.
<http://gltrs.grc.nasa.gov/GLTRS>

Ohio Aerospace Institute contact:

Dr. Ali Abdul-Aziz, 216-433-6729,
Ali.Abdul-aziz@grc.nasa.gov

Authors: Dr. Ali Abdul-Aziz,
Dr. George Y. Baaklini, and
Dr. Ramakrishna T. Bhatt

Headquarters program office: OAT

Programs/Projects:

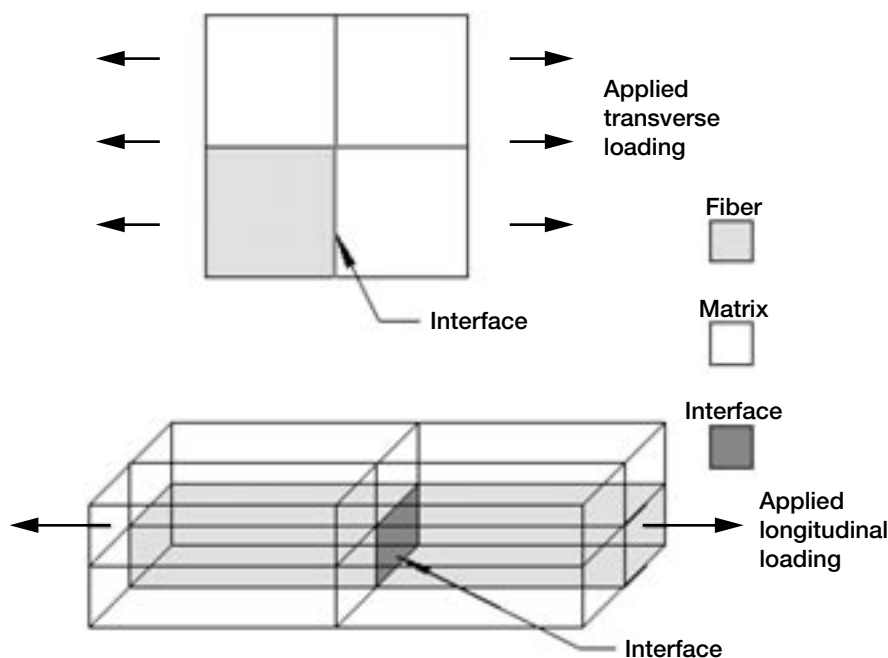
HOTPC, RLV, Spaceliner 100

Local Debonding and Fiber Breakage in Composite Materials Modeled Accurately

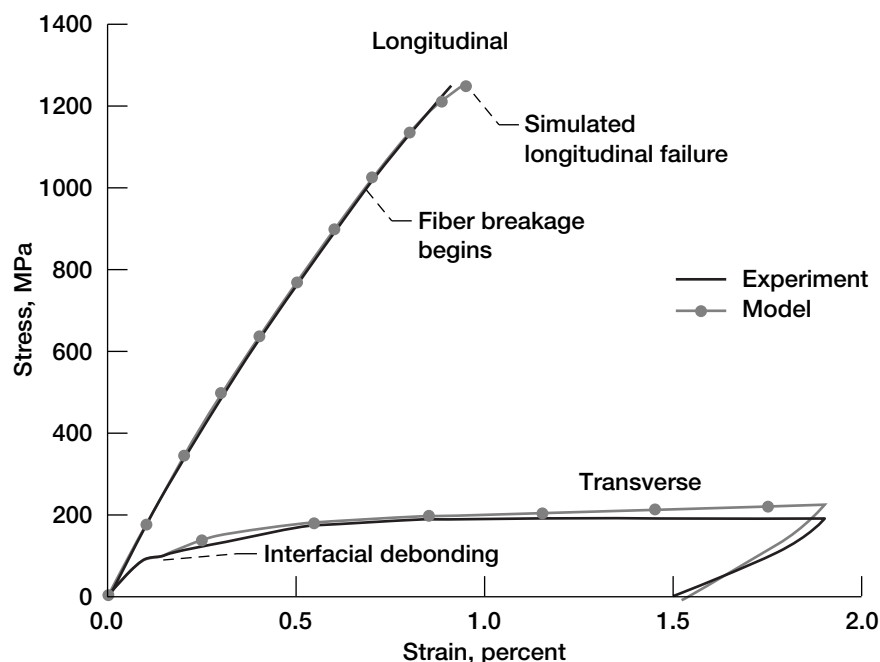
A prerequisite for full utilization of composite materials in aerospace components is accurate design and life prediction tools that enable the assessment of component performance and reliability. Such tools assist both structural analysts, who design and optimize structures composed of composite materials, and materials scientists who design and optimize the composite materials themselves. NASA Glenn Research Center's Micromechanics Analysis Code with Generalized Method of Cells (MAC/GMC) software package (<http://www.grc.nasa.gov/WWW/LPB/mac>) addresses this need for composite design and life prediction tools by providing a widely applicable and accurate approach to modeling composite materials. Furthermore, MAC/GMC serves as a platform for incorporating new local models and capabilities that are under development at NASA, thus enabling these new capabilities to progress rapidly to a stage in which they can be employed by the code's end users.

A recent effort (done in conjunction with the Ohio Aerospace Institute (NCC3-650)) that has leveraged many of the existing capabilities of MAC/GMC is the development and implementation of a new interfacial model (ECI) to simulate internal debonding (or local failure) within composite

materials. This model is unique in that it allows stress reduction to occur in the region of the composite local to the failure event as interfacial separation continues. In addition, the ECI model can be applied to simulate both transverse fiber-matrix interfacial debonding and longitudinal fiber breakage in continuously reinforced composite plies. For interfacial debonding, a simulated weak interface is placed at the fiber-matrix interface, whereas for longitudinal fiber breakage, a simulated weak interface (which will represent a fiber break) is placed within the fiber itself (see the following figure). To allow more accurate



Application of the ECI debonding model to transverse interfacial debonding and longitudinal fiber breakage.



Simulated and experimental longitudinal and transverse tensile response of SCS-6/TIMETAL21S at 650 °C.

simulation of composites and to incorporate the statistical nature of fiber strength, researchers must employ more complex (and realistic) geometric representations (refs. 1 and 2). Sample results of MAC/GMC with the ECI model are shown in the final figure. In the longitudinal simulation, the model agrees well with the experiment not only for the composite deformation, but also for the global failure of the composite. The transverse simulation does an excellent job capturing the details of the knee associated with debonding. The ECI model also functions in concert with the other features in MAC/GMC such as arbitrary time-dependent multiaxial loading histories, laminate analysis, yield/damage surface generation, and an interface with the ABAQUS finite element package.

References

1. Bednarczyk, Brett A.; and Arnold, Steven M.: A New Local Failure Model With Application to the Longitudinal Tensile Behavior of Continuously Reinforced Titanium Composites. NASA/TM-2000-210027, 2000. <http://gltrs.grc.nasa.gov/GLTRS>
2. Bednarczyk, Brett A.; and Arnold, Steven M.: A New Local Debonding Model With Application to the Transverse Tensile and Creep Behavior of Continuously Reinforced Titanium Composites. NASA/TM-2000-210029, 2000. <http://gltrs.grc.nasa.gov/GLTRS>

Glenn Contact:

Dr. Steven M. Arnold, 216-433-3334, Steven.M.Arnold@grc.nasa.gov

Authors: Dr. Brett A. Bednarczyk and Dr. Steven M. Arnold

Headquarters program office: OAT

Programs/Projects:

ASTP, RLV Focused, RLV MMC Turbopump Housing—Rocketdyne

Micromechanics-Based Inelastic Finite Element Analysis Accomplished Via Seamless Integration of MAC/GMC With ABAQUS

A critical issue in the micromechanics-based analysis of composite structures becomes the availability of a computationally efficient homogenization technique (see the figure to the right): one that is (1) capable of handling the sophisticated, physically based, viscoelastoplastic constitutive and life models for each constituent, (2) able to generate accurate displacement and stress fields at both the macro and the micro levels, and (3) compatible with the finite element method. The Generalized Method of Cells (GMC) developed by Paley and Aboudi (ref. 1) is one such micromechanical model that has been shown to predict accurately the overall macro behavior of various types of composites given the required constituent properties.

Specifically, the method provides "closed-form" expressions for the macroscopic composite response in terms of the properties, size, shape, distribution, and response of the individual constituents or phases that make up the material. Furthermore, expressions relating the internal stress and strain fields in the individual constituents in terms of the macroscopically applied stresses and strains are available through strain or stress concentration matrices. These expressions make possible the investigation of failure processes at the microscopic level at each step of an applied load history.

MAC/GMC (ref. 2) enhances the basic capabilities of GMC by providing a modular framework wherein (1) various thermal, mechanical (stress or strain control), and thermomechanical load histories can be imposed, (2) different integration algorithms can be selected, (3) a variety of material constitutive models (both deformation and life) can be utilized and/or implemented, (4) a variety of fiber architectures (both unidirectional, laminate, and woven) can be easily accessed through their corresponding representative volume elements contained within the supplied library of representative volume elements or input directly by the user, and (5) graphical postprocessing of the macro and/or micro field quantities is made available. Consequently, the availability of MAC/GMC (see <http://www.grc.nasa.gov/WWW/LPB/mac>) now provides industry, academia, and government engineers and materials scientists with a comprehensive, computationally efficient, user-friendly micromechanics analysis tool that can easily and accurately design/analyze multiphase (composite) materials

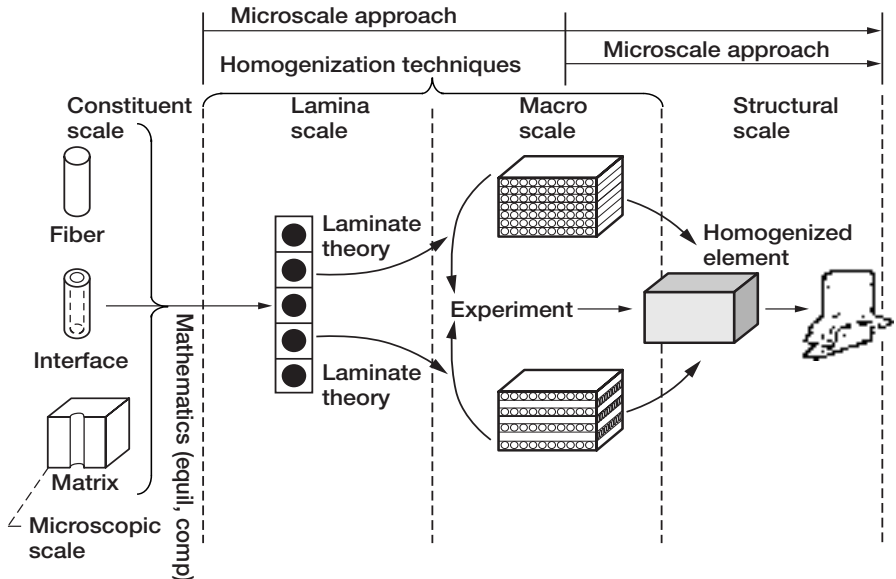
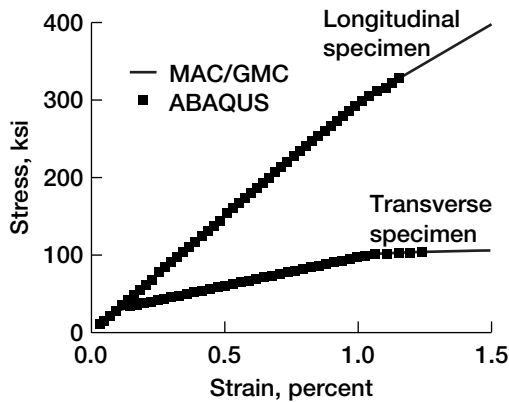


Illustration of levels of scale and approaches for composite analysis.

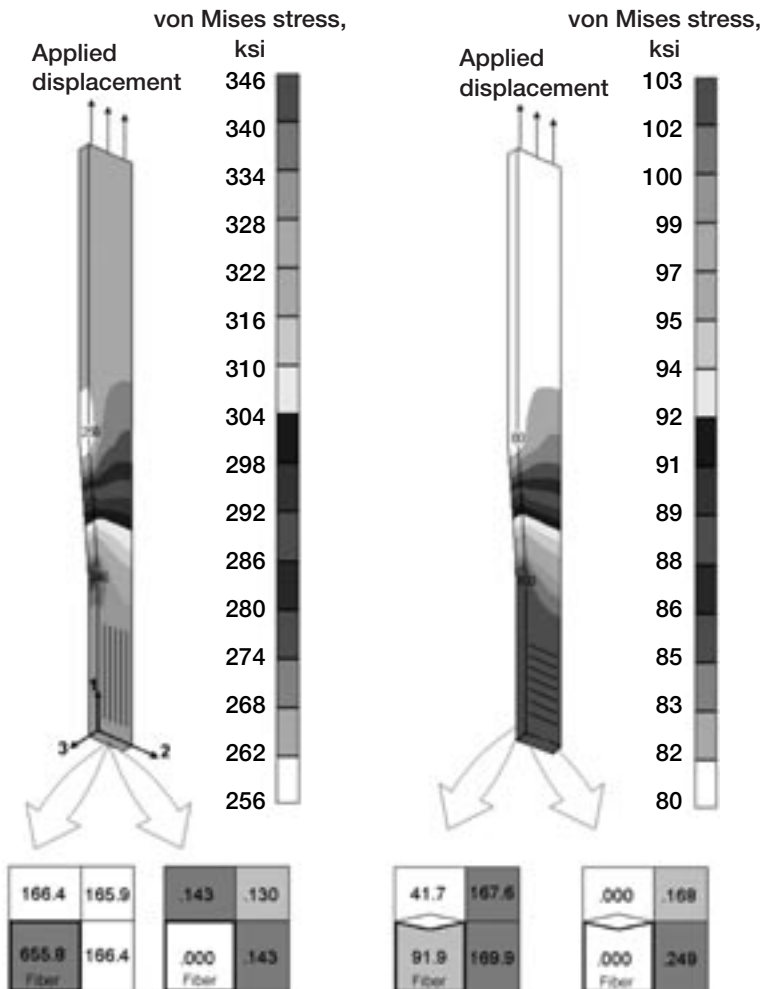
for a given application. MAC/GMC is also ideally suited for conducting sensitivity/parametric studies (i.e., "what-if" scenarios) in the design and analysis of advanced composite materials (e.g., metal matrix composites, polymer matrix composites, and ceramic matrix composites). Furthermore, MAC/GMC can be interfaced directly with standard linear and nonlinear finite element analysis packages (through their respective user-definable constitutive routines) for cost-effective large-scale component design and analysis. Recently, in cooperation with the University of Akron such a seamless interface was achieved for HKS's nonlinear finite element code, ABAQUS. For clarity, this finite element implementation of MAC/GMC has been given its own unique name, FEAMAC.



Longitudinal specimen,
fibers in one direction

Longitudinal specimen,
fibers in two directions

Macro Fields



Micromechanics-based structural analysis of two 432-element idealizations of 33-vol % SCS-6/TIMETAL 21S dog bone test specimens, longitudinally and transversely reinforced. Top: Macrolevel stress-strain response. Bottom: Multilevel ABAQUS results using FEAMAC to represent material behavior.

To date, over 40 industrial and academic customers have used or are using MAC/GMC for a variety of applications. In particular, FEAMAC is being employed by the Goodyear Tire and Rubber Co. and the NASA Glenn Research Center to understand the influence of cord architecture on the behavior and performance of their tires, and by Glenn and Boeing, Rocketdyne Division, to design and analyze a metal matrix composite (MMC) housing on a large 400,000 thrust class turbopump. For illustration purposes, see the following figure: two 432-element (C3D8) idealizations of a 33-vol % SCS-6/TIMETAL 21S test specimen, longitudinally and transversely reinforced, are analyzed. In the top part of the figure to the left, a comparison is made of the macro response prediction resulting from MAC/GMC and that coming from the center element within the gauge length (where FEAMAC is providing the viscoplastic material response at all integration points throughout the specimen). Clearly, the agreement is excellent. Furthermore, in the bottom part of this figure, the macro von Mises stress contours for both specimens and the corresponding in situ microstress and inelastic strain field within each constituent are illustrated at the end of the applied tension test. Note that in the transverse specimen, fiber-matrix debonding has been enabled as indicated by the diamond-shaped interface in the bottom part of the figure.

References

1. Paley, M.; and Aboudi, J.: Micromechanical Analysis of Composites by the Generalized Cells Model. Mech. Mater., vol. 14, no. 2, 1992, pp. 127-139.
2. Arnold, S.M., et al.: Micromechanics Analysis Code With Generalized Method of Cells (MAC/GMC) User Guide. Ver. 3.0. NASA/TM-1999-209070, 1999. <http://gltrs.grc.nasa.gov/GLTRS>

Glenn contact: Dr. Steven M. Arnold, 216-433-3334, Steven.M.Arnold@grc.nasa.gov

Authors: Dr. Steven M. Arnold and D. Trowbridge

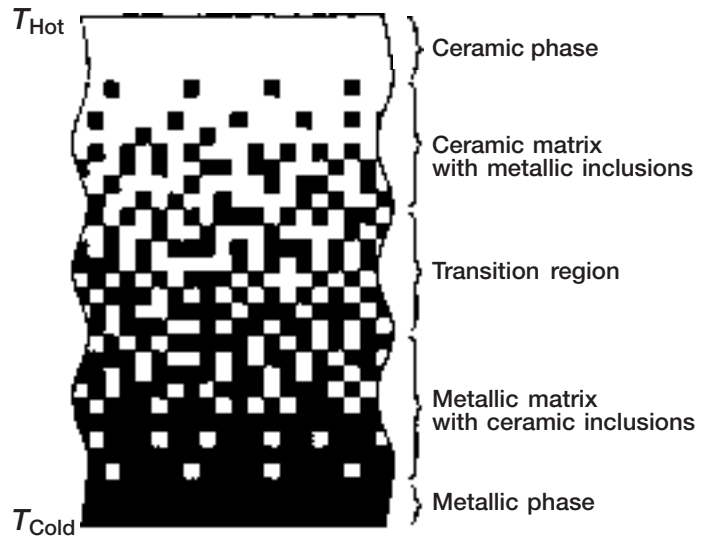
Headquarters program office: OAT

Programs/Projects: RLV, ASTP, RLV Focused

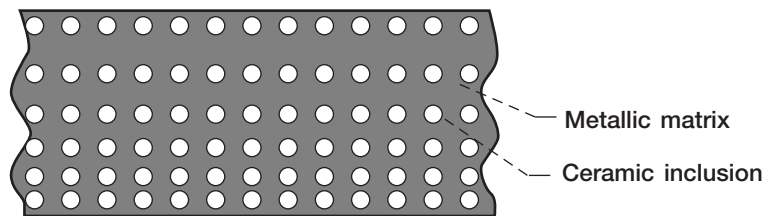
Higher-Order Theory for Functionally Graded Materials

Functionally graded materials (FGM's) are a new generation of engineered materials wherein the microstructural details are spatially varied through nonuniform distribution of the reinforcement phase(s), see the top figure. Engineers accomplish this by using reinforcements with different properties, sizes, and shapes, as well as by interchanging the roles of the reinforcement and matrix phases in a continuous manner (ref. 1). The result is a microstructure that produces continuously or discretely changing thermal and mechanical properties at the macroscopic or continuum scale. This new concept of engineering the material's microstructure marks the beginning of a revolution both in the materials science and mechanics of materials areas since it allows one, for the first time, to fully integrate the material and structural considerations into the final design of structural components. Functionally graded materials are ideal candidates for applications involving severe thermal gradients, ranging from thermal structures in advanced aircraft and aerospace engines to computer circuit boards. Owing to the many variables that control the design of functionally graded microstructures, full exploitation of the FGM's potential requires the development of appropriate modeling strategies for their response to combined thermomechanical loads. Previously, most computational strategies for the response of FGM's did not explicitly couple the material's heterogeneous microstructure with the structural global analysis. Rather, local effective or macroscopic properties at a given point within the FGM were first obtained through homogenization based on a chosen micromechanics scheme and then subsequently used in a global thermomechanical analysis.

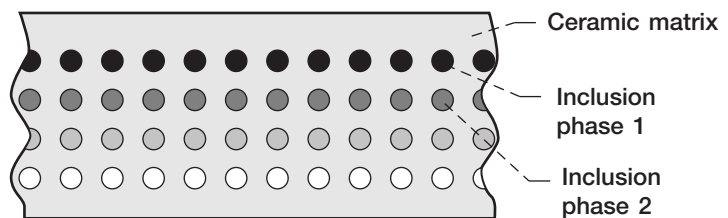
Reference 2 provides a detailed review and description of the full generalization of a new Cartesian-coordinate-based higher order theory for functionally graded materials developed by the University of Virginia in conjunction with the NASA Glenn Research Center over the past several years. This theory circumvents the problematic use of the standard micromechanical approach, based on the concept of a representative volume element, commonly employed in the analysis of functionally graded composites by explicitly coupling the local (microstructural) and global (macrostructural) responses. The theoretical framework is based on volumetric averaging of the various field quantities, together with the imposition of boundary and



(a) Continuously graded microstructure.



(b) Discretely graded microstructure.



(c) Multiphase graded microstructure.

Examples of different types of functionally graded microstructures.

interfacial conditions in an average sense between the subvolumes used to characterize the composite's functionally graded microstructure. The generalization outlined involved the extension of the theoretical framework to enable the analysis of

materials characterized by spatially variable microstructures in all three directions. Specialization of the generalized theoretical framework to previously published versions of the higher order theory for materials functionally graded in one and two directions was demonstrated. Reference 2 summarizes the major findings obtained with the one- and two-directional versions of the higher order theory. The results illustrate both the fundamental issues related to the influence of microstructure on microscopic and macroscopic quantities governing the response of composites and technologically important applications. A major issue addressed was the applicability of the classical homogenization schemes in the analysis of functionally graded materials. The technologically important applications illustrate the utility of functionally graded microstructures in tailoring the response of structural components in a variety of applications involving uniform and gradient thermomechanical loading.

References

1. Hirai, T.: Functional Gradient Materials. Processing of Ceramics, pt. 2, vol. 17B, Richard J. Brook, et al., eds., Weinheim, New York, NY, 1996, pp. 293–341.

2. Aboudi, J.; Pindera, M.J.; and Arnold, S.M.: Higher-Order Theory for Functionally Graded Materials. Composites Part B—Engineering, vol. 30, no. 8, 1999, pp. 777–832.

Glenn contact:

Dr. Steven M. Arnold, 216–433–3334,
Steven.M.Arnold@grc.nasa.gov

Authors: Prof. J. Aboudi,
 Prof. M.J. Pindera, and
 Dr. Steven M. Arnold

Headquarters program office: OAT

Programs/Projects: HOTPC

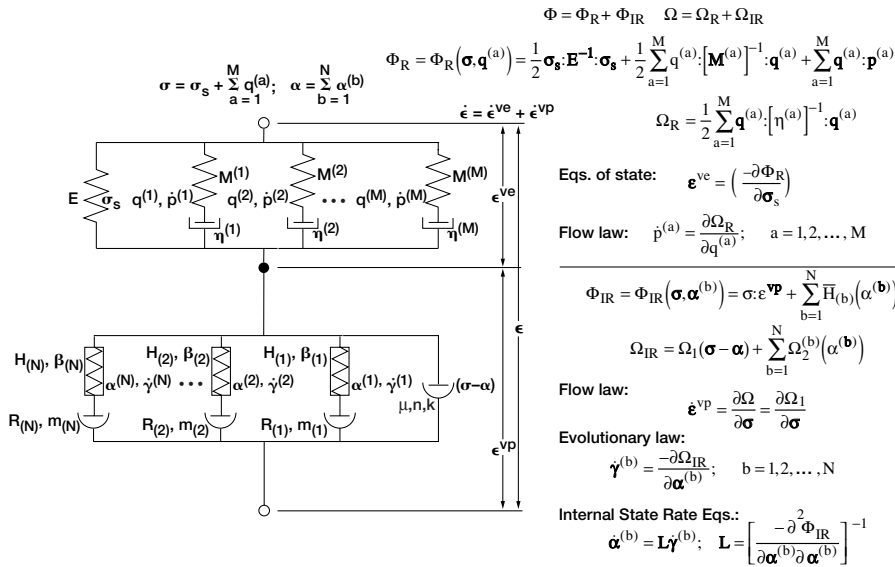
Awards: Life Prediction Best Branch
 Paper 2000

General Multimechanism Reversible-Irreversible Time-Dependent Constitutive Deformation Model Being Developed

Since most advanced material systems (for example metallic-, polymer-, and ceramic-based systems) being currently researched and evaluated are for high-temperature airframe and propulsion system applications, the required constitutive models must account for both reversible and irreversible time-dependent deformations. For example, considering that most aerospace engine designs are typically limited to the quasi-linear stress and strain regimes, the reversible time-dependent response component becomes dominant in comparison to the irreversible component. Alternatively, one can envision another extreme case (e.g., in polymer- and rubber-based systems under varying temperatures) in which a purely reversible viscous response is present. And lastly, an obvious natural extension for general applicability is the middle ground in which a combined reversible and irreversible representation is required. Furthermore, since an integral part of continuum-based computational methodologies (be they microscale- or macroscale-based) is an accurate and computationally efficient constitutive model to describe the deformation behavior of the materials of interest, extensive research efforts have been made over the years on the phenomenological representations of constitutive material behavior in the inelastic analysis of structures. From a more recent and comprehensive perspective (ref. 1), the NASA Glenn Research Center in conjunction with the University of Akron has emphasized concurrently addressing three important and related areas: that is, (1) mathematical formulation, (2) algorithmic developments for updating (integrating) the external (e.g., stress) and internal state variables, as well as (3) parameter estimation for characterizing the model. This concurrent perspective to constitutive modeling has enabled the overcoming of the two major obstacles to fully utilizing these sophisticated time-dependent (hereditary) constitutive models in practical engineering analysis. These obstacles are

- (1) lack of efficient and robust integration algorithms and
- (2) difficulties associated with characterizing the large number of required material parameters, particularly when many of these parameters lack obvious or direct physical interpretations.

Recently, a coupled fully associative viscoelastoplastic model was formulated (refs. 1 to 4), with sufficient generality in its potential functions to permit systematic introduction of multiple mechanisms for both viscoelastic (reversible) and viscoplastic (irreversible) response components (see the figure). The notions of strain and stress partitioning have been introduced, leading to the additive decomposition of strain into reversible and irreversible parts, and the partitioning of the stress into (1) its equilibrium (σ_e) and nonequilibrium ($q^{(a)}$) parts in the reversible region and (2) the internal ($\alpha^{(a)}$) and overstress



Summary of the stress and strain partitioning of the General Multimechanism Hereditary behavior model.

$(\sigma - \alpha)$ components in the irreversible region. The viscoelastic part utilizes the concept of equilibrium stress, leading to a rate dependency upon instantaneous loading, as well as to a unique limiting state of elastic deformation for an infinite amount of time. The viscoplastic formulation accounts for both nonlinear kinematic hardening and static recovery submechanisms. This general, multimechanism, hereditary deformation model has been shown to accurately represent a wide spectrum of material response under different loading conditions for the case of titanium alloys. Examples include (1) rate-dependent (effective) material tangent stiffness during initial loading or any subsequent reversed loading, (2) pure transient response (e.g., in creep or relaxation) within the reversibility region, (3) anelastic behavior upon stress reversal, irrespective of the load level, as well as (4) the many response features that are common to "unified viscoplastic" formulations already existing (e.g., rate-sensitivity, creep-plasticity interaction, and thermal recovery).

References

1. Saleeb, A.F., et al.: A General Hereditary Multimechanism-Based Deformation Model With Application to the Viscoelastoplastic Response of Titanium Alloys. *Int. J. Plasticity*, To be published Mar. 2001.
2. Arnold, S.M.; and Saleeb, A.F.: On the Thermodynamic Framework of Generalized Coupled Thermoelastic-Viscoplastic-Damage Modeling. *Int. J. Plast.*, vol. 10, no. 3, 1994, pp. 263–278.
3. Saleeb, A.F.; and Arnold, S.M.: A General Reversible Hereditary Constitutive Model. Pt. 1: Theoretical Developments, NASA TM–107493, 1997. <http://gltrs.grc.nasa.gov/GLTRS>
4. Arnold, S.M.; Saleeb, A.F.; and Castelli, M.G.: A General Reversible Hereditary Constitutive Model. Pt. 2: Application to a Titanium Alloy, NASA TM–107494, 1997. <http://gltrs.grc.nasa.gov/GLTRS>

Glenn contact:

Dr. Steven M. Arnold, 216–433–3334, Steven.M.Arnold@grc.nasa.gov

Authors: Prof. A.F. Saleeb and Dr. Steven M. Arnold

Headquarters program office: OAT

Programs/Projects: Trailblazer/GTX

Nondestructive Evaluation Approaches Developed for Material Characterization in Aeronautics and Space Applications

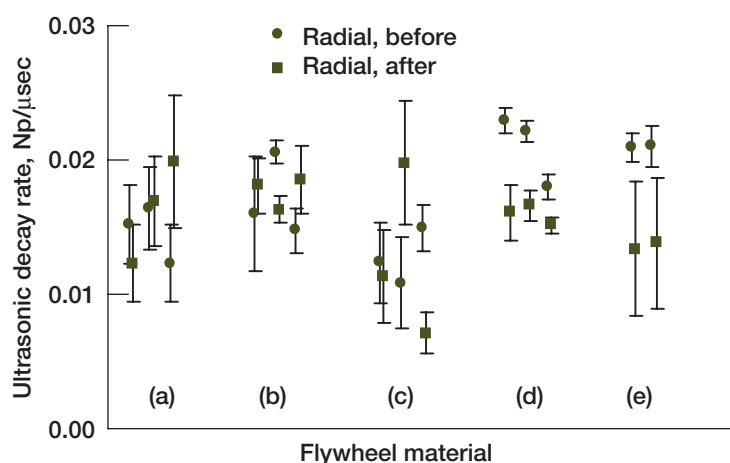
At the NASA Glenn Research Center, nondestructive evaluation (NDE) approaches were developed or tailored for characterizing advanced material systems. The emphasis was on high-temperature aerospace propulsion applications. The material systems included monolithic ceramics, superalloys, and high-temperature composites. In the aeronautics area, the major applications were cooled ceramic plate structures for turbine applications, γ -TiAl blade materials for low-pressure turbines, thermoelastic stress analysis for residual stress measurements in titanium-based and nickel-based engine materials, and acousto-ultrasonics for creep damage assessment in nickel-based alloys. In the space area, applications consisted of

cooled carbon-carbon composites for gas generator combustors and flywheel rotors composed of carbon-fiber-reinforced polymer matrix composites for energy storage on the International Space Station. The role of NDE in solving manufacturing problems, the effect of defects on structural behavior, and the use of NDE-based finite

element modeling are discussed in reference 11. NDE technology needs for improved microelectronic and micromechanical systems as well as health monitoring of micromaterials and microcomponents are briefly discussed in reference 11, and many relevant papers can be found in reference 12.

The aeronautic applications include (1) cooled ceramic vane material optimization (refs. 1 and 2), (2) the resistance to defects of superalloy γ -TiAl blade materials (ref. 3), (3) thermoelastic stress analysis that can gauge residual stress in Ti- and Ni-based materials (refs. 4 and 5), and (4) creep damage/remaining life in superalloys by acousto-ultrasonics (ref. 6). The space applications focus was on assuring material/component quality and uniformity via the NDE of cooled carbon-carbon composites for gas generator combustors, and on demonstrating the importance of integrating NDE and the finite element method (FEM) for the rapid, reduced-cost proof testing and material development of advanced polymer matrix composites for a flywheel-energy-based storage system (refs. 7 to 10).

The critical role of nondestructive evaluation as a material characterization modality was demonstrated for several aerospace applications. NDE was successfully used for ceramic process optimization and γ -TiAl effect of defect investigation on fatigue life. Thermoelastic stress analysis was found to be a viable NDE method to monitor the residual stress-state of structural materials. Acousto-ultrasonics parameters could quantify creep damage starting at 50 percent of used-up life, and they correlated well with the time-to-failure and used-up life in superalloys. Microfocus radiography and computed tomography in conjunction with finite element modeling and fracture analysis proved to be useful for the rapid, reduced-cost proof testing and material development of advanced composites. Lastly, acousto-ultrasonics was able to classify flywheel material systems and gauge degradation due to spin testing of composite rotors (see the figure). The reader is directed to study reference 11 for more details.



Acousto-ultrasonic measurements along the profile of the stepped creep specimen (75.7 ksi 1350 °F and 260 hr). Indicated are percentages of used-up life.

References

1. Bhatt, Ramakrishna T., et al.: Minimally Cooled Ceramics and Fiber Reinforced Ceramic Matrix Composite Turbine Components: A Progress Report. HITEMP Review 1999, NASA/CP-1999-208915, 1999. Available from the Subsonic Systems Office, NASA Glenn Research Center.
2. Klosterman, D., et al.: Automated Fabrication of Monolithic Ceramics and Ceramic Matrix Composites (CMCs) Using a Novel Rapid Prototyping Method. *Ceram. Eng. Sci. Proc.*, vol. 19, no. 3, 1998, pp. 291-301.
3. Lerch, Bradley A., et al.: Effect of Defects on the Fatigue Life of Gamma-TiAl. NASA/CP-1999-208915, 1999, pp. 30-1 to 30-11. Available from the Subsonic Systems Office, NASA Glenn Research Center.
4. Gyekenyesi, Andrew L.; and Baaklini, George Y.: Thermoelastic Stress Analysis: The Mean Stress Effect in Metallic Alloys. *Nondestructive Evaluation of Aging Materials and Composites III*, George Y. Baaklini, Carol A. Lebowitz, and Eric S. Boltz, eds., SPIE, Bellingham, WA, 2000.
5. Gyekenyesi, Andrew L.; and Baaklini, George Y.: Quantifying Residual Stresses by Means of Thermoelastic Stress Analysis. *Nondestructive Evaluation of Aging Materials and Composites IV*, George Y. Baaklini, Carol A. Lebowitz, and Eric S. Boltz, eds., SPIE, Bellingham, WA, 2000.
6. Kautz, H.E., et al.: NDE of Creep Tested and Thermally Aged Udimet 520 Nickel Based Superalloy. ASNT 2000 Spring Conference and 9th Annual Research Symposium, Birmingham, Alabama. To be published.
7. Abdul-Aziz, Ali, et al.: Challenges in Integrating Nondestructive Evaluation and Finite Element Methods for Realistic Structural Analysis. *Nondestructive Evaluation of Aging Materials and Composites IV*, George Y. Baaklini, Carol A. Lebowitz, and Eric S. Boltz, eds., SPIE, Bellingham, WA, 2000.

8. Olszewski, Mitchell, et al.: On the Fly or Under Pressure; Flywheel and Accumulator Energy-Storage Devices. Mech. Eng., vol. 110, no. 6, 1988, pp. 50–58.
9. Coppa, A.P.: Flywheel Containment and Safety Considerations. Keckler, C.R.; Bechtel, R.T.; and Groom, N.J.: An Assessment of Integrated Flywheel System Technology. NASA CP-2346, 1984, pp. 243–264.
10. Abdul-Aziz, A.; Baaklini, G.Y.; and Trudell, J.: Structural Analysis of Composite Flywheels: An Integrated NDE and FEM Approach. To be published as NASA/TM-2001-210461, 2001. <http://gltrs.grc.nasa.gov/GLTRS>
11. Baaklini, G.Y., et al.: NDE for Material Characterization in Aeronautic and Space Applications. NASA/TM-2000-210474, 2000. <http://gltrs.grc.nasa.gov/GLTRS>
12. Smart Structures and Materials, V.K. Vardan, ed., Proceedings of SPIE, vol. 3673, 1999.

Glenn contacts:

Dr. George Y. Baaklini, 216-433-6016, George.Y.Baaklini@grc.nasa.gov;
Harold E. Kautz, 216-433-6015, Harold.E.Kautz@grc.nasa.gov;

Dr. Andrew L. Gyekenyesi,
216-433-8155,
Andrew.L.Gyekenyesi@grc.nasa.gov;
and Dr. Ali Abdul-Aziz, 216-433-6729,
Ali.Abdul-aziz@grc.nasa.gov

Cleveland State University contact:

Richard E. Martin, 216-433-3684,
Richard.E.Martin@grc.nasa.gov

Authors: Dr. George Y. Baaklini, Harold
E. Kautz, Dr. Andrew L. Gyekenyesi,
Dr. Ali Abdul-Aziz, and Richard E. Martin

Headquarters program office: OAT

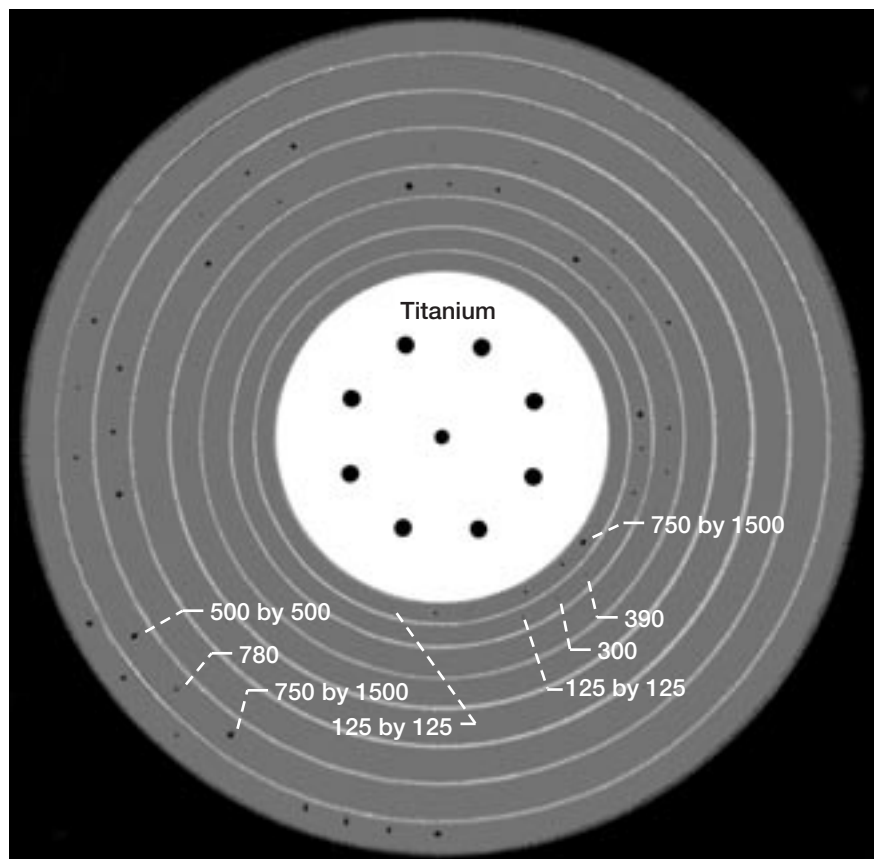
Programs/Projects:

AvSP, FESS, RSL, HOTPC

Nondestructive Evaluation Methodologies Developed for Certifying Composite Flywheels

Manufacturing readiness of composite rotors and certification of flywheels depend in part on the maturity of nondestructive evaluation (NDE) technology for process optimization and quality assurance, respectively. At the NASA Glenn Research Center, the capabilities and limitations of x-ray-computed tomography and radiography, as well as advanced ultrasonics were established on NDE ring and rotor standards with electrical discharge machining (EDM) notches and drilled holes. Also, intentionally seeded delamination, tow break, and insert of bagging material were introduced in hydroburst-rings to study the NDE detection capabilities of such anomalies and their effect on the damage tolerance and safe life margins of sub-scale rings and rotors. Examples of possible occurring flaws or anomalies in composite rings as detected by NDE and validated by destructive metallography are shown. The general NDE approach to ensure the quality of composite rotors and to help in the certification of flywheels is briefly outlined.

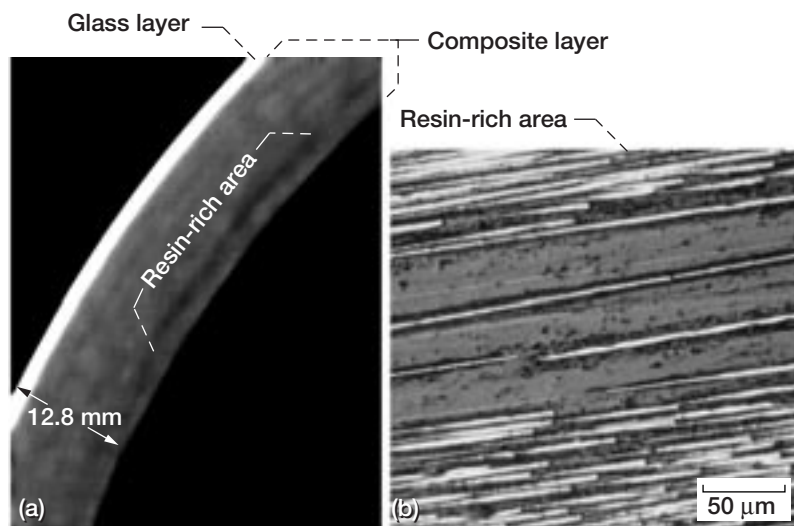
Using the flywheel technology for energy storage systems is gaining broader support, more than it did for



Computed tomography slice of a multilayered rotor standard (composite rim and titanium hub) with EDM notches and drilled holes set (125 by 125, 300 diameter, 390 diameter, 500 by 500, 780 diameter, and 750 by 1500) in each layer. This set was duplicated in a spiral fashion starting at the innermost ring near the inner diameter and finishing at the outermost ring near the outer diameter. All dimensions given in micrometers.

the last 25 years (refs. 1 to 4) because of current support from NASA and U.S. Air Force space programs. The drive is not only to improve energy storage systems where the state of charge can be known but also to concurrently perform attitude control depending on the specific application for a given spacecraft (ref. 5). Some of the major challenges in the flywheel technology for the International Space Station include high-speed rotors and carbon-reinforced composite materials that can meet the safe-life design requirements, reliability and durability to end-of-life, flight certification, and safety constraints while delivering the high energy density needed (ref. 6). This research was limited to the NDE of composite flywheel rotors and rings that are targeted under the flywheel energy storage system program (ref. 7). These composite rotors are to be flown on the International Space Station as a replacement for a battery charge/discharge unit.

Findings demonstrated that EDM notches as small as 125 by 125 μm and drilled holes as small as 300 μm in diameter can be detected in a thick multilayered rotor by using x-ray computed tomography (see the figure on the preceding page). At the ring level, x-ray microfocus radiography, x-ray computed tomography, and pulse echo ultrasonic scans were able to detect EDM notches as small as 125 by 125 μm and drilled holes as small as 300 μm in diameter. Intentionally seeded delamination, tow break, and insert of bagging material were easily detected in hydroburst rings by using the ultrasonic pulse echo method. Possible occurring anomalies like delaminations in polymer matrix composite layers, voids in glass layers, and resin-rich regions in the composite layers (see the following figure), were all detected by NDE and verified by metallography. The general NDE approach to ensure the quality of composite rotors and to help in the certification of flywheels is described in greater detail in reference 8.



Computed tomography detected the presence of (a) resin-rich area, which was substantiated by the photomicrograph shown in (b).

References

1. DeTersa, S.J.: Materials for Advanced Flywheel Energy-Storage Devices. MRS Bulletin, vol. 24, no. 11, 1999, pp. 51–56.
2. Olszewski, Mitchell, et al.: On the Fly or Under Pressure; Flywheel and Accumulator Energy-Storage Devices. Mech. Eng., vol. 110, 1988, pp. 50–58.
3. Ashley, Steven: Flywheels Put a New Spin on Electric Vehicles. Mech. Eng., vol. 115, 1993, pp. 44–51.
4. Moritz, Brad: Composites Maximize Energy Storage in Industrial Flywheels. High-Performance Composites, 1998, pp. 21–24.
5. Brown, Peter J.: Flywheels in Space. Launchspace Magazine, Sep. 2000, pp. 22–25. <http://www.launchspace.com/archive/2000/081400.htm> Accessed Jan. 23, 2001.
6. Konno, Kevin: Certification of High Speed Composite Flywheel Rotors for the International Space Station. Presented at the Power Systems Conference, San Diego, CA, Oct. 31 to Nov. 2, 2000.
7. Aerospace Flywheel Development Overview. NASA Power & Propulsion Office. <http://space-power.grc.nasa.gov/ppo/flywheel/> Accessed Jan. 23, 2001.
8. Baaklini, G.Y., et al.: NDE for Material Characterization in Aeronautic and Space Applications. NASA/TM–2000–210474, 2000.

Glenn contacts: Dr. George Y. Baaklini, 216–433–6016, Fax 216–977–7150, George.Y.Baaklini@grc.nasa.gov; and Kevin E. Konno, 216–433–8373, Kevin.E.Konno@grc.nasa.gov

Cleveland State University contact: Richard E. Martin, 216–433–3684, Richard.E.Martin@grc.nasa.gov

University of Texas contact: Richard Thompson, 512–232–1615, r.thompson@mail.utexas.edu

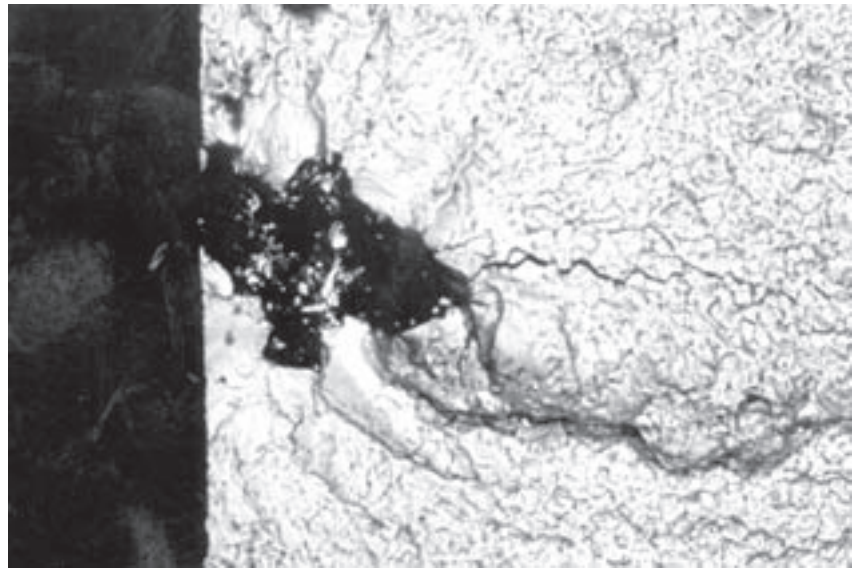
Authors: Dr. George Y. Baaklini, Kevin E. Konno, Richard E. Martin, and Richard Thompson

Headquarters program office: OAT

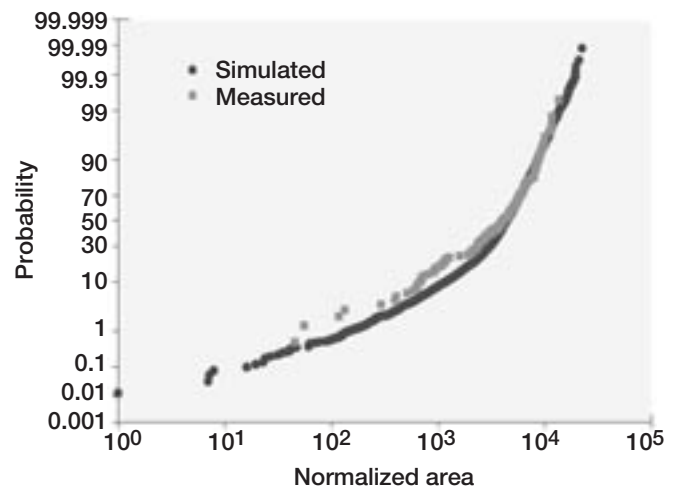
Programs/Projects: FESS, RSL

Ceramic Inclusions in Powder Metallurgy Disk Alloys: Characterization and Modeling

Powder metallurgy alloys are increasingly used in gas turbine engines, especially in turbine disk applications. Although powder metallurgy materials have many advantages over conventionally cast and wrought alloys (higher strength, higher temperature capability, etc.), they suffer from the rare occurrence of ceramic defects (inclusions) that are inherent to the powder atomization process. These inclusions can have a potentially large detrimental effect on the durability of individual components. An inclusion in a high stress location can act as a site for premature crack initiation and thereby considerably reduce the fatigue life. Because these inclusions are exceedingly rare, they typically do not reveal themselves in the process of characterizing the material for a particular application (the cumulative volume of the test bars in a fatigue life characterization is typically on the order of a *single* actual component). Ceramic inclusions have, however, been found to be the root cause of a number of catastrophic engine failures. To investigate the effect of these inclusions in detail, we have undertaken a study where known populations of ceramic particles, whose composition and morphology are designed to mimic the "natural" inclusions, are added to the precursor powder. Surface-connected inclusions have been found to have a particularly large detrimental effect on fatigue life; therefore, the quantity of ceramic "seeds" added is calculated to ensure that a minimum number will intersect the surface of the fatigue test bars. Because the ceramic inclusions are irregularly shaped and have a tendency to break up in the process of extrusion and forging, a method of calculating the probability of occurrence and expected intercepted surface area was needed. We have developed a Monte Carlo simulation to determine the distributions of these parameters and have verified the simulated results with observations of ceramic inclusions found in macroscopic slices from extrusions and forgings. Fatigue specimens have been machined from Udimet 720 (a powder metallurgy superalloy) forgings, to determine the effects of the inclusions on fatigue life. The ultimate goal of this study will be to use probabilistic methods to determine the reliability detriment that can be attributed to these ceramic inclusions. This work has been supported by the Ultra Safe and Ultra-Efficient Engine Technologies programs.



Crack emanating from a surface-connected ceramic inclusion.



Comparison of observed and simulated intercepted surface area of seeded ceramic inclusions.

Glenn contacts:

Peter J. Bonacuse, 216-433-3309, Peter.J.Bonacuse@grc.nasa.gov;
Jack Telesman, 216-433-3310, Ignacy.Telesman@grc.nasa.gov; and
Timothy P. Gabb, 216-433-3727, Timothy.P.gabb@grc.nasa.gov

Author: Peter J. Bonacuse

Headquarters program office: OAT

Programs/Projects: Ultra Safe, UEET

Test Standard Developed for Determining the Life Prediction Parameters of Advanced Structural Monolithic Ceramics at Elevated Temperatures

Advanced monolithic ceramics like ceramic matrix composites (CMC's) and continuous-fiber-reinforced ceramic matrix composites (CFCC's) are candidate materials for high-temperature structural applications in heat engines. However, the process of slow crack growth often limits the service life of structural monolithic ceramic components. Hence, it is important to develop an appropriate test methodology to determine accurately the slow crack growth parameters required for component life prediction. This methodology also should be useful in determining the influences of component processing and composition variables on the slow crack growth behavior of newly developed or existing materials, thereby allowing the component processing and composition to be tailored and optimized to specific needs.

In 1998, the authors initiated the development of a test method to determine the life prediction parameters of advanced structural monolithic ceramics at elevated temperatures. Conducted at the NASA Glenn Research Center, the work was done for the C28 Advanced Ceramics Committee of the American Society for Testing and Materials (ASTM). The draft standard written by the authors had gone through all the required balloting and was established in 2000 as a new ASTM test method, ASTM C1465-00, "Standard Test Method for Determination of Slow Crack Growth Parameters of Advanced Ceramics by Constant Stress-Rate Flexural Testing at Elevated Temperatures." This new standard is to be published in the year 2001 Annual Book of ASTM Standards, Vol. 15.01.

Briefly, the test method employs constant stress-rate (or dynamic fatigue) testing to determine strengths as a function of the applied stress rate at elevated temperatures. The merit of this test method lies in its simplicity: Strengths are measured in a routine manner at four or more applied stress rates by applying a constant displacement rate or constant load rates. The slow crack growth parameters necessary for life prediction are then determined from a simple relationship between the strength and the applied stress rate. Some of the limiting factors such as creep, material deterioration, and crack-tip morphological change that are often encountered at higher test temperatures have been also taken into account to minimize their effects on the determination of slow crack growth parameters.

Currently, this test method is being extended to various continuous-fiber-reinforced ceramic matrix composites in tension at elevated temperatures to see if the test method is applicable to those composite materials (refs. 1 and 2). It has been found that a good relationship between ultimate strength and applied test rate existed and that reasonable agreement was observed within the experimental range between constant stress-rate and constant stress testing. This is a promising result since life prediction parameters of even composite materials would be determined by this simple, fast test method, allowing one to achieve a significant test-time saving. Furthermore, this method would be very useful in screening com-

posite materials in terms of slow crack growth or damage accumulation behavior within a limited time frame.

Glenn has maintained an active leadership role in the standardization of the life prediction testing of advanced monolithic ceramics within ASTM. The authors also wrote a companion ambient-temperature standard, ASTM C 1368-97, "Standard Test Method for Determination of Slow Crack Growth Parameters of Advanced Ceramics at Ambient Temperature."

References

1. Choi, Sung R.; and Gyekenyesi, John P.: Effect of Loading Rate on Strength of Nicalon™/CAS CFCC at Elevated Temperature. Proceedings of the Seventh Annual International Conference on Composites Engineering, David Hui, ed., ICCE/7, 2000, pp. 299-300.
2. Choi, S.R; and Gyekenyesi, J.P.: Effect of Load Rate on Tensile Strength of Various Continuous Fiber-Reinforced Ceramic Composites at Elevated Temperatures. Presented at the 25th Cocoa Beach Conference (Paper S2-0650-01), Jan. 21-26, 2001, Cocoa Beach, FL. Ceram. Eng. Sci. Proc., vol. 22, 2001.

Ohio Aerospace Institute contact:

Dr. Sung R. Choi, 216-433-8366,
Sung.R.Choi@grc.nasa.gov

Glenn contact: Dr. John P. Gyekenyesi,
216-433-3210,
John.P.Gyekenyesi@grc.nasa.gov

Authors: Dr. Sung R. Choi and
Dr. John P. Gyekenyesi

Headquarters program office: OAT

Programs/Projects:
ZCET, HOTPC, UEET

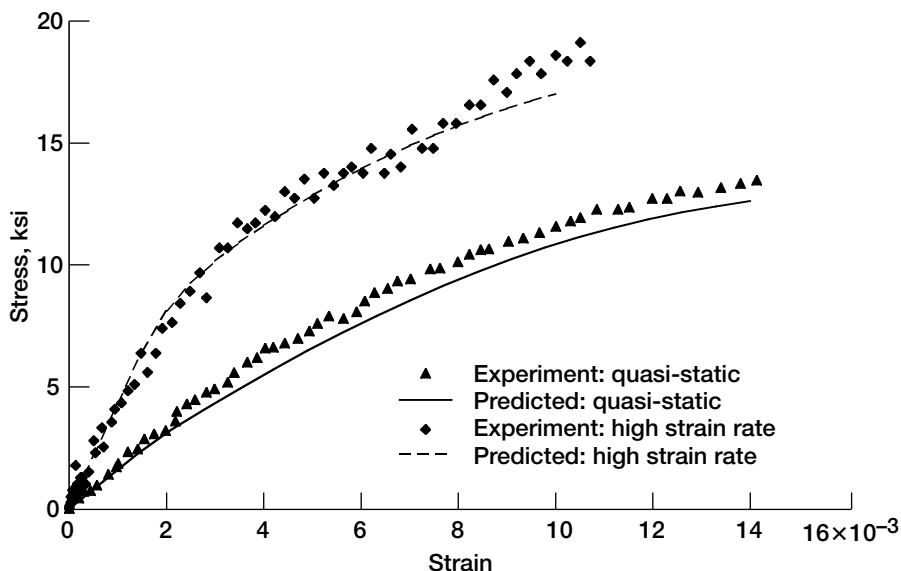
High Strain Rate Behavior of Polymer Matrix Composites Analyzed

Procedures for modeling the high-speed impact of composite materials are needed for designing reliable composite engine cases that are lighter than the metal cases in current use. The types of polymer matrix composites that are likely to be used in such an application have a deformation response that is nonlinear and that varies with strain rate. To characterize and validate material models that could be used in the design of impact-resistant engine cases, researchers must obtain material data over a wide variety of strain rates. An experimental program has been carried out through a university grant with the Ohio State University to obtain deformation data for a representative polymer matrix composite for strain rates ranging from quasi-static to high rates of several hundred per second. This information has been used to characterize and validate a constitutive model that was developed at the NASA Glenn Research Center.

To obtain the material data, Glenn's researchers designed and fabricated test specimens of a toughened epoxy resin and a carbon-fiber-reinforced composite that could be used in fan-containment applications. Quasi-static tests at low strain rates and split Hopkinson bar tests at high strain rates were then conducted at the Ohio State University. The tests indicated that both the stiffness and strength were highly strain-rate dependent for the resin. Furthermore, the strain rate dependence of the stiffness and strength were also observed for a variety of uniaxial composites with different fiber orientation angles. The resin data were used to characterize a constitutive model that was developed at Glenn to simulate the rate-dependent,

deformation response of the toughened epoxy matrix material. The composite data were used to validate a composite micromechanics model which incorporates the polymer constitutive equations and was also developed at Glenn that predicts the rate-dependent deformation response of a composite based on the properties and response of the individual constituents.

In the figure, the tensile stress-strain curve of a uniaxial [45°] polymer matrix composite is shown for both quasi-static and high strain rates. The rate dependence of the deformation response can be easily seen in the figure, with the stiffness and strength of the material increasing with strain rate. Results predicted using the developed analytical model are also shown for both strain rates. The predicted results compare well with the experimentally obtained values, indicating that the analytical model is valid over a wide variety of strain rates. Further tests and analyses will be conducted on additional fiber and resin combinations, as well as on multidirectional laminates with various ply layups.



Experimental and predicted tensile response of a representative [45°] polymer matrix composite for quasi-static and high strain rates.

Glenn contacts: Dr. Robert K. Goldberg, 216-433-3330, Robert.K.Goldberg@grc.nasa.gov; Dr. Gary D. Roberts, 216-433-3244, Gary.D.Roberts@grc.nasa.gov; and Dr. J. Michael Pereira, 216-433-6738, J.M.Pereira@grc.nasa.gov

Authors: Dr. Robert K. Goldberg and Dr. Gary D. Roberts

Headquarters program office: OAT

Programs/Projects: Ultra Safe

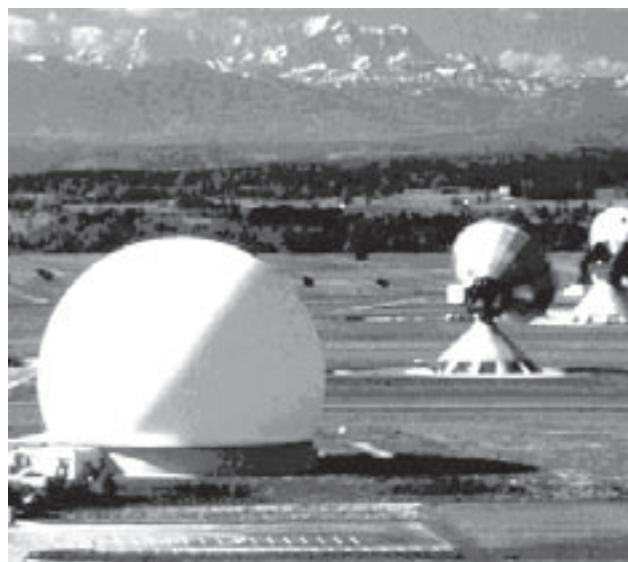
Biaxial Testing of High-Strength Fabric Improves Design of Inflatable Radar Domes

Large radar installations around the globe continuously watch the skies, unobtrusively providing security to the United States; these systems have been in active use for the past 50 years. Often situated in extreme environments, the radar dishes require shielding from the harsh elements. Air-inflated domes (over 100 ft in diameter) are one structure of choice for providing this essential protection. The radomes are constructed from high-strength fabric that is strong enough to withstand the inflation pressure, high winds, and other environmental loads, yet transparent to the microwave signal to allow precise radar mapping. This fabric is woven from glass fibers for high strength and embedded in a polytetrafluoroethylene resin matrix, akin to the nonstick coatings used on cookware.

Recently, there have been increasing demands for larger radome installations at locations with more severe wind environments, combined with greater reliability requirements. This has driven a need to better understand the mechanical properties of the material. On the basis of previous fabric testing for the design of aircraft emergency evacuation chutes, Raytheon Company, Electronic Systems Division, contacted the NASA Glenn Research Center's Life Prediction Branch to discuss using Glenn's testing and analysis capabilities. A cost-reimbursable Space Act Agreement was rapidly negotiated to conduct a series of biaxial tests of the glass-Teflon (DuPont) composite material in Glenn's Benchmark Test Facility.

The Chemfab Corporation supplied 36- by 36-in. cruciform fabric specimens in several different new designs, and new load-application fixtures were fabricated for the 100,000-lb-capacity Benchmark Test Facility in-plane load frame to accommodate the specimens. An optical full-field strain measurement system based on speckle-pattern correlation was modified to accommodate the large geometry.

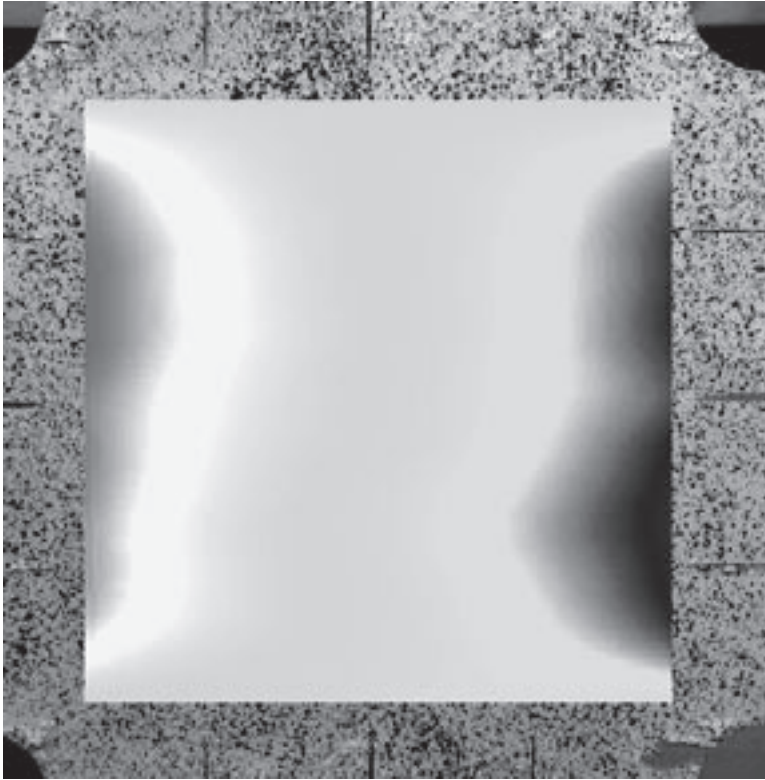
The ongoing testing program will accurately characterize the highly nonlinear, anisotropic, time- and cycle-dependent nature of the fabric. Deformation extensional and rotational moduli and Poisson's ratios along the principal material axes will be determined for over 80 load levels and load ratios. Currently midway through the program, the test results already are proving useful in improved understanding of the material at previously unobtainable high test loads. In addition, the specimen design has evolved to a degree that will allow valid strength testing.



Air-supported, 160-foot diameter fabric radome installed at Raisting, Germany.



Benchmark Test Facility in-plane biaxial load frame with fabric specimen mounted.



Fabric specimen under equibiaxial load with full-field strain pattern superimposed.

The results of this extensive testing program ultimately will allow higher-fidelity design and analysis of inflatable domes, as well as other structures fabricated from the glass-Teflon material. In the end, Glenn's testing will

lead to more efficient and greater use, higher durability, longer life, and improved safety and reliability of fabric material designs.

Find out more about this research:

Raytheon Company—Electronic Systems Division:

<http://www.raytheon.com/es/es.htm>

Chemfab Corporation:

<http://www.chemfab.com>

NASA Glenn Research Center:

<http://www.grc.nasa.gov>

Glenn's Life Prediction Branch:

<http://www.grc.nasa.gov/WWW/LPB>

Glenn contacts:

David L. Krause, 216-433-5465, David.L.Krause@grc.nasa.gov; and Dr. Paul A. Bartolotta, 216-433-3338, Paul.A.Bartolotta@grc.nasa.gov

Authors: David L. Krause and Dr. Paul A. Bartolotta

Headquarters program office: OAT

Programs/Projects: DoD

NASA Software of the Year, GENOA-PFA, Given 2000 R&D 100 Award

GENOA-PFA, marketed currently by Alpha Star Corporation, is an enhanced commercial version of the Composite Durability Structural Analysis (CODSTRAN) computer program that was originally developed in-house at NASA Glenn Research Center specifically for polymer-matrix composite structures. Alpha Star Corporation and the University of Clarkson have made substantial developments to the code under the NASA Small Business Innovation Research and University Grant support. The code won the NASA Software of the year award in 1999 and was given the 2000 R&D 100 Award. The current GENOA-PFA can simulate the initiation and progression of damage, ultimately leading to global fracture in advanced composite structures under various loading and environmental conditions. It offers a number of capabilities beyond those of programs developed previously for similar purposes; these capabilities make GENOA-PFA preferable for use in analyzing the durability and damage tolerance of

complex aero and space structures that have fiber reinforcements formed as two- and even three-dimensional weaves and braids.

GENOA-PFA implements a progressive-fracture methodology, the basic concept of which is that a structure fails when flaws that may initially be small (even microscopic) grow and/or coalesce to a critical dimension such that the structure no longer has an adequate safety margin to

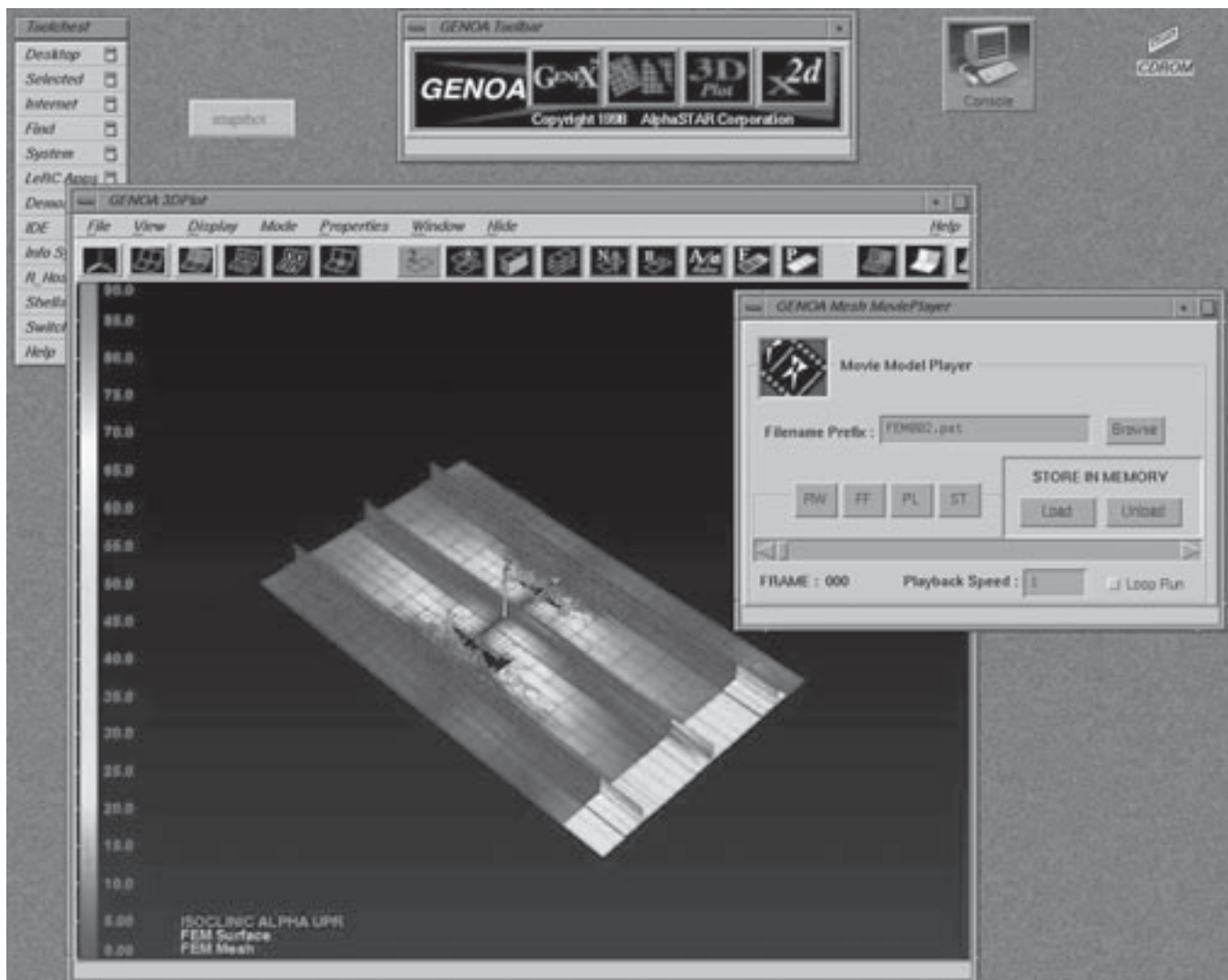
avoid catastrophic global fracture. Damage is considered to progress through five stages: (1) initiation, (2) growth, (3) accumulation (coalescence of propagating flaws), (4) stable propagation (up to a critical dimension), and (5) unstable or very rapid propagation (beyond the critical dimension) to catastrophic failure. The computational simulation of progressive failure involves formal procedures for identifying the five different stages of damage at each stage and relating the amount of damage at each stage to the overall behavior of the deteriorating structure. Typical applications of GENOA are shown in the accompanying figures.

Some of the salient features of GENOA-PFA software follow:

- Inclusion of material nonlinearities through the periodic updating of stiffnesses and inclusion of geometric nonlinearities through Lagrangian updating
- Simulation of the initiation, growth, and ultimate failure of a material under static, cyclic, creep, and impact loads

- Identification of the fractional contributions of various possible composite failure modes involved in critical damage events
- Determination of the sensitivities of failure modes to such design parameters as fiber volume fractions, ply thicknesses, fiber orientations, and thicknesses of adhesive bonds

Over 20 customers from industry, academia, and Government agencies nationwide utilize GENOA for the durability and life analysis of



GENOA-PFA graphical user interface showing a simulation of composite damage and fracture propagation via CODSTRAN. Act 3 stringer composite wing panel.

advanced composite structures. Some of the selected industry users are Boeing, Rockwell Aerospace, AlliedSignal, and McDonnell Douglas. University users include Case Western Reserve University, Clarkson University, and the University of California at Santa Barbara. Government agency users include NASA and Wright-Patterson Air Force Base.

Bibliography

Chamis, C.C.; Murthy, P.L.N.; and Minnetyan, L.: Progressive Fracture of Polymer Matrix Composite Structures. Theoret. Applied Fracture Mechan., vol. 25, no. 1, 1996, pp. 1–15.

Huang, Dade: GENOA Progressive Failure Analysis Program: Computational Simulation of Three-Dimensional Fiber Reinforced Composites. Vol. 1—Theoretical Manual, Alpha STAR Corporation, Los Angeles, CA, 1998.

GENOA Progressive Failure Analysis Module for 2D/3D Laminate/Woven/Braided/Stitched Polymer Matrix Composites, User's Manual, ver. 7.0, Alpha Star Corporation, Los Angeles, CA, 1999.

Glenn contacts:

Dr. Pappu L.N. Murthy, 216–433–3332, Pappu.L.Murthy@grc.nasa.gov; and Dr. Christos C. Chamis, 216–433–3252, Christos.C.Chamis@grc.nasa.gov

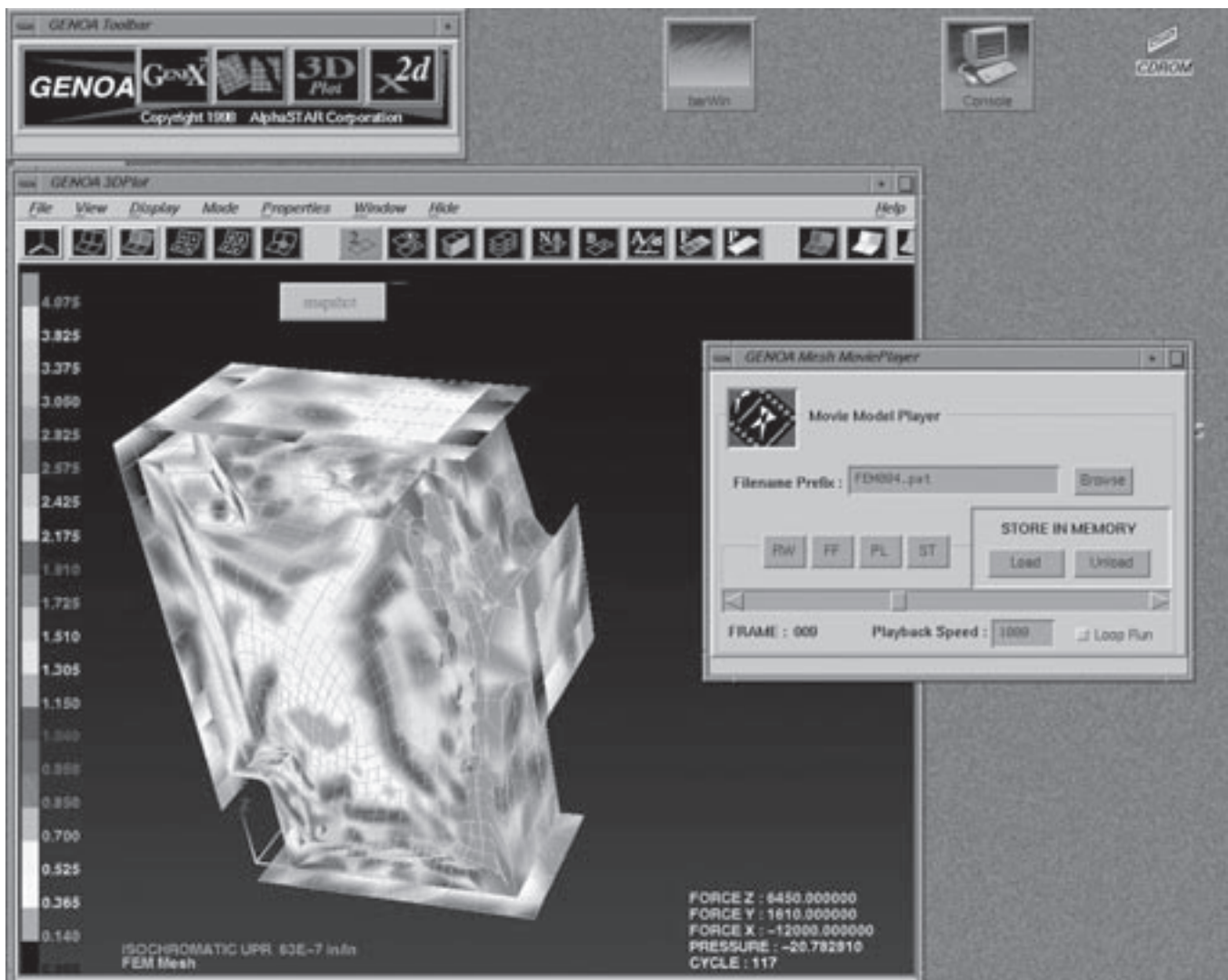
Author: Dr. Pappu L.N. Murthy

Headquarters program office: OAT

Programs/Projects: Base R&T

Special recognition:

2000 R&D 100 Award and 1999 NASA Software of the Year Award



GENOA–PFA graphical user interface showing a simulation of composite damage and fracture propagation via CODSTRAN. Airborne laser reactor housing.

Uncertainties in the Thermal and Mechanical Properties of Particulate Composites Quantified

Particle-reinforced composites are candidate materials for a wide variety of aerospace and nonaerospace applications. The high costs and technical difficulties involved with the use of many fiber-reinforced composites often limit their use in many applications. Consequently, particulate composites have emerged as viable alternatives to conventional fiber-reinforced composites. Particulate composites can be processed to near net shape—potentially reducing the manufacturing costs. They are candidate materials where shock or impact properties are important. For example, particle-reinforced metal matrix composites have shown great potential for many automotive applications. Typically, these materials are aluminum matrix reinforced with SiC or TiC particles. Reinforced concrete can also be thought of as a particle-reinforced composite. In situ ceramics can be modeled as particulate composites and are candidate materials for many high-temperature applications. The characterization of these materials is fundamental to their reliable use. It has been observed that the overall properties of these composites exhibit scatter because of the uncertainty in the constituent material properties, and fabrication-related parameters.

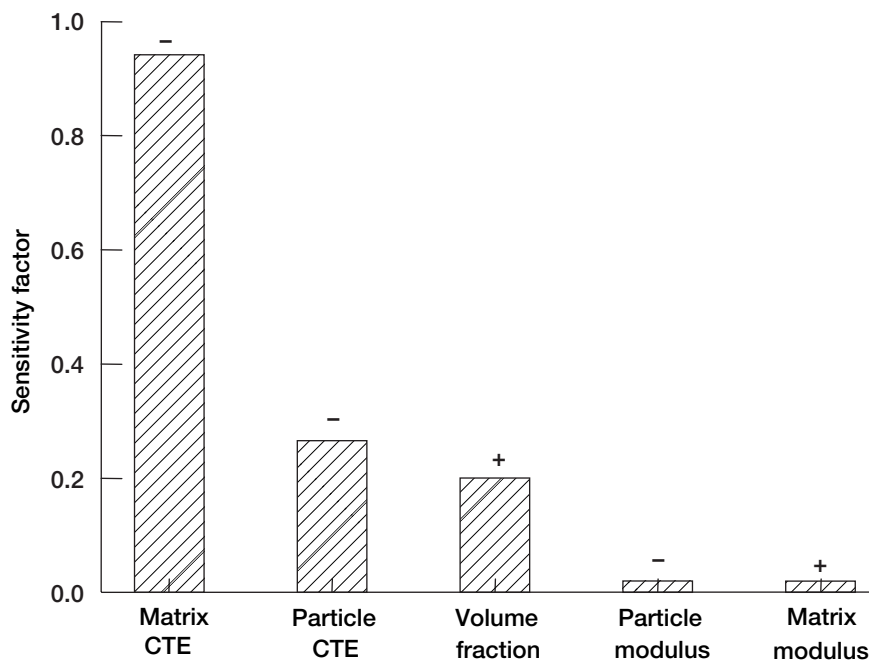
The observed scatter in the global composite behavior or “response” is usually caused by the existence of uncertainties in the basic or “primitive” variables. Primitive variables are properties or parameters that participate at the lowest or micromechanics level in defining a global or homogenized property. Volume fractions and individual constituent properties such as moduli, thermal expansion coefficients, thermal conductivities,

and strengths are examples of primitive variables. They are assumed to be independent and have their own statistical distributions. Response variables are those that characterize such composite behavior as the composite moduli, thermal properties, and strengths.

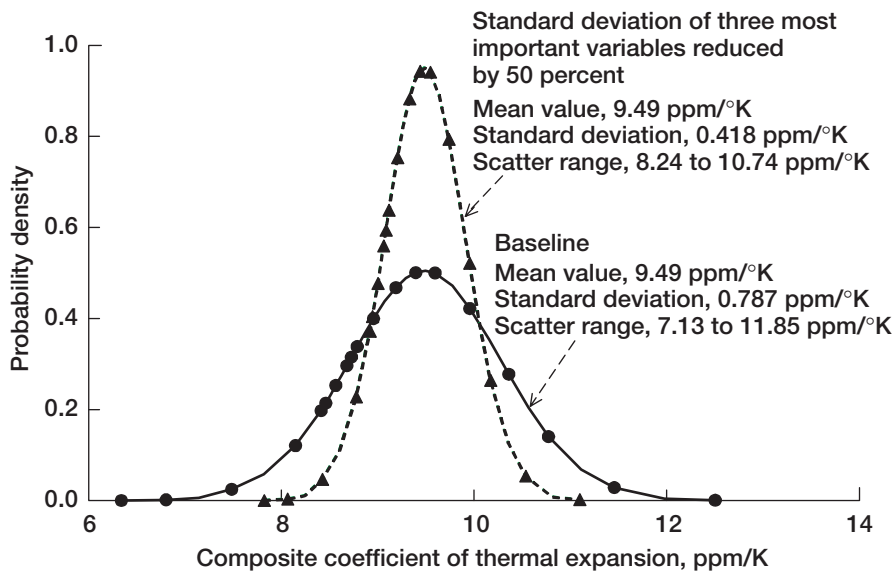
This approach to quantify probabilistic composite behavior, which was developed at the NASA Glenn Research Center, combines the micromechanics of particulate composites with a fast probability integration technique. The role of micromechanics equations that are programmed in a computer code ICAN/PART, is to provide functional relationships that tie the constituent properties to the equivalent composite behavior. The role of the fast probability integration technique is to perform probabilistic analyses by utilizing the properties generated by the micromechanics equations. The combined procedure yields probabilistic distribution and density functions of global composite properties. Furthermore, the procedure also identifies and ranks the sensitivities of the various primitive variables on the global composite property and its scatter. This technique is far more efficient than a standard Monte-Carlo technique where a large number of simulations are needed to generate such information. The figures show sample results from the analysis.

Bibliography

Mital, Subodh K.; and Murthy, Pappu L.N.: Quantifying Uncertainties in the Thermo-Mechanical Properties of Particulate Reinforced Composites. *J. Reinf. Plast. Comp.*, vol. 19, no. 8, 2000, pp. 657–678.



Sensitivity factors of composite coefficients of thermal expansion.



Probability density function of composite thermal expansion coefficient.

Glenn contact:

Dr. Pappu L.N. Murthy, 216-433-3332,
Pappu.L.Murthy@grc.nasa.gov

University of Toledo contact:

Subodh K. Mital, 216-433-3261,
Subodh.K.Mital@grc.nasa.gov

Authors: Dr. Pappu L.N. Murthy and
 Subodh K. Mital

Headquarters program office: OAT

Programs/Projects: Base R&T

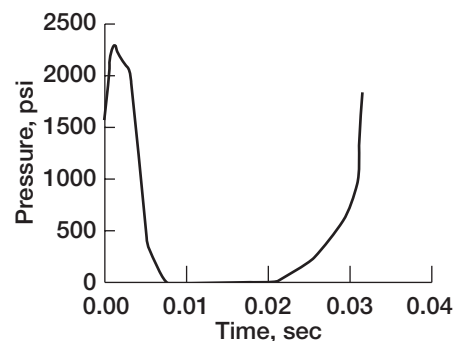
Transient Reliability Analysis Capability Developed for CARES/*Life*

The CARES/*Life* software developed at the NASA Glenn Research Center provides a general-purpose design tool that predicts the probability of the failure of a ceramic component as a function of its time in service. This award-winning software has been widely used by U.S. industry to establish the reliability and life of a brittle material (e.g., ceramic, intermetallic, and graphite) structures in a wide variety of 21st century applications.

Present capabilities of the NASA CARES/*Life* code include probabilistic life prediction of ceramic components subjected to fast fracture, slow crack growth (stress corrosion), and cyclic fatigue failure modes. Currently, this code can compute the time-dependent reliability of ceramic structures subjected to simple time-dependent loading. For example, in slow crack growth failure conditions CARES/*Life* can handle sustained and linearly increasing time-dependent loads, whereas in cyclic fatigue applications various types of repetitive constant-amplitude loads can be accounted for. However, in real applications applied loads are rarely that simple but vary with time in more complex ways such as engine startup, shutdown, and dynamic and vibrational loads. In addition, when a given component is subjected to transient environmental and or thermal conditions, the material properties also vary with time. A methodology has now been developed to allow the CARES/*Life* computer code to perform reliability analysis of ceramic components undergoing transient thermal and mechanical loading. This means that CARES/*Life* will be able to analyze

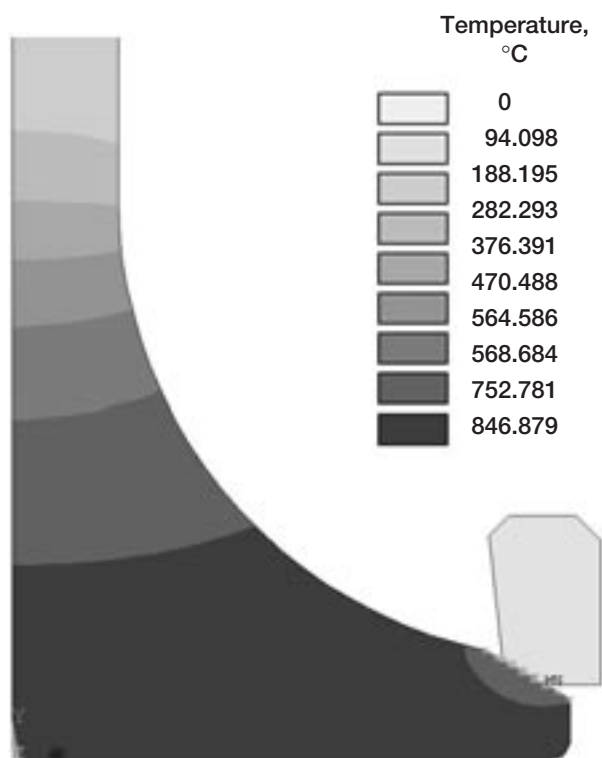
finite element models of ceramic components that simulate dynamic engine operating conditions. The methodology developed is generalized to account for material property variation (on strength distribution and fatigue) as a function of temperature. This allows CARES/*Life* to analyze components undergoing rapid temperature change—in other words, components undergoing thermal shock. In addition, the capability has been developed to perform reliability analysis for components that undergo proof testing involving transient loads. This methodology was developed for environmentally assisted crack growth (crack growth as a function of time and loading), but it will be extended to account for cyclic fatigue (crack growth as a function of load cycles) as well.

An example involving a ceramic exhaust valve subjected to combustion cycle loads is presented to demonstrate the viability of this methodology and the CARES/*Life* program. The valve is designed to be used in heavy duty diesel engines. Replacement of the metal exhaust valves with ceramic valves would prolong valve life and permit higher operating temperatures. The valves were made of NT-551 silicon nitride material. Simple specimens (four-point-bend rectangular bars, four-point-bend cylindrical bars, and tensile specimens) were tested in fast fracture and dynamic fatigue modes to extract the Weibull and slow crack growth parameters for NT-551 as a function of temperature. These parameters were used to predict the probability of failure of the valve versus the number of operating cycles. For this example, the valves were assumed to degrade because of slow crack growth and not significantly from cyclic fatigue—which is typical behavior for many ceramic materials. The figure to the right represents one pressure cycle applied to the valve face.



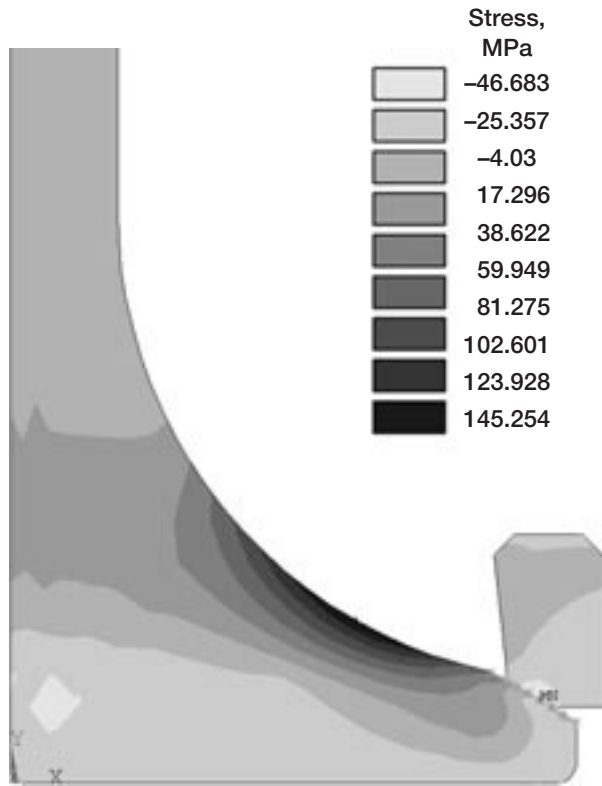
Pressure variation applied to the face of a ceramic valve during a typical engine combustion cycle.

The pressure is applied to the valve's face and other exposed surfaces within the cylinder. In addition, thermal stresses due to the temperature distribution in the valve are superposed to the mechanical stresses. The next figure shows the approximate mean thermal profile in the valve. Steady-state thermal analysis using the ANSYS finite element analysis code was conducted to compute these temperatures. This figure shows that the temperature is maximum near the valve face and decays towards the valve seat and stem.

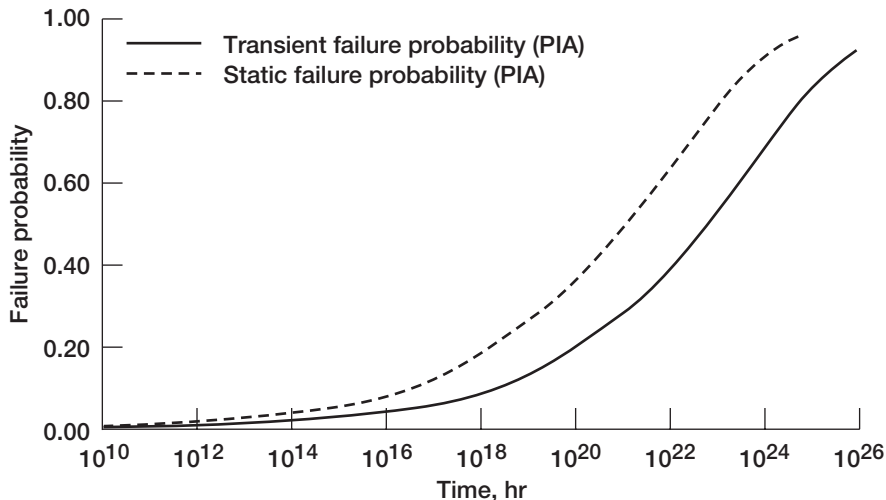


Mean thermal profile in the ceramic diesel exhaust valve.

The transient reliability analysis was conducted by dividing the load history into 29 time steps; during each, the load was assumed to be constant. The loads corresponding to these time steps were modeled into ANSYS finite element analysis code, which yielded the stress results for these 29 time steps (stress history). The next figure (facing page) highlights the first principal thermomechanical stress distribution in the valve at the moment of maximum applied pressure (the most critical point of the load history). From the figure, it is apparent that the maximum stress location is at the valve radius. The valve's stress history and other relevant terms (temperature, volume, material properties, element number, etc.) were subsequently read into CARES/*Life*. The failure probability as a function of time (number of cycles converted to time according to 1 cycle = 0.0315 sec) was then computed using the transient reliability analysis described previously. The final figure shows the transient reliability curve as a function of time (load cycles). As can be seen from that figure, the probability of failure increases with time. It is apparent from the figure that this ceramic valve is very reliable. After 1 hr of operation, the failure probability P_f



First principal stress distribution in the diesel exhaust valve at the moment of maximum applied pressure.



Transient and static probability of failure as a function of time for the ceramic valve. PIA, principle of independent action.

is predicted to be 6×10^{-5} (6 in 100,000 valves would have failed), whereas after 8.7 million hr of operation the P_f would be 9.4×10^{-4} (approximately 9 in 10,000 valves would have failed). A static reliability analysis using the maximum load level (load step 6 in this analysis) during the load cycle was performed and compared with the transient reliability analysis based on the actual transient loading. The final figure contains the results of this analysis. As can be seen from this figure, the static loading at the maximum level yielded higher failure probabilities (more conservative) in comparison to the transient loading case. Between 9 and 9×10^{15} hr of operation, the failure probability based on static analysis at maximum stress is double the failure probability based on transient analysis. For example, after 1000 hr of operation, transient reliability analysis predicted that approximately 2 in 10,000 valves would have failed, whereas maximum static reliability analysis predicted that approximately 4 in 10,000 valves would have failed. These results, showing higher failure probabilities for the static loading compared with the transient loading, make sense since the valve is not even loaded for some time during each combustion cycle. Therefore, depending on the structure and loading, making the assumption that static reliability analysis at the maximum load level can produce close results using the actual loading is not always accurate. Such static analysis can lead to oversized structures.

Glenn contact:

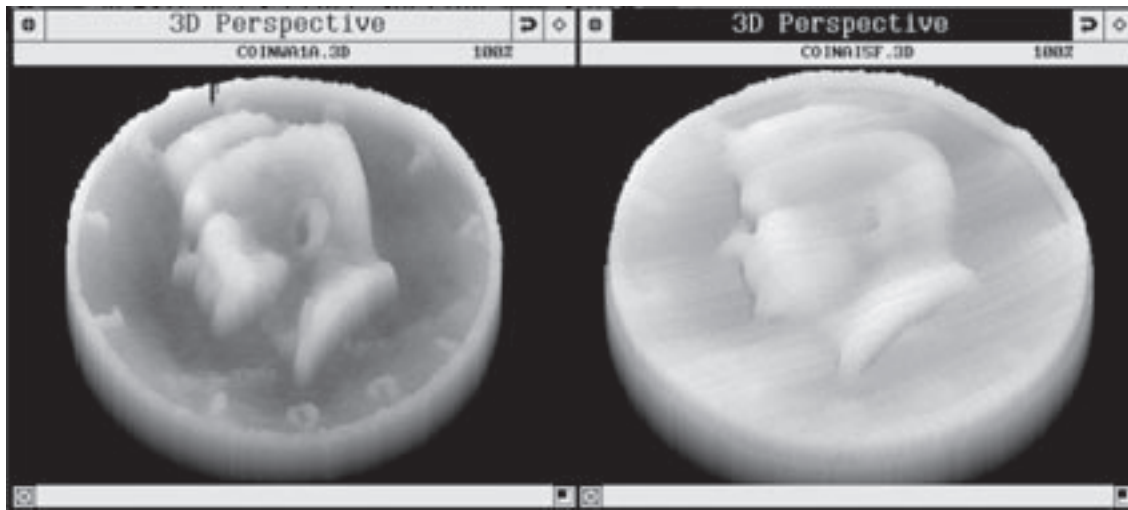
Noel N. Nemeth, 216-433-3215,
Noel.N.Nemeth@grc.nasa.gov

Author: Noel N. Nemeth

Headquarters program office: OAT

Programs/Projects: HOTPC

High-Frequency Focused Water-Coupled Ultrasound Used for Three-Dimensional Surface Depression Profiling



Water-coupled versus air-coupled ultrasonic surface profiling. Left: 25-MHz water-coupled, three-dimensional view. Right: 1-MHz air-coupled, three-dimensional view.

To interface with other solids, many surfaces are engineered via methods such as plating, coating, and machining to produce a functional surface ensuring successful end products. In addition, subsurface properties such as hardness, residual stress, deformation, chemical composition, and microstructure are often linked to surface characteristics. Surface topography, therefore, contains the signatures of the surface and possibly links to volumetric properties, and as a result serves as a vital link between surface design, manufacturing, and performance. Hence, surface topography can be used to diagnose, monitor, and control fabrication methods. At the NASA Glenn Research Center, the measurement of surface topography is important in developing high-temperature structural materials and for profiling the surface changes of materials during microgravity combustion experiments.

A prior study demonstrated that focused air-coupled ultrasound at 1 MHz could profile surfaces with a 25- μm depth resolution and a 400- μm lateral resolution over a 1.4-mm depth range. In this work, we address the question of whether higher frequency focused water-coupled ultrasound can improve on these specifications. To this end, we employed 10- and 25-MHz focused ultrasonic transducers in the water-coupled mode. The surface profile results seen in this investigation for 25-MHz water-coupled ultrasound, in comparison to those for 1-MHz air-coupled ultrasound, represent an 8 times improvement in depth resolution (3 vs. 25 μm seen in practice), an improvement of at least 2 times in lateral resolution (180 vs. 400 μm calculated and observed in practice), and an improvement in vertical depth range of 4 times (calculated).

In most cases, impressive topographical representations were obtained for all samples when they were compared with diamond-tip profiles and measurements from micrometers. The method is completely nondestructive, requires only water as a coupling fluid, and can profile large areas

limited only by the scan limits of the particular ultrasonic system. Using an optimized configuration, it is reasonably rapid and has all quantitative analysis facilities online including two- and three-dimensional visualization capability, extreme value filtering (for faulty data), and leveling capability. The most significant factor affecting practical utilization of the water-coupled ultrasonic method of surface profiling as described in this study is the scattering effect when high-frequency ultrasound encounters nonperpendicular surfaces and does not reflect back to the transducer. It was shown that in some cases, extreme value filtering with nearest neighbors averaging replacement algorithms can be employed successfully to obtain an accurate topological representation even in the presence of major scatter. Overall quantitative agreement, however, remains difficult in the presence of significant scatter.

The major advantage of ultrasonic surface profiling over more

conventional profiling methods is its large area/high-speed capability and applicability to curved surfaces. The major disadvantage is it significantly reduced lateral and depth resolution capabilities in comparison with the conventional methods. This work was done at Glenn and at Sonix, Inc.

Bibliography

Roth, Don J., et al.: Using High Frequency Focused Water-Coupled Ultrasound for 3-D Surface Depression Profiling. NASA/TM-1999-209268, 1999. <http://gltrs.grc.nasa.gov/GLTRS>

Glenn contact:

Dr. Don J. Roth, 216-433-6017,
Don.J.Roth@grc.nasa.gov

Authors: Don J. Roth, Mike F. Whalen,
J. Lynne Hendricks, and James R. Bodis

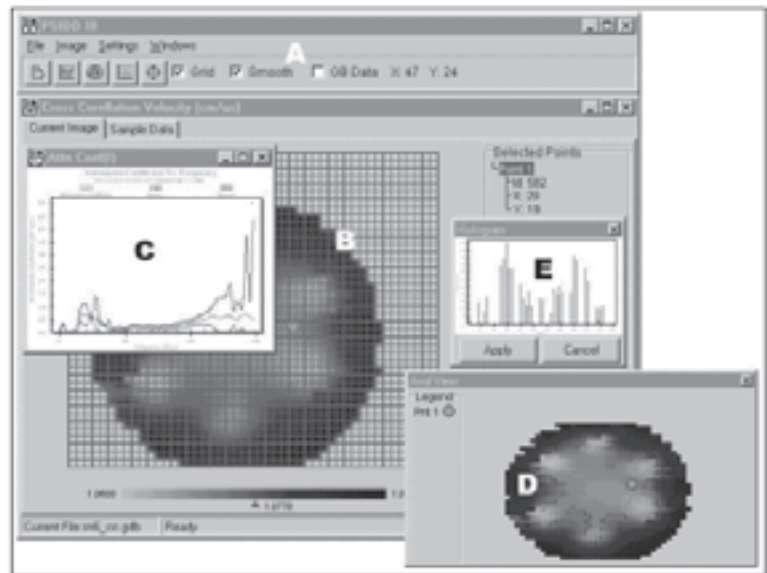
Headquarters program office: OAT

Programs/Projects: HITEMP,
COMMTECH, Space Act Agreement

Ultrasonic Data Display and Analysis System Developed (Including Fuzzy Logic Analysis) for the Windows-Based PC

Post-Scan Interactive Data Display (PSIDD) III is a user-oriented Windows-based system that facilitates the display and comparison of ultrasonic contact measurement data obtained at NASA Glenn Research Center's Ultrasonic Nondestructive Evaluation measurement facility. The system is optimized to compare ultrasonic measurements made at different locations within a material or at different stages of material degradation. PSIDD III provides complete analysis of the primary waveforms in the time and frequency domains along with the calculation of several frequency-dependent properties including phase velocity and attenuation coefficient and several frequency-independent properties, like the cross correlation velocity. The system allows image generation on all the frequency-dependent properties at any available frequency (limited by the bandwidth used in the scans) and on any of the frequency-independent properties. From ultrasonic contact scans, areas of interest on an image can be studied with regard to underlying raw waveforms and derived ultrasonic properties by simply selecting the point on the image. The system offers various modes of indepth comparison between scan points. Up to five scan points can be selected for comparative analysis at once. The system was developed with Borland Delphi software (Visual Pascal) and is based on an SQL data base. It is ideal for the classification of material properties or the location of microstructure variations in materials. Along with the ultrasonic contact measurement software that it is partnered with, this system is technology ready and can be transferred to users worldwide.

This software culminates over 10 years of work from inception to finish. The original implementation was on a VAX computer system custom to Glenn's nondestructive evaluation laboratory, and it did not include fuzzy logic analysis capability. In 1997, we decided to port the entire system to Windows running on an IBM-compatible personal computer (PC). As such, PSIDD III would enjoy the benefits of a graphically oriented environment. This would allow information to be seamlessly passed between PSIDD and other systems for reporting or presentation use. Also, the interface would



Ultrasonic data display and analysis screen elements.

be much simpler for the end user by replacing the original cursor control unit with a mouse. PSIDD III was developed jointly by Glenn and the University of Toledo.

Bibliography

Lovelace, Jeffrey J., et al.: PSIDD3: Post-Scan Ultrasonic Data Display System for the Windows-Based PC Including Fuzzy Logic Analysis. NASA/TM-2000-210065, 2000. <http://gltrs.grc.nasa.gov/GLTRS>

Glenn contact:

Dr. Don J. Roth, 216-433-6017,
Don.J.Roth@grc.nasa.gov

Authors: Jeffrey J. Lovelace, Krzysztof J. Cios, Dr. Don J. Roth, and Wei N. Cao

Headquarters program office: OAT

Programs/Projects: HITEMP, UEET

Fan Flutter Analysis Capability Enhanced

The trend in the design of advanced transonic fans for aircraft engines has been toward the use of complex high-aspect-ratio blade geometries with a larger number of blades and higher loading. In addition, integrally bladed disks or blisks are being considered in fan designs for their potential to reduce manufacturing costs, weight, and complexity by eliminating attachments. With such design trends, there is an increased possibility within the operating region of part-speed stall flutter (self-excited vibrations) that is exacerbated by the reduced structural damping of blisk fans. To verify the aeroelastic soundness of the design, the NASA Glenn Research Center is developing and validating an accurate aeroelastic prediction and analysis capability. Recently, this capability was enhanced significantly as described here.

The propulsion aeroelastic analysis capability is based on a three-dimensional unsteady aerodynamic Reynolds-averaged Navier-Stokes turbomachinery code TURBO. This code can accurately model viscous flow effects that play an important role in certain aeroelastic problems such as flutter with flow separation, flutter at high loading conditions near the stall line (stall flutter), and flutter in the presence of shock and boundary-layer interaction. Recently, a preprocessor code (named AE-prep) was developed that performs the functions of the modeshape interpolation and grid deformation. This preprocessor allows the most recent version of the TURBO code (versions 4.2) to be used for aeroelastic analysis without the long delays previously associated with the merging of the aeroelastic modifications into each new version of TURBO. Thus, the aeroelastic analysis can benefit from all the new and improved features present in the latest versions of the TURBO code: namely, improved steady and unsteady viscous flow modeling with algebraic or $k-\epsilon$ turbulence models, improved ability to use startup solutions from other codes such as the APNASA code, real gas modeling, namelist input capability, cross-platform portability, and improved memory management with the FORTRAN 90 code. For fan flutter analysis near the stall line, the newly added capability to use a $k-\epsilon$ turbulence model is considered to be an extremely significant enhancement.

The AE-prep aeroelastic preprocessor and the TURBO code have been and continue to be exercised for flutter analysis as part of the verification and validation efforts. Standard test configurations and actual fan designs have been used as part of the verification and validation. Researchers at Honeywell Engines and Systems have also successfully exercised the TURBO code for the flutter analysis of experimental fan designs.

University of Toledo contacts:

Milind A. Bakhle, 216-433-6037,
Milind.A.Bakhle@grc.nasa.gov; and
Rakesh Srivastava, 216-433-6045,
Rakesh.Srivastava@grc.nasa.gov

Glenn contact:

George L. Stefko, 216-433-3920,
George.L.Stefko@grc.nasa.gov

Authors: Milind A. Bakhle, Rakesh Srivastava, and George L. Stefko

Headquarters program office: OAT

Programs/Projects: UEET

Cross-Axis Proportional Gains Used to Control Gyroscopic Effects in a Magnetic-Bearing-Supported Flywheel

For magnetic-bearing-supported high-speed machines with significant gyroscopic effects, it is necessary to stabilize both forward and backward tilt whirling modes. Instability or the low damping of these modes can prevent the attainment of desired shaft speeds. Previous work elsewhere showed that cross-axis derivative gain in the magnetic bearing control law can improve the stability of the forward whirl mode, but it is commonly recognized that derivative gains amplify high-frequency noise and increase the required control effort. At the NASA Glenn Research Center, it has been shown previously that a simple cross-axis proportional gain can add stability (without adding noise) to either forward whirl or backward whirl, depending on the sign of the gain, but that such a gain destabilizes the other mode.

It has been predicted by Glenn analysis that both modes can be stabilized by cross-axis proportional gains by utilizing the large-frequency separation of the two modes at speeds where the gyroscopic effects are significant. We use a modal controller that decouples the tilt and center-of-mass-translation modes. Only the tilt modes exhibit speed-dependent gyroscopic effects. The key to

controlling them by the present method is to stabilize the backward whirl tilt mode with the appropriate sign of cross-axis proportional gain in the control law, but to include a low-pass filter on that gain term to restrict its effect only to the low-frequency backward-whirl mode. A second cross-axis term with the opposite sign and a high-pass filter stabilizes the forward whirl, which can have a frequency one or two orders of magnitude higher than the backward whirl, permitting very independent action of the two terms. Because the physical gyroscopic torques are proportional to the spinning speed of the shaft, it is convenient to gain-schedule the cross-axis control terms by making them proportional to shaft speed. This has the added benefit of avoiding a somewhat awkward zero-speed splitting of the tilt-mode eigenvalues.

Phase lags in the closed loop do place a limit on the speed at which this simple method is effective, but if the phase lags are known, a modification of the method can extend the benefits to extremely high speeds. The action of the cross-axis gain is really to provide phase lead in the control to counteract phase lags in the rest of the closed loop. The displacement of one axis leads or lags the other by 90° and can be used with an appropriate gain to provide up to that amount of phase lead. However, at a shaft speed such that the forward whirl frequency reaches a value where the system phase lag reaches 90° , the method, as outlined so far, fails. But a linear combination of the two tilt displacements can have any desired phase (up to 360°) with respect to one of the displacements. An appropriate linear combination can be formed for any forward whirl mode frequency at which the external system phase lag is known, and that combination can provide adequate phase lead for forward whirl stability at any shaft speed. Implementation would require knowledge of the system transfer function and gain scheduling with respect to rotor speed. This extension of the method has been verified by eigenvalue analysis but not tested experimentally.

The basic method was experimentally demonstrated on the "DEV1" energy storage flywheel unit at Glenn at speeds up to 20,000 rpm. At that speed, the forward-whirl mode frequency was about 240 Hz and the backward-whirl frequency was about 15 Hz. Spectral density measurements of the shaft displacements confirmed that the two gain terms acted independently on the two modes. Each gain could be increased to reduce the affected spectral density peak to insignificance or, by using a small gain of the opposite sign, the modal damping could be reduced in order to sharpen the spectral density peak for accurate frequency measurement.

Glenn contact:

Dr. Gerald V. Brown, 216-433-6047,
Gerald.V.Brown@grc.nasa.gov

Glenn/U.S. Army Research Laboratory contact:

Albert F. Kascak, 216-433-6024,
Albert.F.Kascak@grc.nasa.gov

Authors: Dr. Gerald V. Brown and
Albert F. Kascak

Headquarters program office: OAT

Programs/Projects:

Flywheel Technology, FESS

DC Control Effort Minimized for Magnetic-Bearing-Supported Shaft

A magnetic-bearing-supported shaft may have a number of concentricity and alignment problems. One of these involves the relationship of the position sensors, the centerline of the backup bearings, and the magnetic center of the magnetic bearings. For magnetic bearings with permanent magnet biasing, the average control current for a given control axis that is not bearing the shaft weight will be minimized if the shaft is centered, on average over a revolution, at the magnetic center of the bearings. That position may not yield zero sensor output or center the shaft in the backup bearing clearance.

The desired shaft position that gives zero average current can be achieved if a simple additional term is added to the control law. Suppose that the instantaneous control currents from each bearing are available from measurements and can be input into the control computer. If each control current is integrated with a very small rate of accumulation and the result

is added to the control output, the shaft will gradually move to a position where the control current averages to zero over many revolutions. This will occur regardless of any offsets of the position sensor inputs. At that position, the average control effort is minimized in comparison to other possible locations of the shaft. Nonlinearities of the magnetic bearing are minimized at that location as well.

A satisfactory simplification of the method is possible in most

situations. For frequencies where power amplifier phase lags are negligible, the actuator control current is proportional to the control output command for transconductance mode power amplifiers. Thus, an integral of the output command to each amplifier, added to that output, will achieve the same effect. Even at frequencies where there is appreciable amplifier phase lag, the slowly building integral should still be effective.

The effectiveness of the simplified method (integration of control output) was demonstrated on a magnetic-bearing-supported energy-storage flywheel (DEV1) at the NASA Glenn Research Center. Previous tests of the flywheel had required repeated sensor offset adjustments as rotor speed changed to keep the average current for each axis near zero. (The presumed cause of the speed dependence was severe sensor runout interacting with various dynamic effects and system frequency response.) The present method maintained zero average control current throughout the speed range without any operator attention. The integral gain was chosen so that the time constant for approach to the final shaft position was a few seconds. An unexpected benefit was that the average motor current required at any rotor speed was reduced as well, presumably because of better centering of the motor rotor within its stator.

The method was also applied to the thrust bearing of the rig, which has a vertically oriented axis. In this situation with permanent magnet bias, the control effort is minimized with the axial bearing thrust disk higher than midway between the two stator disks. The axial control current becomes zero there, and the shaft weight is carried by the bias field because the magnetic gap is smaller above the thrust disk than below.

Glenn contact:

Dr. Gerald V. Brown, 216-433-6047,
Gerald.V.Brown@grc.nasa.gov

Author: Dr. Gerald V. Brown

Headquarters program office: OAT

Programs/Projects:

Flywheel Technology, FESS

Synchronous Control Effort Minimized for Magnetic-Bearing-Supported Shaft

Various disturbances that are synchronous with the shaft speed can complicate radial magnetic bearing control. These include position sensor target irregularities (runout) and shaft imbalance. The method presented here allows the controller to ignore all synchronous harmonics of the shaft position input (within the closed-loop bandwidth) and to respond only to asynchronous motions. The result is reduced control effort.

A previous article in this report outlined a method for automatic centering of a shaft in radial magnetic bearings, which achieves zero average control current. That was done by adding a very slowly building integral of the control current to the control output. (Using an integral of the controller output command rather than measured current can be a simpler alternative.) The method for rejecting synchronous disturbances is an extension of that method. We presume that the shaft's angular (spin) position θ is always known (from a once-per-revolution pulse, for example). For each actuator degree of freedom, an array of integrals of control output O is calculated and stored. Each integral $I(n)$ is approximated by a sum that receives a new contribution n samples after each one-per-revolution pulse:

$$I(n) = (1 - f \lg) [I(n) + \alpha I(n - 1) + \alpha I(n + 1)] + (1 - 2 \alpha) \lg O(n)$$

where \lg is a small gain (such as 0.02) and $f \lg$ is a "forgetter" factor. The terms containing α are discussed in the last paragraph of this article. Thus at a given speed, we are integrating the control effort required whenever

the shaft has a particular angular position and are storing that in one element of the array. Adding that element in the array to the control output whenever the shaft angle is θ results eventually in the magnetic bearing producing no synchronous control force at that shaft angle. The output for the n th sample after the one-per-revolution is

$$O(n) = PD_control_etc(n) + I(n) + \{cg [I(n + 1) - I(n - 1)]\} / \Delta t$$

where $PD_control_etc(n)$ is the control output for whatever control law is used, Δt is the time between samples, and the presence of the term containing Δt is explained in the last paragraph of this article. The $I(n)$ array acts like a feed-forward function. Spurious synchronous sensor runout signals come into the controller and contribute

to $PD_control_etc(n)$ but are cancelled out by $I(n)$. Furthermore, the shaft is allowed to revolve about its principle inertia axis rather than about its geometrical centerline, reducing the control effort due to imbalance as well as reducing the forces transmitted to the housing. The shaft runs like a supercritical shaft at all speeds.

The method was demonstrated on a magnetic-bearing-supported energy-storage flywheel (DEV1) at the NASA Glenn Research Center. The runout of the radial sensors was very serious, amounting to 15 to 20 percent of the backup bearing gap of 8 mils (0.2 mm). The sensor runout produced apparent (but spurious) displacements at least an order of magnitude higher than the real shaft dynamics. Moving notch filters had previously been needed to keep the sensor runout from causing power amplifier saturation at high shaft speeds. Spectral density measurements of the sensor signals showed that the present method reduced synchronous harmonic content by factors of 3 to 10 at shaft speeds up to 20,000 rpm.

If explicit synchronous feed-forward signals are introduced to deal with unbalance, the array $I(n)$ converges to the difference between its former values and the feed-forward function.

Several implementation details were developed on an ad hoc basis. The required size of the array is equal to the number of samples in one shaft revolution at the lowest speed at which the method will be used. We used arrays of 1500 to 2000 elements with a controller sample rate of 60 μ sec and could introduce the integrals at shaft speeds somewhat below 1000 rpm. Note that the number of active elements in the array becomes much smaller at high speeds; there are only 50 samples per revolution at 20,000 rpm. We do not need to change the array dimension with speed; rather the code automatically uses only as many elements as required in one revolution. The array was continually smoothed by a degree of averaging of adjacent elements. This was affected by the terms containing α , which was arbitrarily set somewhere between 0 and 0.25. This aids in letting the array adapt to changing speeds. Furthermore, each element was gradually eroded to remove contributions of the distant past by using a

forgetter factor $(1 - fI_g)$, which is very slightly less than one, where f was of order 1. Each element is, thus, a geometric average of the control effort exerted for n samples after the one-per-revolution pulse, smoothed somewhat in time. Finally, to avoid an instability that would otherwise develop in the array, a derivative of the array with respect to θ was added to the control output, with an empirically determined gain cg of the order of 0.005.

If the shaft speed is set low, the actual sensor runout, which is difficult to measure otherwise, can be obtained by allowing the synchronous rejection to converge and then recording the sensor output. This measurement is relatively uncontaminated by closed-loop effects that would otherwise prevent direct measurement of runout on the levitated shaft.

Glenn contact:

Dr. Gerald V. Brown, 216-433-6047,
Gerald.V.Brown@grc.nasa.gov

Author: Dr. Gerald V. Brown

Headquarters program office: OAT

Programs/Projects:

Flywheel Technology, FESS

Fail-Safe Magnetic Bearing Controller Demonstrated Successfully

The Structural Mechanics and Dynamics Branch has successfully demonstrated a fail-safe controller for the Fault-Tolerant Magnetic Bearing rig at the NASA Glenn Research Center. The rotor is supported by two 8-pole redundant radial bearings, and coil failing situations are simulated by manually shutting down their control current commands from the controller cockpit. The effectiveness of the controller was demonstrated when only two active coils from each radial bearing could be used (that is, 14 coils failed). These remaining two coils still levitated the rotor and spun it without losing stability or desired position up to the maximum allowable speed of 20,000 rpm.

This demonstration disproved the existing fault-tolerant control theory, which cannot solve the distribution matrix of reduced flux density for the case of just two coils. A significant amount of real-time noise levels were calculated by using a moving average (MA) filter and a programmable S-function block. Also, a centralized

modal controller was demonstrated to better control the dynamic behavior over system modes. A graphical-user-interface-based control cockpit and a whirling feature to investigate gyroscopic effects were also demonstrated.

This extremely valuable demonstration could help to ease the controversial safety issue of magnetic suspension technology for advanced high-speed rotating turbomachinery in case of system faults in the main bearing components. A simple PID controller generated autonomous corrective actions for the failed coil situations without losing the load capacity to meet the NASA mission of doing things faster, better, and cheaper.

Glenn contacts:

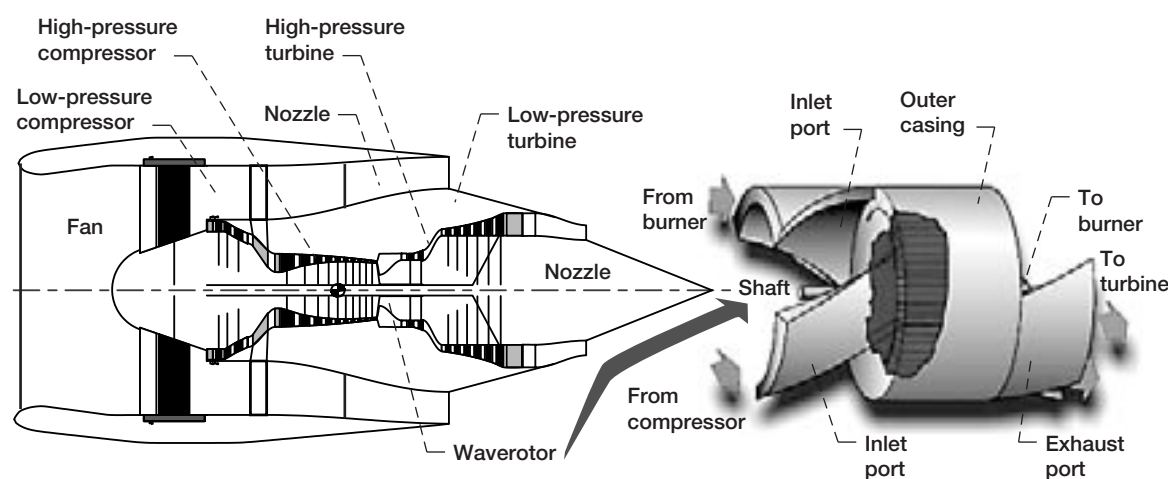
Dr. Benjamin B. Choi, 216-433-6040, Benjamin.B.Choi@grc.nasa.gov; and Andrew J. Provenza, 216-433-6025, Andrew.J.Provenza@grc.nasa.gov

Authors: Dr. Benjamin B. Choi and Andrew J. Provenza

Headquarters program office: OAT

Programs/Projects: TCT, FESS

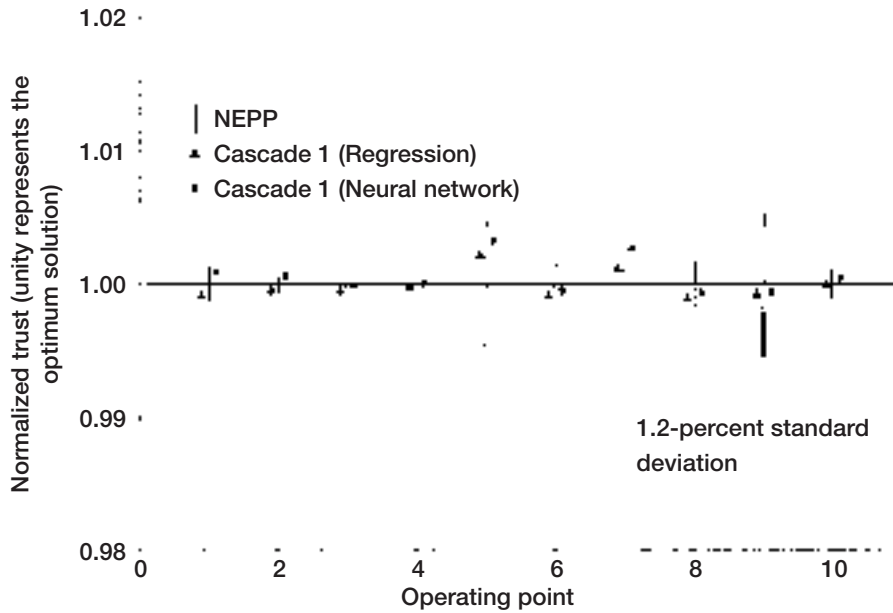
Engine With Regression and Neural Network Approximators Designed



Subsonic waverotor-topped gas turbine engine.

At the NASA Glenn Research Center, the NASA engine performance program (NEPP, ref. 1) and the design optimization testbed COMETBOARDS (ref. 2) with regression and neural network analysis-approximators have been coupled to obtain a preliminary engine design methodology. The solution to a high-bypass-ratio subsonic waverotor-topped turbofan engine, which is shown in the preceding figure, was obtained by the simulation depicted in the preceding figure. This engine is made of 16 components mounted on two shafts with 21 flow stations. The engine is designed for a flight envelope with 47 operating points. The design optimization utilized both neural network and regression approximations, along with the cascade strategy (ref. 3). The cascade used three algorithms in sequence: the method of feasible directions, the sequence of unconstrained minimizations technique, and sequential quadratic programming. The normalized optimum thrusts obtained by the three methods are shown in the following figure: the cascade algorithm with regression approximation is represented by a triangle, a circle is shown for the neural network solution, and

a solid line indicates original NEPP results. The solutions obtained from both approximate methods lie within one standard deviation of the benchmark solution for each operating point. The simulation improved the maximum thrust by 5 percent. The performance of the linear regression and neural network methods as alternate engine analyzers was found to be satisfactory for the analysis and operation optimization of air-breathing propulsion engines (ref. 4).



Optimum solution for the waverotor-topped subsonic engine.

References

1. Klann, John L.; and Snyder, Christopher A.: NEPP Programmers Manual. NASA TM-106575, 1994.
2. Guptill, James D., et al.: CometBoards Users Manual Release 1.0. NASA TM-4537, 1996. <http://gltrs.grc.nasa.gov/GLTRS>

3. Patnaik, Surya N.; Coroneos, R.M.; and Hopkins, D.A.: A Cascade Optimization Strategy for Solution of Difficult Design Problems. *Int. J. Numer. Meth. Engrg.*, vol. 40, no. 12, 1997, pp. 2257-2266.
4. Patnaik, Surya N., et al.: Cascade Optimization for Aircraft Engines With Regression and Neural Network Analysis—Approximators. NASA/TM-2000-209177, 2000. <http://gltrs.grc.nasa.gov/GLTRS>

Ohio Aerospace Institute contact:

Dr. Surya N. Patnaik, 216-433-5916, Surya.N.Patnaik@grc.nasa.gov

Glenn contact:

Dale A. Hopkins, 216-433-3260, Dale.A.Hopkins@grc.nasa.gov

Authors: Dr. Surya N. Patnaik and Dale A. Hopkins

Headquarters program office: OAT

Programs/Projects:

Ultra Safe, UEET, HSR

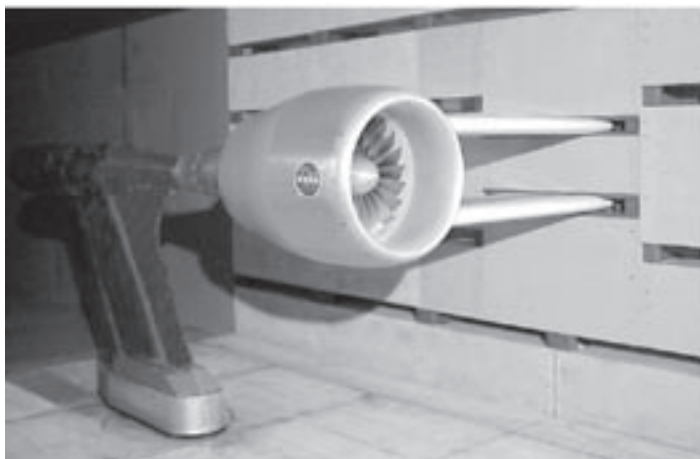
Turbofan Noise Studied in Unique Model Research Program in NASA Glenn's 9- by 15-Foot Low-Speed Wind Tunnel

A comprehensive aeroacoustic research program called the Source Diagnostic Test was recently concluded in NASA Glenn Research Center's 9- by 15-Foot Low Speed Wind Tunnel. The testing involved representatives from Glenn, NASA Langley Research Center, GE Aircraft Engines, and the Boeing Company. The technical objectives of this research were to identify the different source mechanisms of noise in a modern, high-bypass turbofan aircraft engine through scale-model testing and to make detailed acoustic and aerodynamic measurements to more fully understand the physics of how turbofan noise is generated.

The Source Diagnostic Test research program was conducted using a one-sixth-scale model of the bypass section representative of current technology turbofan engines, which included the fan, stators, and nacelle. The fan consisted of 22 wide-chord fan blades and was driven by Glenn's Ultra High Bypass Propulsion Simulator—a 5000-shp air-driven turbine designed for testing



Source Diagnostic Test turbofan engine simulator installed in Glenn's 9- by 15-Foot Low-Speed Wind Tunnel.



Rotor Alone Nacelle configuration with externally supported nacelle during Source Diagnostic Test.

turbofan aircraft engine models in a wind tunnel environment. The stator vane assembly, located behind the fan and used to provide support for the nacelle as well as to straighten the swirling flow from the fan, included several hardware configurations to investigate the effect of vane number and vane blade geometry on acoustics and aerodynamic performance. In order to isolate and characterize the fan noise from the stator noise, an innovative test technique was successfully developed at Glenn, which isolated the fan in the nacelle. Called the Rotor Alone Nacelle (RAN), this system used an external strut arrangement to support the nacelle externally and thereby allow the stator vanes to be removed. During testing, a laser ranging system was used to measure the distance from the nacelle to the model centerbody. A sophisticated two-axis translating table and control system then used these centerbody measurements to automatically move the nacelle and external strut assembly to keep the fan centered in the nacelle. In addition to keeping the nacelle centered over the fan, realistic fan tip clearances representative of a turbofan engine were also achieved.

The extensive, year-long testing program allowed a comprehensive data base of aerodynamic and acoustic performance parameters to be obtained using unique and innovative measurement techniques. Fan and stator vane performance was measured using fixed pressure and temperature rakes, and a translating multiprobe pressure rake was used to measure stator wakes. Fan thrust and power and the stator vane thrust were measured using rotating and static force balances. Steady and unsteady surface pressures on the stator vanes were measured using removable, instrumented vanes. Details of the velocity and turbulence components in the fan flow field were obtained using Laser Doppler Velocimetry (LDV) and, for the first time at NASA, two-point turbulence measurements using multicomponent, multiprobe hotwire anemometry.

A special LDV window mounted over the fan tip allowed details of the flow to be obtained. Farfield acoustics were measured using a translating microphone assembly to provide sideline measurements. Acoustic duct

modes within the nacelle were measured simultaneously by 180 dynamic pressure sensors, located at three axial areas in the nacelle, and a rotating microphone assembly in front of the fan and behind the stator vanes.

The extensive acoustic and aerodynamic data base created as a result of this research will be used by NASA and the U.S. aerospace industry as a guide for future acoustic research in turbofan engine noise-reduction technologies. More computationally efficient and more accurate fan-noise-prediction computer codes will be developed and validated using these data.

Glenn contact:

Christopher E. Hughes, 216-433-3924,
Christopher.E.Hughes@grc.nasa.gov

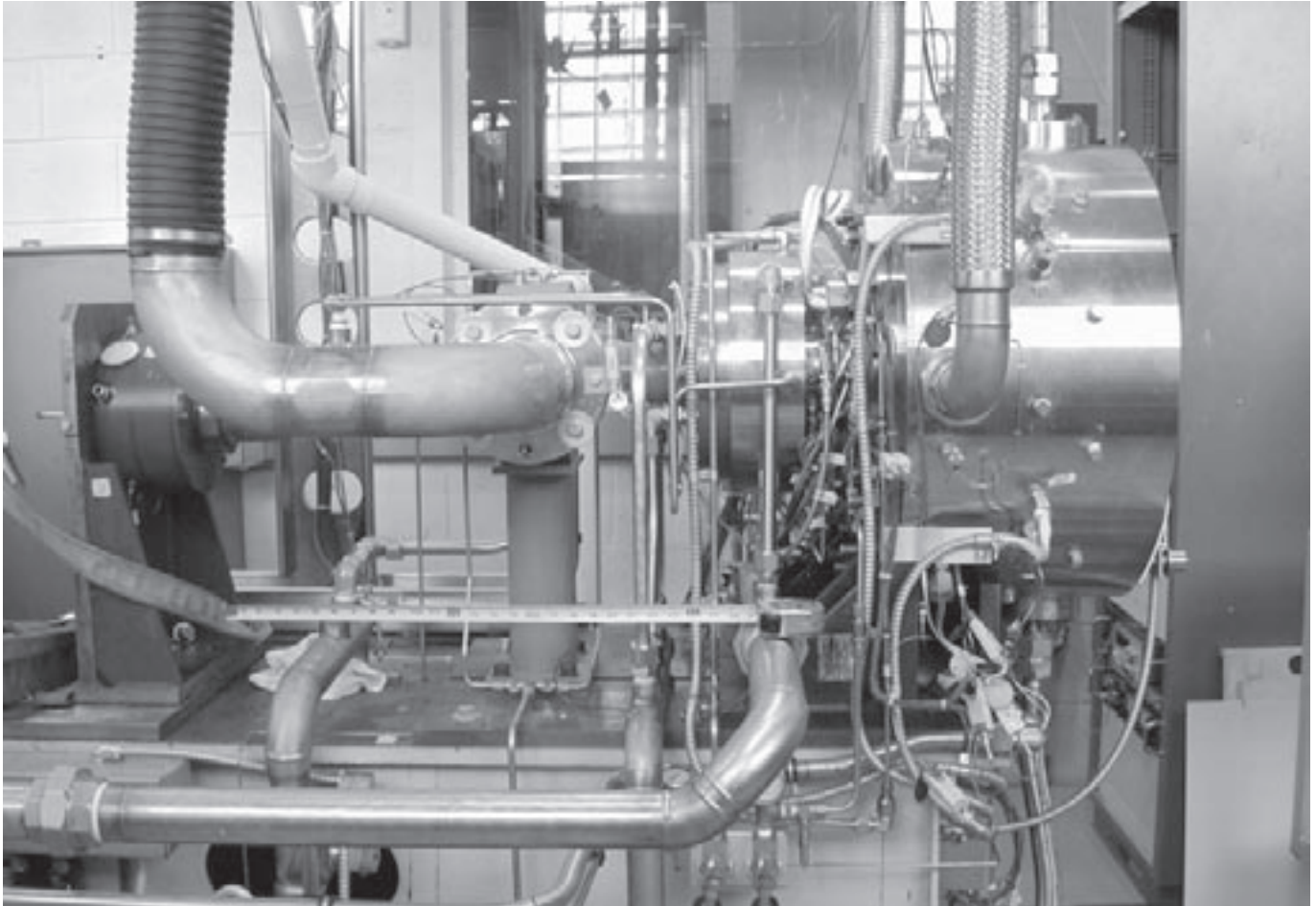
Author: Christopher E. Hughes

Headquarters program office: OAT

Programs/Projects:

Quiet Aircraft Technology, Aerospace
Vehicle Systems Technology

New High-Temperature Turbine Seal Rig Installed



High-Temperature Seal Rig installation completed.

Current NASA program goals for aircraft engines and vehicle performance include reducing direct operating costs for commercial aircraft by 3 percent in large engines and 5 percent in regional engines, reducing engine fuel burn up to 10 percent, and reducing engine oxides of nitrogen emissions by more than 50 percent. Significant advancements in current gas turbine engines and engine components, such as seals, are required to meet these goals. Specifically, advanced seals have been identified as critical in meeting engine goals for specific fuel consumption, thrust-to-weight ratio, emissions, durability, and operating costs. In a direct effort to address and make progress toward these goals, researchers at the NASA Glenn Research Center have developed a unique high-temperature, high-speed engine seal test rig to evaluate seals under the temperature, speed, and pressure conditions anticipated for next-generation turbine engines. Newly installed, this seal test rig has capabilities beyond those of any existing seal rigs. It can test air seals (i.e., labyrinth, brush, and new seal concepts) at temperatures of up to 1500 °F and pressures up to 100 psid (even higher pressures are possible at lower temperatures), and at all surface speeds anticipated in future NASA (Ultra-Efficient Engine Technology, UEET) and

Integrated High-Performance Turbine Engine Technology (IHPTET) engine programs. In addition, seals can be tested offset from the rotor centerline, in the rotor runout condition,¹ and with simulated mission profiles. Support for this new rig was provided by Glenn, the U.S. Air Force, and the U.S. Army.

For more information about turbine seal work at Glenn, please visit the following web pages:

Glenn's Mechanical Components Branch: <http://www.grc.nasa.gov/WWW/5900/5950/>

¹With the rotor outer diameter eccentric to the rotor inner diameter.

Glenn's Turbine Seal Branch:

<http://www.grc.nasa.gov/WWW/TurbineSeal/TurbineSeal.html>

Bibliography

Steinetz, Bruce M.; Hendricks, Robert C.; and Munson, John: Advanced Seal Technology Role in Meeting Next Generation Turbine Engine Goals. NASA/TM-1998-206961, 1998. <http://gltrs.grc.nasa.gov/GLTRS>

Glenn/U.S. Army Research Laboratory contact:

Irebert R. Delgado, 216-433-3935, Irebert.R.Delgado@grc.nasa.gov

Glenn contact:

Margaret P. Proctor, 216-977-7526, Margaret.P.Proctor@grc.nasa.gov

Author: Irebert R. Delgado

Headquarters program office: OAT

Programs/Projects:

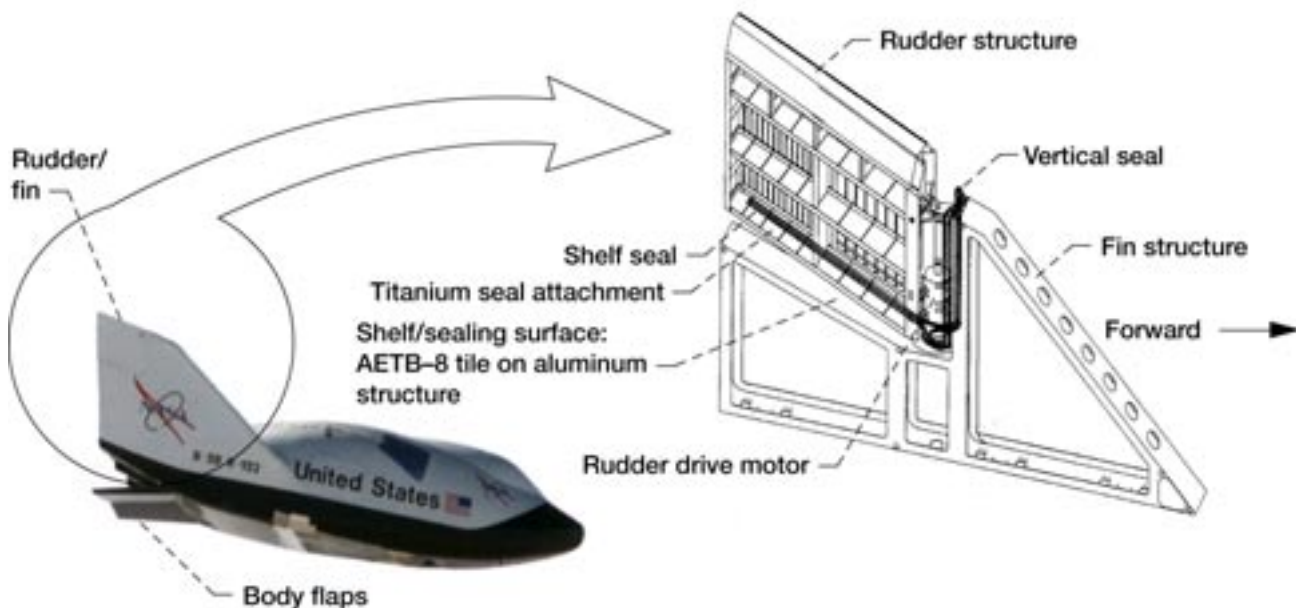
UEET, TCT, IHPTET, HITEMP, HSR, FQE

Rudder/Fin Seals Investigated for the X-38 Re-Entry Vehicle

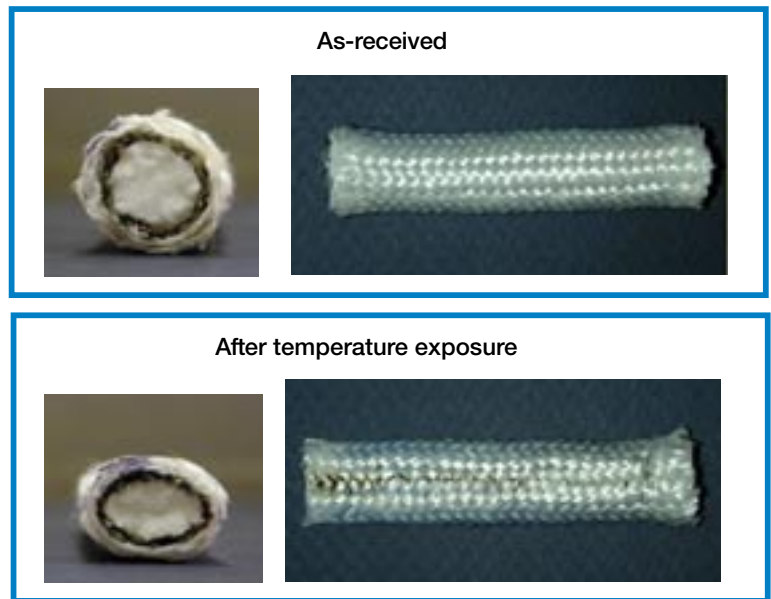
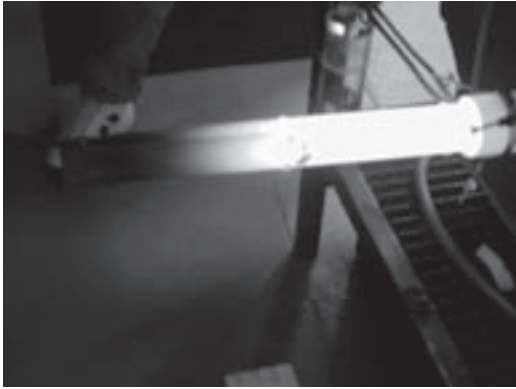
NASA is currently developing the X-38 vehicle that will demonstrate the technologies required for a crew return vehicle for the International Space Station. This vehicle will serve both as an ambulance for medical emergencies and as an evacuation vehicle for the manned space station. Control surfaces on the X-38 require high-temperature seals to limit hot gas ingestion and transfer of heat to underlying low-temperature structures to prevent these structures from becoming too hot and possibly causing the loss of the vehicle. Working with the NASA Johnson Space Center, the Seals Team at the NASA Glenn Research Center completed a series of tests to characterize baseline seal designs for the rudder/fin interfaces of the X-38. The structure of the rudder/fin assembly and its associated seals are shown in the following illustration.

A thermal analysis done by Johnson on the rudder/fin seal assembly predicted peak seal temperatures of 1900 °F during re-entry of the X-38

vehicle. On the basis of this analysis, Glenn conducted temperature exposure tests on the baseline seal design to simulate exposure of the seals to these extreme temperatures and to determine the effects that this exposure has on the seals. Specimens were placed into a tube furnace in a compressed state and heated at 1900 °F for 7 min (see the figure on the left, facing page). Examination of the seals after temperature exposure revealed that they took on a permanent set and lost resiliency, becoming stiffer and



X-38 rudder/fin seal assembly with rudder/fin structure and seal locations. (AETB-8 is the shuttle tile material.)



Left: Temperature exposure of X-38 seals at 1900 °F. Right: Seals before and after 1900 °F temperature exposure.

less flexible. Although this is not a concern for single-use X-38 seals, it is a concern for future reusable re-entry vehicles. The permanent set of the seals after temperature exposure is shown in the figure on the right.

Glenn performed room-temperature compression tests to determine load versus linear compression, unit loads, contact areas, stiffness, and resiliency characteristics for as-received and temperature-exposed seals. The temperature-exposed seals were stiffer and less resilient than the as-received seals, but the measured unit loads and contact pressures for both conditions were below the limits that Johnson had set as goals for the seals. In the rudder/fin seal location, the seals are in contact with shuttle thermal tiles and are moved across the tiles as the rudder is rotated during re-entry. Low seal unit loads and contact pressures are required to limit the loads on these tiles and minimize any damage that the seals could cause.

Flow tests were conducted on the seals under ambient temperatures to examine their leakage characteristics at different compression levels and gap sizes in both the as-received condition and after temperature exposure. Glenn measured seal flow rates 4.5 times higher than Johnson's preliminary flow goal. On the basis of this finding, Glenn recommended that more detailed thermal analyses be run to account for flow through the seals and to reassess the maximum seal temperatures. Johnson subsequently performed additional analyses that showed that the higher leakage flow would not cause a significant increase in seal temperatures.

Glenn's tests have identified several areas where the X-38 seals have met Johnson's goals and other areas where future work should be completed to ensure that the proper final seal selection is made. Glenn and Johnson are currently defining what additional work needs to be done to develop the final rudder/fin seal design for the X-38 vehicle.

Find out more about this work:

Structural seals and thermal barriers:
<http://www.grc.nasa.gov/WWW/structuralseal/>

High-temperature, flexible, fiber preform seal:
http://www.grc.nasa.gov/WWW/TU/InventYr/1996Inv_Yr.htm

Glenn's Mechanical Components Branch: <http://www.grc.nasa.gov/www/5900/5950/>

Bibliography

Dunlap, Patrick H., Jr.; Steinetz, Bruce M.; and Curry, Donald M.: Rudder/Fin Seal Investigations for the X-38 Re-Entry Vehicle. NASA/TM-2000-210338/REV1 (AIAA Paper 2000-3508), 2000. <http://www.grc.nasa.gov/WWW/structuralseal/papers/TM-2000-210338.pdf> and <http://gltrs.grc.nasa.gov/GLTRS>

Glenn contacts:

Patrick H. Dunlap, Jr., 216-433-6374, Patrick.H.Dunlap@grc.nasa.gov; and Dr. Bruce M. Steinetz, 216-433-3302, Bruce.M.Steinetz@grc.nasa.gov

Authors: Patrick H. Dunlap, Jr. and Dr. Bruce M. Steinetz

Headquarters program office: OAT
Programs/Projects: X-38

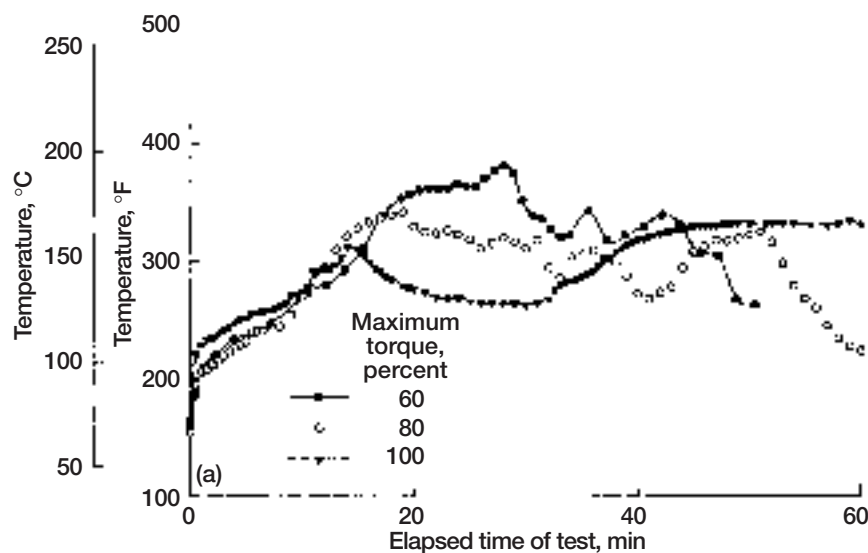
Vapor/Mist Used to Lubricate Gears After Loss of Primary Lubrication System

Loss of lubrication in rotorcraft drive systems is a demanding requirement placed on drive system manufacturers. The drive system must operate for at least 30 minutes once the primary lubrication system has failed. This test is a military requirement that must be passed prior to certification of the aircraft. As new aircraft engines, operating at higher speeds, are fielded, the

requirements for the drive system become increasingly more difficult. Also, the drive system must be lightweight, which minimizes the opportunity to use the gear bodies to absorb the tremendous amount of heating that takes place. In many cases, the amount of heat generated because of the high speed and load requires an emergency lubrication system that negatively impacts the aircraft's weight, complexity, and cost.

A single mesh spur gear test rig is being used at the NASA Glenn Research Center to investigate possible emergency lubrication system improvements that will minimize the impact of having these systems onboard rotorcraft. A technique currently being investigated uses a vapor/mist system to lubricate the contacting surfaces after the primary lubrication system has been shut down. A number of tests were conducted in which the vapor/mist used the same lubricant as the primary system, but at a greatly reduced flow rate. Each test was initiated with the primary lubrication system operational and at steady-state conditions for a given speed and load. Then the primary lubrication system was shut down, and the vapor/mist lubrication system was initiated. An example of the tests conducted is shown in the figures.

These preliminary tests have uncovered a mechanism that provides a lubricious, carbonaceous solid on the surface that actually reduces the surface temperature of the meshing gear teeth during operation. Surface analysis of the carbonaceous solid revealed it was graphitic. This mechanism is the synthetic lubricant "coking" on the



Top: Effect of load on mist-fed lubrication after primary lubrication was terminated. Tests conducted at 10,000 rpm; pitch line velocity, 46.6 m/sec (152.7 ft/min).
Bottom: Posttest photograph after primary lubrication terminated and gear was mist lubricated.

active profile of the gears, which reduces the friction between the contacting gear surfaces. The level of load affects the onset of this mechanism: the higher the load, the sooner coking takes place. Future work will investigate several other factors that could improve the already promising results that have been attained.

Find out more about this research: <http://www.grc.nasa.gov/WWW/5900/5950>

Bibliography

Morales, Wilfredo; and Handschuh, Robert F.: A Preliminary Study on the Vapor/Mist Phase Lubrication of a Spur Gearbox. NASA/TM—1999-208833 (Also ARL-TR-1912), 1999. <http://gltrs.grc.nasa.gov/GLTRS>

Handschuh, Robert F.; and Morales, Wilfredo: Lubrication System Failure Baseline Testing on an Aerospace Quality Gear Mesh. NASA/TM—2000-209954 (Also ARL-TR-2214), 2000. <http://gltrs.grc.nasa.gov/GLTRS>

Glenn/U.S. Army Research Laboratory

contacts: Dr. Robert F. Handschuh, 216-433-3969, Robert.F.Handschuh@grc.nasa.gov; and Dr. Wilfredo Morales, 216-433-6052, Wilfredo.Morales@grc.nasa.gov

Authors: Dr. Robert F. Handschuh and Dr. Wilfredo Morales

Headquarters program office: OAT

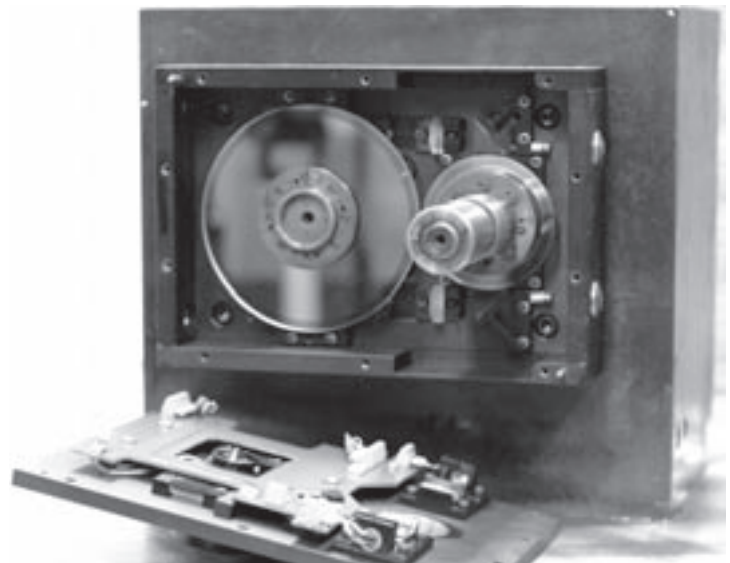
Programs/Projects: Rotorcraft Base Program, Propulsion Systems R&T, NASA Ames Rotorcraft Program

New Gear Transmission Error Measurement System Designed

The prime source of vibration and noise in a gear system is the transmission error between the meshing gears. Transmission error is caused by manufacturing inaccuracy, mounting errors, and elastic deflections under load. Gear designers often attempt to compensate for transmission error by modifying gear teeth. This is done traditionally by a rough "rule of thumb" or more recently under the guidance of an analytical code. In order for a designer to have confidence in a code, the code must be validated through experiment.

NASA Glenn Research Center contracted with the Design Unit of the University of Newcastle in England for a system to measure the transmission error of spur and helical test gears in the NASA Gear Noise Rig. The new system measures transmission error optically by means of light beams directed by lenses and prisms through gratings mounted on the gear shafts. The amount of light that passes through both gratings is directly proportional to the transmission error of the gears. A photodetector circuit converts the light to an analog electrical signal.

To increase accuracy and reduce "noise" due to transverse vibration, there are parallel light paths at the top and bottom of the gears. The two signals are subtracted via differential amplifiers in the electronics package. The output of the system is 40 mV/ μm , giving a resolution in the time domain of better than 0.1 μm , and discrimination in the frequency domain of better than 0.01 μm .



Optical and electronic components of the new transmission error measurement system. Note the reflections in the two mirrorlike gratings. The sizes of the gratings are proportional to the size of the gears, which have a 1.8:1 ratio.

The new system will be used to validate gear analytical codes and to investigate mechanisms that produce vibration and noise in parallel axis gears.

Bibliography

Oswald, Fred B.; and Townsend, Dennis P.: Influence of Tooth Profile Modification on Spur Gear Dynamic Tooth Strain. NASA TM-106952 (ARL-TR-778 and AIAA Paper 95-3050), 1995. <http://gltrs.grc.nasa.gov/GLTRS>

Atkins, I.; Hofmann, D.A.; and Haigh, J.: The Ultra Low Noise Gearbox. Marine Engineering Challenges for the 21st Century, INEC 2000, 2000.

Find out more from Glenn's Mechanical Components Branch:

<http://www.grc.nasa.gov/WWW/5900/5950>

Glenn contact:

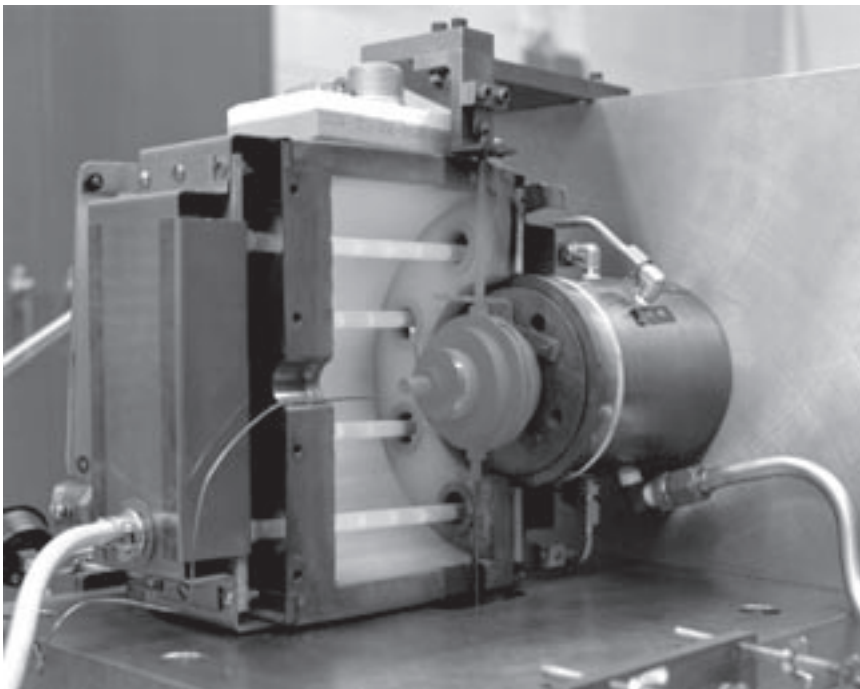
Fred B. Oswald, 216-433-3957,
Fred.Oswald@grc.nasa.gov

Author: Fred B. Oswald

Headquarters program office: OAT

Programs/Projects: Rotorcraft SILNT

Oil-Free Turbomachinery Being Developed



High-speed Oil-Free foil air bearing operating red-hot with PS304 solid lubricant coating (test rig cover removed for photograph).

NASA and the Army Research Laboratory (ARL) along with industry and university researchers, are developing Oil-Free technology that will have a revolutionary impact on turbomachinery systems used in commercial and military applications. System studies have shown that eliminating an engine's oil system can yield significant savings in weight, maintenance, and operational costs. The Oil-Free technology (foil air bearings, high-temperature coatings, and advanced modeling) is being developed to eliminate the need for oil lubrication systems on high-speed turbomachinery such as turbochargers and gas turbine engines that are used in aircraft propulsion systems. The Oil-Free technology is enabled by recent breakthroughs in foil bearing load capacity, solid lubricant coatings, and computer-based analytical modeling. During the past fiscal year, a U.S. patent was awarded for the NASA PS300 solid lubricant coating, which was developed at the NASA Glenn Research Center. PS300 has enabled the successful operation of foil air bearings to temperatures over 650 °C and

has resulted in wear lives in excess of 100,000 start/stop cycles. This leapfrog improvement in performance over conventional solid lubricants (limited to 300 °C) creates new application opportunities for high-speed, high-temperature Oil-Free gas turbine engines. On the basis of this breakthrough coating technology and the world's first successful demonstration of an Oil-Free turbocharger in fiscal year 1999, industry is partnering with NASA on a 3-year project to demonstrate a small, Oil-Free turbofan engine for aeropropulsion.

Bibliography

DellaCorte, C., et al.: Performance and Durability of High Temperature Foil Air Bearings for Oil-Free Turbomachinery. NASA/TM-2000-209187/REV1 (Also ARL-TR-2202), 2000. <http://gltrs.grc.nasa.gov/GLTRS>

DellaCorte, Christopher.; and Edmonds, Brian J.: PS300, Self-Lubricating, Readily Polished High Temperature Composite Coating. U.S. Patent 5,866,518, Dec. 1999.

Glenn contact: Dr. Christopher DellaCorte, 216-433-6056,
Christopher.Dellacorte@grc.nasa.gov

Authors: Dr. Christopher DellaCorte and Dr. Mark J. Valco

Headquarters program office: OAT

Programs/Projects: Base R&T

Special recognition:

A patent was awarded for NAS PS300 (U.S. Patent 5,866,518).



2, (Space) 0

Space Communications

Phased-Array Satcom Antennas Developed for Aeronautical Applications

The Advanced Communications (AC) for Aeronautics research at the NASA Glenn Research Center integrates both aeronautics and space communications technologies to achieve the national objective of upgrading the present National Airspace System infrastructure by responding to the agency's aviation capacity and safety goals. One concept for future air traffic management, free flight, presents a significantly increased demand for communications systems capacity and performance in comparison to current air traffic management practices. Current aeronautical communications systems are incapable of supporting the anticipated demands, and the new digital data communications links that are being developed, or are in the early stages of implementation, are not primarily designed to carry the data-intensive free flight air traffic management (ATM) communications loads. Emerging satellite communications technologies are the best potential long-term solution to provide the capacity and performance necessary to enable a mature free flight concept to be deployed.

NASA AC/ATM funded the development of a Boeing-designed Ku-band transmit phased-array antenna, a combined in-house and contract effort. Glenn designed and integrated an Aeronautical Mobile Satellite Communications terminal based on the transmit phased-array antenna and a companion receive phased-array antenna previously developed by Boeing.

One such advanced satellite communications concept that has the potential to provide a significant increase in aeronautical communications system capacity and performance is the Ku-band phased-array antenna. In a development effort jointly funded and carried out by Glenn and Boeing, a broadband (active) antenna that can transmit at 256 kbps was developed. NASA Glenn then successfully integrated the transmit phased-array antenna and a companion receive phased-array antenna previously developed by Boeing into a mobile testbed. In preliminary demonstrations, the transmit and receive portions of the terminal were shown to function successfully, and basic antenna pointing and tracking and modem performance were verified. Successful demonstration of both transmit and receive antennas is the first step in fusing the technologies needed to support a fully digital data-based integrated communications network, including satellite and ground-based communication links, as contrasted with the primarily analog voice transmit environment of the current environment. This technology promises a 100-fold improvement in communications capability to and from a transport aircraft.

Some of the many advantages offered by these Ku-band antennas are electronic steering, which requires no moving mechanical parts, higher reliability, and a high bandwidth capability. In addition, the flat, conformal

mechanical design yields a lower profile, reducing drag and increasing fuel savings. On a systems level, Ku-band phased-array antennas will reduce overall costs because of their lower recurring manufacturing costs. And finally, the Ku-band antenna offers a multiple, independent-beam capability; one antenna can operate with multiple satellites. From a commercial standpoint, the NASA-supported development of the transmit antenna has enabled Boeing to conceive, develop, and market an entirely new business, called Connexion by Boeing, which is the first two-way broadband communication link to commercial aircraft.

Glenn contacts:

Robert J. Kerczewski, 216-433-3434,
Robert.J.Kerczewski@grc.nasa.gov;
Konstantinos S. Martzaklis,
216-433-8966,
Konstantinos.S.Martzaklis@grc.nasa.gov;
and Michael J. Zernic, 216-433-5286,
Michael.J.Zernic@grc.nasa.gov

Author: Robert J. Kerczewski

Headquarters program office: OAT

Programs/Projects:

ARC, AvSP (NASA Langley), AC/ATM (NASA Glenn), AATT, Aviation System Capacity, WINCOMM (NASA Glenn), WxAP, AvSP

Status of the Direct Data Distribution (D³) Experiment

NASA Glenn Research Center's Direct Data Distribution (D³) project will demonstrate an advanced, high-performance communications system that transmits information from an advanced technology payload carried by a NASA spacecraft in low Earth orbit (LEO) to a small receiving terminal on Earth. The space-based communications package will utilize a solid-state, K-band phased-array antenna that electronically steers the radiated energy beam toward a low-cost, tracking ground terminal, thereby providing agile, vibration-free, electronic steering at reduced size and weight with increased reliability. The array-based link will also demonstrate new digital processing technology that will allow the transmission of substantially increased amounts of latency-tolerant data collected from the LEO spacecraft directly to NASA field centers, principal investigators, or into the commercial terrestrial communications network. The technologies demonstrated by D³ will facilitate NASA's transition from using Government-owned communication assets to using commercial communication services.



Flight mockup of the Direct Data Distribution (D³) experiment in a GSFC Hitchhiker-G Canister.

The hardware for D³ will incorporate advanced technology components developed under the High Rate Data Delivery (HRDD) Thrust Area of NASA's Office of Aerospace Technology Space Base Program at Glenn's Communications Technology Division. The flight segment components will include the electrically steerable phased-array antenna, which is being built by the Raytheon System Corporation and utilizes monolithic microwave integrated circuit (MMIC) technology operating at 19.05 GHz; and the digital encoder/modulator chipset, which uses four-channel orthogonal frequency division multiplexing (OFDM). The encoder/modulator will use a chipset developed by SICOM, Inc., which is both bandwidth and power efficient. The ground segment components will include a low-cost, open-loop tracking ground terminal incorporating a cryoreceiver to minimize terminal size without compromising receiver capability. The project is planning to hold a critical design review in the second quarter of fiscal year 2002.

D³ is a work area under the Advanced Communications campaign within the Space Operations Technology Project of NASA Johnson Space Center's Space Operations Management Office.

In fiscal year 2000, the D³ team, composed of both civil servants and ZIN Technology contractor personnel, completed several major activities. The prototype version of the OFDM modulator board was completed and is currently being tested by Communications Technology Division personnel. The thermal and structural designs of the flight payload were completed based on the NASA Goddard Space Flight Center

Hitchhiker-G carrier. A flight mockup, shown in the figure, was fabricated and assembled to aid in the internal layout of the D³ avionics. The team successfully completed the optical proof-of-concept testing of various LEO spacecraft. This test focused on open-loop tracking of LEO spacecraft based on position information derived from simple two-line orbital element sets downloaded from the Internet. An inexpensive optical tracking pedestal was procured for the test, and various LEO spacecraft (including the shuttles and the International Space Station) were successfully tracked during their overhead passes from locations in northeast Ohio.

Glenn contact:

Lawrence W. Wald, 216-433-5219,
Lawrence.W.Wald@grc.nasa.gov

Author: Lawrence W. Wald

Headquarters program office: OSF

Programs/Projects:

HEDS, SOMO (NASA Johnson), Earth
Science, Space Science

Aeronautical-Satellite-Assisted Process Being Developed for Information Exchange Through Network Technologies (Aero-SAPIENT)

Communications technologies are being developed to address safety issues during aviation travel. Some of these technologies enable the aircraft to be in constant bidirectional communications with necessary systems, people, and other aircraft that are not currently in place today. Networking technologies, wireless datalinks, and advanced avionics techniques are areas of particular importance that the NASA Glenn Research Center has contributed.

Glenn, in conjunction with the NASA Ames Research Center, NASA Dryden Flight Research Center, and NASA Langley Research Center, is investigating methods and applications that would utilize these communications technologies. In mid-June 2000, the flight readiness of the network and communications technologies were demonstrated via a simulated aircraft. A van simulating an aircraft was equipped with advanced phased-array antennas (Advanced Communications/Air Traffic Management (AC/ATM) Advanced Air Transportation Technologies (AATT) project) that used com-

mercial Ku-band satellite communications to connect Glenn, Dryden, and Ames in a combined system ground test. This test simulated air-ground bidirectional transport of real-time digital audio, text, and video data via a hybrid network configuration that demonstrated the flight readiness of the network and communications technologies. Specifically, a Controller Pilot Data Link Communications application was used with other applications to demonstrate a multiprotocol capability via Internet-protocol encapsulated ATN (Aeronautical Telecommunications Network) data packets.



Glenn van simulating an aircraft in ground tests.

The significance of this combined ground test is its contribution to the Aero Information Technology Base Program Level I milestone (Software Technology investment area) of a real-time data link for the National Airspace System. The objective of this milestone was to address multiprotocol technology applicable for real-time data links between aircraft, a satellite, and the ground as well as the ability to distribute flight data with multilevel priorities among several sites.

The impact of this achievement contributes to the maturation of airborne networking for safety-critical and noncritical data, the reduction in redundant data links, and enhanced information integrity for safety.

Also, with the support of the Glenn Director's Discretionary Fund program and continued collaboration with the Army Research Lab and Embry Riddle University, progress was made in the applicability of silicon carbide to avionics. During fiscal year 2000, optimized silicon carbide mixer diodes were fabricated and packaged in preparation for benchmark testing. Also, a patent was issued for Wide Dynamic Range RF (radiofrequency) Mixers Using Wide Band-Gap Semiconductors (U.S. patent 6,111,452).

The significance of this material and design is the reduction of the RF receiver circuits' susceptibility to undesired interference. This interference reduction increases the communication link performance and the ability of pilots to navigate in poor weather. Furthermore, the rejection of intermodulation distortion products enables a wider dynamic range, more efficient performance of very high frequency (VHF) data links, and more efficient spectrum utilization.

The impact of its applicability to avionics will improve aviation safety by decreasing navigation instrument malfunctions and communication dropouts. Also, it may improve electronic device electromagnetic compatibility (e.g., the use of personal portable electronics during air travel).

Plans are in place to perform an initial flight test in fiscal year 2001 of the communication and network technologies used in the June 2000 ground test. The aircraft to be used is Dryden's DC-8, which routinely conducts airborne science missions. Therefore, this progress to enable bidirectional transport of real-time digital audio, text, and video data will not only benefit improvements within the National Airspace System but NASA science missions as well.

Glenn contact:

Michael J. Zernic, 216-433-5286,
Michael.J.Zernic@grc.nasa.gov

Author: Michael J. Zernic

Headquarters program office: OAT

Programs/Projects: IT Base,
Aero-SAPIENT, AvSP, AATT, AC/ATM

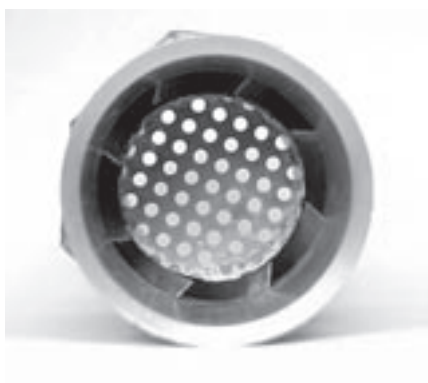
Microgravity Science

Technology Being Developed at Lawrence Berkeley National Laboratory: Ultra-Low-Emission Combustion Technologies for Heat and Power Generation

The Combustion Technologies Group at Lawrence Berkeley National Laboratory has developed simple, low-cost, yet robust combustion technologies that may change the fundamental design concept of burners for boilers and furnaces, and injectors for gas turbine combustors.

The new technologies utilize lean premixed combustion and could bring about significant pollution reductions from commercial and industrial combustion processes and may also improve efficiency.

The technologies are spinoffs of two fundamental research projects: (1) an inner-ring burner insert for lean flame stabilization developed for NASA-sponsored reduced-gravity combustion experiments and (2) a low-swirl burner developed for Department of Energy Basic Energy Sciences research on turbulent combustion.



LBNL low-NO_x burner showing 20-kW flame at 25 vol % excess air and 15-ppm NO_x (3 vol % O₂). Left: With ring stabilizer insert. Right: Without insert.

The ring stabilizer insert is a simple device. It is adaptable to many existing burner designs and enables them to maintain a steady ultralean premixed flame. The inner-ring insert is highly effective even under intense turbulence and produces complete combustion, but at the same time it lowers the emissions of oxides of nitrogen (NO_x) and carbon monoxide (CO). It has been tested in several interesting applications and produced very promising results. In a laboratory study, when ring inserts were fitted to a multiport burner of a domestic forced air-furnace, the resulting efficiency was increased and emissions were well below current air quality standards. A leading U.S. water heater manufacturer has tested ring stabilizer inserts in a product prototype and scaled its design to operate up to 200 kW.

Discovered in 1991, low-swirl flame stabilization is a novel combustion concept that is counter to conventional high-swirl methods. Low-swirl burners can burn premixed ultralean fuel/oxidizer mixtures. Two versions of the low-swirl burner have been developed. One uses very small air jets to generate low-swirl; the other uses a patented vane-swirler designed especially to produce the divergent flow pattern needed to sustain the flame.

The feasibility of using the low-swirl concept for larger heating and power-generating systems has been demonstrated. A low-swirl burner capable of operating beyond 1 MW recently tested in a research furnace showed the same low emissions (less than 10-ppm NO_x and 20-ppm CO) and high combustion efficiency. For gas turbines, a concept prototype of a low-swirl injector was successfully tested in a gas turbine manufacturer's facility. These tests have established the potential of using low-swirl devices for power generation. Lawrence Berkeley National Laboratory is seeking industrial partners for commercialization.

Discovery and development of our combustion technologies are prime examples of the fruits of basic research. Basic understanding of the operating principles of these technologies was the key to the successful scaling of the burners from 15 kW to over 1 MW and to designing injectors for testing in gas turbines.

To support the development of this technology for other pressurized combustion systems, Lawrence Berkeley National Laboratory is building a laboratory-scale facility to study lean, premixed combustion with high inlet pressures and temperatures.

Glenn contact:

Paul S. Greenberg, 216-433-3621,
Paul.S.Greenberg@grc.nasa.gov

Author: Robert K. Cheng

Headquarters program office: OBPR

Programs/Projects:

Microgravity Science

Microscale Particulate Classifiers (MiPAC) Being Developed

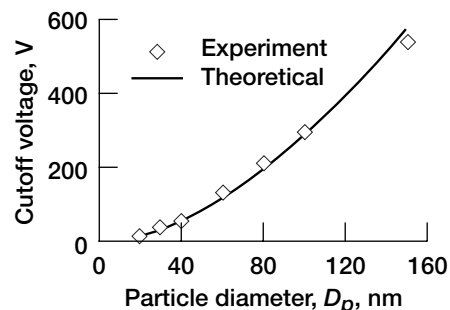
The NASA Glenn Research Center is developing microscale sensors to characterize atmospheric-borne particulates. The devices are fabricated using MEMS (microelectromechanical systems) technologies. These technologies are derived from those originally developed in support of the semiconductor processing industry. The resulting microsensors can characterize a wide range of particles and are, therefore, suitable to a broad range of applications.

This project is supported under a collaborative program called the Glenn Microsystems Initiative. The initiative comprises members of NASA Glenn Research Center, various university affiliates from the State of Ohio, and a number of participating industrial partners. Funding is jointly provided by NASA, the State of Ohio, and industrial members. The work described here is a collaborative arrangement between researchers at Glenn, the University of Minnesota, The National Institute of Standards and Technology (NIST), and the Cleveland State University. Actual device fabrication is conducted at Glenn and at the laboratories of Case Western Reserve University. Case Western is also located in Cleveland, Ohio, and is a participating member of the initiative. The principal investigator for this project is Paul S. Greenberg of Glenn.

Two basic types of devices are being developed, and target different ranges of particle sizes. The first class of devices, which is used to measure nanoparticles (i.e., particles in the range of 0.002 to 1 μm), is based on the technique of Electrical Mobility Classification. This technique also affords the valuable ability of measuring the electrical charge state of the particles. Such information is important in the understanding of agglomeration mechanisms and is useful in the development of methods for particle repulsion. The second type of device being developed, which utilizes optical scattering, is suitable for particles larger than 1 μm . This technique also provides information on particle shape and composition.

Applications for these sensors include fundamental planetary climatology, monitoring and filtration in spacecraft, human habitation modules and related systems, characterization of particulate emissions from propulsion and power systems, and as early warning sensors for both space-based and terrestrial fire detection. These devices are also suitable for characterizing biological compounds such as allergens, infectious agents, and biotoxic agents.

The project team recently demonstrated the performance of a prototype microscale electrical mobility classifier, which is intended for applications to particles as small as a few nanometers. Excellent agreement was observed between modeling calculations and the observed performance.



MiPAC cutoff voltage versus particle size. Flow rate, 203 cm^3/min .

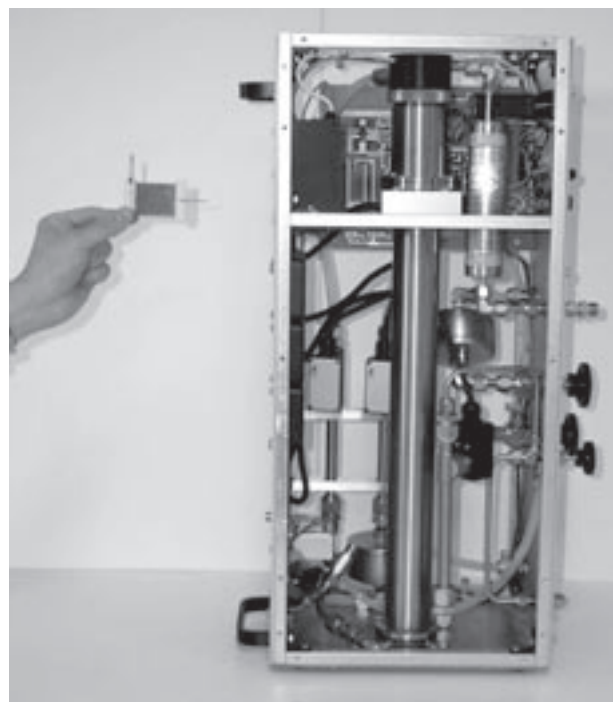
Glenn contact: Paul S. Greenberg,
216-433-3621,
Paul.S.Greenberg@grc.nasa.gov

Author: Paul S. Greenberg

Headquarters program office:
OSS, OAT

Programs/Projects:

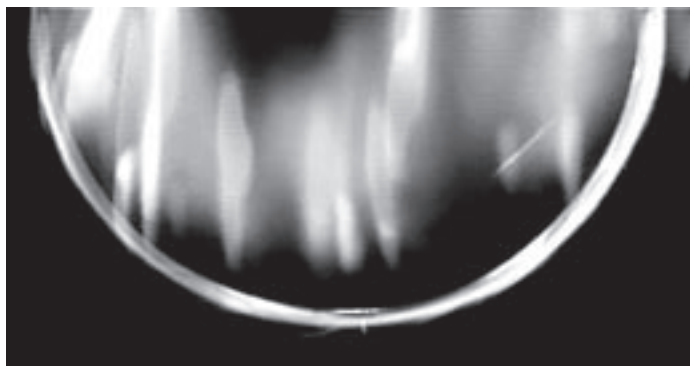
Microgravity Science, Aerospace
Propulsion, Mars Planetary Missions



Prototype microscale electrical mobility classifier shown with conventional macroscale device.

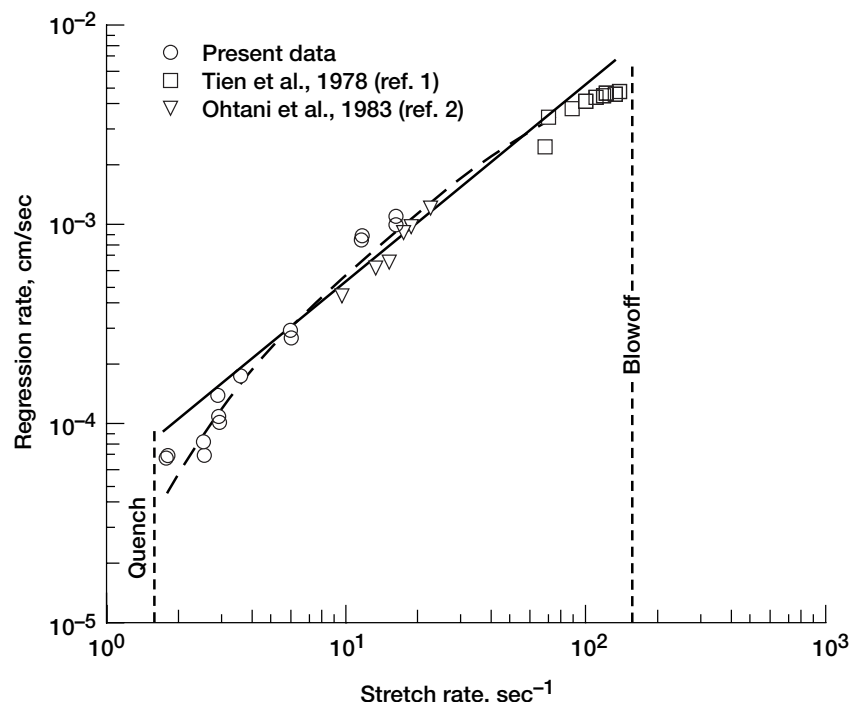
Ceiling Fires Studied to Simulate Low-Gravity Fires

A unique new way to study low-gravity flames in normal gravity has been developed. To study flame structure and extinction characteristics in low-stretch environments, a normal gravity low-stretch diffusion flame was generated using a cylindrical PMMA sample of varying large radii, as shown in the photograph. These experiments have demonstrated that low-gravity flame characteristics can be generated in normal gravity through the proper use of scaling. On the basis of this work, it is feasible to apply this concept toward the development of an Earth-bound method of evaluating material flammability in various gravitational environments from normal gravity to microgravity, including the effects of partial gravity low-stretch rates such as those found on the Moon (1/6g) or Mars (1/3g).



Burning of large-radius cylinder of polymethylmethacrylate (PMMA) under low stretch.

During these experiments, the surface regression rates for PMMA were measured for the first time over the full range of flammability in air, from blowoff at high stretch, to quenching at low stretch, as plotted in the graph. The solid line drawn through the central portion of the data ($3 < a < 100 \text{ sec}^{-1}$) has a slope of unity, which indicates regression is proportional to stretch. The figure coordinates assume that the values of stretch are equivalent, whether derived from forced stretch or from buoyant stretch. The excellent correlation of the regression-rate data over the two-order-of-magnitude variation of stretch shows the reasonableness of this assumption.



Regression rate data versus stretch rate over the range of flammability for PMMA in air.

At very low stretch, which is equivalent to reduced gravity, uniform flame burning was not achieved, starting at 3 sec^{-1} , where departure from the linear correlation occurs. Unstable flamelets are observed in this region. Similarly, the overall low stretch extinction limit is marked simply as a quench limit, which means that no type of flame was visible at these low stretch rates.

Find out more about this research:

<http://www.grc.nasa.gov/WWW/ERB/ce13b.htm>

References

1. Tien, J.S., et al.: Combustion and Extinction in the Stagnation-Point Boundary Layer of a Condensed Fuel. *Combustion and Flame*, vol. 33, 1978, pp. 55–68.
2. Ohtani, H.; Akita, K.; and Hirano, T.: An Analysis of Bottom Stagnation Region Combustion of Polymeric Material Pieces Under Natural Convection. *Combustion and Flame*, vol. 53, 1983, pp. 33–40.

Glenn contact:

Dr. Sandra L. Olson, 216–433–2859,
Sandra.L.Olson@grc.nasa.gov

Author: Dr. Sandra L. Olson

Headquarters program office: OBPR

Programs/Projects:

Microgravity Science

TIGER Burned Brightly in JAMIC

The Transition From Ignition to Flame Growth Under External Radiation in 3D (TIGER-3D) experiment, which is slated to fly aboard the International Space Station, conducted a series of highly successful tests in collaboration with the University of Hokkaido using Japan's 10-sec JAMIC drop tower. The tests were conducted to test engineering versions of advanced flight diagnostics such as an infrared camera for detailed surface temperature measurements and an infrared spectroscopic array for gas-phase species concentrations and temperatures based on detailed spectral emissions in the near infrared.

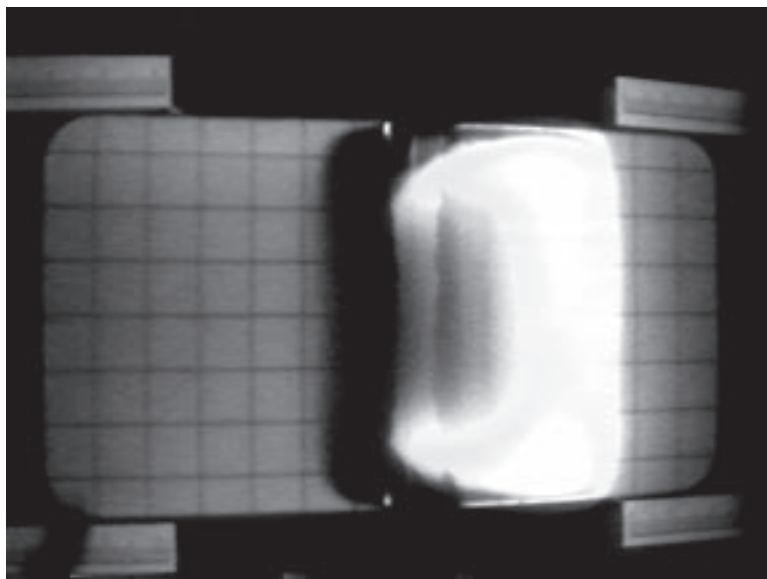
Shown in the top figure is a visible light image and in the bottom figure is an infrared image at $3.8\ \mu\text{m}$ obtained during the microgravity tests. The images show flames burning across cellulose samples against a slow wind of a few centimeters per second (wind is from right to left). These flow velocities are typical of spacecraft ventilation systems that provide fresh air for the astronauts. The samples are ignited across the center with a hot wire, and the flame is allowed to spread upwind and/or downwind. As these images show, the flames prefer to spread upwind, *into* the fresh air, which is the exact opposite of flames on Earth, which spread much faster downwind, or *with* the airflow, as in forest fires.

These experiments show that fire safety aboard spacecraft cannot be extrapolated from fire safety on Earth, and must be studied carefully to develop an accurate understanding of fire behavior under the conditions found aboard spacecraft.

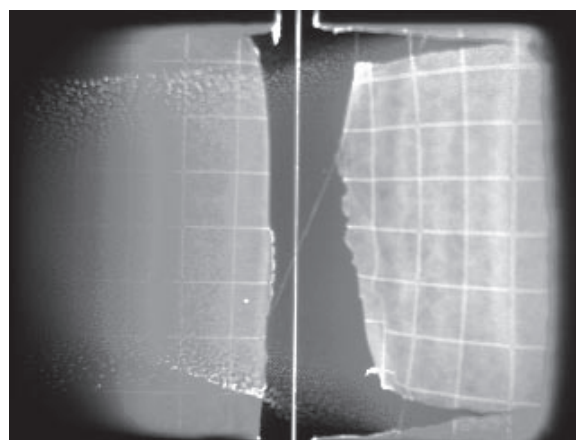
The fire safety strategy in a spacecraft is (1) to detect any fire as early as possible, (2) to keep any fire as small as possible, and (3) to extinguish any fire as quickly as possible. This suggests that a material that undergoes a momentary ignition but then extinguishes might be tolerable, but a material that permits a transition to flame spread would significantly increase the fire hazard in a spacecraft. If the transition does not take place, fire growth does not occur. Therefore, it is critical to understand what process controls the transition from ignition to subsequent flame spread both upstream and downstream. Furthermore, if the transition occurs, it is important to be able to predict subsequent flame growth from the ignited area. This would characterize the potential fire hazard by calculating the heat-release rate, which is one of the most important properties in expressing the size of a fire.

Find out more about this research:

<http://www.fire.nist.gov/bfrlpubs/fire99/PDF/f99126.pdf>



Visible image of flame spread over cellulose sheet. 1-cm-square grid pattern on sample.



Infrared image at $3.8\ \mu\text{m}$ of cellulose radiant heat loss as it pyrolyzes beneath the flame. Soot from the flame can be seen streaming from the flame zone as well. The igniter wire is in the center of the image.

Glenn contact:

Dr. Sandra Olson, 216-433-2859,
Sandra.L.Olson@grc.nasa.gov

Authors: Dr. Sandra L. Olson and
Dr. Takashi Kashiwagi

Headquarters program office: OBPR

Programs/Projects:
Microgravity Science

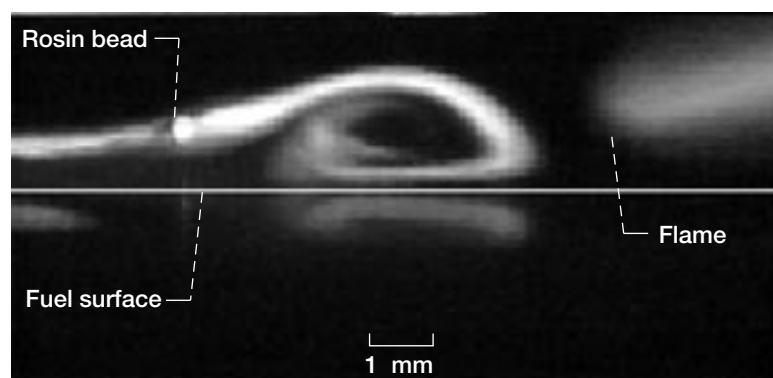
Spread Across Liquids Continues to Fly

The physics and behavior of a flame spreading across a flammable liquid is an active area of research at the NASA Glenn Research Center. Spills of fuels and other liquids often result in considerable fire hazards, and much remains unknown about the details of how a flame, once ignited, moves across a pool. The depth of the liquid or size of the spill, the temperature, and wind, if any, can all complicate the combustion processes. In addition, with the advent of the International Space Station there may be fire hazards associated with cleaning, laboratory, or other fluids in space, and it is essential to understand the role that gravity plays in such situations.

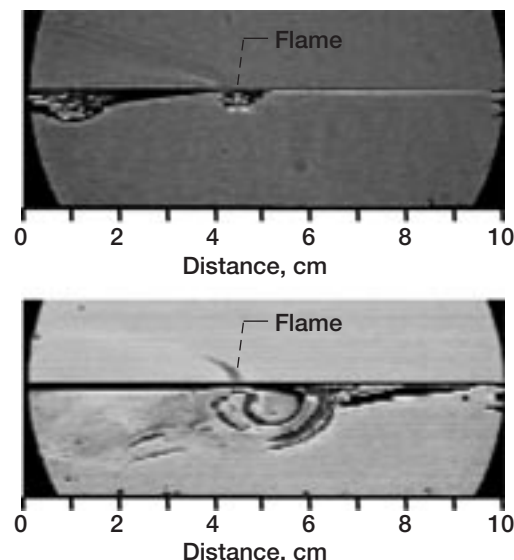
The Spread Across Liquids (SAL) experiment is an experimental and computational effort dedicated to understanding the detailed mechanisms of flame spread across a flammable liquid initially below its flashpoint temperature. The experimental research is being carried out in-house by a team of researchers from Glenn, the National Center for Microgravity Combustion, and Zin Technologies, with computer modeling being provided via a grant with the University of California, Irvine. Glenn's Zero Gravity Facility is used to achieve short microgravity periods, and normal gravity testing is done in the Space Experiments Laboratory. To achieve longer periods of microgravity, the showcase SAL hardware flies aboard a sounding rocket launched from White Sands Missile Range, New Mexico, approximately once per year. In addition to extended microgravity, this carrier allows the use of detailed diagnostics that cannot be employed in a drop tower.

SAL was first reported on in Glenn's 1995 Research & Technology report (ref. 1) when it was the first microgravity combustion experiment to have flown on a sounding rocket. Since that time, three more launches have been performed, with a fourth scheduled for December 2000.

As reported in 1995, a most surprising result was obtained when the flame spread slowly and steadily across the pools, as opposed to rapidly spread-

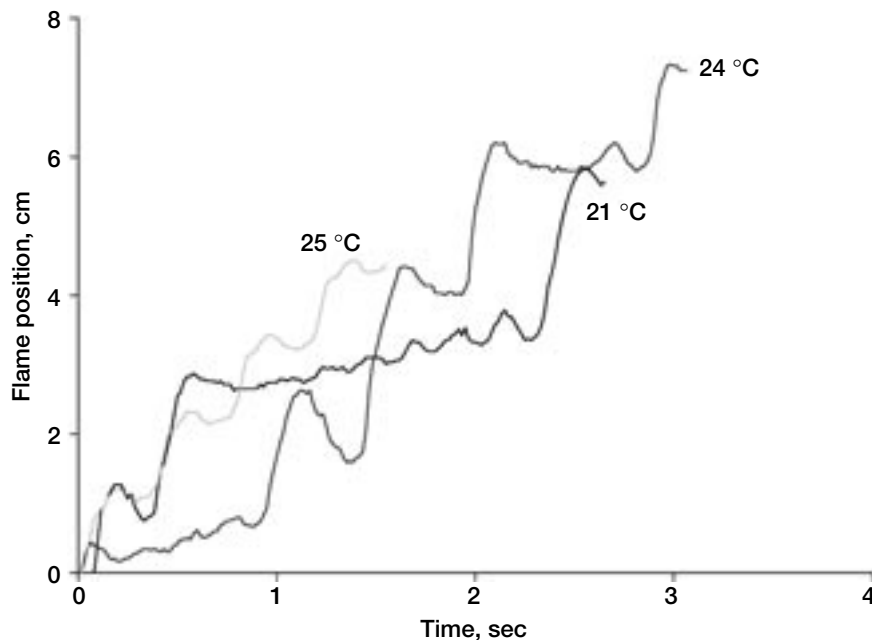


Side-view smoke visualization of the recirculation cell ahead of a flame spreading over 1-butanol. Flame is nearing the end of the crawl phase of the pulsation cycle. The smoke wire is perpendicular to the image at the location of the rosin bead. Note surface reflection.



Side view of subsurface temperature fields for a flame spreading across 1-butanol. Top: In 1g, the flame pulsates, and a new vortex forms each time it jumps. Bottom: In microgravity, the flame spreads steadily and slowly, and the vortex is much larger and travels with the flame.

ing and pulsating as it does in normal gravity. Since then, this result has been further confirmed at a variety of opposed airflow velocities, ranging from 5 to 30 cm/sec. At the lowest speeds, the flame initially spread slowly and then flashed and extinguished, whereas at the higher speeds steady, complete propagation was achieved. That the flame did not spread at opposed airflows of 5 cm/sec was regarded as unusual, since even solid materials support flame spread at much lower velocities, and take much more energy to pyrolyze. It is believed the difference may be due to a large vortex that forms in the liquid and carries heat deep into the pool. In normal gravity, this vortex is kept near the surface by buoyancy, but not so in microgravity. See the figures at the top of this page for a comparison. Using smoke tracers, a gas-phase recirculation cell that had been



Flame position versus time for three different liquid temperatures in a shallow tray (2 mm deep) in microgravity. Higher temperatures lead to more rapid flame pulsations and faster flame spread.

predicted approximately 30 years ago, but never realized, was finally visualized in both normal and microgravity (see the image at the bottom of the preceding page).

Ironically, the numerical model initially predicted that the flame would pulsate in microgravity. The experimental results dictated that the model needed to be revised, and changes to the diffusion coefficient and the addition of a heat-loss term finally brought the model and experiments into alignment. For the first time the model predicts the correct flame spread behavior regardless of gravitational level without the need to adjust chemical rate parameters. This will allow parametric runs to determine the effect of several variables that cannot all be tested in flight.

In fiscal year 2000, experiments in Glenn's Zero Gravity Facility focused on much shallower pools than used previously, 2 mm rather than 25 mm.

These are more realistic of a liquid spill, and have led for the first time to pulsating flame spread in microgravity (see the graph to the left). This indicates that buoyancy is not needed for the pulsation process. A new shallow tray filling system was designed, and the next flight of SAL will test both a deep tray at elevated temperature and a shallow tray.

Reference

1. Ross, Howard D.: Spread Across Liquids: The World's First Microgravity Combustion Experiment on a Sounding Rocket. 1995 Research & Technology. NASA TM-107111, 1996, pp. 137-138.
<http://www.grc.nasa.gov/WWW/RT1995/6000/6711r.htm>

Glenn contact:

Dr. Howard D. Ross, 216-433-2562,
Howard.D.Ross@grc.nasa.gov

National Center for Microgravity

Research contact:

Fletcher J. Miller, 216-433-8845,
FletcherJ.Miller@grc.nasa.gov

Author: Fletcher J. Miller

Headquarters program office: OBPR

Program/Projects:

Microgravity Science

Special recognition

Top 15 Microgravity Science Division Achievements 1983-1998; NASA Group Achievement Award, 1996.

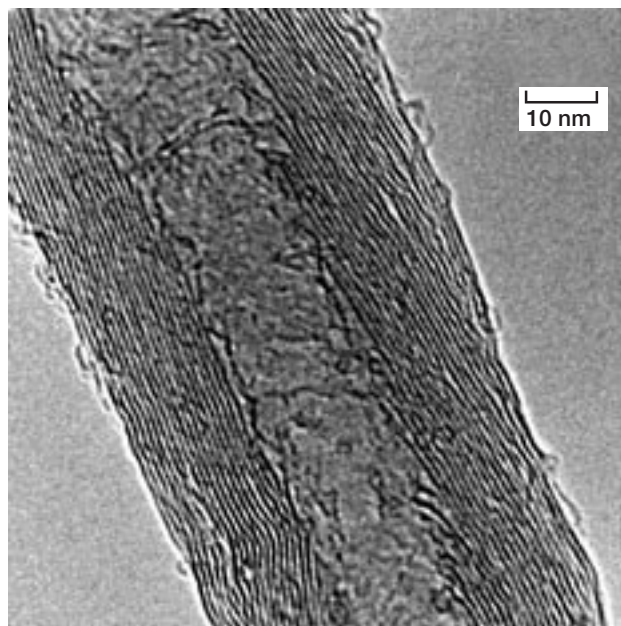
Flame Synthesis Used to Create Metal-Catalyzed Carbon Nanotubes

Metal-catalyzed carbon nanotubes are highly ordered carbon structures of nanoscale dimensions. They may be thought of as hollow cylinders whose walls are formed by single atomic layers of graphite. Such cylinders may be composed of many nested, concentric atomic layers of carbon or only a single layer, the latter forming a single-walled carbon nanotube. This article reports unique results using a flame for their synthesis.

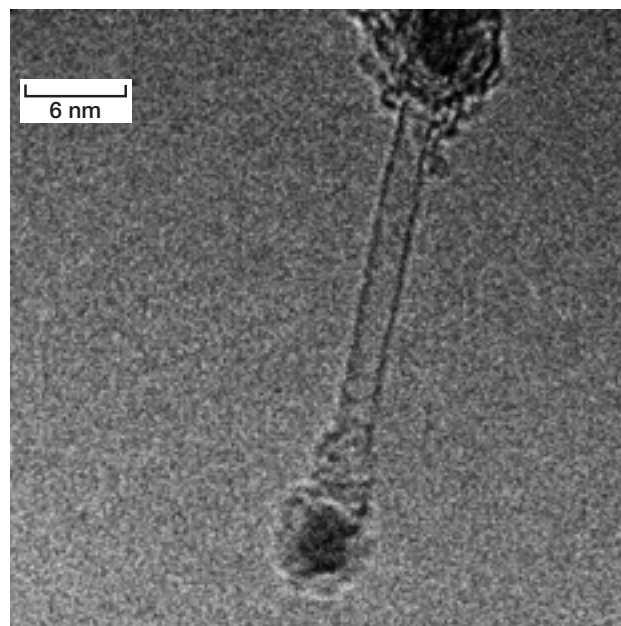
Only recently were carbon nanotubes discovered within an arc discharge and recognized as fullerene derivatives. Today metal-catalyzed carbon nanotubes are of great interest for many reasons. They can be used as supports for the metal catalysts like those found in catalytic converters. Open-ended nanotubes are highly desirable because they can be filled by other elements, metals or gases, for battery and fuel cell applications. Because of their highly crystalline structure, they are significantly stronger than the commercial carbon fibers that are currently available (10 times as strong as steel but possessing one-sixth of the weight). This property makes them highly desirable for strengthening polymer and ceramic composite materials.

Current methods of synthesizing carbon nanotubes include thermal pyrolysis of organometallics, laser ablation of metal targets within hydrocarbon atmospheres at high temperatures, and arc discharges. Each of these methods is costly, and it is unclear if they can be scaled for the commercial synthesis of carbon nanotubes. In contrast, flame synthesis is an economical means of bulk synthesis of a variety of aerosol materials such as carbon black. Flame synthesis of carbon nanotubes could potentially realize an economy of scale that would enable their use in common structural materials such as car-body panels.

The top figure is a transmission electron micrograph of a multiwalled carbon nanotube. The image shows a cross section of the atomic structure of the nanotube. The dark lines are individual atomic layer planes of carbon, seen here in cross section. They form a nested series of concentric cylinders, much like the growth rings on a tree. This sample was obtained by the supported catalyst method, whereby the nanoscale catalysts are dispersed on a substrate providing their support. The substrate with catalyst particles was immersed within an acetylene diffusion flame to which nitrogen had been added to eliminate soot formation. Upon removal from the flame, the nanotubes were dispersed on a holder suitable for electron microscopy. Although not seen in the figure, the tube diameter reflects that of the catalyst particle.



Cross section of a multiwalled carbon nanotube.



Single-walled carbon nanotube showing that a single atomic layer of graphite forms the hollow cylinder.

The bottom figure is a transmission electron micrograph of a single-walled carbon nanotube. Only a single graphite layer of carbon

(one layer plane of graphite) is rolled upon itself so as to form a seamless cylinder. The nanotube was obtained by sampling material from a flame using a probe that was rapidly inserted and retracted from the flame to minimize flame perturbations. In these experiments, catalyst particles were seeded into the flame by thermal decomposition of a suitable precursor compound. Upon reaching a suitable temperature within the flame, the catalyst particle initiated nanotube formation. Given buoyancy-induced convection, the total residence time for the catalyst particle within the flame environment is less than 1/10 of a second, limited by buoyancy-induced convection. Experiments conducted in a low-gravity environment will help us understand the limitations imposed by such short residence times upon nanotube growth and structure.

This work, awarded through NRA-98-HEDS-01, is funded by the Microgravity Science Division at NASA headquarters and is being performed

through a NASA cooperative agreement (NAC3-546) with The National Center for Microgravity Research monitored by the NASA Glenn Research Center.

Glenn contact: Dr. Randy L. Vander Wal, 216-433-9065, Randall.L.VanderWal@grc.nasa.gov

Author: Dr. Randy L. Vander Wal

Headquarters program office: OBPR

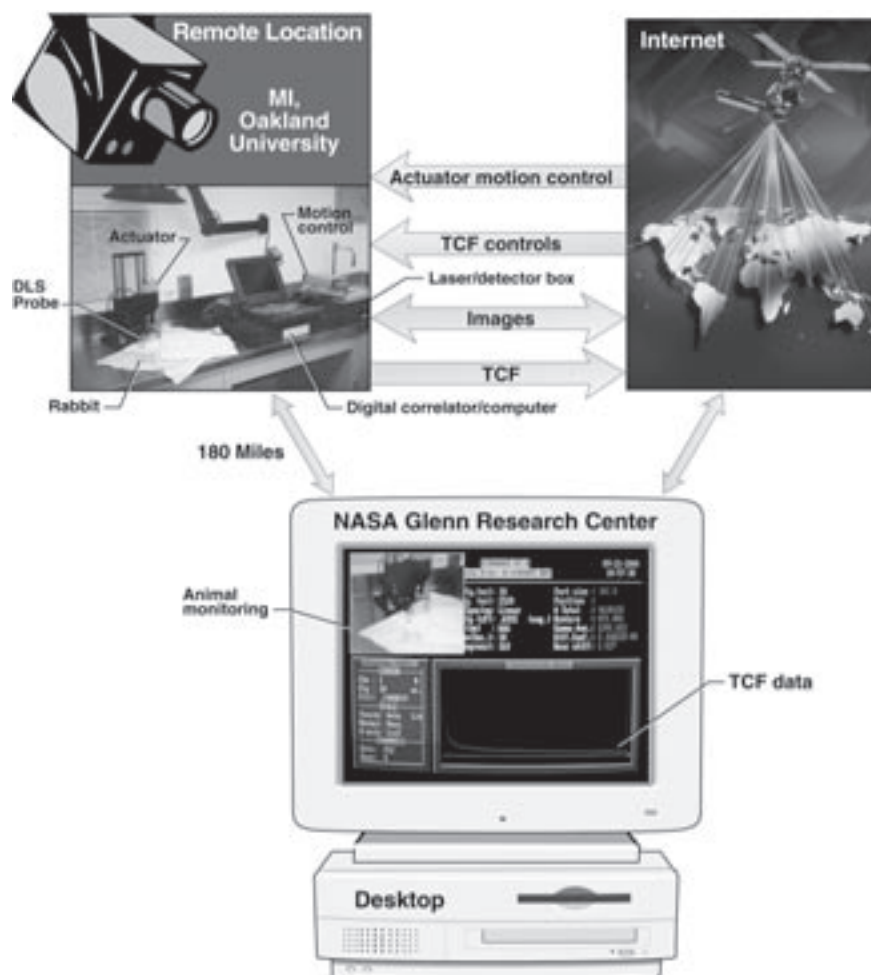
Programs/projects:
Microgravity Science

Applications in Bioastronautics and Bioinformatics: Early Radiation Cataracts Detected by Noninvasive, Quantitative, and Remote Means

Human exploration of Mars is a key goal in NASA's exploration planning in the next 20 years. Maintaining crew health and good vision is certainly an important aspect of achieving a successful mission. Continuous radiation exposure is a risk factor for radiation-induced cataracts in astronauts because radiation exposure in space travel has the potential of accelerating the aging process (ref. 1). A patented compact device (ref. 2) based on the technique of dynamic light scattering (DLS) was designed for monitoring an astronaut's ocular health during long-duration space travel. This capability of early diagnosis, unmatched by any other clinical technique in use today, may enable prompt initiation of preventive/curative therapy. An Internet web-based system integrating photon correlation data and controlling the hardware to monitor cataract development in vivo at a remote site in real time (teleophthalmology) is currently being developed. The new technology detects cataracts very early (at the molecular level). Cataract studies onboard the International Space Station will be helpful in quantifying any adverse effect of radiation to ocular health.

The normal lens in a human eye, situated behind the cornea, is a transparent tissue. It contains 35 wt % protein and 65 wt % water. Aging, disease (e.g., diabetes), smoking, dehydration, malnutrition, and exposure to ultraviolet light and ionizing radiation can cause agglomeration of the lens proteins. Protein aggregation can take place anywhere in the lens, causing

lens opacity. The aggregation and opacification could produce nuclear (central portion of the lens) or cortical (peripheral) cataracts. Nuclear and posterior subcapsular (the membrane's capsule surrounds the whole lens) cataracts, being on the visual optical axis of the eye, cause visual impairment that can finally lead to blindness. The lens proteins, in their native state, are small in size. As a cataract develops, this size grows from a few nanometers (transparent) to several micrometers (cloudy). Ansari and Datiles have shown that DLS can detect cataracts at least two to three orders of magnitude earlier noninvasively and quantitatively than the best imaging (Scheimpflug) techniques in clinical use today (ref. 3).



Bioinformatics system currently under development. TCF, time correlation function.

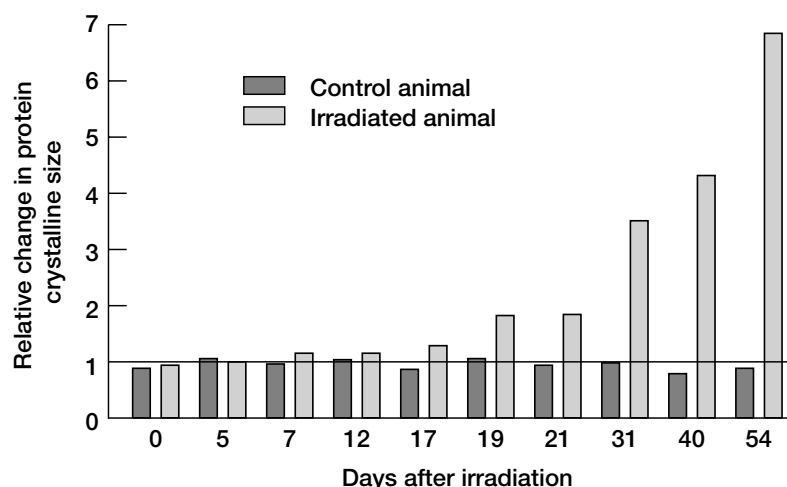
One important aspect of monitoring an astronaut's ocular health is the ability to collect data noninvasively, frequently, easily, and quickly, and to send it to Earth for examination by expert ophthalmologists in real time. Here on Earth such a device will make it easy to monitor human health in remote and underserved areas of the world (e.g., Polynesia, Africa, etc.) and to monitor defense personnel (naval ships, army battalions) at remote combat locations. As shown in the following figure, we are setting up a system in cyberspace to conduct DLS/cataract evaluation measurements. The system has two components. First, a digital camera, microphone/speaker, a fiber-optic probe equipped with actuators, detector, and a digital correlator are located at the testing site (an animal facility in this case). The output of the digital correlator and the camera is connected to an Internet site via the telephone lines. The second component consists of an operator at a desktop at another location (the NASA Glenn Research Center in this case) controlling the experiment and collecting data. The functional keys on the computer keypad are used to direct the fiber-optic probe at a desired location in the animal eye to collect data in 2 to 5 sec.

Recently, we conducted experiments to test our technology in collaboration with Dr. Frank Giblin at Oakland University in Michigan on his animal-radiation model. X-ray exposure accelerated the aging process. DLS can

detect radiation cataract much earlier noninvasively and quantitatively. Our approach provides good reproducibility and single endpoint measurements in terms of lens protein crystalline size. We see changes in the lens nucleus as early as 1 week after the radiation exposure. However, traditional methods still show the lens nucleus to be transparent until 9 to 10 weeks after the x-ray irradiation. The DLS method would be very useful to monitor early damage to ocular tissues in a space environment so that countermeasures could be taken. It can be a useful tool for guaranteeing astronauts' and cosmonauts' safety onboard the International Space Station, in transit to and from Mars, and during Mars exploration. A DLS-bioinformatics system presently under development has the potential to provide online monitoring of an astronaut's ocular health noninvasively, quantitatively, and remotely, perhaps beginning a new era of celestial teleophthalmology.

References

1. White, Ronald J.: Weightlessness and the Human Body. *Sci. Amer.*, vol. 279, no. 3, 1998, pp. 58-63.
2. Ansari, Rafat R., et al.: Fiber-Optic Imaging Probe Developed for Space Used to Detect Diabetes Through the Eye. 1999 Research & Technology. NASA/TM-2000-209639, 2000, pp. 143-145. <http://www.grc.nasa.gov/WWW/RT1999/6000/6712ansari.html>
3. Ansari, Rafat R.: Fiber Optic Imaging Probe. U.S. Patent 5,973,779, Mar. 1997.
4. Ansari, Rafat R.; Datiles, Manuel B.; and King, James F.: New Clinical Instrument for the Early Detection of Cataract Using Dynamic Light Scattering and Corneal Topography. *Proceedings of the Ophthalmic Technologies X*, vol. 3908, SPIE, Bellingham, WA, 2000, pp. 38-49.



Environmental ocular toxicity: effects of x-ray irradiation.

National Center for Microgravity Research contact:

Dr. Rafat R. Ansari, 216-433-5008,
Rafat.R.Ansari@grc.nasa.gov

Authors: Dr. Rafat R. Ansari, James F. King, and Frank J. Giblin

Headquarters program office: OBPR

Programs/Projects:
 Microgravity Science

Novel Shapes of Miscible Interfaces Observed

The dynamics of miscible displacements in a cylindrical tube are being investigated experimentally and numerically, with a view to understand the complex processes that occur, for example, in enhanced oil recovery, hydrology, and filtration (refs. 1 and 2). We have observed complex shapes of the interface between two liquids that mix with each other when the less viscous liquid is displaced by the more viscous one in a tube.

A less viscous fluid that displaces a more viscous fluid is known to propagate in the form of a "finger," and a flight experiment proposed by Maxworthy et al. (ref. 3) to investigate the miscible-interface dynamics is currently being developed by NASA.

From the current theory of miscible displacements, which was developed for a porous medium satisfying Darcy's law (see ref. 1), it can be shown that in the absence of gravity the interface between the fluids is destabilized and thus susceptible to fingering only when a more viscous fluid is displaced by a less viscous one. Therefore, if the interface is initially flat and the more viscous fluid displaces the less viscous fluid, the interface ought to be stable and remain flat. However, numerical simulations by Chen and Meiburg (ref. 4) for such displacement in a cylindrical tube show that the interface is unstable and a finger of the more viscous fluid is indeed formed.

Preliminary experiments performed at the NASA Glenn Research Center show that not only can fingering occur when the more viscous fluid displaces a less viscous one in a cylindrical tube, but also that under certain conditions the advancing finger achieves a sinuous or snakelike shape. These experiments were performed using silicone oils in a vertical pipette of small diameter. In the initial configuration, the more viscous fluid rested on top of the less viscous one, and the interface was nominally flat. A dye was added to the upper liquid for ease of observation of the interface



Formation of an axisymmetric finger; viscosity ratio, 2.

between the fluids. The flow was initiated by draining the lower fluid from the bottom of the pipette, at speeds less than 0.1 mm/sec.

When the upper fluid was twice as viscous as the lower fluid, an axisymmetric finger of the more viscous fluid was observed to form (see the figure on the preceding page). When the viscosity ratio was 10, the steady-state shape attained by the interface was not axisymmetric. Rather, the upper liquid had a sinuous shape as it flowed down the pipette (see the figure to the right).

This study is ongoing. We plan to modify our apparatus so that the more viscous fluid can be injected from either end of the tube. This will not only enable better control of the displacement in comparison to the draining technique we have used, but also ascertain the role played by buoyancy forces in the experiments. We plan to vary the viscosity ratio and the volumetric flow rate in the tube, while maintaining as small a density difference between the fluids as possible.

References

1. Homsy, G.M.: Viscous Fingering in Porous-Media. *Annu. Rev. Fluid Mech.*, vol. 19, 1987, pp. 271–311.
2. Petitjeans, P.; and Maxworthy, T.: Miscible Displacements in Capillary Tubes. 1—Experiments. *J. Fluid Mech.*, vol. 326, 1996, pp. 37–56.
3. Maxworthy, Tony; and Meiburg, Eckart: The Dynamics of Miscible Interfaces: A Space Flight Experiment. Science Requirements Document, First Draft, University of Southern California, Los Angeles, CA, Mar. 2000.
4. Chen, C.Y.; and Meiburg, E.: Miscible Displacements in Capillary Tubes. 2—Numerical Simulations. *J. Fluid Mech.*, vol. 326, 1996, pp. 57–90.

National Center for Microgravity Research contacts:

Dr. Ramaswamy Balasubramaniam, 216–433–2878,
Ramaswamy.Balasubramaniam@grc.nasa.gov; and
 Dr. Nasser Rashidnia, 216–433–3622, Nasser.Rashidnia@grc.nasa.gov

Authors: Dr. Ramaswamy Balasubramaniam and Dr. Nasser Rashidnia

Headquarters program office: OBPR

Programs/Projects: Microgravity Science



Sinuous shape of the interface; viscosity ratio, 10.

Gas-Liquid Two-Phase Flows Through Packed Bed Reactors in Microgravity

The simultaneous flow of gas and liquid through a fixed bed of particles occurs in many unit operations of interest to the designers of space-based as well as terrestrial equipment. Examples include separation columns, gas-liquid reactors, humidification, drying, extraction, and leaching. These operations are critical to a wide variety of industries such as petroleum, pharmaceutical, mining, biological, and chemical. NASA recognizes that similar operations will need to be performed in space and on planetary bodies such as Mars if we are to achieve our goals of human exploration and the development of space. The goal of this research is to understand how to apply our current understanding of two-phase fluid flow through fixed-bed reactors to zero- or partial-gravity environments.

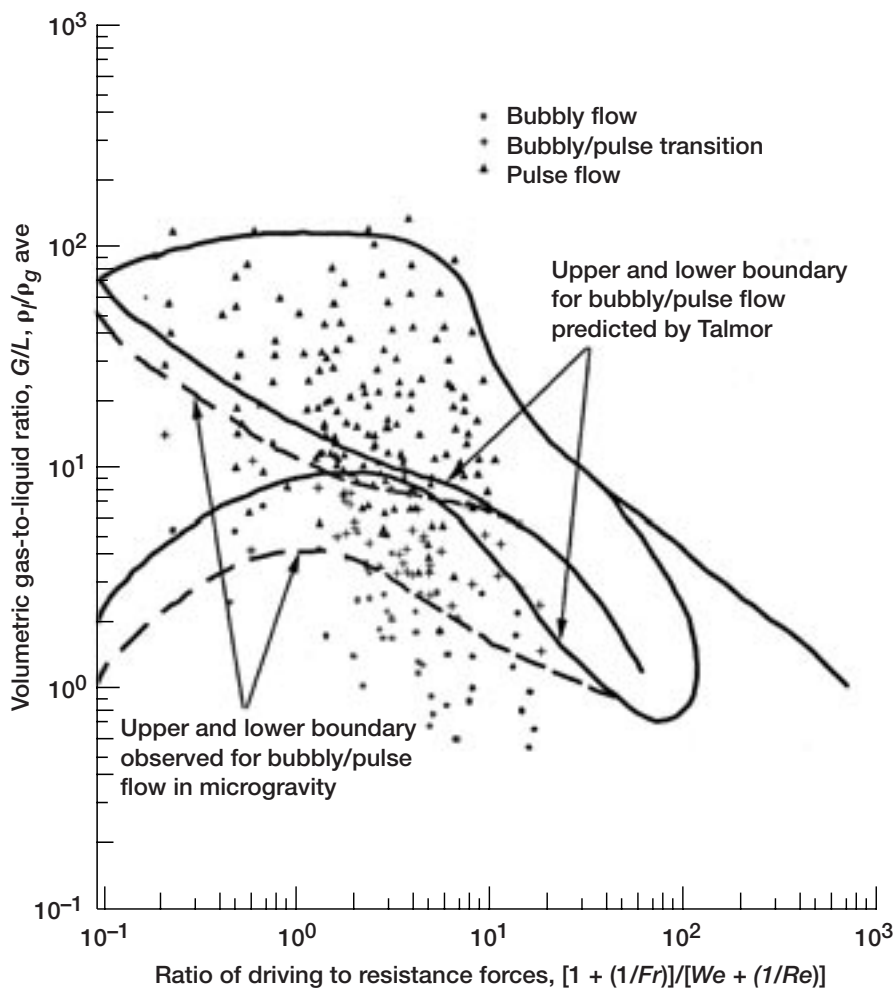
Previous experiments by NASA have shown that reactors designed to work on Earth do not necessarily function in a similar manner in space. Two experiments, the Water Processor Assembly and the Volatile Removal

Assembly have encountered difficulties in predicting and controlling the distribution of the phases (a crucial element in the operation of this type of reactor) as well as the overall pressure drop.

To address this problem, the NASA Glenn Research Center has begun an in-house study on the effects of a microgravity environment on gas-liquid flow through a packed bed reactor. The initial study compares an established flow regime map developed by E. Talmor in 1977



Researchers Eric Dao (University of Houston) and Brian Motil (Glenn) work on a packed bed reactor experiment on NASA's KC-135 aircraft.



Flow map for two-phase downflow through packed beds in microgravity.

(ref. 1) to similar flow conditions under microgravity. The Talmor map uses dimensionless quantities that account for the effects of gravity. In theory, by adjusting the gravity term, this map should also be applicable to reduced gravity.

Four different flow patterns or regimes exist for nonfoaming systems in normal-gravity flows. Two of the flow regimes can be classified as "gas continuous" because the gas phase occupies most of the void space within the column. At both low gas and low liquid flow rates, trickle or channeled flow is observed. In this important flow regime, the liquid phase trickles down the packing, driven mainly by the draining force of gravity. The liquid forms a laminar film that frequently does not wet the entire packing surface, and interaction between the phases is relatively low. As the gas flow is increased, the liquid film becomes turbulent and eventually the gas flow is strong enough to suspend droplets of liquid. This flow regime is generally called spray or mist flow. At higher liquid flow rates and relatively low gas flow, the continuous phase is now liquid and the gas phase is uniformly dispersed in small bubbles throughout the column. This regime is called bubbly flow. Finally, an interesting flow regime exists for a specific range of gas and liquid flow rates called the pulse flow regime. This flow regime can be observed as the liquid flow is increased beyond trickle flow until pulses (traveling waves) of liquid can be observed. The waves quickly grow until they span the entire cross section of the column.

The experimental apparatus used to compare flow regimes in microgravity was flown on NASA's KC-135 aircraft (photograph). The results are shown in the graph. The black lines indicate Talmor's predictions based on normal

gravity testing of concurrent downflow conditions. The data shown are from the microgravity testing and are used to generate the new curves (dashed lines). This series of tests indicate a significant shift in the pulse and bubbly flow regimes. The onset of pulse flow is shown to occur at a much lower gas-to-liquid ratio than is predicted. Research is ongoing with plans to develop a more comprehensive model.

Reference

1. Talmor, E.: Two-Phase Downflow Through Catalyst Beds. *AIChE J.*, vol. 23, no. 6, 1977, pp. 868–878.

Glenn contact:

Brian J. Motil, 216–433–6617,
Brian.J.Motil@grc.nasa.gov

Authors:

Brian J. Motil and Vemuri Balakotaiah

Headquarters program office: OBPR

Programs/Projects:

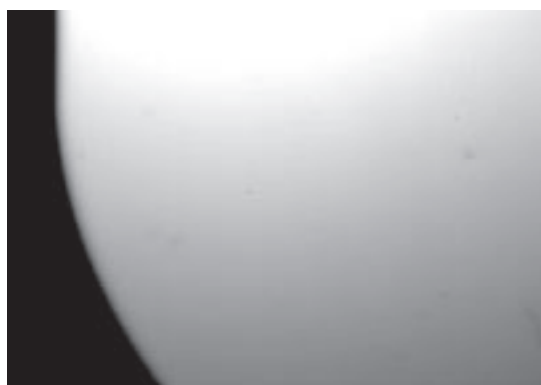
Microgravity Science

How Does a Liquid Wet a Solid? Hydrodynamics of Dynamic Contact Angles

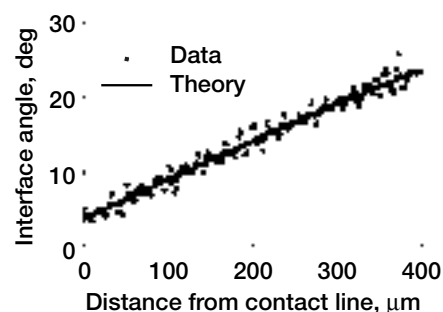
A contact line is defined at the intersection of a solid surface with the interface between two immiscible fluids. When one fluid displaces another immiscible fluid along a solid surface, the process is called dynamic wetting and a “moving” contact line (one whose position relative to the solid changes in time) often appears. The physics of dynamic wetting controls such natural and industrial processes as spraying of paints and insecticides, dishwashing, film formation and rupture in the

eye and in the alveoli, application of coatings, printing, drying and imbibition of fibrous materials, oil recovery from porous rocks, and microfluidics.

The contact angle, the angle formed at the intersection of the solid and the fluid-fluid interfaces, is a key material property needed to determine the shape of the fluid-fluid interface. It serves as the boundary condition for a differential equation describing the interface shape. In static capillary systems (e.g., the water meniscus formed on a clean glass plate), the static contact angle is routinely used for this purpose. The preceding image shows a magnified view near the contact line of a static meniscus formed by poly-dimethylsiloxane (silicone oil) on clean Pyrex: the air is clear, the fluid below is dark, and the vertical straight line at the top right is a Pyrex glass immersed in the fluid. Since silicone oil wets glass “perfectly,” its contact angle is very close to zero. The preceding graph shows the angle between the solid and the tangent to the static interface of the shadow-



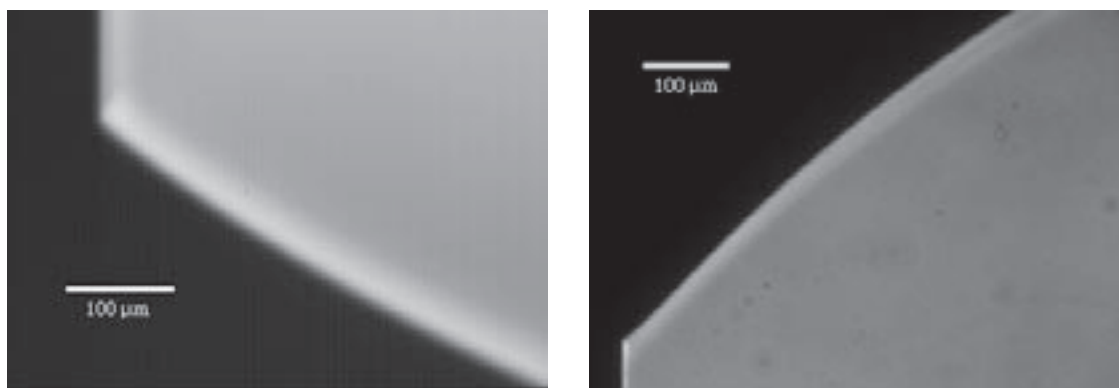
Shadowgraph of the static meniscus of silicone oil on Pyrex (Corning, Corning, NY). Field of view is about 600 μm in the horizontal direction. The fluid slightly overfills a Teflon beaker, 10 cm in diameter. A Pyrex tube, 2.54 cm in diameter, is immersed in the fluid. Because of the slight overfill, the meniscus appears above the beaker rim and can, thus, be imaged optically.



Static meniscus of silicone oil on Pyrex: The angle between the solid and the interface tangent is shown versus the distance from the contact line from image analysis of the picture in the first figure. The slope extrapolates to a static contact angle, $\approx 4^\circ$, at the contact line. The solid line shows the best fit of the static capillary theory. The theory's only adjustable parameter is the contact angle.

graph image, as a function of the distance to the contact line, r . The solid line is the solution of the static capillary theory (ref. 1). Clearly, the slope may be safely extrapolated to the contact line, $r = 0$, at which point the angle equals the static contact angle of the system.

In dynamic systems, however, the “dynamic” contact angle is not well defined. For example, when a silicone oil of viscosity $\mu = 10$ poise (1000 times more viscous than



Dynamic interface shape of silicone oil on Pyrex. Left: Ca , 0.01. Right: Ca , 0.1. Because of the high viscous forces near the contact line at $Ca = 0.1$, the macroscopic meniscus is bent into depression. Thus, the liquid is clear and the air is dark.

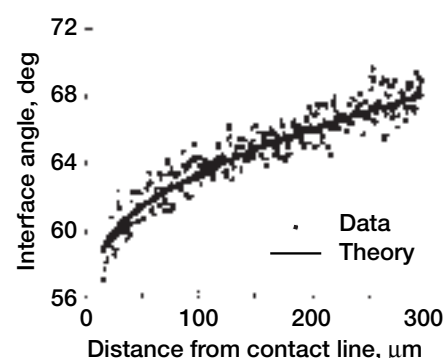
water) and surface tension $\sigma = 20$ dyn/cm advances on Pyrex with velocity $U = 0.02$ cm/sec, the image on the left shows that the dynamic contact angle is close to 67° . The controlling factor for the observed dynamic contact angle is the dimensionless group known as the capillary number, $Ca = U\mu/\sigma$. When $Ca = 0.1$, silicone oil forms a contact angle close to 120° (right image).

Despite their well-behaved appearance, these dynamic interfaces are fundamentally different from static interfaces. The final two graphs show that, when the dynamic interface shape is digitized and the angle is plotted versus the distance from the contact line, the slope does not attain a well-defined limit at the contact line ($r = 0$). Viscous forces dramatically bend the interface near the contact line. This suggests that, in contrast to the static contact angle (see the first graph, preceding page), the dynamic contact angle is not a well-defined quantity—it is not at all clear where on the interface one should apply the slope condition in order to calculate the interface shape. Nevertheless, a dynamic contact angle is still necessary to calculate the interface shape in dynamic conditions, the pressure drop necessary to move a meniscus in a capillary tube, and the spreading dynamics of small droplets.

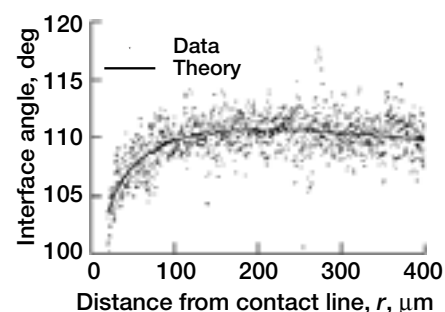
Principal investigator Professor Stephen Garoff of Carnegie Mellon University and coinvestigator Enrique Ramé of the National Center for Microgravity Research in Fluids and Combustion have been studying these systems for about 10 years. The objectives are

- (1) Identify and measure material-dependent, geometry-independent properties for describing dynamic wetting predicted in theoretical analyses valid at a low Ca .
- (2) Test the theories by measuring the property in two different geometries and using it to predict the flow in a third geometry.
- (3) Generate geometry-independent dynamic contact angle information outside the range of the validity of the theory ($Ca \sim 1$).

By using an asymptotic theory valid at $Ca \ll 1$ (ref. 2) and measurements of the interface near the contact line, we can extract a material parameter describing wetting dynamics. This parameter can be translated to geometries different from that where the measurement was performed, giving



Angle between solid and tangent to the interface versus distance from contact line at $Ca = 0$. The solid line shows the best fit of the dynamic theory (ref. 2). The theory's only adjustable parameter is a property that controls dynamic wetting and whose role is that of an "apparent" contact angle.



Angle between solid and tangent to the interface versus distance from contact line at $Ca = 0$. The solid line shows the best fit of the dynamic theory (ref. 2).

the approach predictive power. When Ca is not $\ll 1$, a geometry-free region of flow near the contact line must first be identified; then the interface shape and velocity field measured in that region can be used as boundary conditions for actual calculations. During the last year, as part of our ground-based program, we have begun to understand some subtleties of unsteady wetting behavior through a series of controlled experiments; a manuscript describing this work is in preparation.

The NASA Glenn Research Center is in the process of developing flight hardware to conduct a microgravity experiment to study the microscale phenomena in the vicinity of the moving contact line. In the absence of gravity, the region dominated by capillary force is enlarged, allowing detailed observations of flow and meniscus shape.

References

1. Huh, Chuh; and Scriven, L.E.: Shapes of Axisymmetric Fluid Interfaces of Unbounded Extent. *J. Colloid Interface Sci.*, vol. 30, no. 3, 1969, pp. 323–337.
2. Dussan, E.B.; Ramé, E.; and Garoff, S.: On Identifying the Appropriate Boundary-Conditions at a Moving Contact Line—An Experimental Investigation. *J. Fluid Mech.*, vol. 230, 1991, pp. 97–116.
3. Stoev, K.; Ramé, E.; and Garoff, S.: Effects of Inertia on the Hydrodynamics Near Moving Contact Lines. *Phys. Fluids*, vol. 11, no. 11, 1999, pp. 3209–3216.
4. Stoev, K., et al.: The Effects of Thin Films on the Hydrodynamics Near Moving Contact Lines. *Phys. Fluids*, vol. 10, no. 8, 1998, pp. 1793–1803.
5. Ramé, E.: The Interpretation of Dynamic Contact Angles Measured by the Wilhelmy Plate Method. *J. Colloid Interface Sci.*, vol. 185, no. 1, 1997, pp. 245–251.
6. Chen, Q.; Ramé, E.; and Garoff, S.: The Velocity Field Near Moving Contact Lines. *J. Fluid Mech.*, vol. 337, 1997, pp. 49–66.
7. Chen, Q.; Ramé, E.; and Garoff, S.: Experimental Studies on the Parametrization of Liquid Spreading and Dynamic Contact Angles. *Colloids Surf. A—Physicochemical and Engineering Aspects*, vol. 116, nos. 1–2, 1996, pp. 115–124.
8. Ramé, E.; and Garoff, S.: Microscopic and Macroscopic Dynamic Interface Shapes and the Interpretation of Dynamic Contact Angles. *J. Colloid Interface Sci.*, vol. 177, 1996, pp. 234–244.
9. Chen, Q.; Ramé, E.; and Garoff, S.: The Breakdown of Asymptotic Hydrodynamic Models of Liquid Spreading at Increasing Capillary Number. *Phys. Fluids*, vol. 7, no. 11, 1995, pp. 2631–2639.
10. Garoff, Stephen, et al.: Microscale Hydrodynamics Near Moving Contact Lines. Second Microgravity Fluid Dynamics Conference. NASA CP–3276, 1994, pp. 95–99.

National Center for Microgravity Research contact:

Dr. Enrique Ramé, 216–433–2842, Enrique.Rame@grc.nasa.gov

Author: Enrique Ramé

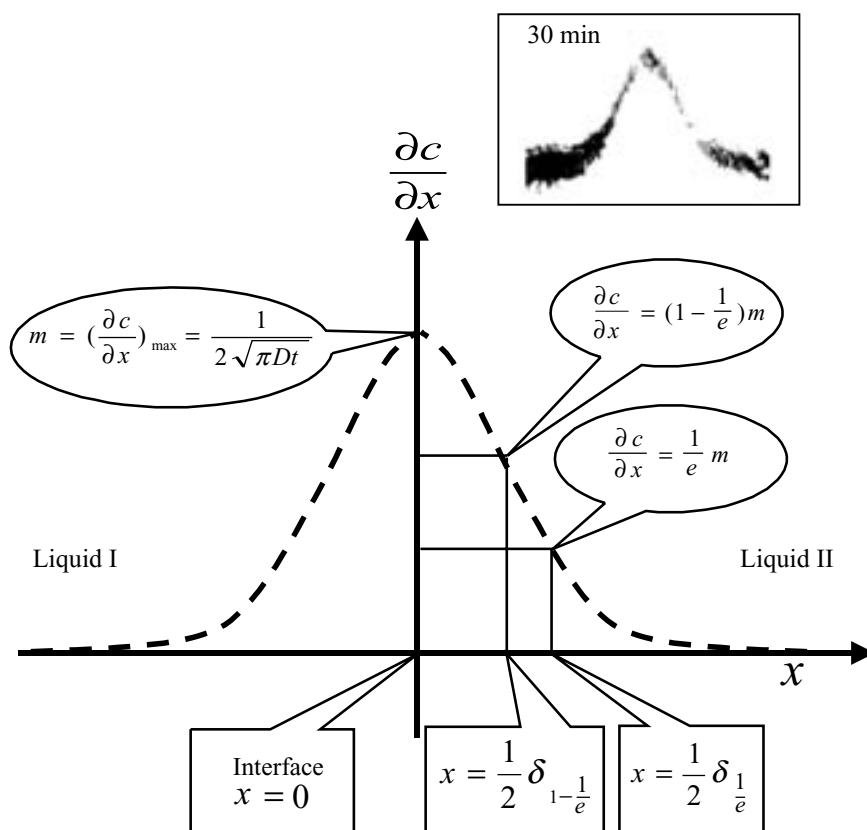
Headquarters program office: OBPR

Programs/Projects:
Microgravity Science

Diffusivity Measurements Made Instant and Easy

A compact common path interferometer (CPI) system has been developed to measure the diffusivity of liquid pairs. The CPI is an optical technique that can be used to measure changes in the gradient of the refraction index of transparent materials. It uses a shearing interferometer that shares the same optical path from a laser light source to the final imaging plane. The molecular diffusion coefficient of liquids can be determined from the physical relations between changes in the optical path length and liquid phase properties. When the data obtained by using the CPI have been compared with similar results from other techniques, the instrument has been demonstrated to be far superior to other instruments for measuring the diffusivity of miscible liquids while staying very compact and robust (ref. 1). Because of its compactness and ease of use, the CPI has been adopted for use in studies of interface dynamics as well as other diffusion-controlled process applications (ref. 2). This progress will permit experiments in microgravity that can quantitatively answer basic science questions about mass and thermal diffusion and their effect in transport processes. This instrument is a spinoff of a diagnostic development for microgravity fluid physics experiments at the NASA Glenn Research Center that has used optics and electronics existing in the fluid physics laboratory for feasibility studies.

Optical diagnostic techniques have become an integral part of many areas of measurement applications in industrial and research laboratories. Many types of interferometers and their phase-shifted versions have been used as instruments for measuring optical wave fronts for lens testing and combustion and fluid flow diagnostics. One of these, the point diffraction interferometer, is considered to be robust (see, for example, ref. 3) because it has a common-path design. The point diffraction interferometer is difficult to align and has a limited measurement range for liquid-phase applications. Interferometry and schlieren techniques have been widely used for many years



A typical traced fringe (concentration gradient profile $\partial c/\partial x$) near the interface after fluids came in contact (inset shows the actual fringe after 30 min). Typical straightforward data points for diffusivity D calculations are also shown on the traced shifted fringe. (Note: All dimensions are normalized by the maximum m value.)

for gas-flow-visualization. On the other hand, the CPI, which is basically a Wollaston prism Polarizer in combination with an analyser (crystalline quartz retardation plate) is used instead of a point diffraction interferometer unit. The advantage of using the CPI over other optical techniques is that it can make quantitative measurements in liquids with the large index of refraction variations that often occur in interface dynamics studies. This can be simply accomplished by using different prism polarizers for each particular experimental condition.

Miscible fluid flows are important in enhanced oil recovery, fixed bed regeneration, hydrology, and filtration. The dynamics of miscible interfaces is an active area of research that has been identified to benefit from experimentation in reduced gravity. The diffusivity is an important thermophysical property in such experiments. Its measurement is required to determine the ranges for experimental parameters such as the displacement speed, so that the effects of convection and diffusion are in optimal balance.

Recently, a new approach was developed that uses the CPI to measure the diffusivity of a pair of miscible fluids at any instant after they come in contact. The mathematical model underlying this new approach has been defined (ref. 4). The results are in excellent agreement with existing

available data and are far more reliable because of a real-time measurement approach. Results of the first set of measurements have been published by Rashidnia et al. (ref. 1). The physical property data measured by the CPI will greatly help in defining the test results and the mathematical modeling of an experiment planned (ref. 2) to be conducted on the International Space Station in 2005.

References

1. Rashidnia, N., et al.: Measurement of the Diffusion Coefficient of Miscible Fluids Using Both Interferometry and Weiner's Method. Presented at the Fourteenth Symposium on Thermo-physical Properties (Boulder, CO), June 2000.
2. Maxworthy, Tony; and Meiburg, Eckart: The Dynamics of Miscible Interfaces: A Space Flight Experiment. Science Requirements Document, First Draft, Univ. of Southern California, Los Angeles, CA, Mar. 2000.
3. Mercer, Carolyn R.; and Rashidnia, Nasser: Common-Path Phase-Stepped Interferometer for Fluid Measurements. CD Rom Proceedings of the 8th International Symposium on Flow Visualization (Sorrento, Italy), Sep. 1998, pp. 256.1–256.9.
4. Rashidnia, N.: Novel Diffusivity Measurement, Optical Technique. Proceedings of the Ninth (Millennium) International Symposium of Flow Visualization, Flow Visualization IX. G.M. Carlomango and I. Grant, eds., 2000, pp. 451.1–451.8.

Glenn contact:

Dr. Nasser Rashidnia, 216–433–3622, Nasser.Rashidnia@grc.nasa.gov

Author: Dr. Nasser Rashidnia

Headquarters program office: OBPR

Programs/Projects:

Microgravity Science

Growth and Morphology of Supercritical Fluids, a Fluid Physics Experiment Conducted on Mir, Complete

The Growth and Morphology of Supercritical Fluids (GMSF) is an international experiment facilitated by the NASA Glenn Research Center and under the guidance of U.S. principal investigator Professor Hegseth of the University of New Orleans and three French coinvestigators: Daniel Beysens, Yves Garrabos, and Carole Chabot. The GMSF experiments were concluded in early 1999 on the Russian space station Mir. The experiments spanned the three science themes of near-critical phase separation rates, interface dynamics in near-critical boiling, and measurement of the spectrum of density fluctuation length scales very close to the critical point. The fluids used were pure CO_2 or SF_6 . Three of the five thermostats used could adjust the sample volume with the scheduled crew time. Such a volume adjustment enabled variable sample densities around the critical density as well as pressure steps (as distinct from the usual temperature steps) applied to the sample.

The French-built ALICE II facility was used for these experiments. It allows tightly thermostated (left photograph) samples (right photograph) to be controlled and viewed/measured. Its diagnostics include interferometry, shadowgraph, high-speed pressure measurements, and microscopy. Data were logged on DAT tapes, and PCMCIA cards and were returned to Earth only after the mission was over.

The ground-breaking near critical boiling experiment has yielded the most results with a paper published in Physical Review Letters (ref. 1). The boiling work also received press in Science Magazine (ref. 2). This work showed that, in very compressible near-critical two-phase pure fluids, a

vapor bubble was induced to temporarily overheat during a rapid heating of the sample wall. The temperature rise in the vapor was 23-percent higher than the rise in the driving container wall. The effect is due to adiabatic compression of the vapor bubble by the rapid expansion of fluid near the boundary during heatup. Thermal diffusivity is low near the critical point, so getting heat out of the compressed bubble is observably slow. This gives the appearance of a backward heat flow, or heat flow from a cold surface to a warm fluid.

References

1. Wunenburger, et al.: Thermalization of a Two-Phase Fluid in Low Gravity: Heat Transferred From Cold to Hot. Phys. Rev. Lett., vol. 84, no. 18, May 2000, p. 4100.
2. Science Magazine, May 5, 2000, p. 789.

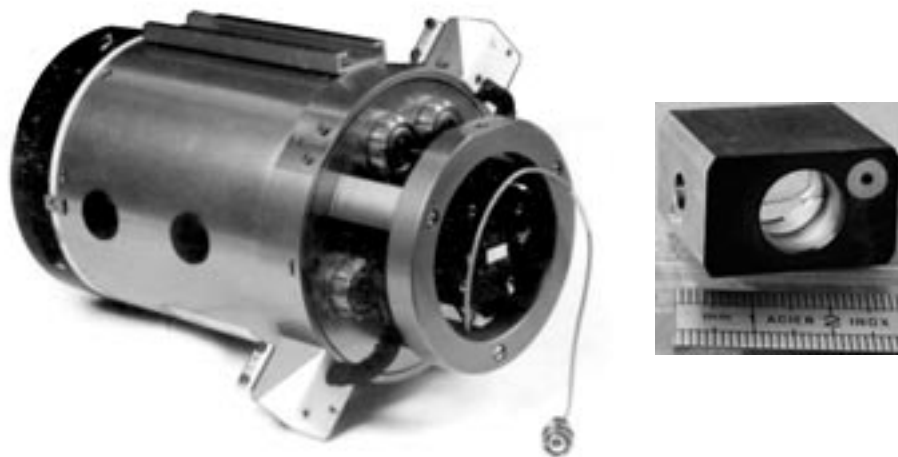
Glenn contacts:

Dr. R. Allen Wilkinson, 216-433-2075, R.A.Wilkinson@grc.nasa.gov; and Monica Hoffmann, 216-433-6765, Monica.I.Hoffmann@grc.nasa.gov

Author: Dr. R. Allen Wilkinson

Headquarters program office: OBPR

Programs/Projects:
Microgravity Science



Left: ALICE II Thermostat for critical fluid samples enables stable temperature control ($\pm 50 \mu\text{C rms}$) and optical diagnostics like interferometry and microscopy. Right: Typical copper-bodied cell with sapphire windows and filled with SF_6 to roughly 38 atm and a density of 0.73 g/cm^3 . The typical fluid volume is less than 1 cm^3 .

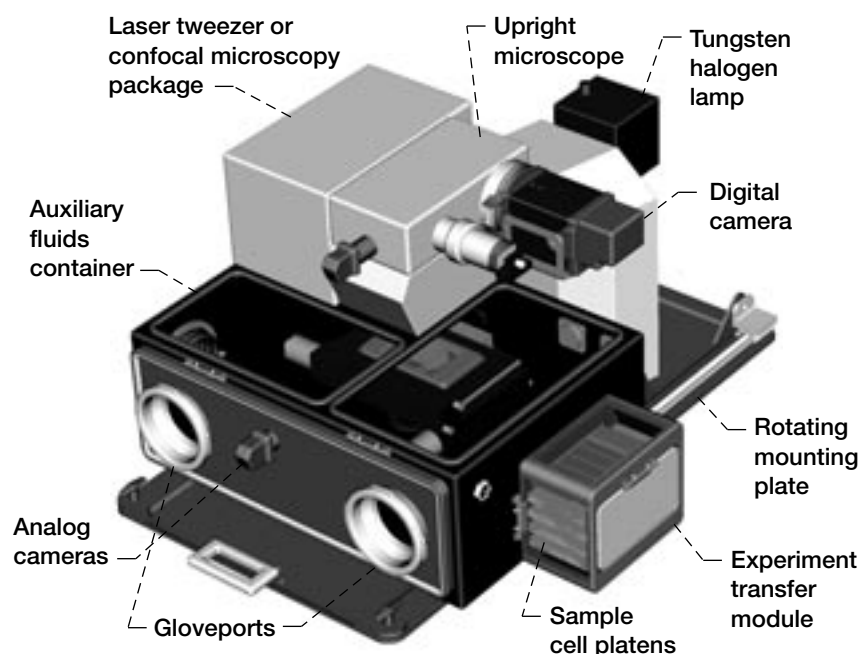
Light Microscopy Module: An On-Orbit Microscope Planned for the Fluids and Combustion Facility on the International Space Station

The Light Microscopy Module (LMM) is planned as a fully remotely controllable on-orbit microscope subrack facility, allowing flexible scheduling and control of fluids and biology experiments within NASA Glenn Research Center's Fluids and Combustion Facility on the International Space Station.

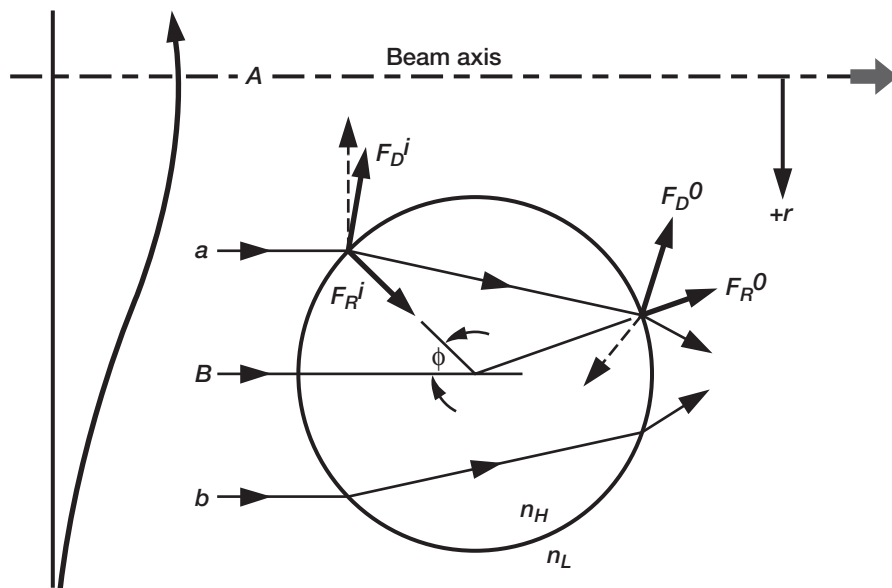
Within the Fluids and Combustion Facility, four fluids physics experiments will utilize an instrument built around a light microscope. These experiments are the Constrained Vapor Bubble experiment (Peter C. Wayner of Rensselaer Polytechnic Institute), the Physics of Hard Spheres Experiment-2 (Paul M. Chaikin of Princeton University), the Physics of Colloids in Space-2 experiment (David A. Weitz of Harvard University), and the Low Volume Fraction Colloidal Assembly experiment (Arjun G. Yodh of the University of Pennsylvania). The first experiment investigates heat conductance in microgravity as a function of liquid volume and heat flow rate to determine, in detail, the transport process characteristics in a curved liquid film. The other three experiments investigate various complementary aspects of the nucleation, growth, structure, and properties of colloidal crystals in microgravity and the effects of micromanipulation upon their properties. Key diagnostic capabilities for meeting the science requirements of the four experiments include video microscopy to observe sample features including basic structures and dynamics, interferometry to measure vapor bubble thin film thickness, laser tweezers for colloidal particle manipulation and patterning, confocal microscopy to provide enhanced three-dimensional

visualization of colloidal structures, and spectrophotometry to measure colloidal crystal photonic properties.

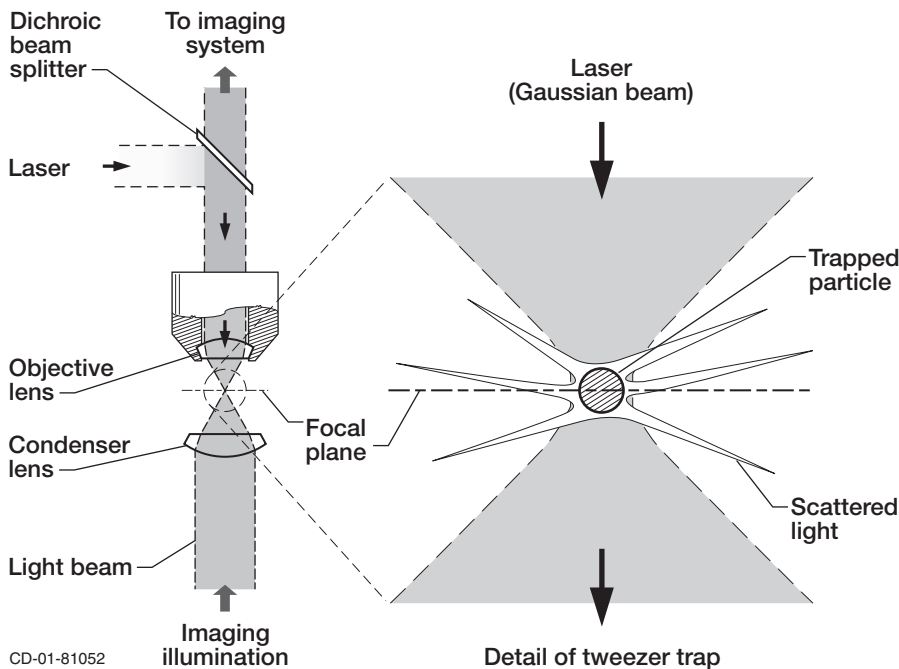
The LMM concept is built around a commercially available upright style microscope. The microscope will house several different objectives, corresponding to magnifications of $\times 10$, $\times 50$, $\times 63$, and $\times 100$. Features of the LMM include cameras, an interchangeable laser tweezer (or confocal) package, tungsten halogen lamps, an auxiliary fluids container with gloveports, an experiment transfer module, and a rotating mounting plate. The multiport imaging head on the top of the microscope provides a motorized slider to select the sensor or sensors to which the images are directed. The rotating mounting plate allows the LMM to be rotated for easy access to the sample area when in a nonoperating mode. The auxiliary fluids container prevents liquid droplets (immersion oil or leaking sample material) from escaping into the cabin or into electronics in the Fluids and Combustion Facility. Glove ports allow access to the sample area for cleaning, before opening the box for sample platen changeout or reconfiguration. The experiment transfer module, which can accommodate up to five sample cell platens, is configured adjacent to the auxiliary fluids container, which has a pass-through for the samples. The experiment transfer module will be loaded with sample platens on the ground and will provide contained storage until the samples are used in the experiment.



Light microscopy module on rotating mounting plate.



the tweezers will be scanned through a fixed array of points across the field of view to induce patterns that are either commensurate or incommensurate with the equilibrium configuration of the colloidal crystal. They also will be used to measure the viscosity of the fluid. A particle is trapped and video images taken as it is translated in an oscillatory fashion through the field of view. The velocity just before the particle falls out of the trap is measured from the video record and, along with the known force and particle diameter, is used to calculate the sample dynamic viscosity (or crystal shear modulus).



CD-01-81052

Concept of laser tweezers: trapping of particles by radiation pressure.

During 2000, the LMM Team at Glenn successfully used laser tweezers to trap colloidal particles. Currently, the LMM project is in the requirements definition and preliminary design phase. A preliminary design review will be conducted in mid-2001. This work was performed under NASA contracts NAS3-99155 (Federal Data Corporation) and NAS3-98008 (Dynamics).

Glenn contact:

Michael P. Doherty, 216-433-6641,
Michael.P.Doherty@grc.nasa.gov

Authors:

Michael P. Doherty, Susan M. Motil,
 John H. Snead, and Dr. DeVon W. Griffin

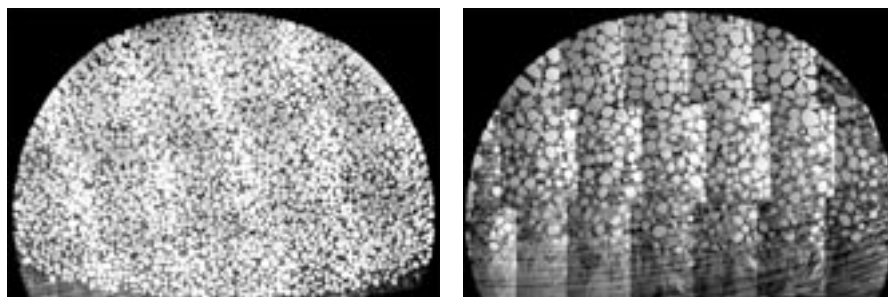
Headquarters program office: OBPR

Programs/Projects:

Microgravity Science

Laser tweezers will be implemented using a custom-built system based on a 1064-nm Nd:YAG laser, beam-focusing optics, and two acousto-optic deflectors to steer the trap within the field of view of the microscope. Laser tweezers simply is the trapping of a colloidal particle using radiation pressure by focusing a laser beam through a high numerical aperture lens and striking the particle. Tweezers will be employed to displace a particle by one or more lattice constants from its equilibrium position. In addition,

Coarsening Experiment Being Prepared for Flight



50-percent solid-phase sample near surface. Left: Coarsened 10 hr (on Earth). Right: Coarsened 3 days (on Earth).

The Coarsening in Solid-Liquid Mixtures-2 (CSLM-2) experiment is a materials science space flight experiment whose purpose is to investigate the kinetics of competitive particle growth within a liquid matrix. During coarsening, small particles shrink by losing atoms to larger particles, causing the larger particles to grow. In this experiment, solid particles of tin will grow (coarsen) within a liquid lead-tin eutectic matrix. The following figures show the coarsening of tin particles in a lead-tin eutectic as a function of time. By conducting this experiment in a microgravity environment, we can study a greater range of solid volume fractions, and the effects of sedimentation present in terrestrial experiments will be negligible. The CSLM-2 experiment is slated to fly onboard the International Space Station. The experiment will be run in the Microgravity Science Glovebox installed in the U.S. Laboratory module.

The coarsening of particles within a matrix is a phenomenon that occurs in many metallic and other systems. For example, the second-phase particles in high-temperature turbine blade materials undergo coarsening at the operating temperature of the turbine. The coarsening process degrades the strength of the blade because turbine alloys containing a few large particles are weaker than those containing many small ones. Coarsening occurs in liquid-phase sintered materials such as tungsten carbide-cobalt, iron-copper, dental amalgam for fillings, and porcelain. The growth of liquid droplets in a vapor phase that occurs inside rain clouds (particularly near the equator, where the vapor pressure of water is high) is a commonplace example of the coarsening phenomenon. The CSLM-2 study will help define the mechanisms and rates of coarsening that govern all these systems.

In fiscal year 2000, the CSLM-2 project designed the experimental flight hardware. The flight hardware consists of two separable pieces of equipment, the sample-processing unit and the electronic control unit, as shown in the final figure. The sample-processing unit incorporates a small electric sample heater with a water quench system. The heater consists of a circular sample holder plate sandwiched by two thin-film kapton heaters with a circular ring heater around the perimeter. The holder plate has four cylindrical sample holes with five platinum resistance temperature devices for temperature monitoring and control.

The electronic control unit contains the power supply, electrical control, and data storage components. There are three toggle switches on the front of the electronic control unit that allow a crew member to power up the unit, activate the experiment run, and abort the run with quench. There are also three indicator lights and a liquid crystal display (LCD) that show the status of the experiment and the temperatures of the resistance temperature devices in the sample holder. The temperature-time data from the experiment run are stored on a hard disk located in the electronic control unit and telemetered to the NASA Telescience Support Center after experiment completion.

The CSLM-2 experiment runs do not need to be attended by an astronaut after activation. There is no need for real-time orbit-to-ground telemetry directly from the experimental apparatus. Non-real-time data will be downlinked via the Microgravity Science Glovebox laptop connected to the CSLM-2 hardware by a RS-422 data downlink.



CSLM-2 hardware mockup with cables.

Find out more about CSLM-2: <http://cslm.zin-tech.com>

Bibliography

Alkemper, J., et al.: Dynamics of Late-Stage Phase Separation: A Test of Theory. *Phys. Rev. Lett.*, vol. 82, no. 13, 1999, pp. 2725–2758.

Calderon, H.A., et al.: Ostwald Ripening in Concentrated Alloys. *Acta. Metall.*, vol. 42, no. 3, 1994, pp. 991–1000.

Snyder, V.A.; Alkemper, J.; and Voorhees, P.W.: The Influence of Temperature Gradients on Ostwald Ripening. *Metal. Mat. Trans.*, vol. 30A, 1999, pp. 2341–2348.

Snyder, V.A.; Alkemper, J.; and Voorhees, P.W.: The Development of Spatial Correlations During Ostwald Ripening: A Test of Theory. *Acta Mater.*, vol. 48, 2000, pp. 2689–2701.

Snyder, V.A.; Alkemper, J.; and Voorhees, P.W.: Transient Ostwald Ripening and the Disagreement Between Steady-State Coarsening Theory and Experiment. To be published in *Acta Mater.*

Alkemper, J.; and Voorhees, P.W.: Quantitative Serial Sectioning Analysis. To be published in *J. Microscopy*.

Glenn contacts:

Dr. Walter Duval, 216–433–5023,
Walter.M.Duval@grc.nasa.gov; and
J. Mark Hickman, 216–977–7105,
John.M.Hickman@grc.nasa.gov

Author: J. Mark Hickman

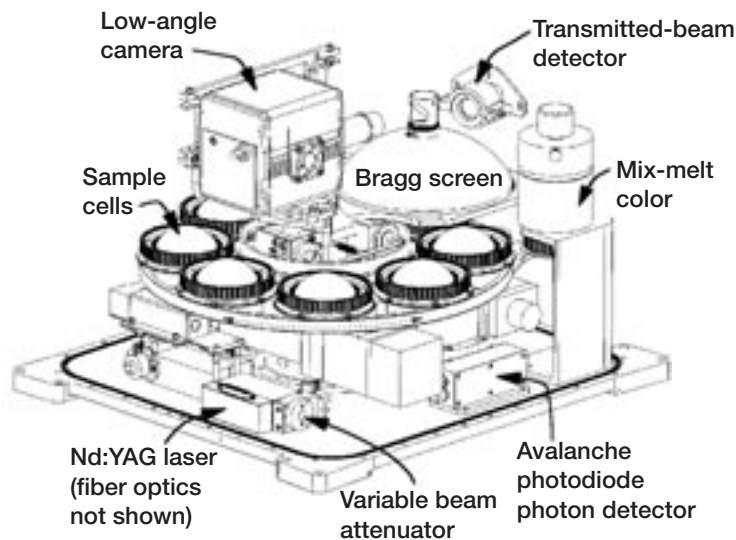
Headquarters program office: OBPR

Programs/Projects:
Microgravity Science

Physics of Colloids in Space (PCS) Flight Hardware Developed

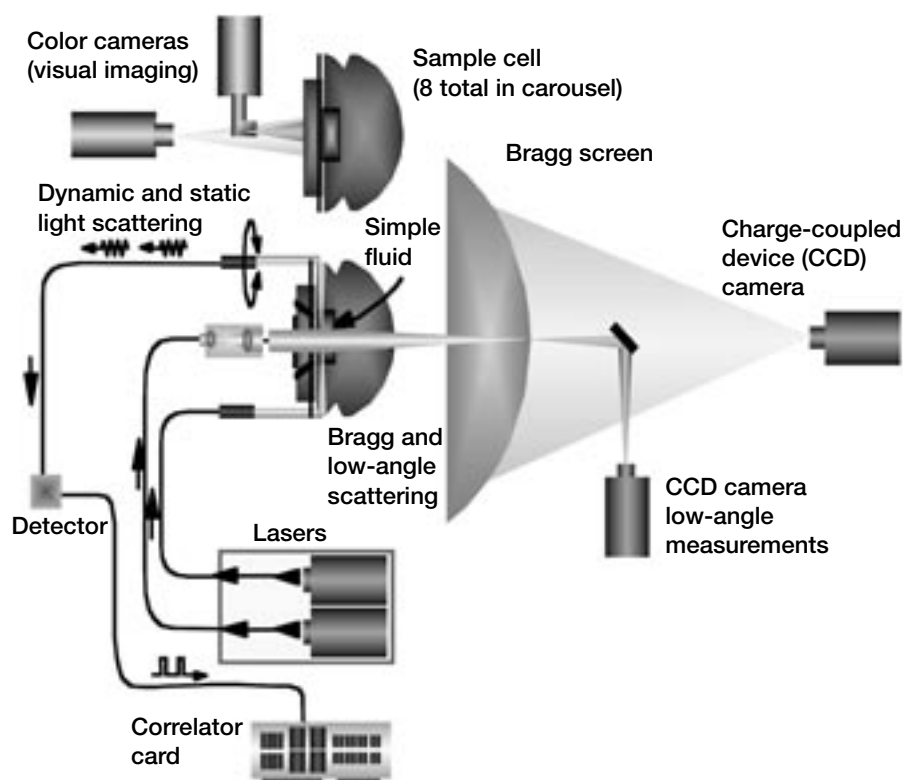
The Physics of Colloids in Space (PCS) experiment is a Microgravity Fluids Physics investigation that will be located in an Expedite the Process of Experiments to Space Station (EXPRESS) Rack. The investigation will be conducted in the International Space Station U.S. laboratory, Destiny, over a period of approximately 10 months during the station assembly period from flight 6A through flight UF-2. This experiment will gather data on the basic physical properties of colloids by studying three different colloid systems with the objective of understanding how they grow and what structures they form. A colloidal suspension consists of fine particles (micrometer to submicrometer) suspended in a fluid—for example, paints, milk, salad dressings, and aerosols. The long-term goal of this investigation is to learn how to steer the growth of colloidal suspensions to create new materials and new structures. This experiment is part of a two-stage investigation conceived by Professor David Weitz of Harvard University along with Professor Peter Pusey of the University of Edinburgh. The experiment hardware was developed by the NASA Glenn Research Center through contracts with Dynacs, Inc., and ZIN Technologies.

The PCS experiment hardware is composed of an Avionics Section unit and a Test Section unit, each approximately 47 by 50 by 56 cm. The Test Section and Avionics Section are accommodated side by side in an EXPRESS Rack occupying four Middeck Locker equivalents (the equivalent volume of a standard Middeck Locker). The PCS hardware uses the EXPRESS Rack



PCS Test Section internal assembly.

utilities of power, air-cooling, water-cooling, and communication for data and commanding telemetry. The Avionics Section provides the power distribution, the data acquisition and processing, and the command and data communication. The Test Section contains eight colloid samples and all the diagnostic instrumentation.



PCS science diagnostics.

The Avionics Section, which is a two-drawer assembly, has been assembled, verified, and delivered to the NASA Kennedy Space Center for integration into the flight EXPRESS Rack. The Test Section has been assembled and also has completed verification testing. The Test Section, which contains the science diagnostics, has been subjected to rigorous performance testing by the project and principal investigator's team. These diagnostics are based primarily on light-scattering instrumentation, which was in majority developed under a previous flight experiment, the Physics of Hard Spheres Experiment (PHaSE). Dynamic and static light scattering is provided via a 532-nm Nd-Yag laser and fiber-coupled avalanche photodiode. Two detection fibers cover scattering angles from 11° to 169° and 191° to 349° , respectively. Bragg scattering over the range of 10° to 60° uses a second Nd-Yag laser and an optical screen and digital camera to image the scattered Bragg rings from the colloid samples. Additional optics and another digital camera capture the laser light scattered at low angles of 0.3° to 6.0° . Via the electronics and data processing provided by the Avionics Section, both static and dynamic data are obtained from the small scattering angle optics/camera.

The Test Section and Avionics Section have been installed in the flight EXPRESS Rack at Kennedy and have undergone interface verification testing. The Test Section returned to Glenn for final sample processing and installation, and final performance and interface verification. It then will be delivered to Kennedy for integration into the space shuttle Middeck for launch on 6A.

Find out more about this research:

Physics of Colloids in Space:

<http://microgravity.grc.nasa.gov/6712/PCS.htm>

Experimental Soft Condensed Matter Group:

<http://www.deas.harvard.edu/projects/weitzlab/>

Glenn contact:

John M. Koudelka, 216-433-2852,
John.M.Koudelka@grc.nasa.gov

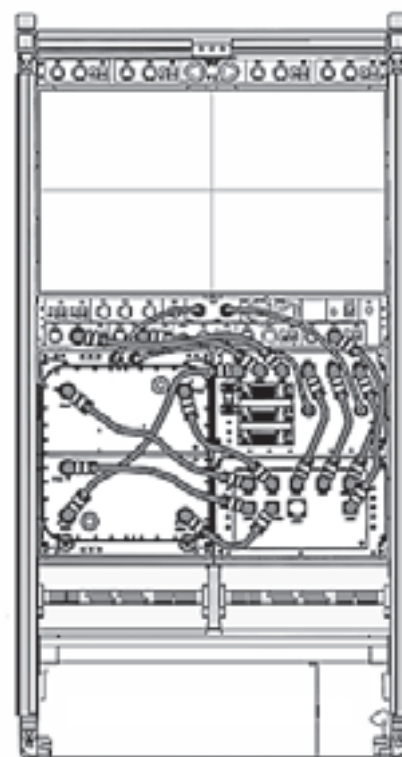
National Center for Microgravity Research contact:

Dr. Rafat R. Ansari, 216-433-5008,
Rafat.R.Ansari@grc.nasa.gov

Author: John M. Koudelka

Headquarters program office: OBPR

Programs/Projects: Microgravity Science, ISS payloads, Flight 6A, PCS



PCS in EXPRESS Rack.

Extensional Rheology Experiment Developed to Investigate the Rheology of Dilute Polymer Solutions in Microgravity

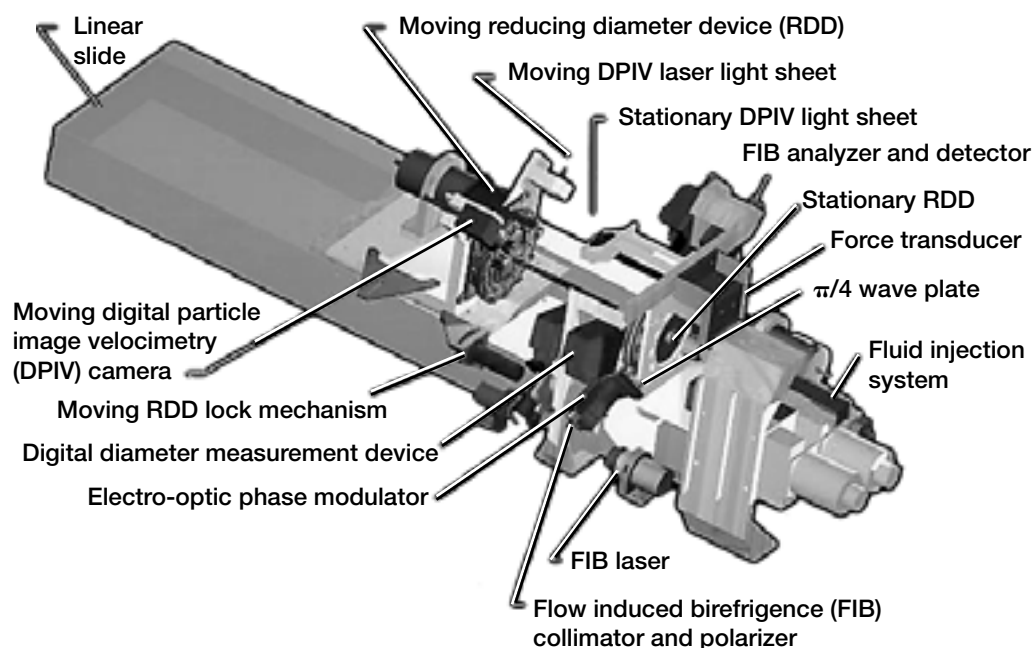
A fundamental characteristic of fluid is viscosity; that is, the fluid resists forces that cause it to flow. This characteristic, or parameter, is used by manufacturers and end-users to describe the physical properties of a specific material so that they know what to expect when a material, such as a polymer, is processed through an extruder, a film blower, or a fiber-spinning apparatus. Normally, researchers will report a shear viscosity that depends on the rate of an imposed shearing flow. Although this type of characterization is sufficient for some processes, simple shearing experiments do not provide a complete picture of what a processor may expect for all materials.

Extensional stretching flows are common in many polymer-processing operations such as extrusion, blow molding, and fiber spinning. Therefore, knowledge of the complete rheological (ability to flow and be deformed) properties of the polymeric fluid being processed is required to accurately predict and account for the flow behavior. In addition, if numerical simulations are ever able to serve as a priori design tools for optimizing polymer processing operations such as those described above, an accurate knowledge of the extensional viscosity of a polymer system and its variation with temperature, concentration, molecular weight, and strain rate is critical.

The Extensional Rheology Experiment (ERE) deals with the flow of polymers when they are subjected to stress and with their behavior after they have been deformed. The two primary objectives of the experiment are (1) to determine the extensional viscosity in a uniaxial stretching flow for

dilute polymer solutions and their subsequent relaxation behavior after extensional deformation and (2) to measure the transient birefringence during deformation and relaxation. (Birefringence is the difference in the index of refraction of a material between polarization states. When light passes through birefringent materials, like certain crystals and polymers, it is refracted in two different directions, depending on the polarization state of the light. Researchers can tell what the light is doing inside the material by measuring the birefringence. This gives them scientific information about how the material's molecules are behaving without having to disturb them.)

ERE was developed at the NASA Glenn Research Center under contract with Zin Technologies Inc. ERE is designed to fly on a Terrier



Computer model image of extensional rheology experiment test section identifying components and subsystems. Direction of stretch is to the left. The stretching fluid is illustrated in the center, between the reducing diameter devices (RDD's). This figure appears in color in the online version of this article (<http://www.grc.nasa.gov/WWW/RT2000/6700/6728logsdon.html>).

Black Brant sounding rocket. Suborbital sounding rockets provide several minutes of useful microgravity time for conducting experiments without the effects of gravity. In the case of ERE, fluid sagging due to gravity prevents making these rheological measurements, particularly at low deformation rates.

The ERE hardware consists of three sections: (1) the avionics package, which contains all electronics systems for power, control, and data acquisition, (2) experiment package A, and (3) experiment package B. Each experiment package contains a test section. The experiment packages are operated independently, and each performs a single test matrix point per flight. The test sections consist of a computer-controlled linear slide mechanism to cause the fluid deformation, a set of moving and stationary reducing diameter devices (RDD's), a flow-induced birefringence (FIB) apparatus, a digital diameter measurement system, and a digital particle image velocimetry (DPIV) system (see the figure).

Each RDD causes a 4:1 reduction in the diameter of the fluid column during the stretch to minimize shear stresses in the fluid. The stationary RDD on each slide has a very sensitive force transducer to measure the force induced by the deformation. The fluid is deployed between the RDD's by a fluid injection system. The DPIV system is used to record fluid motion near the endplates (RDD's) by illuminating glass spheres that were mixed in the fluid. A laser light sheet illuminates an axial plane (along the direction of flow) of the filament, allowing a charge-coupled device (CCD) camera to capture the position of these spheres. From DPIV postprocessing of the captured images, axial and radial fluid velocities can be computed.

The extent that the polymer chain has been deformed during stretch and relaxation is measured with a single-point flow-induced birefringence system developed at Glenn. This phase-modulated system simultaneously measures the retardance (degree of orientation of the polymer chains) and extinction angle (chain orientation angle relative to the flow direction) of the polymer chains as a function of time. The laser-micrometer-based digital diameter measurement system provides the fluid filament diameter necessary for the flow-induced birefringence calculation.

Assembly and testing of the ERE payload was completed in fiscal year 2000. The first two experiments will investigate the extensional viscosity of a non-Newtonian fluid (0.025 wt % high-molecular-weight monodisperse polystyrene dissolved in oligomeric polystyrene oil) at extensional deformation rates of 0.2083 sec^{-1} (slow stretch rate) and 2.6042 sec^{-1} (fast stretch

rate). The first sounding rocket launch was conducted at the White Sands Missile Range in New Mexico on July 6, 2000.

The data from this first flight did not provide the desired scientific results. Several anomalies occurred. The RDD mechanisms did not function properly, resulting in nonideal fluid deformation. This impacted the FIB measurements by deflecting the incident laser beam away from the optical detector due to increased curvature of the fluid column. The force measurement on one of the test sections was also compromised because of larger than expected friction in some cross-roller bearings. (The magnitude of expected forces is in the range of milligrams to several grams.) Finally, reflective particles in the fluid used for flow visualization and flow velocity measurements were not sufficiently distributed in the fluid, preventing postflight DPIV analysis. A post-flight failure investigation was conducted. Causes and corrective action for each of the anomalies have been identified.

Glenn contacts:

Kirk A. Logsdon, 216-433-2836, Kirk.A.Logsdon@grc.nasa.gov; and Nancy R. Hall, 216-433-5643, Nancy.R.Hall@grc.nasa.gov

Author: Kirk A. Logsdon

Headquarters program office: OBPR

Programs/Projects:

Microgravity Science

Compact Microscope Imaging System Developed

The Compact Microscope Imaging System (CMIS) is a diagnostic tool with intelligent controls for use in space, industrial, medical, and security applications. The CMIS can be used in situ with a minimum amount of user intervention. This system, which was developed at the NASA Glenn Research Center, can scan, find areas of interest, focus, and acquire images automatically. Large numbers of multiple cell experiments require microscopy for in situ observations; this is only feasible with compact microscope systems.

CMIS is a miniature machine vision system that combines intelligent image processing with remote control capabilities. The software also has a user-friendly interface that can be used independently of the hardware for post-experiment analysis.

CMIS has potential commercial uses in the automated online inspection of precision parts, medical imaging, security industry (examination of currency in automated teller machines and fingerprint identification in secure entry locks), environmental industry (automated examination of soil/water samples), biomedical field (automated blood/cell analysis), and microscopy community.

CMIS will improve research in several ways:

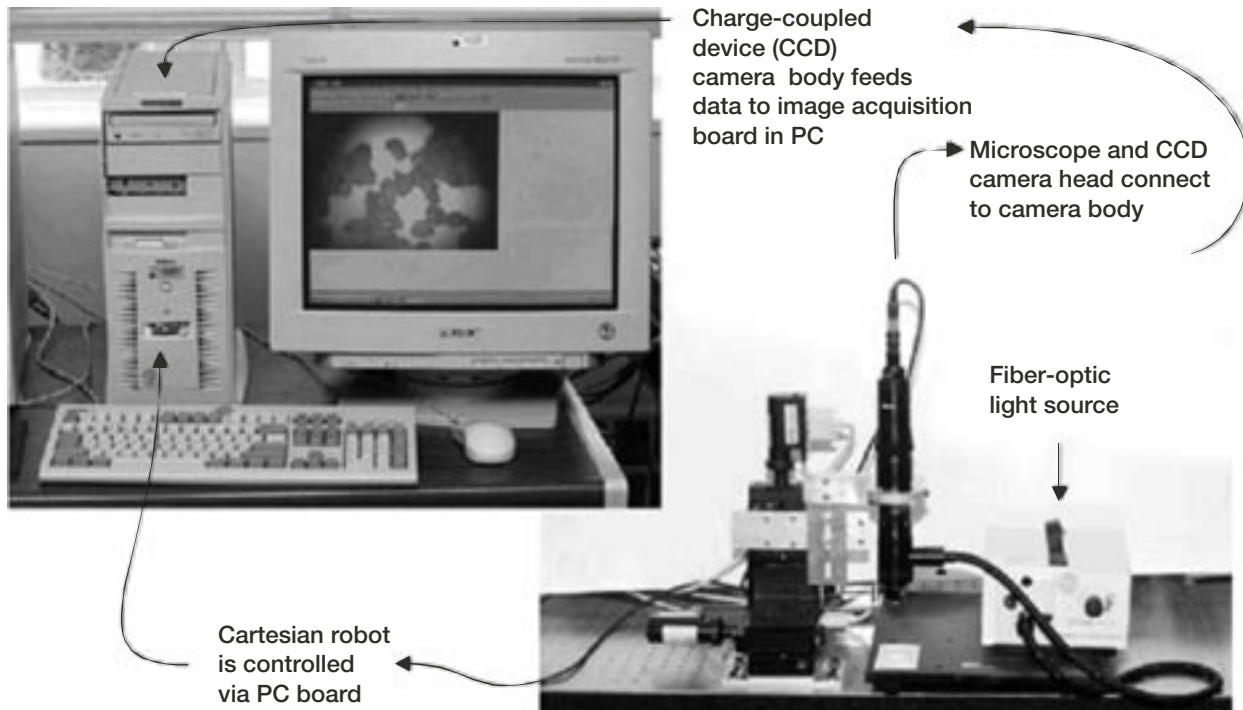
(1) It will expand the capabilities of MSD experiments utilizing microscope technology.

(2) It may be used in lunar and Martian experiments (Rover Robot).

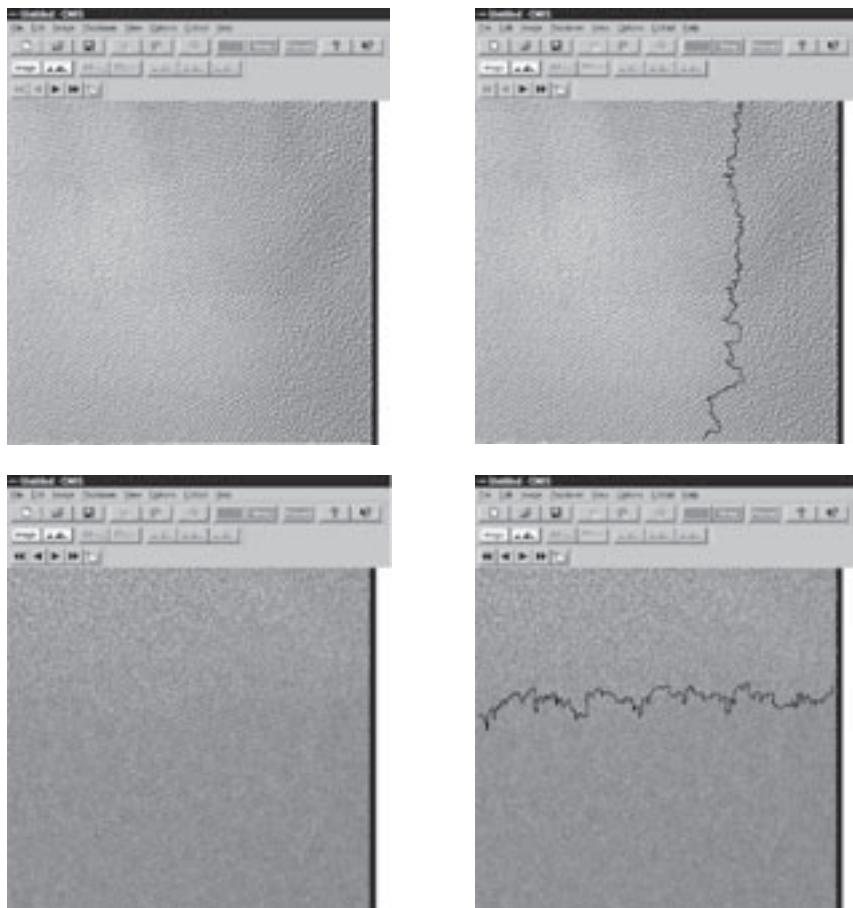
(3) Because of its reduced size, it will enable experiments that were not feasible previously.

(4) It may be incorporated into existing shuttle orbiter and space station experiments, including glove-box-sized experiments as well as ground-based experiments.

This is a true innovation in the field of microscopy and will be incorporated into future microscopy experiments in the microgravity program. The work of the CMIS research team (Dr. Mark McDowell, Stephanie Grasson, Elizabeth Gray, and Rick Rogers) was such a significant contribution to science that it has won the Imaging Solution of the Year award from Advanced Imaging for the field of medical imaging, bioscience, and scientific analysis.



Compact Microscope Imaging System (CMIS).



Automatic phase-change detection has finally been accomplished. After image averaging, brightness slicing, and optimal filtering to isolate the solid area, the CMIS algorithm traces the contours to find the largest solid region, which determines the interface (dark line). Top left: Raw data exhibiting vertical disorder/order interface. Top right: Interface located by CMIS is shown as a darker line. Bottom left: Raw data exhibiting disorder/order interface. Bottom right: Interface located by CMIS is shown as a darker line. This figure appears in color in the online version of this article (<http://www.grc.nasa.gov/WWW/RT2000/6700/6728mcdowell.html>).

Find out more about CMIS:

<http://cmis.grc.nasa.gov>

Glenn contact:

Dr. Mark McDowell, 216-433-8161,
drmm@easy.grc.nasa.gov

Author: Dr. Mark McDowell

Headquarters program office: OBPR

Programs/Projects:

Microgravity Science

Special recognition:

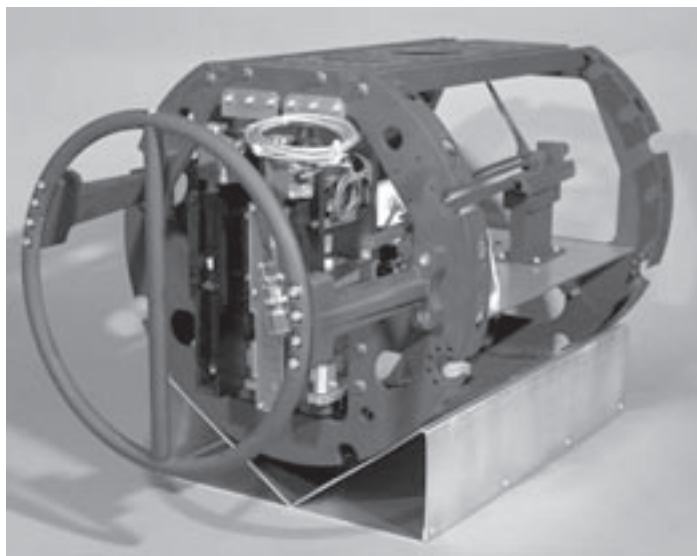
Imaging Solution of the Year award from Advanced Imaging for the field of medical imaging, bioscience and scientific analysis. Advanced Imaging magazine is an international magazine that highlights the latest state-of-the-art advancements in imaging processing.

Multiuser Droplet Combustion Apparatus Developed to Conduct Combustion Experiments

A major portion of the energy produced in the world today comes from the combustion or burning of liquid hydrocarbon fuels in the form of droplets. However, despite vigorous scientific examinations for over a century, researchers still lack a full understanding of many fundamental combustion processes of liquid fuels. Understanding how these fuel droplets ignite, spread, and extinguish themselves will help us develop more efficient ways of energy production and propulsion, as well as help us deal better with the problems of combustion-generated pollution and fire hazards associated with liquid combustibles. The ability to conduct more controlled experiments in space, without the complication of gravity, provides scientists with an opportunity to examine these complicated processes closely.

The Multiuser Droplet Combustion Apparatus (MDCA) supports this continued research under microgravity conditions. The objectives are to improve understanding of fundamental droplet phenomena affected by gravity, to use research results to advance droplet combustion science and technology on Earth, and to address issues of fire hazards associated with liquid combustibles on Earth and in space.

MDCA is a multiuser facility designed to accommodate different combustion science experiments. The modular approach permits the on-orbit replacement of droplet combustion principal investigator experiments such as different fuels, droplet-dispensing needles, and droplet-tethering mechanisms. Large components such as the avionics, diagnostics, and base-plate remain on the International Space Station to reduce the launch mass of new experiments. MDCA is also designed to operate in concert with ground systems on Earth to minimize the involvement of the crew during orbit.



MDCA chamber insert assembly—reusable hardware to accommodate different combustion experiments.



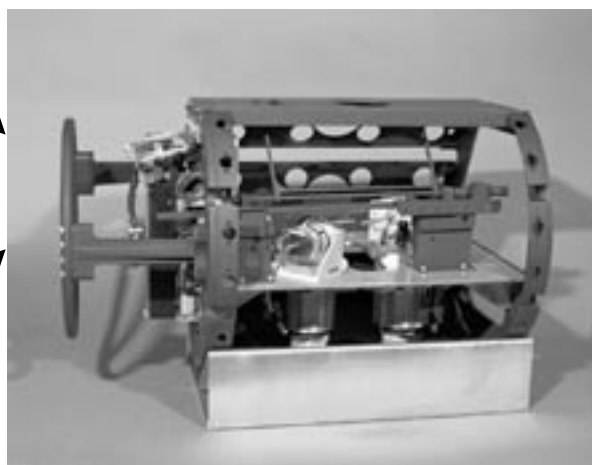
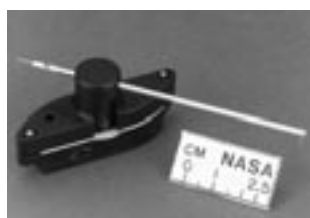
The Combustion Integrated Rack (CIR) provides diagnostics, power, data storage and processing, fluid control, interconnection, and crew-ground interfaces. It also contains the principal-investigator-specific hardware.

MDCA will conduct experiments using the Combustion Integrated Rack (CIR) of the NASA Glenn Research Center's Fluids and Combustion Facility onboard the space station. This facility is a multiuser, microgravity science laboratory with three individually powered space station racks that accommodate both combustion and fluid experiments. MDCA, in conjunction with CIR-provided common hardware, will allow for cost-effective extended access to the microgravity environment, not possible on previous space flights.

For the first phase, plans call for four principal investigators to study the combustion of small, spherical



Fuel syringe

Retractable
indexing fiber

Dispensing needle



Hot wire igniter

Principal investigator-specific hardware allows unique fuels as well as variable droplet diameters, deployment conditions, and diagnostics.

droplets of pure and bicomponent fuels. Isolated liquid fuel droplets remain the easiest to study because of their well-defined system. Three of the investigators will study the combustion of single droplets in a quiescent environment. The Droplet Combustion Experiment-2 reflight investigation will further explore droplet combustion behaviors, especially related to extinction phenomena. These were first observed during its first flight on the Microgravity Science Laboratory-1 flight in the Spacelab Module onboard space shuttle flights STS-83 and -94 in April and July 1997. The Bi-Component Droplet Combustion Experiment has its focus on the internal liquid fluid dynamics and combustion of bi-component fuel droplets. This experiment will be the first to study how each fuel species and their capillary forces drive the internal flow dynamics and combustion of a burning droplet. Sooting behaviors of droplets are the focus of the Sooting Effects in Droplet Combustion Investigation. The goal of this experiment is to measure and sample soot generated from a burning droplet. An understanding of the formation of soot and how it travels is important in fire safety. In contrast to the first three droplet investigations in a quiescent environment, the Dynamic Droplet Combustion Experiment plans to investigate the effects of small convective flows on the droplet during combustion such as may be found in the ventilation systems of space vehicles. This will improve the understanding of enhanced fire safety margins in spacecraft.

The MDCA hardware consists of the chamber insert assembly, avionics package, and a multiple array of diagnostics. The MDCA chamber insert assembly offers interchangeable fuel systems, igniter systems, droplet-tethering mechanisms, and droplet-dispensing systems. Additional diagnostics hardware will be provided by the CIR of the Fluids and Combustion Facility. The CIR will also provide the structural support for the chamber

insert assembly and diagnostics, the utilities for the avionics and diagnostics, and the mixing capability for principal-investigator-specific combustion chamber environments. In concert with the CIR, the MDCA allows for interchangeability and reorientation of the chamber insert assembly and diagnostics to meet principal investigator needs. Different combustion chamber environments will be controlled by the Fluids and Combustion Facility fuel/oxidizer management assembly system.

Glenn contact:

Craig A. Myhre, 216-433-8741,
Craig.A.Myhre@grc.nasa.gov

Author: Craig A. Myhre

Headquarters program office:
OBPR (MRD)

Programs/Projects:
Microgravity Science

Combustion Module-2 Preparations Completed for SPACEHAB Mission Including the Addition of a New Major Experiment

The Combustion Module-1 (CM-1) was a large, state-of-the-art space shuttle Spacelab facility that was designed, built, and operated on STS-83 and STS-94 by a team from the NASA Glenn Research Center composed of civil servants and local support contractors (Analex and Zin Technologies). CM-1 accomplished the incredible task of providing a safe environment to support flammable and toxic gases while providing a suite of diagnostics for science measurements more extensive than any prior shuttle experiment (or anything since). Finally, CM-1 proved that multiple science investigations can be accommodated in one facility, a crucial step for Glenn's Fluids and Combustion Facility developed for the International Space Station. However, the story does not end with CM-1. In 1998, CM-2 was authorized to take the CM-1 accomplishments a big step further by completing three major steps:

- (1) Converting the entire experiment to operate in a SPACEHAB module
- (2) Conducting an extensive hardware refurbishment and upgrading diagnostics (e.g., cameras, gas chromatograph, and numerous sensors)
- (3) Adding a new, completely different combustion experiment.



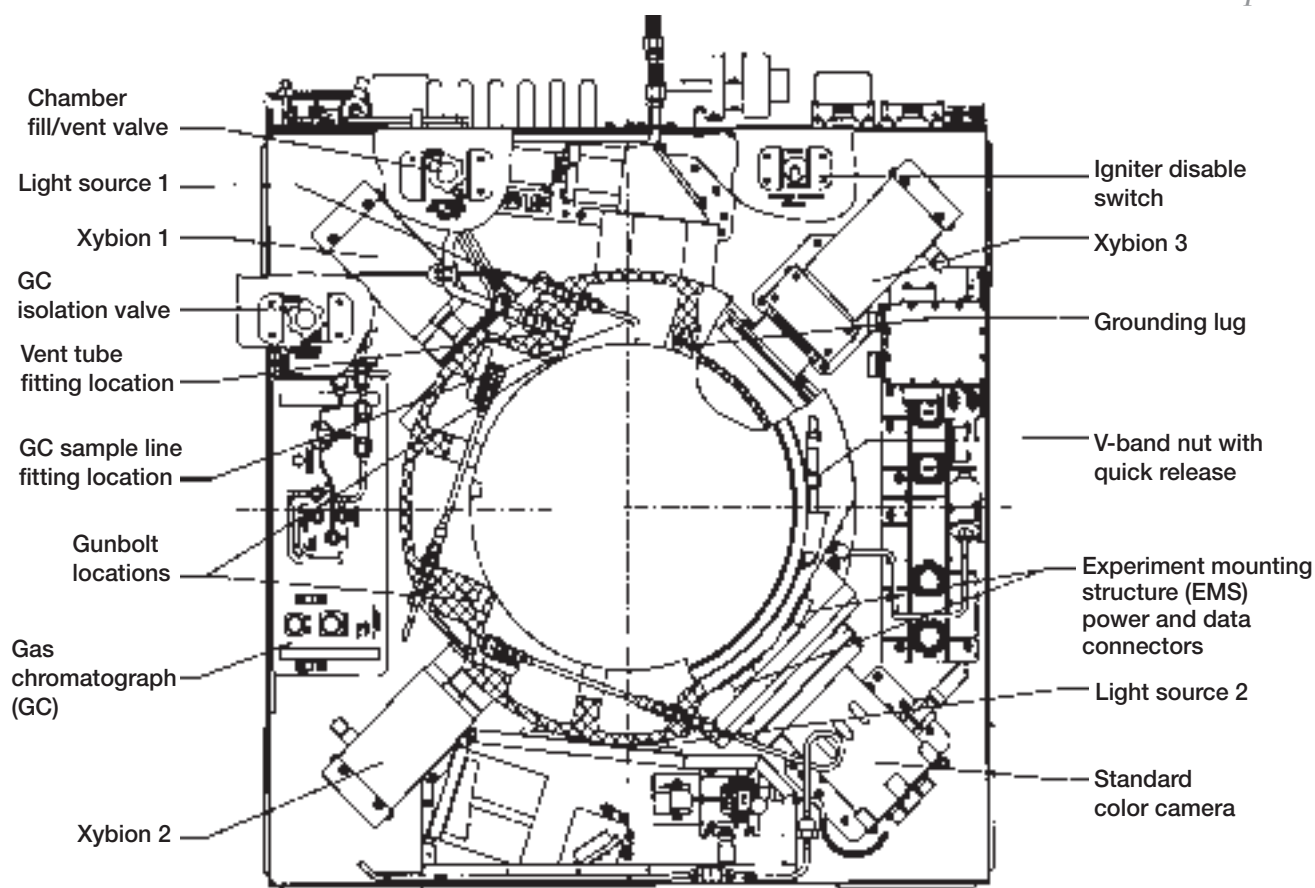
Combustion Module-2 flight system in SPACEHAB racks.

CM-2 has successfully completed these new tasks using only one-eighth the resources of CM-1.

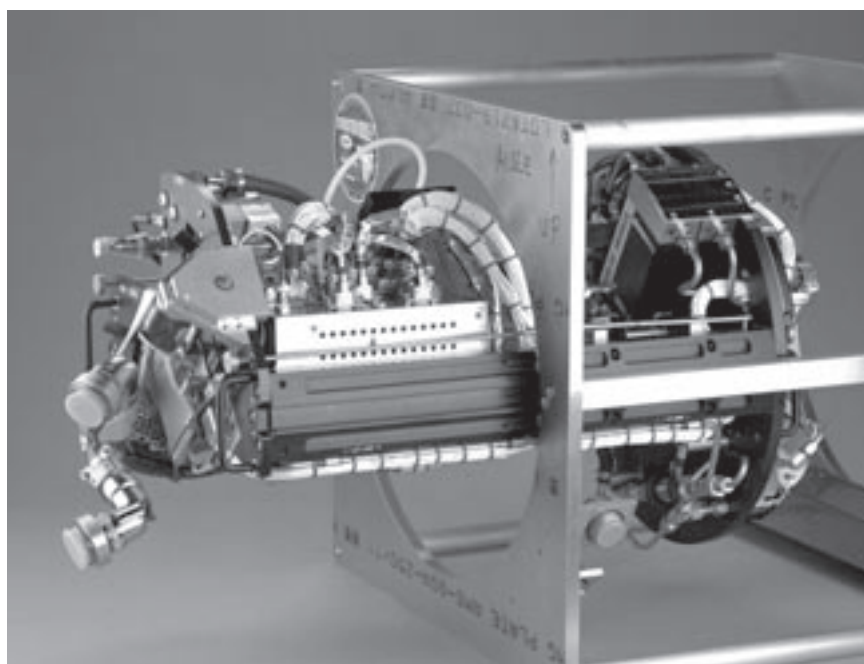
NASA funds combustion research with practical relevance in mind: to improve fuel efficiency, health (reduce pollutants), and fire safety both on Earth and in space. The overall purpose of CM-2 is to host three major combustion experiments:

- Laminar Soot Processes-2 (LSP-2)
- Structure of Flame Balls at Low Lewis-number-2 (SOFBALL-2)
- Water Mist Fire Suppression Experiment (Mist)

To accommodate just LSP-2 and SOFBALL-2, the CM-2 team needed to convert the facility from Spacelab to SPACEHAB and to conduct an extensive refurbishment and requalification for flight safety and science needs. The SPACEHAB conversion impacted every engineering interface including physical layout, structures (dynamics and stress), and thermal, electrical, data, software, and safety controls. For example, given the higher launch loads and the fact that CM-1 was qualified for only one flight, a special structural qualification approach was developed using a combination of low-level rack system vibration testing and analysis to minimize the risk to the CM-2 hardware. As in CM-1, flight rack integration was accomplished at Glenn, saving time and risk for the conversion process. The final flight assembly is shown in this photograph. Internal to CM-2, there was also a significant effort including extensive pressure system refurbishment and retesting



Combustion Module-2 experiment package diagnostics for Mist.



Water Mist Fire Suppression Experiment mounting structure.

as well as upgrades and/or fixes to most diagnostics based on CM-1 experience. For example, six of the seven CM-2 cameras were modified in some way to improve performance. The schematic shows the core of CM-2, the experiment package, with the Mist experiment diagnostics highlighted.

The third accomplishment of CM-2 is the successful integration of a new experiment, Mist. Unlike LSP and SOFBALL, Mist is a commercially sponsored experiment through the Commercial Center for Applications of Combustion in Space (CCACS). Also, unlike LSP and SOFBALL, the Mist chamber insert, or experiment mounting structure, was developed and built by CCACS, with the Glenn team

serving as consultants (see the final photograph). Mist was able to utilize the existing CM-2 chamber, cameras, gas chromatograph, data processing and storage, and experiment control computers without any modifications to the CM-2 hardware. Unique software and system integration activities were accomplished by the CM-2 team in partnership with the Mist CCACS personnel. This partnership provided further evidence to validate the multiuser approach technically, and provided a role model for the Fluids and Combustion Facility to use during future cooperative efforts on the International Space Station.

The CM-2 preflight efforts culminated at the end of fiscal year 2000 with the completion of a successful verification program and shipment to the launch site for SPACEHAB integration and testing. CM-2 is part of the SPACEHAB Research Double Module planned to be flown on STS-107.

Find out more about microgravity combustion research at Glenn:

<http://microgravity.grc.nasa.gov/combustion>

Glenn contacts:

Ann P. Over, 216-433-6535, Ann.P.Over@grc.nasa.gov; and

David T. Frate, 216-433-8329, David.T.Frate@grc.nasa.gov

Author: Ann P. Over

Headquarters program office: OBPR

Programs/Projects:

Microgravity Science, STS-107
SPACEHAB Research Double Module
Mission, Center for Commercial
Applications of Combustion in Space

Special recognition:

LSP-1 and SOFBALL-1 research results
published extensively including the
acclaimed Special Issue on Microgravity
Combustion, in the Combustion and
Flame Journal, published by the Com-
bustion Institute.

Experiments Developed to Study Microgravity Smoldering Combustion

The overall objective of the Microgravity Smoldering Combustion (MSC) research program is to understand and predict smoldering combustion under normal and microgravity (near-zero-gravity) conditions to help prevent and control smolder-originated fires, in both environments. Smoldering is defined as a nonflaming, self-sustaining, propagating, exothermic surface reaction. If a material is sufficiently permeable, smoldering is not confined to its outer surface, but can propagate as a reaction wave through the interior of the material. The MSC program will accomplish its goals by conducting smolder experiments on the ground and in a space-based laboratory, and developing theoretical models of the process. Space-based experiments are necessary because smoldering is a very slow process and, consequently, its study in a microgravity environment requires extended periods of time that can only be achieved in space. Smoldering can occur in a variety of processes ranging from the smolder of porous insulating materials to underground coal combustion. Many materials can sustain smoldering, including wood, cloth, foams, tobacco, other dry organic materials, and charcoal. The ignition, propagation, transition to flaming, and extinction of the smolder reaction are controlled by complex, thermochemical mechanisms that are not well understood. As with many forms of combustion, gravity affects the availability of the oxidizer and the transport of heat, and therefore, the rate of combustion.

The smoldering combustion of porous materials has been studied both experimentally and theoretically, usually in the context of fire safety. Smoldering encompasses a number of fundamental processes, including heat

and mass transfer in a porous media; endothermic pyrolysis of combustible material; ignition, propagation, and extinction of heterogeneous exothermic reactions at the solid-gas pore interface; and the onset of gas phase reactions (flaming) from existing surface reactions. Smoldering presents a serious fire risk because the combustion can propagate slowly in a material's interior and go undetected for long periods of time. It typically yields a substantially higher conversion of fuel to toxic compounds than does flaming (though more slowly), and may undergo a sudden transition to flaming.

Common examples of smoldering hazards are the initiation of forest fires by smoldering embers and of building fires from undetected smoldering in packing material



Microgravity smoldering combustion. Left: After modification. Right: Before modification.

insulation and furniture cushioning. Various studies since the early 1970's have shown that more than 40 percent of U.S. fire deaths can be attributed to smoldering household furniture. Smolder of cable insulation, another common fire hazard, is of particular concern in the space program—to date there have been a few minor incidents of overheated and charred cables and electrical components reported on space shuttle flights. Recently, with the establishment of the International Space Station and other planned space facilities, there has been an increased interest in the study of smoldering in microgravity to prevent or minimize the effect of a smolder-initiated fire.

The complexity of the smolder process requires the use of approximations in theoretical models and simplifications in experiments. The removal of gravity substantially simplifies smolder investigations because the influence of buoyancy on the heat and mass transport processes is removed. Instabilities induced by density stratification and problems related to sedimentation and collapse of the porous fuel and char are absent in microgravity. Furthermore, such experiments as well as a complementary theoretical foundation are necessary to assess the fire risk of a space-based installation.

The MSC investigation is being led by Professor A.C. Fernandez-Pello, the principal investigator, of the University of California at Berkeley. Dr. David L. Urban, of the NASA Glenn Research Center, is the project scientist. Two flight units have been built at Glenn by a team of civil servants and contractors, and have flown on the space shuttle: one on STS-69 and one on STS-77. The smoldering test material on both flights was unretarded urethane furniture foam. Each unit contained two test sections. Unit one had one test section with opposed (to the direction of burn) flow, and one with quiescent conditions. Unit two tested another opposed case (a different flow rate), and another quiescent case, the latter at higher oxygen content.

All tests were with oxygen-nitrogen mixtures. On the basis of these results, the project improved the smolder tracking system for reflight. The first units employed a video system, but the data were not as useful in low gravity as in Earth gravity. However, the experiment was able to track the combustion progress because the fuel sample included 10 thermocouples that provide an axial and radial temperature history of the smolder propagation. The modified units use an ultrasonic imaging system (UIS), which was developed and tested by the Glenn team. The UIS uses arrays of speakers and receivers on opposite sides of the foam test piece test sections to track the progress of the flame front. The original hardware design used a clear quartz cylinder to hold the foam fuel test sample to permit imaging of the smolder process, but this material is brittle and not amenable to the machining necessary to mount the speakers and receivers. After much searching and testing, the team located a polyimide resin material that could both withstand the high temperatures and had the toughness to be machined to the necessary tolerances. In addition to the UIS, the reflight experiment hardware comprises the main structure, two aluminum combustion chambers, an igniter power unit, a common igniter, two flow systems to deliver the oxidizer gas mixture, a battery, a data acquisition and control system, and a power control unit. Other hardware improvements, especially to the oxidizer gas delivery system, have been incorporated in the latest MSC reflight design. The first unit has been completed, and the second is now in the final testing process. Both are in line to fly on the shuttle as "Get-Away-Specials," as did the previous units. The experiments

are based on what was learned on the previous flights. They are opposed and forward flows on the first reflight payload, and forward flows and quiescent conditions on the second, with changes in various parameters. It is expected that the results of these studies will provide new insights into the mechanisms involved in the smoldering process and result in specific recommendations for reducing the risk of fires both on Earth and in space.

Glenn contact:

Franklin Vergilii, 216-433-6733, Fax 216-433-8050, Franklin.Vergilii@grc.nasa.gov

Author: Franklin Vergilii

Headquarters program office: OBPR

Programs/Projects: Microgravity Science



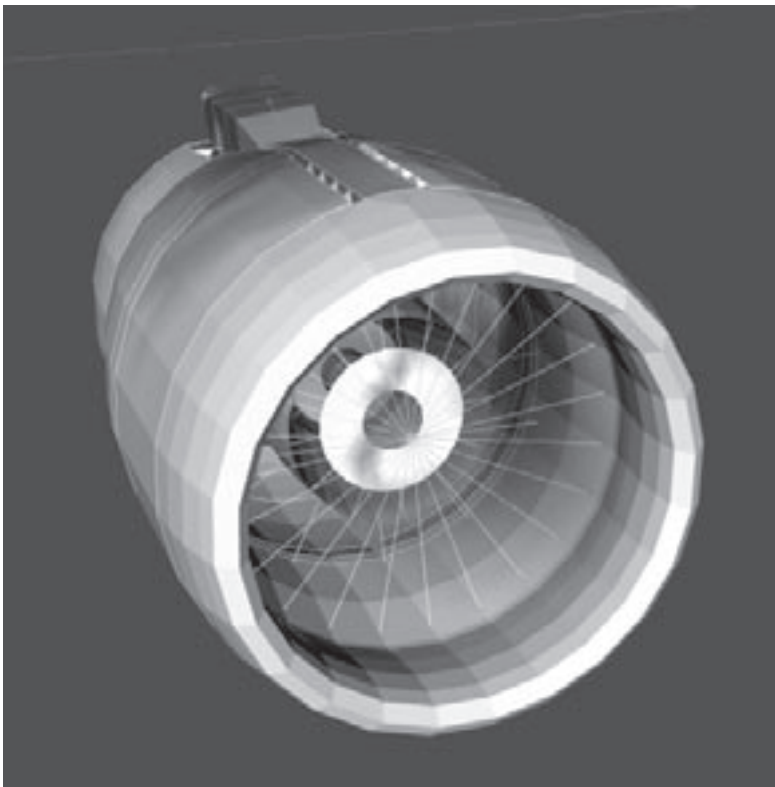
Engineering and Technical Services

Computer Services

Virtual Reality Used to Serve the Glenn Engineering Community

There are a variety of innovative new visualization tools available to scientists and engineers for the display and analysis of their models. At the NASA Glenn Research Center, we have an ImmersaDesk, a large, single-panel, semi-immersive display device. This versatile unit can interactively display three-dimensional images in visual stereo. Our challenge is to make this virtual reality platform accessible and useful to researchers. An example of a successful application of this computer technology is the display of blade out simulations.

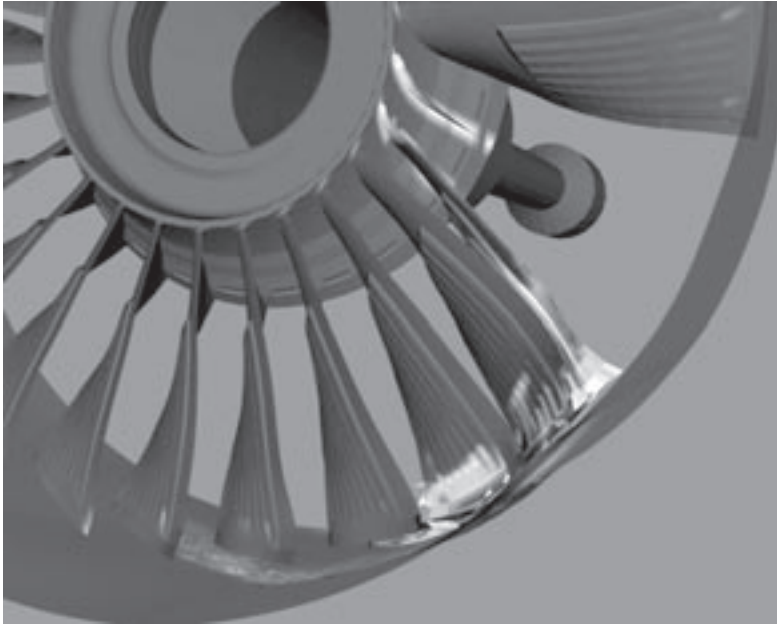
NASA Glenn structural dynamicists, Dr. Kelly Carney and Dr. Charles Lawrence, funded by the Ultra Safe Propulsion Project under Base R&T, are researching blade outs, when turbine engines lose a fan blade during operation. Key objectives of this research include minimizing danger to the aircraft via effective blade containment, predicting destructive loads due to the imbalance following a blade loss, and identifying safe, cost-effective designs and materials for future engines.



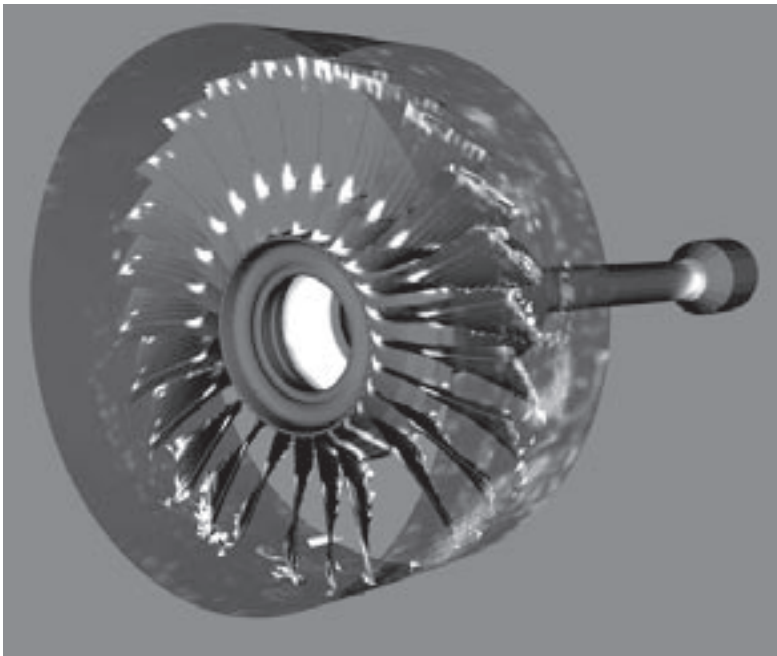
Glenn engineers, in collaboration with industry partners, model jet engines to predict loads due to blade loss. When displayed in a time sequence on the ImmersaDesk, subtle effects become apparent.

A blade out event is dramatic, complex, and fast moving. It is an excellent application for the ImmersaDesk platform. The event is modeled over time in a computer simulation. Physics-based modeling is used to predict the complex interactions between the fan rotor, the remaining fan blades, and the engine casing during a blade loss. Colors show a selected variable, such as plastic strain (images appear in color in the online version of this article: <http://www.grc.nasa.gov/WWW/RT2000/7000/7180carney.html>). The time steps of the simulation are displayed in sequence. To view the model on the ImmersaDesk, researchers wear stereoscopic goggles with liquid-crystal lenses. As a result, the model has depth and it is easier to interpret the physical events and mechanical interactions. Using a hand-held wand, a researcher can rotate, translate, and zoom the model interactively in real time. The researcher has now entered into semi-immersive virtual reality. Other observers, also wearing goggles, can watch as the three-dimensional model is manipulated. The display can be interactive or, if desired, a sequence can be captured and replayed as an animation.

As a part of the blade out research, Glenn engineers are working with engineers from Boeing Commercial Aircraft, GE Aircraft Engines, and Pratt & Whitney to develop new computer simulation tools for analyzing engine airframe structural systems. Glenn's physics-based computer simulations were



Researchers can use an interactive wand to zoom in for closeups of their models. This fan interaction simulation shows the dramatic results of a blade loss.



This fan interaction model can be viewed in stereo from all angles on the ImmersaDesk while cycling through the time steps of the traumatic blade out event.

successfully demonstrated on the ImmersaDesk for a large group of visiting representatives from those industry partners. In addition to being useful onsite for such collaborations, the ImmersaDesk is portable and can be shipped offsite for use at conferences and expositions so that NASA visualizations can be presented to a wider audience.

Find out more about this research:

Ultra Safe Propulsion Project:

<http://www.grc.nasa.gov/WWW/AERO/base/UltraSafe.htm>

ImmersaDesk R2:

<http://fakespacesystems.com/products/deskr2.html>

Engine System Dynamics—The Structural Mechanics and Dynamics Branch:

http://sdwww.grc.nasa.gov/5900website/5930/structural_mechanics/Rotor%20Dynamics/System%20Dynamics.html

Researcher Dorothy Carney:

http://gvis.grc.nasa.gov/people/personal_pages/carney/carney.html

Glenn contact:

Dorothy V. Carney, 216-433-8261,
Dorothy.V.Carney@grc.nasa.gov

Author: Dorothy V. Carney

Headquarters program office: OAT

Programs/Projects:

Aerospace Propulsion and Power
R&T Base Program, Ultra Safe Propulsion Project

Special recognition:

Featured on FOX-8 local TV news coverage and in The Plain Dealer following the Concorde crash in July 2000, featured by software vendor CEI at their web site and in a press release, and published on the HPCwire, an industry feed for high-performance computing.

Facilities and Test Engineering

Multimillion Dollar Construction Project Completed in Glenn's Icing Research Tunnel

Over the last year, the Glenn Research Center's Icing Research Tunnel (IRT) underwent a major \$5.2 million rehabilitation project as part of the Construction of Facilities program. The scope of the project included redesign and replacement of the 55-yr-old heat exchanger, the addition of fan outlet guide vanes for flow conditioning downstream of the 25-ft-diameter fan,

and redesign and replacement of the C and D corner-turning vanes. The purpose of the rehabilitation was to replace old portions of the infrastructure and to improve the aerodynamic flow quality in the tunnel.



Demolition of the IRT's original heat exchanger and turning vanes.



IRT's new 1650-ton heat exchanger.

After the construction phase was completed, the IRT facility engineers and technician staff successfully completed the Integrated Systems Testing. Next, a full calibration of the IRT's aerothermodynamics and icing cloud characteristics was completed. Results of these calibrations indicate that the temperature uniformity of the tunnel has improved significantly with variation across the tunnel cross section minimized to ± 1 °F. Flow angularity and turbulence intensity in the test section and settling chamber also improved. The achievable velocity in the test section during icing tests increased because of a reduction in the pressure drop across the heat exchanger and in the frost buildup.

Calibration tests were completed in July 2000, and the IRT's first research test program was successfully completed in early August. With the completion of the extensive facility modifications, the IRT is well positioned to support both NASA icing research programs and private industry customers well into the future.

Find out more about Glenn's IRT facility:

<http://www.grc.nasa.gov/WWW/IRT/>

Glenn contacts:

David W. Sheldon, 216-433-5662,
David.W.Sheldon@grc.nasa.gov; and
Susan L. Kevdzija, 216-977-7547,
Susan.L.Kevdzija@grc.nasa.gov

Author: Susan L. Kevdzija

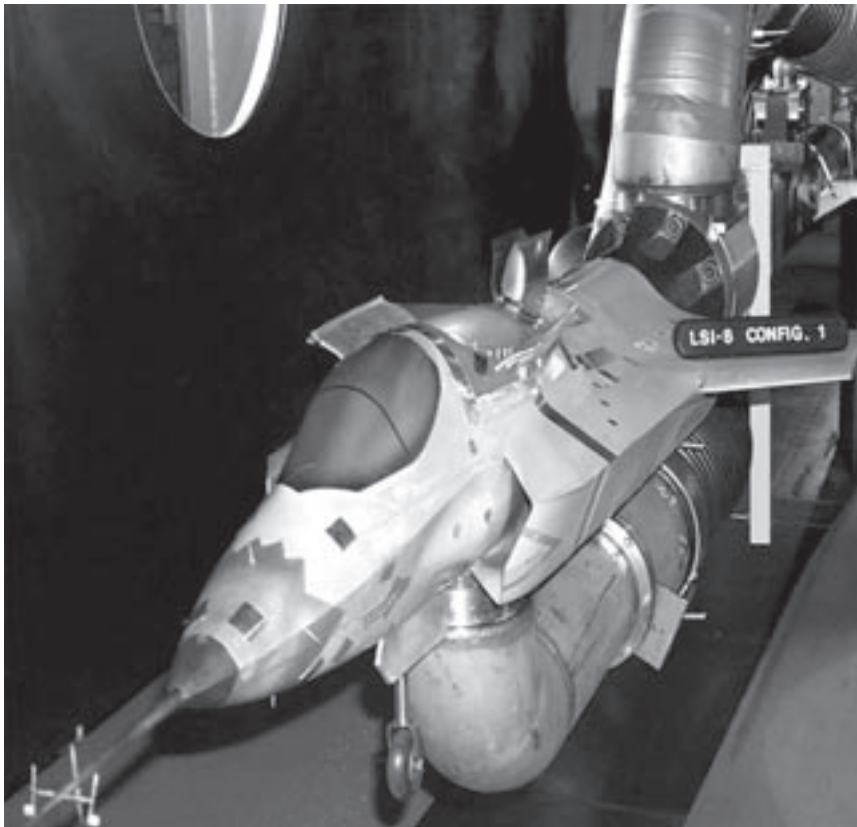
Headquarters program office: OAT

Programs/Projects: AvSP, AOS



Newly installed "C" corner fiberglass turning vanes in the IRT.

Abe Silverstein 10- by 10-Foot Supersonic Wind Tunnel Validated for Low-Speed (Subsonic) Operation



Lockheed Martin Joint Strike Fighter concept demonstration aircraft model installed at Glenn's 10- by 10-Foot Supersonic Wind Tunnel.

The NASA Glenn Research Center and Lockheed Martin Corporation tested an aircraft model in two wind tunnels to compare low-speed (subsonic) flow characteristics. Objectives of the test were to determine and document the similarities and uniqueness of the tunnels and to validate that Glenn's 10- by 10-Foot Supersonic Wind Tunnel (10×10 SWT) is a viable low-speed test facility. Results from two of Glenn's wind tunnels compare very favorably and show that the 10×10 SWT is a viable low-speed wind tunnel.

The Subsonic Comparison Test was a joint effort by NASA and Lockheed Martin using the Lockheed Martin's Joint Strike Fighter Concept Demonstration Aircraft model. Although Glenn's 10×10 and 8×6 SWT's have many similarities, they also have unique characteristics. Therefore, test data were collected for multiple model configurations at various vertical locations

in the test section, starting at the test section centerline and extending into the ceiling and floor boundary layers.

The stated test objectives are as follows:

- Verify that the 10×10 SWT is a viable subsonic test facility.
- Compare and validate model data of the 10×10 SWT versus the 8×6 SWT at multiple low-speed conditions and model positions.

In conclusion,

1. The 10×10 SWT is a viable low-speed test facility (from the standpoint of data quality), allowing flight speed to be varied from 0 to 250 knots.
2. The maneuver range is similar to that for the 8×6 SWT because of existing boundary layers in the 10×10 SWT test section.
3. A comparison of data from the 8×6 and 10×10 SWT's shows that the data are within an acceptable range. Most data are within a 0.5-percent range, with some data in a range up to 1 percent that may have resulted from adding unmatched parameters, such as angle of attack, angle of slip, and exhaust flow.

Glenn contacts:

Albert L. Johns, 216-433-3972,
Albert.L.Johns@grc.nasa.gov; and
Thomas R. Hoffman, 216-433-5637,
Thomas.R.Hoffman@grc.nasa.gov

Author: Thomas R. Hoffman

Headquarters program office: OAT

Programs/Projects:

Propulsion Systems R&T

Engineering Design and Analysis

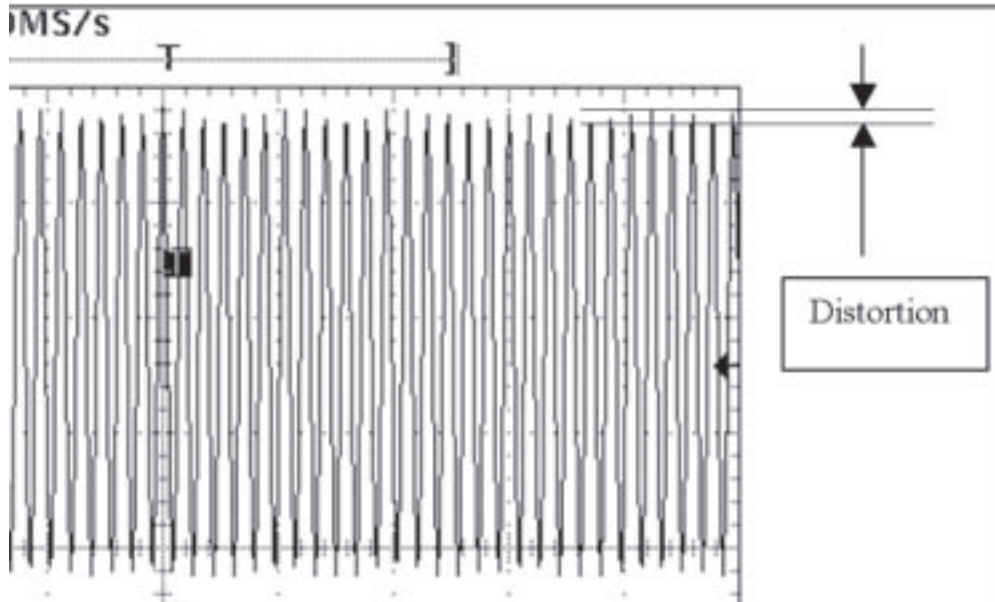
Sub-Nyquist Distortions in Sampled One- and Two-Dimensional Signals Studied

Hardware testing frequently involves the acquisition of waveform and instrumentation signals, which are often recorded on waveform recorders, oscillographs, and video recorders. Years ago, the waveforms were viewed as analog records, as drawn by a paper strip chart pen or electron beam on a cathode ray tube screen. One of the problems in the past was that the analog electronics may not have been able to accurately display the full amplitude of a signal if the real-time signals exceeded the frequency response bandwidth of the recording device.

The advent of digital oscilloscopes, waveform recorders, and video frame-grabbers solved many of the frequency response problems, though not all. A restriction on digital waveform acquisition is well known by people in the instrumentation field. Put simply, the sampling frequency must be at least twice the frequency of any signal to be sampled, or vice versa; the signals must be filtered so that none of the signal frequencies are higher than one-half the sample rate (the Nyquist Limit). Then, per Shannon's Sampling

Theorem (1949, ref. 1), any sampled signal can be reconstructed for viewing on a display device. If any signals exceed the Nyquist frequency limit, error signals called aliases occur in the output display.

The common assumption is that once the system signals and sample rates obey all the sampling requirements, there are no other front-end sampling issues. (There may be other requirements issues, such as having enough memory or disk space for storing all the samples.)



Waveform peak distortion captured with a digital oscilloscope at 1 million samples per second. Input frequency was 6/53 of that, or 113.20754 kHz.

Recently we showed (see above) that other sampling considerations apply when signals are much lower in frequency than the sample rate. Similar to a beat-note in an out-of-tune musical instrument, there is a distortion introduced into the displayed record that is most noticeable at the signal waveform peaks. Investigations have shown that the distortion in the signal peaks results in a modulation similar to a form of amplitude modulation (AM) on a radio signal. The signal frequencies of concern are those that are a fraction of a harmonic of the sample rate, in which the numerical ratio in the fraction has all the common primes factored out.

Unfortunately, there are literally hundreds of possible ratios (such as 6/53 in the figure) that can cause the distortion. The impact of having these false modulation signals in the record depends on the application. Through no fault of the manufacturers of waveform recorders and oscilloscopes, these distortion products can confuse and frustrate customers who are not familiar with the implications of sampling. A full publication on this topic is available (ref. 2).

References

1. Shannon, C.E.: Communication in the Presence of Noise. Proc. IRE, vol. 37, Jan. 1949, pp. 10–21.
2. Williams, G.L.: Sub-Nyquist Distortions in Sampled Data, Waveform Recording, and Video Imaging. NASA/TM–2000-210381, 2000. <http://gltrs.grc.nasa.gov/GLTRS>.

Glenn contact:

Glenn L. Williams, 216–433–2389,
Glenn.L.Williams@grc.nasa.gov

Author: Glenn L. Williams

Funding office: Engineering and Technical Services (NASA Glenn)

Programs/Projects:

Digital waveform technology, digital video recording technology

High-Voltage Droplet Dispenser Developed

Various techniques have been applied to deploying individual droplets for many applications, such as the study of the combustion of liquid fuels. Isolated droplet studies are useful in that they allow phenomena to be studied under well-controlled and simplified conditions. A high-voltage droplet dispenser has been developed that is extremely effective in dispensing a wide range of droplets. The dispenser is quite unique in that it utilizes a droplet bias voltage, as well as an ionization pulse, to release the droplet.

The droplet is deployed from the end of a needle. A flat-tipped, stainless steel needle attached to a syringe dispenses a known value of liquid that hangs on the needle tip. Somewhat below the droplet is an annular ring electrode. A bias voltage, followed by a voltage pulse, is applied to attract the droplet sufficiently to pull it off the needle. The droplet and needle are oppositely charged relative to the annular electrode. The needle is negatively charged, and the annular ring is positively charged.

The circuit of the droplet dispenser configuration described here is shown in the diagram. Power supply PS2 energizes DC/DC converter PS4 to produce the desired bias voltage for the droplet. A bias voltage on the order of 3 kV was found to be effective. PS4 charges capacitor C2 through current-limiting resistor R9. Bleed resistor R8 discharges C2 for safety when the circuit is not in use. Diodes D5 and D6 protect PS4 from inductive spikes. The droplet is charged via steering diode D4 and current-limiting resistor R7. Power supply PS1 energizes DC/DC converter PS3 to charge capacitor C1 via current-limiting resistor R1. Charging C1 to 100 V was found to be effective. Bleed resistor R2 discharges C1 for safety when the circuit is not in use. SCR1 conducts when S1 is depressed momentarily to produce a microsecond pulse in the primary winding of transformer T1. Diodes D1 and D2 protect SCR1 from inductive spikes. A pulse of 12 kV is produced at the secondary winding of T1 with C1 charged to 100 V, but

the circuit can produce a pulse up to 40 kV. The pulse provides ionization energy to the droplet via steering diode D3 and current-limiting resistors R3, R4, R5, and R6 to release the droplet. Multiple resistors are used to handle the high-voltage pulse.

In use, PS1 and PS2 are set to the minimum voltage levels and are turned on along with PS5. Power supplies PS1 and PS2 are then set to the desired voltage level. Finally, S1 is depressed momentarily to release the droplet. The circuit shown was developed for manual control, but it is readily adaptable to microprocessor-controlled applications.

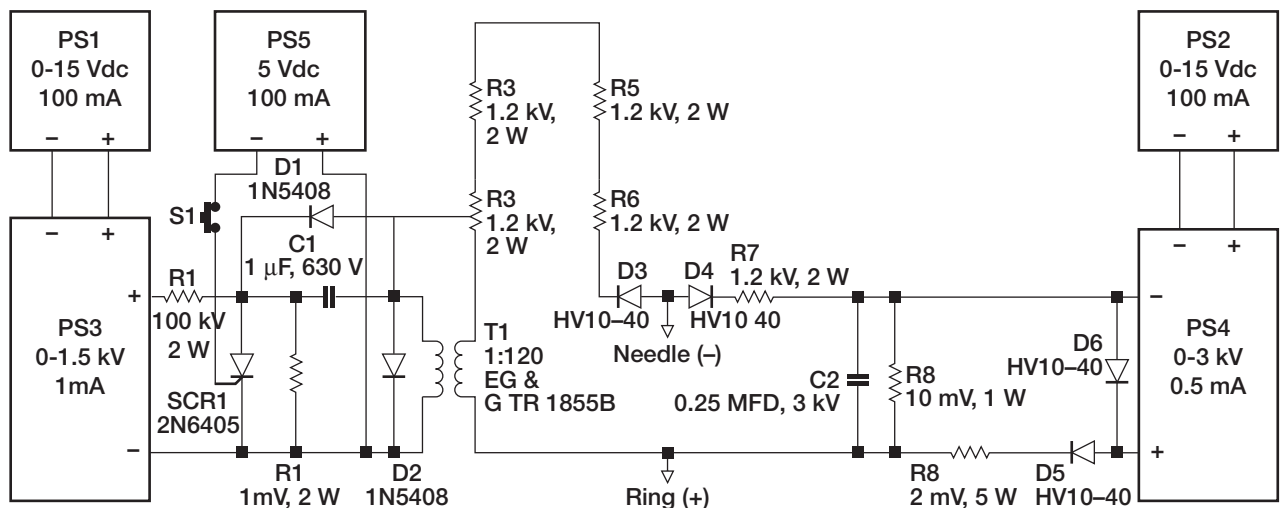
Glenn contact:

Dennis J. Eichenberg, 216-433-8360,
Dennis.J.Eichenberg@grc.nasa.gov

Authors: Dennis J. Eichenberg and
 Dr. Randy L. Vander Wal

Headquarters program office: OBPR

Programs/Projects:
 Microgravity Science



Electrical circuit diagram of high-voltage droplet dispenser.

Acoustical Testing Laboratory Developed to Support the Low-Noise Design of Microgravity Space Flight Hardware

The NASA John H. Glenn Research Center at Lewis Field has designed and constructed an Acoustical Testing Laboratory to support the low-noise design of microgravity space flight hardware. This new laboratory will provide acoustic emissions testing and noise control services for a variety of customers, particularly for microgravity space flight hardware that must meet International Space Station limits on noise emissions. These limits have been imposed by the space station to support hearing conservation, speech communication, and safety goals as well as to prevent noise-induced vibrations that could impact microgravity research data.

The Acoustical Testing Laboratory consists of a 23 by 27 by 20 ft (height) convertible hemi/anechoic chamber and separate sound-attenuating test support enclosure. Absorptive 34-in. fiberglass wedges in the test chamber provide an anechoic environment down to 100 Hz. A spring-isolated floor system affords vibration isolation above 3 Hz. These criteria, along with very low design background levels, will enable the acquisition of accurate and repeatable acoustical measurements on test articles, up to

a full space station rack in size, that produce very little noise. Removable floor wedges will allow the test chamber to operate in either a hemianechoic or anechoic configuration, depending on the size of the test article and the specific test being conducted. The test support enclosure functions as a control room during normal operations but, alternatively, may be used as a noise-control enclosure for test articles that require the operation of noise-generating test support equipment.

The Acoustical Testing Laboratory will provide a comprehensive array of acoustical testing services, including sound power level testing per ANSI S12.34 and ANSI S12.35. A multichannel PC-based acoustical data acquisition system allows simultaneous acquisition and real-time analysis of signals to facilitate the identification of equipment noise sources and transmission paths. Acoustical Testing Laboratory will function as a design verification facility, producing data to document requirements compliance and, more importantly, as an in-house lab where noise-control design strategies can be actively pursued and integrated into the overall design of flight hardware early in the life of each project.

The Acoustical Testing Laboratory was designed and constructed to meet the requirements of the Fluids and Combustion Facility project and was funded by the Microgravity Sciences Division. Acoustical design requirements were provided by the Engineering Design and Analysis Division, with technical facilities-engineering support from the Facilities Test and Engineering Division (FTED).



The Acoustical Testing Laboratory test chamber is a convertible hemi/anechoic facility with 34-in.-deep fiberglass wall and ceiling wedges. Removable floor wedge pallets incorporate a walking surface above the wedge tips.

Construction was managed by the FTED Construction Management Branch and implemented under Glenn Research Center's 8A construction program. The anechoic chamber and test-support enclosure were designed, fabricated, and installed by Eckel Industries of Cambridge, Massachusetts. The Acoustical Testing Laboratory will be operated by the Engineering Design and Analysis Division, joining their other vibroacoustic test services: the Structural Dynamics Laboratory and the Microgravity Emissions Laboratory.

Find out more on the World Wide Web: <http://acousticaltest.grc.nasa.gov>

Glenn contact:

Beth A. Cooper, 216-433-3950,
Beth.A.Cooper@grc.nasa.gov

Author: Beth A. Cooper

Headquarters program office:

OSF (Space Operations)

Programs/Projects:

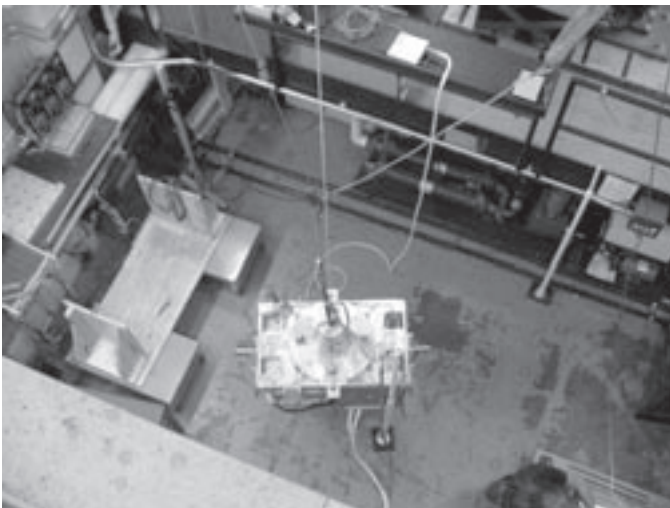
Microgravity Science, FCF

Microgravity Emissions Laboratory Developed

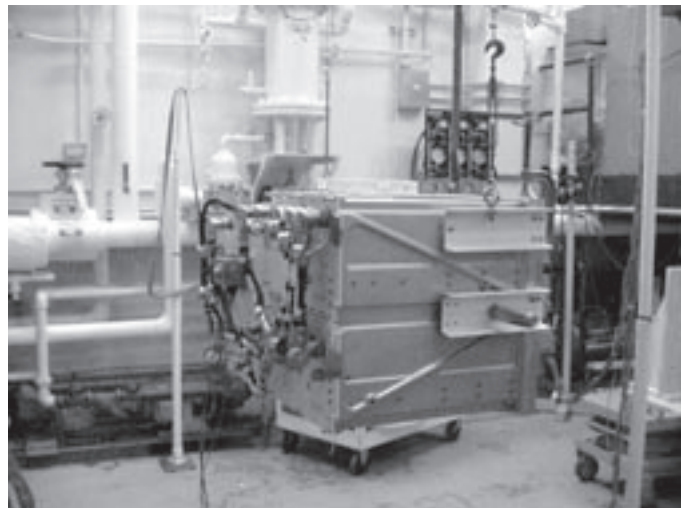
The Microgravity Emissions Laboratory (MEL) was developed for the support, simulation, and verification of the International Space Station microgravity environment. The MEL utilizes an inertial measurement system using acceleration emissions generated by various operating components of the space station. These emissions, if too large, could hinder the science performed on the space station by disturbing the microgravity environment.

Typical test components are disk drives, pumps, motors, solenoids, fans, and cameras. These components will produce inertial forces, which disturb the microgravity on-orbit station environment. These components, usually housed within a station rack, must meet acceleration limits imposed at the rack interface for minimizing the onboard station-operating environment. The NASA Glenn Research Center developed this one-of-a-kind laboratory for testing components and, eventually, rack-level configurations. The MEL

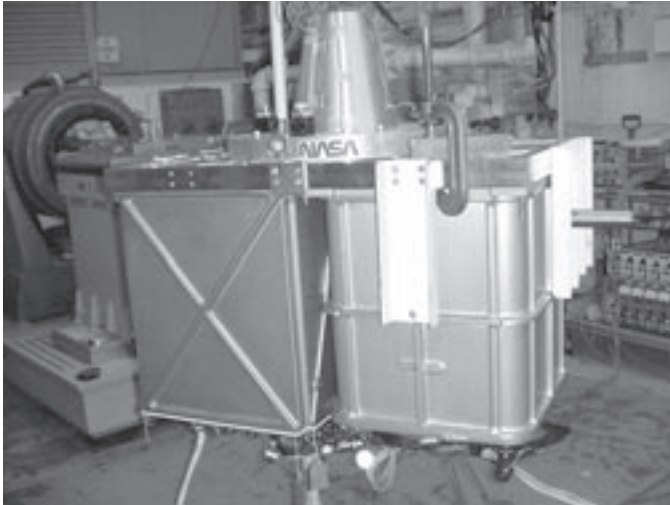
approach is to measure the component's generated inertial forces. This force is a product of the full diagonal mass matrix including the test setup (the center of gravity, mass moment of inertia, and weight) and the resolved diagonal rigid-body acceleration determined from measurements using the 10 apparatus accelerometers. The mass matrix can be test derived. The bifilar torsional pendulum method is used to measure the moment of inertia for the test component.



View from above the Physics of Colloids in Space MEL testing in progress.



Mass moment of inertia test setup.



MEL testing of the Physics of Colloids in Space experiment.

MEL is a low-frequency (0.15- to 0.4-Hz) isolator. The lateral frequencies are established with the pendulum, and the vertical mode is lowered with a zero-rate spring mechanism. This mechanism reduces the system's vertical frequencies to approximately 0.3 Hz. It suspends the measurement apparatus with the attached test unit by a long cable. The system allows the test article to float freely similar to a zero-g condition above 1 Hz. The measured motion of the rigid body is characterized through the MEL test, and the accelerometer data is postprocessed to calculate the rigid-body component forces and moments at the center of gravity/interface of the test unit.

MEL was developed for the Fluids and Combustion Facility through Glenn's Microgravity Sciences Division. It is located in Glenn's Structural Dynamics Laboratory. Engineering models of the Fluids and Combustion Facility's Optics Bench and Air Thermal Control Unit were tested in fiscal year 2001. Testing can be requested by using the MEL Web site: <http://www.grc.nasa.gov/WWW/MEL>.

Glenn contact:

Thomas W. Goodnight, 216-433-2381, Thomas.W.Goodnight@grc.nasa.gov; and Anne M. McNelis, 216-433-8880, Anne.M.McNelis@grc.nasa.gov

Authors: Thomas W. Goodnight and Anne M. McNelis

Headquarters program office: OSF

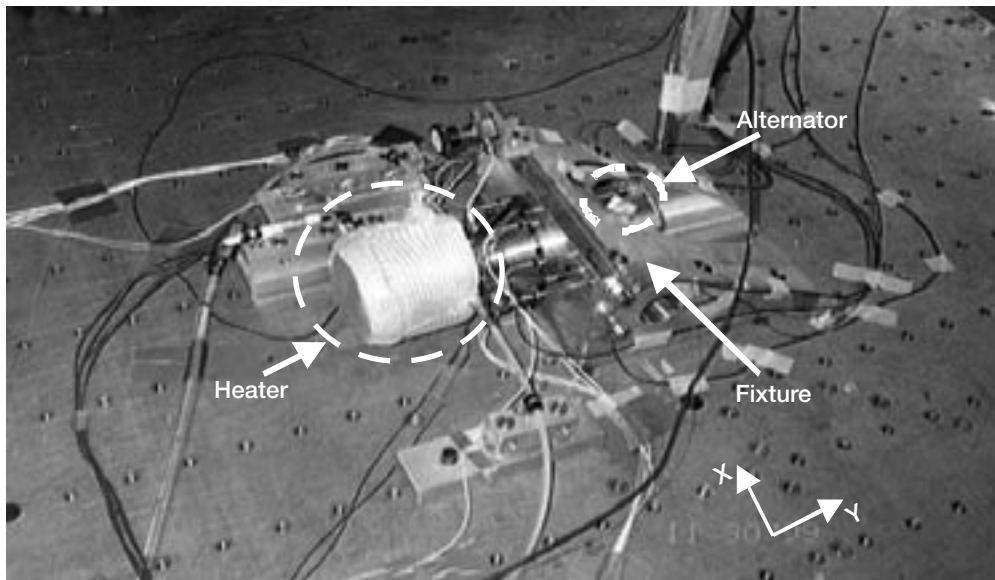
Programs/Projects: Microgravity Science, FCF, SAMS, MAMS, PCS

Vibration Test Demonstrated Dynamic Capability of an Operating Stirling Convertor

The NASA Glenn Research Center and the U.S. Department of Energy are currently developing a high-efficiency, long-life, free piston Stirling convertor for use as an advanced spacecraft power system for future NASA missions. As part of this development, a Stirling Technology Demonstrator Converter (TDC), developed by Stirling Technology Company for the Department of Energy, was vibration tested at Glenn's Structural Dynamics Laboratory in November and December 1999. This testing demonstrated that the Stirling TDC is able to withstand the harsh random vibration (20 to 2000 Hz) seen during a typical spacecraft launch and to survive with no structural damage or functional power performance degradation, thereby enabling its use in future spacecraft power systems.

Glenn and Stirling personnel conducted tests on a single 55 We TDC. The purpose was to characterize the TDC's structural response to vibration and to determine if the TDC could survive the vibration criteria established by the Jet Propulsion Laboratory for launch environments. The TDC was operated at full-stroke and full power conditions during the vibration testing.

It was tested in two orientations, with the direction of vibration parallel and perpendicular to the TDC's moving components (displacer and piston). The TDC successfully passed a series of sine and random vibration tests. The most severe test was a 12.3grms random vibration test (peak vibration level of 0.2 g²/Hz from 50 to 250 Hz) with test durations of 3 min per axis. The random vibration test levels were chosen to simulate, with margin, the maximum anticipated launch vibration conditions.



Vibration testing of the Stirling Technology Demonstrator Converter.

As a result of this very successful vibration testing and successful evaluations in other key technical readiness areas, the Stirling power system is now considered to be a viable technology for future application for NASA spacecraft missions. Possible usage of the Stirling power system would be to supply onboard electric spacecraft power for future NASA deep-space missions, performing as an attractive alternative to Radioisotope Thermo-electric Generators. Use of the Stirling technology is also being considered as the electric power source for future Mars rovers, whose mission profiles may exclude the use of photovoltaic power systems (such as exploring at high Martian latitudes or for missions of lengthy durations). Glenn's Thermo-Mechanical Systems Branch provides Stirling technology expertise under a Space Act Agreement with the Department of Energy. Additional vibration testing, by Glenn's Structural Systems Dynamics Branch, is planned to continue to demonstrate the Stirling power system's vibration capability as its technology and flight system designs progress.

Find out more about this research:

Glenn's Structural Dynamics Laboratory:

<http://www.grc.nasa.gov/WWW/SDL/Home.html>

Glenn's Thermo-Mechanical Systems Branch:

<http://www.grc.nasa.gov/WWW/tmsb>

Bibliography

Hughes, William O.; McNelis, Mark E.; and Goodnight, Thomas W.: Vibration Testing of an Operating Stirling Converter. NASA/TM-2000-210526, 2000. <http://gltrs.grc.nasa.gov/GLTRS>

Goodnight, Thomas W.; Hughes, William O.; and McNelis, Mark E.: Dynamic Capability of an Operating Stirling Converter. AIAA Paper 2000-2839, 2000. NASA/TM-2000-210527. <http://gltrs.grc.nasa.gov/GLTRS>

Thieme, Lanny G.; and Schreiber, Jeffrey G.: NASA GRC Technology Development Project for a Stirling Radioisotope Power System. AIAA Paper 2000-2480, 2000. NASA/TM-2000-210246. <http://gltrs.grc.nasa.gov/GLTRS>

Glenn authors and contacts:

William O. Hughes, 216-433-2597, William.O.Hughes@grc.nasa.gov; Thomas W. Goodnight, 216-433-2381, Thomas.W.Goodnight@grc.nasa.gov; and Mark E. McNelis, 216-433-8395, Mark.E.McNelis@grc.nasa.gov

Author: William O. Hughes

Headquarters program office:

OSS (MPDD), Flight Program Division

Programs/Projects:

Power and On-Board Propulsion/
Stirling Engine Technology

CM-2 Environmental/Modal Testing of SPACEHAB Racks

Combined environmental/modal vibration testing has been implemented at the NASA Glenn Research Center's Structural Dynamics Laboratory. The benefits of combined vibration testing are that it facilitates test article modal characterization and vibration qualification testing.

The Combustion Module-2 (CM-2) is a space experiment that will launch on shuttle mission STS-107 in the SPACEHAB Research Double Module. The CM-2 flight hardware is integrated into a SPACEHAB single and double rack. CM-2 rack-level combined vibration testing was recently completed on a shaker table to characterize the structure's modal response and verify the random vibration response. Control accelerometers and limit force gauges, located between the fixture and rack interface, were used to verify the input excitation. Results of the testing were used to verify the loads and environments for flight on the shuttles.

The CM-2 is a combustion science experiment consisting of eight packages that are integrated into SPACEHAB single and double racks (see the photograph). The CM-2 hardware is a reflight of CM-1 hardware, which was designed and environmentally qualified for SpaceLab and flew on STS-83 (April 4, 1997) and STS-94 (July 1, 1997). The CM-2 design loads and vibration environments for SPACEHAB are higher than for CM-1, requiring requalification of the CM-2 hardware for mission assurance.

The application of combined environmental/modal testing for the CM-2 flight program was a cost-effective way to reduce the design load factors and verify the package environments for mission assurance. The advantage of rack-level testing is it provides flight boundary conditions to the package. Performing rack-level testing instead of individual package level tests saved the program one-half the testing time. Furthermore, the one-fourth flight rack tests reduced the fatigue exposure to the CM-2 commercial, vibration-

sensitive electronic hardware. Integrated rack-level testing provided the inertial effect of mass attenuation, reducing the package interface random vibration response. By reducing the CM-2 package loads and vibration environments, the CM-2 program saved the cost of hardware requalification and redesign. This research was presented at the 7th International Congress on Sound and Vibration in Garmisch-Partenkirchen, Germany, July 5, 2000 (ref. 1). More information about CM-2 is available in references 2 and 3.

References

1. McNelis, Mark E.; Goodnight, Thomas W.; and Farkas, Michael A.: CM-2 Environmental/Modal Testing of SPACEHAB Racks. Proceedings of the 7th International Congress on Sound and Vibration, Garmisch-Partenkirchen, Germany, July 4-7, 2000.
2. Combustion Module-2 (CM-2): SPACEHAB Double Rack With Protoflight Packages Sinusoidal Resonance Survey and $\frac{1}{4}$ Flight Level Vibration Characterization Test Report. Structural Dynamics Laboratory Test Report SDL-TR 99-34, NASA Glenn Research Center, Dec. 7, 1999.
3. Combustion Module-2 (CM-2): SPACEHAB Single Rack With Protoflight Packages Sinusoidal Resonance Survey and $\frac{1}{4}$ Flight Level Vibration Characterization Test Report. Structural Dynamics Laboratory Test Report SDL-TR 99-29, NASA Glenn Research Center, Dec. 30, 1999.

Glenn contact:

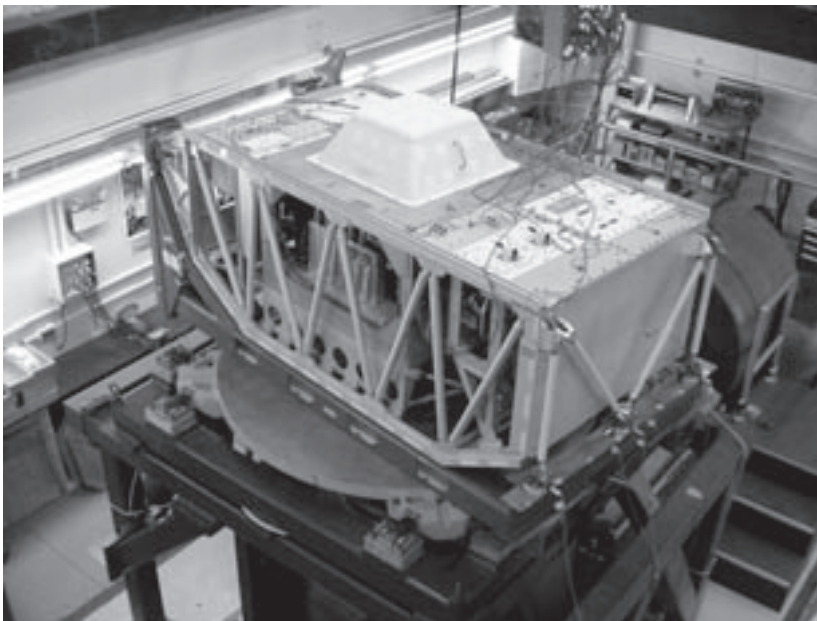
Mark E. McNelis, 216-433-8395,
Mark.McNelis@grc.nasa.gov

Author: Mark E. McNelis and
Thomas W. Goodnight

Headquarters program office: OBPR

Programs/Projects:

Microgravity Science, CM-2



CM-2 double-rack verification testing.



2, Commercial Technology 0

Microarthroscopy System With Image Processing Technology Developed for Minimally Invasive Surgery

In a joint effort, NASA, Micro Medical Devices, and the Cleveland Clinic have developed a microarthroscopy system with digital image processing. This system consists of a disposable endoscope the size of a needle that is aimed at expanding the use of minimally invasive surgery on the knee, ankle, and other small joints.

This device not only allows surgeons to make smaller incisions (by improving the clarity and brightness of images), but it gives them a better view of the injured area to make more accurate diagnoses. Because of its small size, the endoscope helps reduce physical trauma and speeds patient recovery. The faster recovery rate also makes the system cost effective for patients.

The digital image processing software used with the device was originally developed by the NASA Glenn Research Center to conduct computer simulations of satellite positioning in space. It was later modified to reflect lessons learned in enhancing photographic images in support of the

Center's microgravity program. Glenn's Photovoltaic Branch and Graphics and Visualization Lab (G-VIS) computer programmers and software developers enhanced and sped up graphic imaging for this application. Mary Vickerman at Glenn developed algorithms that enabled Micro Medical Devices to eliminate interference and improve the images.

Glenn contacts:

Kathleen K. Needham, 216-433-2802, Kathleen.K.Needham@grc.nasa.gov; Dr. Sheila G. Bailey, 216-433-2228, Sheila.G.Bailey@grc.nasa.gov; and Mary B. Vickerman, 216-433-5067, Mary.B.Vickerman@grc.nasa.gov

Author: Gynelle C. Steele

Headquarters program office:
OAT (CTD)

Programs/Projects: CTO

Special recognition:
1999 EDI Innovation Award



Microarthroscopy system.

Dynamic Light Scattering Developed to Look Through the Eye's Window Into the Body

Microgravity researcher Dr. Rafat R. Ansari, from the NASA Glenn Research Center, has found that the eye operates much like a camera and is the "window to the body." The eye contains transparent tissue through which light passes, providing us a view of what's going on inside. These transparent tissues represent nearly every tissue type that exists throughout the body. With the correlations and comparisons of these tissues done at Glenn, we hope to improve doctors' ability to diagnose diseases at much earlier stages. The medical community will be able to look noninvasively and quantitatively into a patient's eyes to detect disease before symptoms appear. Since the eye is easily accessed by light, the optical technologies created at Glenn can be used to evaluate its structure and physiology in health, aging, and disease.

These efforts have been concentrated into four areas of study: cataracts, diabetes, age-related macular degeneration (AMD), and Alzheimer's disease. Ophthalmic instruments with dynamic light scattering (DLS) capabilities, which were recently developed at Glenn, can diagnose cataracts at the molecular level. The fiber-optic probe also can be used for the early detection of vitreous diseases, including diabetic retinopathy and asteroid hyalosis. In addition, it can monitor blood sugar and cholesterol levels without taking blood samples.

Age-related macular degeneration, which damages and destroys the central vision of up to one in three people in the United States in their lifetime, has no known cause or cure. It is predicted that this disease may soon take on aspects of an epidemic. We hope to detect this disease earlier by measuring blood flow through the choroids region in the back of the retina and better monitor it with this new technology.

Many of the world's aging population are currently afflicted with Alzheimer's disease. The only current method of diagnosing Alzheimer's is

through an autopsy. Brain tissue is examined through a microscope to detect a protein substance called amyloid, which is deposited in the brains of people with the disease. This research will allow physicians to look into the eye tissue for amyloid protein, the same substance found in the Alzheimer's patient's brain. If the disease is detected at earlier stages, patients may be helped with anti-inflammatories, antioxidants, or hormone replacement therapies.

Using helmet-mounted "space-vision" or night vision goggles (similar to those used by F-16 pilots), doctors will be able to monitor the health of future space travelers and to detect cataracts, diabetic retinopathy, Alzheimer's disease, age-related macular degeneration, and retinal detachment. The goggles will allow doctors to remotely observe electroencephalograms (EEG's) and heart monitors and record body temperatures. This apparatus will also assist patients that live in distant areas with limited medical facilities. The information gathered through the goggles could be transmitted via satellite to doctors and medical personnel at more sophisticated urban medical centers.

Glenn contact:

Laurel J. Stauber, 216-433-2820,
Laurel.Stauber@grc.nasa.gov

National Center for Microgravity Research contact:

Dr. Rafat R. Ansari, 216-433-5008,
Rafat.R.Ansari@grc.nasa.gov

Author: Laurel J. Stauber

Headquarters program office: OBPR

Programs/Projects: HEDS



Dr. Ansari utilizing fiber probe to look into the window of the body.

Computer Model Used to Help Customize Medicine

Dr. Radhakrishnan, a researcher at the NASA Glenn Research Center, in collaboration with biomedical researchers at the Case Western Reserve University School of Medicine and Rainbow Babies and Children's Hospital, is developing computational models of human physiology that quantitate metabolism and its regulation, in both healthy and pathological states. These models can help predict the effects of stresses or interventions, such as drug therapies, and contribute to the development of customized medicine. Customized medical treatment protocols can give more comprehensive evaluations and lead to more specific and effective treatments for patients, reducing treatment time and cost.

Commercial applications of this research may help the pharmaceutical industry identify therapeutic needs and predict drug-drug interactions. Researchers will be able to study human metabolic reactions to particular treatments while in different environments as well as establish more definite blood metabolite concentration ranges in normal and pathological states.

These computational models may help NASA provide the background for developing strategies to monitor and safeguard the health of astronauts and civilians in space stations and colonies. They may also help to develop countermeasures that ameliorate the effects of both acute and chronic space exposure.

Glenn contacts:

Laurel J. Stauber, 216-433-2820,
Laurel.J.Stauber@grc.nasa.gov; and
Krishnan Radhakrishnan,
216-433-8483,
Krishnan.Radhakrishnan@grc.nasa.gov

Author:

Laurel J. Stauber and Jenise Veris

Headquarters program office: OAT

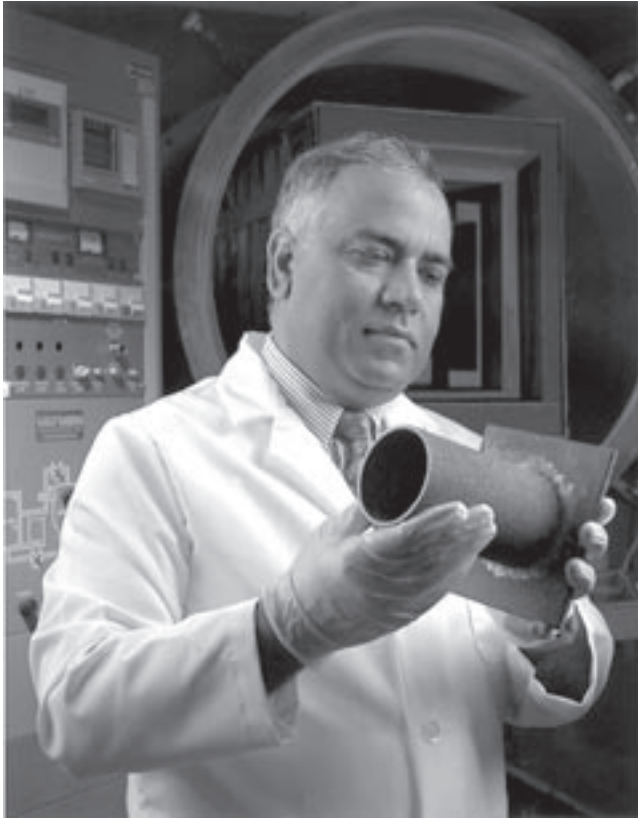
Programs/Projects: Base R&T

Affordable, Robust Ceramic Joining Technology (ARCJoint) Developed

Affordable, Robust Ceramic Joining Technology (ARCJoint) is a method for joining high-temperature-resistant ceramic pieces together, establishing joints that are strong, and allowing joining to be done in the field. This new way of joining allows complex shapes to be formed by joining together geometrically simple shapes. The joining technology at NASA is one of the enabling technologies for the application of silicon-carbide-based ceramic and composite components in demanding and high-temperature applications.

The technology is being developed and tested for high-temperature propulsion parts for aerospace use. Commercially, it can be used for joining ceramic pieces used for high-temperature applications in the power-generating and chemical industries, as well as in the microelectronics industry. This innovation could yield big payoffs for not only the power-generating industry but also the Silicon Valley chipmakers.

This technology, which was developed at the NASA Glenn Research Center by Dr. Mrityunjay Singh, is a two-step process involving first using a paste to join together ceramic pieces and bonding them by heating the joint to 110 to 120 °C for between 10 and 20 min. This makes the joint strong enough to be handled for the final joining. Then, a silicon-based substance is applied to the joint and heated to 1400 °C for 10 to 15 min. The resulting joint is as strong as the original ceramic material and can withstand the same high temperatures.



Dr. Singh holds an ARJoint ceramic component.

Glenn contact:

Gynelle C. Steele, 216-433-8258,
Gynelle.C.Steele@grc.nasa.gov

Dynacs Engineering Company, Inc., contact:

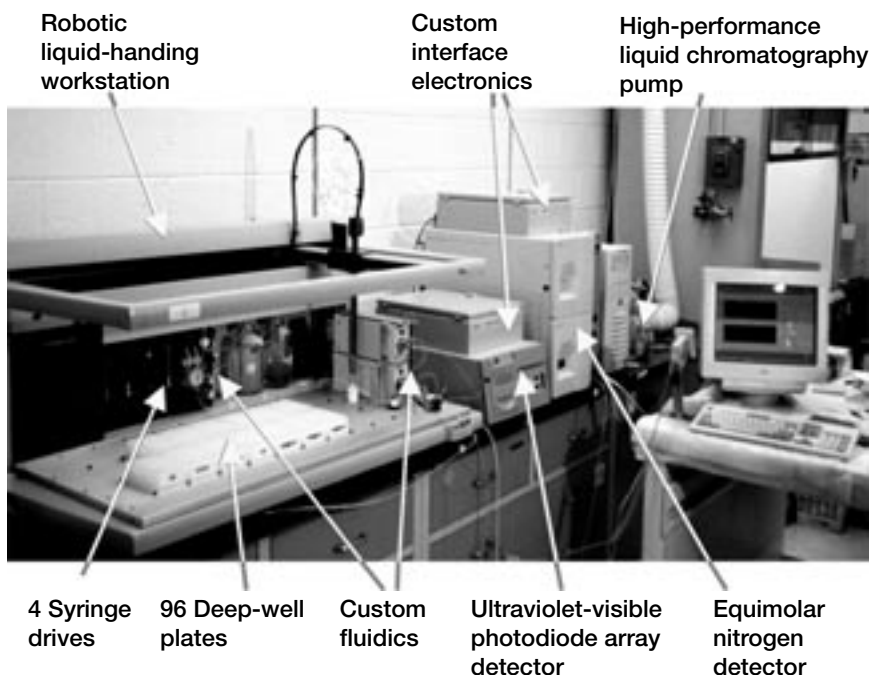
Dr. Mrityunjay Singh, 216-433-8883,
Mrityunjay.Singh@grc.nasa.gov

Author: Gynelle C. Steele

Headquarters program office: OAT

Programs/Projects: CTO

LIFT Tenant Is Off and Running



Analiza LIFT facility.

Lewis Incubator for Technology (LIFT) tenant, Analiza Inc., graduated from the incubator July 2000.

Analiza develops technology and products for the early diagnosis of diseases, quality control of bio-pharmaceutical therapeutics, and other applications involving protein analyses.

Technology links with NASA from existing and planned work are in areas of microfluidics and laser light scattering.

Since their entry in LIFT in May, 1997, Analiza has

- Received a \$750,000 grant from the National Institutes of Health
- Collaborated with a Nobel Prize winner on drug design

- Collaborated with Bristol-Myers Squibb on the characterization of biological therapeutics
- Added a Ph.D. senior scientist and several technicians
- Received significant interest from major pharmaceutical companies about collaborating and acquiring Analiza technology

Glenn contacts:

Gynelle C. Steele, 216-433-8258, Gynelle.C.Steele@grc.nasa.gov; and
Dr. Kim A. Veris, 216-433-6355, Kim.A.Veris@grc.nasa.gov

Author: Gynelle C. Steele

Headquarters program office: OAT (CTD)

Programs/Projects:

Biological therapeutics, drug design, microfluidics, laser light scattering

Definitions of NASA Headquarters Program Offices

OAT	Office of Aerospace Technology
CTD	Commercial Technology Division
OBPR	Office of Biological and Physical Research
MRD	Microgravity Research Division
OSF	Office of Space Flight
OSMA	Office of Safety and Mission Assurance
OSS	Office of Space Science
ATMS	Advanced Technology & Mission Studies Division
MPDD	Mission & Payload Development Division

Definitions of Programs and Projects

AATT	Advanced Air Transportation Technologies
AC/ATM	Advanced Communications for Air Traffic Management
AOS	Aviation Operations Systems
ARC	Aviation Capacity Program
ASTP	Advanced Space Transportation Program
AvSP	Aviation Safety Program
AvSP–SWAP	Aviation Safety Program—System Wide Accident Prevention
CAS	Computational Aerospace Sciences Project
CETDP	Cross-Enterprise Technology Development Program
CM–2	Combustion Module-2 space experiment
COMMTECH	A cooperative technology commercialization program
CTO	Glenn’s Commercial Technology Office
D³	Direct Data Distribution
DDF	Director’s Discretionary Fund (NASA Glenn)
DoD	Department of Defense
FCF	Fluids & Combustion Facility for the International Space Station
FESS	Flywheel Energy Storage System
FQE	Fast Quiet Engine
GMI	Glennan Microsystems Initiative
HEDS	Human Exploration and Development of Space
HITEMP	Advanced High Temperature Engine Materials Technology Program
HOTPC	High Operating Temperature Propulsion Components
HPCCP	High-Performance Computing and Communications Program
HSSO	High-Speed Systems Office
HSR	High-Speed Research
HST	Hubble Space Telescope
ICTD	Integrated Component Technology Demonstrations
IHPTET	Integrated High Performance Turbine Engine Technology
IPC	Intelligent Propulsion Controls
ISCO	Intelligent System Controls and Operations Project
ISS	International Space Station
IT Base	Information Technology Base Program
LTP	Learning Technologies Project
MAMS	Multispectral Atmospheric Mapping Sensor
NEPP	NASA Electronic Parts and Packaging
NGST	Next Generation Space Telescope
PAI	Propulsion-Airframe Integration

PCS	Physics of Colloids in Space
PDE	Pulse Detonation Engine Technology
PET	Photovoltaic Experimental Testbed
RLV	Reusable Launch Vehicles
RSL	Rotor Safe Life
SAMS	Space Acceleration Measurement System
SBIR	Small Business Innovation Research
SERT	Space Solar Power Exploratory Research and Technology
SILNT	Selected Integrated Low-Noise Transmissions for Rotorcraft
SOMO	Space Operations Management Office
SRF	Glenn's Strategic Research Fund
STR	Space Transportation Research
TCT	Technical Communication Terminal
UEET	Ultra Efficient Engine Technology
WINCOMM	Weather Information Communications
WxAP	Weather Accident Prevention Project
X-38	Prototype crew return vehicle for ISS
ZCET	Zero CO ₂ Emission Technology

Index of Authors and Contacts

Both authors and contacts are listed in this index. Articles start on the page numbers following the names.

- A**
Abel, Dr. Phillip B. 16
Abdul-Aziz, Dr. Ali 97, 99, 107
Aboudi, Prof. J. 105
Alexander, J. Iwan D. 92
Alston, Dr. William B. 29
Anderson, Robert C. 78
Ansari, Dr. Rafat R. 149, 162, 191
Arnold, Dr. Steven M. 101, 103, 105, 106
- B**
Baaklini, Dr. George Y. 96, 97, 99, 107, 109
Bailey, Dr. Sheila G. 190
Bakhle, Milind A. 124a
Balasubramaniam, Dr. Ramaswamy 151
Banks, Bruce A. 47, 48, 53
Balakotaiah, Vemuri 152
Baraona, Cosmo R. 37, 39
Bartolotta, Dr. Paul A. 114
Bednarczyk, Dr. Brett A. 101
Bencic, Timothy J. 62
Benson, Tom J. 6
Bhatt, Dr. Ramakrishna T. 34, 99
Blaha, Charles A. 90
Bodis, James R. 122
Bonacuse, Peter J. 111
Bond, Thomas H. 87
Bowles, Dr. Kenneth J. 27
Bozzolo, Dr. Guillermo H. 16
Bright, Michelle M. 64, 74, 75
Brinker, David J. 47
Brown, Dr. Gerald V. 124b, 125, 126
- C**
Cao, Wei N. 123
Carney, Dr. Dorothy V. 176
Chamis, Dr. Christos C. 115
Chato, David J. 94
Chen, Dr. Liang-Yu 58
Cheng, Robert K. 141
Chima, Dr. Rodrick V. 73
Choi, Dr. Benjamin B. 127
Choi, Dr. Sung R. 112
- Cios, Krzysztof J. 123
Cooper, Beth A. 183
Copland, Dr. Evan H. 18, 30
- D**
de Groh, Kim K. 47, 48, 49
DeGroot, Dr. Wilhemus A. 76
Decker, Dr. Arthur J. 63
Delgado, Irebert R. 131
DellaCorte, Dr. Christopher 136
Dever, Joyce A. 48, 50, 53
Doherty, Michael P. 159
Downey, Alan N. 67
Dunlap, Patrick H., Jr. 132
Duval, Dr. Walter 161
- E**
Eckel, Dr. Andrew J. 36
Eichenberg, Dennis J. 182
Ellis, Dr. David L. 24
- F**
Follen, Gregory J. 7, 9
Fox, Dr. Dennis S. 19, 35
Fralick, Gustave C. 90
Frate, David T. 170
Freedman, Marc R. 31
- G**
Gabb, Dr. Timothy P. 22, 111
Georgiadis, Nicholas J. 92
Giblin, Frank J. 149
Giriunas, Julius A. 89
Goldberg, Robert K. 113
Good, Dr. Brian S. 16
Goodnight, Thomas W. 184, 185, 187
Greenberg, Paul S. 141, 142
Griffin, Dr. DeVon W. 159
Gummow, Jonathan D. 49
Gyekenyesi, Dr. Andrew L. 96, 107
Gyekenyesi, Dr. John P. 112
- H**
Hall, Nancy R. 164
Hammoud, Ahmad 54
Hands Schuh, Dr. Robert F. 134
Hathaway, Dr. Michael D. 75
Hendricks, J. Lynne 122
Hickman, J. Mark 161
Hicks, Dr. Yolanda R. 76, 78
Hoffman, Thomas R. 179
Hoffmann, Monica I. 158
Holmes, Richard 24
Hopkins, Dale A. 128
Hughes, Christopher E. 129
Hughes, William O. 185
Hung, Dr. Ching-cheh 51
Hunter, Dr. Gary W. 58
Hurst, Janet B. 32
Hwang, Dr. Danny P. 90
- J**
Jacobson, Dr. Nathan S. 18, 30
Jacqmin, Dr. David A. 94
Jankovsky, Robert S. 42
Jaworske, Dr. Donald A. 47, 52
Jenkins, Phillip P. 37, 40
Johns, Albert L. 179
Juhasz, Albert J. 43
- K**
Kantzos, Peter T. 22
Kascak, Albert F. 124b
Kashiwagi, Takashi 145
Kautz, Harold E. 96, 107
Keller, Dennis A. 24
Kercewski, Robert J. 138
Kevdzija, Susan L. 178
King, James F. 149
Konno, Kevin E. 109
Kory, Carol L. 67
Koudelka, John M. 162
Krasowski, Mchael J. 37, 39
Krause, David L. 114
- L**
Landis, Dr. Geoffrey A. 37, 39, 40
LaPointe, Dr. Michael R. 41
Lee, Dr. Kang N. 35
Lei, Dr. Jih-Fen 58
Lepicovsky, Dr. Jan 73

Lerch, Dr. Bradley A. 24
 Locke, Dr. Randy J. 76, 78
 Logsdon, Kirk A. 164
 Lopez, Isaac 10
 Lovelace, Jeffrey J. 123

M

Manthey, Lori A. 2
 Martin, Lisa C. 90
 Martin, Richard E. 107, 109
 Martzaklis, Konstantinos S. 138
 Mason, Lee S. 42
 McDowell, Dr. Mark 166
 McFarland, Dr. Eric R. 73
 McNelis, Anne M. 184
 McNelis, Mark E. 185, 187
 Meador, Dr. Michael A. 26, 29
 Messer, Russell K. 50
 Miller, Fletcher J. 146
 Miller, Dr. Robert A. 19
 Miller, Sharon K. 47, 48, 53
 Miranda, Dr. Félix A. 71, 72
 Mital, Subodh K. 118
 Morales, Dr. Wilfredo 134
 Moran, Matthew E. 44
 Motil, Brian J. 152
 Motil, Susan M. 159
 Murthy, Dr. Pappu L.N. 115, 118
 Myhre, Craig A. 168

N

Naiman, Cynthia G. 7
 Nathal, Dr. Michael V. 24
 Needham, Kathleen K. 190
 Nemeth, Noel N. 119
 Neudeck, Dr. Philip G. 58
 Nguyen, Dr. Quang-Viet 79
 Noebe, Dr. Ronald D. 16

O

Okojie, Dr. Robert S. 59
 Olson, Dr. Sandra L. 143, 145
 Opila, Dr. Elizabeth J. 30
 Oswald, Fred B. 135
 Over, Ann P. 170

P

Palaszewski, Bryan A. 82, 84, 85
 Patnaik, Dr. Surya N. 128
 Patterson, Richard L. 54
 Paxson, Dr. Daniel E. 66

Pereira, Dr. J. Michael 113
 Petersen, Ruth A. 6, 11
 Pindera, Prof. M.J. 105
 Plachta, David W. 95
 Porro, A. Robert 91
 Powell, J. Anthony 60
 Powers, Charles 50
 Proctor, Margaret P. 131
 Provenza, Andrew J. 127

R

Radhakrishnan, Krishnan 192a
 Ramé, Dr. Enrique 154
 Rashidnia, Dr. Nasser 151, 156
 Ratvasky, Thomas P. 87, 89
 Reed, John A. 9
 Reshotko, Eli 92
 Roberts, Dr. Gary D. 113
 Robinson, R. Craig 35
 Rohn, Douglas A. 84, 85
 Romanofsky, Dr. Robert R. 69
 Ross, Dr. Howard D. 146
 Roth, Dr. Don J. 122, 123

S

Saleeb, Prof. A.F. 106
 Scheiman, David A. 39
 Schreiber, Jeffrey G. 55
 Sechkar, Edward A. 47, 48
 Shaltens, Richard K. 55
 Shaw, Dr. Robert J. 2
 Sheldon, David W. 178
 Simons, Dr. Rainee N. 71, 72
 Singh, Dr. Mrityunjay 33, 192b
 Skoch, Gary J. 74
 Smith, Timothy D. 86
 Snead, John H. 159
 Snyder, Aaron 47, 48
 Soeder, James F. 46
 Srivastava, Rakesh 124a
 Stauber, Laurel J. 191, 192a
 Steele, Gynelle C. 190, 192b, 193
 Stefko, George L. 124a
 Steinetz, Dr. Bruce M. 132
 Strazisar, Dr. Anthony J. 64, 74, 75
 Stueber, Thomas J. 47
 Suder, Dr. Kenneth L. 64, 75

T

Telesman, Jack 22, 111
 Tew, Roy C. 43

Thieme, Lanny G. 43, 55
 Thompson, Richard 109
 Thorp, Scott A. 64, 75
 Tong, Michael T. 4
 Townsend, Jacqueline A. 50
 Trowbridge, D. 103

V

Valco, Dr. Mark J. 136
 Vander Wal, Dr. Randy L. 148, 182
 Van Schalkwyk, Christian 64
 Vergilii, Franklin 172
 Veres, Joseph P. 13
 Veris, Jenise 192a
 Veris, Dr. Kim A. 193
 Vickerman, Mary B. 190

W

Wald, Lawrence W. 139
 Whalen, Mike F. 122
 Wilkinson, Dr. R. Allen 158
 Williams, Glenn L. 180
 Wilson, Jeffrey D. 68
 Wilt, David M. 40
 Wolff, Frederick J. 46
 Wong, Wayne A. 56
 Wooldridge, Eve 50

Y

Yun, Hee Mann 24

Z

Zernic, Michael J. 138, 140
 Zhu, Dr. Dongming 19
 Zona, Kathleen A. 11

REPORT DOCUMENTATION PAGE			Form Approved OMB No. 0704-0188	
Public reporting burden for this collection of information is estimated to average 1 hour per response, including the time for reviewing instructions, searching existing data sources, gathering and maintaining the data needed, and completing and reviewing the collection of information. Send comments regarding this burden estimate or any other aspect of this collection of information, including suggestions for reducing this burden, to Washington Headquarters Services, Directorate for Information Operations and Reports, 1215 Jefferson Davis Highway, Suite 1204, Arlington, VA 22202-4302, and to the Office of Management and Budget, Paperwork Reduction Project (0704-0188), Washington, DC 20503.				
1. AGENCY USE ONLY (Leave blank)		2. REPORT DATE March 2001		3. REPORT TYPE AND DATES COVERED Technical Memorandum
4. TITLE AND SUBTITLE Research & Technology 2000			5. FUNDING NUMBERS None	
6. AUTHOR(S)				
7. PERFORMING ORGANIZATION NAME(S) AND ADDRESS(ES) National Aeronautics and Space Administration John H. Glenn Research Center at Lewis Field Cleveland, Ohio 44135-3191			8. PERFORMING ORGANIZATION REPORT NUMBER E-12565	
9. SPONSORING/MONITORING AGENCY NAME(S) AND ADDRESS(ES) National Aeronautics and Space Administration Washington, DC 20546-0001			10. SPONSORING/MONITORING AGENCY REPORT NUMBER NASA TM-2001-210605	
11. SUPPLEMENTARY NOTES Responsible person, Walter S. Kim, organization code 9400, 216-433-3742.				
12a. DISTRIBUTION/AVAILABILITY STATEMENT Unclassified - Unlimited Subject Categories: 01 and 31 This publication is available from the NASA Center for AeroSpace Information, 301-621-0390.			12b. DISTRIBUTION CODE Distribution: Nonstandard	
13. ABSTRACT (Maximum 200 words) This report selectively summarizes the NASA Glenn Research Center's research and technology accomplishments for the fiscal year 2000. It comprises 138 short articles submitted by staff scientists and engineers. The report is organized into five major sections: Aeronautics, Research and Technology, Space, Engineering and Technical Services, and Commercial Technology. A table of contents and an author index have been developed to assist readers in finding articles of special interest. This report is not intended to be a comprehensive summary of all the research and technology work done over the past fiscal year. Most of the work is reported in Glenn-published technical reports, journal articles, and presentations prepared by Glenn staff and contractors. In addition, university grants have enabled faculty members and graduate students to engage in sponsored research that was reported at technical meetings or in journal articles. For each article in this report, a Glenn contact person has been identified, and where possible, reference documents are listed so that additional information can be easily obtained. The diversity of topics attests to the breadth of research and technology being pursued and to the skill mix of the staff that makes it possible. For more information about research at NASA Glenn, visit us on the World Wide Web (http://www.grc.nasa.gov). This document is available online (http://www.grc.nasa.gov/WWW/RT). For publicly available reports, visit the Glenn Technical Report Server (http://gltrs.grc.nasa.gov/GLTRS).				
14. SUBJECT TERMS Aeronautics; Aerospace engineering; Space flight; Space power; Materials; Structures; Electronics; Space experiments; Technology transfer			15. NUMBER OF PAGES 215	
			16. PRICE CODE A10	
17. SECURITY CLASSIFICATION OF REPORT Unclassified	18. SECURITY CLASSIFICATION OF THIS PAGE Unclassified	19. SECURITY CLASSIFICATION OF ABSTRACT Unclassified	20. LIMITATION OF ABSTRACT	